Univerzita Karlova v Praze

Přírodovědecká fakulta

Studijní program: Vývojová a buněčná biologie

Mgr. Kateřina Bruštíková

Vývoj chemických regulátorů drah mikroRNA a RNAi

Development of chemical regulators of microRNA and RNAi pathways

Disertační práce

Školitel:

Doc. Petr Svoboda, Ph.D.

Praha, 2015

Prohlášení:

Prohlašuji, že jsem disertační práci zpracovala samostatně, a že jsem řádně uvedla a citovala všechny použité informační zdroje a literaturu. Tato práce ani její podstatná část nebyla předložena k získání jiného nebo stejného akademického titulu.

V Praze, 7.6.2015

Kateřina Bruštíková

PODĚKOVÁNÍ

Tuto práci věnuji své mamince…

Její přání, abych Ph.D. „dotáhla do konce“, mě poháněl po celou dobu mé práce.

Tato práce by jen stěží vznikla bez pomoci níže jmenovaných lidí:

V první řadě bych ráda poděkovala Petrovi za to, že mi před lety projevil důvěru a přijal mě do svého týmu. Vážím si ho nejen pro jeho profesionalitu a snahu udělat ze mě vědce schopného mimo jiné i prezentovat výsledky své práce jak psanou, tak ústní formou, ale především pro jeho snad nekonečnou trpělivost, kterou při mém vedení projevil.

V druhé řadě bych ráda poděkovala RNDr. Petru Bartůňkovi CSc., který v rámci spolupráce na tomto projektu zapůjčil několik nezbytných nástrojů, bez kterých by tento projekt nemohl být zrealizován. Za prvé kolekci chemických sloučenin, 30 tisíc nadějných hochů, kteří jen čekají na to, až objevíme jejich skrytý potenciál ovlivnit dráhu mikroRNA. Za druhé, úžasné roboty, jak ze science fiction, bez kterých bych pipetovala ještě dnes. A za třetí Mgr. Davida Sedláka, Ph.D., který mi předal nejen mnoho zkušeností a rad týkajících se optimalizace HTS metod, ale i pár životních lekcí, za které jsem zpětně moc vděčná. Na Davidovi v podstatě stála celá konečná realizace HTS a následná normalizace a prvotní analýza dat, kterou provedl s obdivuhodnou pečlivostí a profesionalitou. Za to mu patří můj velký dík.

Dále bych chtěla poděkovat celému týmu Petra Svobody za vytvoření příjemného prostředí pro práci. Každý člen Svobodovy posádky je naprosto jedinečný a každý z nich mi pomohl svým osobitým způsobem.

Můj dík patří i Markétě Vančurové, která se na této práci podílela kontrolou angličtiny, a to s velkou pečlivostí a podle jejího nejlepšího vědomí a svědomí.

Děkuji i všem dalším kolegům, s kterými jsem mohla konzultovat jednotlivé metody a úskalí, popř. i těm, kteří mi poskytli technickou a materiální podporu.

V neposlední řadě bych ráda poděkovala své rodině. Michalovi a Stelince za jejich trpělivost, toleranci a podporu při dlouhém sepisování této práce. A dále Jarce za to, že hlídala Stelinku a umožnila mi za sebou alespoň občas na pár hodin zavřít dveře a dělat, že existuje jen text přede mnou.

ABSTRAKT

MikroRNA jsou nekódující RNA navozující sekvenčně specifickou inhibici genové exprese na posttranskripční úrovni. MikroRNA představují hlavní skupinu malých endogenních RNA v savčích buňkách. V současnosti je známo více než 2500 lidských mikroRNA, které potencionálně regulují více než 60% lidských genů kódujících proteiny. MikroRNA se účastní většiny buněčných procesů a změny v jejich expresi byly popsány u různých patologií, včetně rakoviny.

V současnosti neexistuje žádná malá chemická sloučenina schopná efektivního ovlivnění aktivity dráhy mikroRNA. Nicméně, malé chemické sloučeniny představují skvělé nástroje pro výzkum procesů, ve kterých dráhy sekvenčně specifického umlčování RNA (RNA silencing) hrají roli. Navíc by mohly být využitelné i pro biotechnologické aplikace a mohly by mít i značný terapeutický potenciál. Tato práce je součástí širokého projektu, jehož konečným cílem je: (i) najít soubor malých molekul umožňujících stimulaci a inhibici drah sekvenčně specifického umlčování RNA a (ii) identifikovat případy, kdy se tyto dráhy vzájemně ovlivňují s jiných buněčnými drahami. Tato práce shrnuje výsledky prvních dvou fází projektu, vývoj vysoce výkonných metod testování s vysokou propustností a vysoce výkonné testování s vysokou propustností (high-throughput screening, HTS) dostupných knihoven malých sloučenin.

Abychom mohli monitorovat aktivitu dráhy mikroRNA, vyvinuli jsme a optimalizovali jednu biochemickou *in vitro* metodu založenou na měření změny fluorescence po modulaci aktivity enzymu Dicer a dále několik metod založených na měření změny luminiscence po modulaci dráhy mikroRNA přímo v buňkách. Naší strategií bylo získat data umožňující třídit výsledky z HTS na základě různých parametrů tak, abychom mohli zohlednit například buněčně-specifické efekty, mikroRNA specifické efekty, popřípadě určit v jaké fázi jsou dráhy sekvenčně specifického umlčování RNA ovlivněny. S pomocí optimalizovaných metod byl proveden HTS ~30,000 malých chemických sloučenin. Kombinací dat ze všech HTS jsme získali desítky potencionálně zajímavých sloučenin, které je potřeba dále ověřit. Vybrané sloučeniny budou dále analyzovány řadou metod s cílem určit jejich farmakokinetické vlastnosti, místo jejich působení na dráhy sekvenčně specifického umlčování RNA a jejich regulační potenciál v různých modelových systémech.

ABSTRACT

MicroRNAs are noncoding RNAs inducing sequence-specific posttranscriptional inhibition of gene expression and represent the major class of small endogenous RNAs in mammalian cells. Over 2,500 of human microRNAs potentially regulating more than 60% of human protein-coding genes have been identified. MicroRNAs participate in the majority of cellular processes, and their expression changes in various diseases, including cancer.

Currently, there is no efficient small chemical compound available for the modulation of microRNA pathway activity. At the same time, small chemical compounds represent excellent tools for research of processes involving RNA silencing pathways, for biotechnological applications, and would have a considerable therapeutic potential. The presented work represents a part of a broader project, whose ultimate goal is: (i) to find a set of small molecules allowing for stimulation or inhibition of RNA silencing and (ii) to identify crosstalks between RNA silencing and other cellular pathways. This thesis summarizes results from the first two phases of the project, the development of high-throughput screening assays and the high-throughput screening (HTS) of available libraries of small compounds.

To monitor the microRNA pathway activity, we developed and optimized one biochemical fluorescence-based *in vitro* Dicer assay and several cell-based luciferase assays. Our strategy was to generate data allowing sorting HTS results according to different parameters, such as cell-type specific effects, miRNA specific effects, or sorting compounds affecting different steps of RNA silencing pathway. Optimized assays were used for HTS of ~30,000 small chemical compounds. The combination of data from all HTS generated tens of interesting hits that need to be further validated. Selected compounds will undergo series of assays to characterize their pharmacokinetic properties, their mode of action, and their regulatory potential in different model systems.

CONTENTS

ABBREVIATIONS

A	**Adenosine**
AGO	**Argonaute**
AMO	**Antagomir**
ATP	**Adenosine triphosphate**
A.U.	**Arbitrary unit**
bp	**Base pair**
BHQ2	**Black Hole Quencher 2**
C	**Cytidine**
CBB-R250	**Coomassie Brilliant Blue-R250**
C. elegans	***Caenorhabditis elegans***
CDS	**Coding sequence**
CHS	**Chalcone synthase**
CLL	**Chronic lymphocytic leukemia**
CMV	**Cytomegalovirus**
Dcr	**Dicer**
DGCR8	**Di George Syndrome critical region gene 8**
DMSO	**Deoxyribonucleic acid**
dpt	**Days post transfection**
dsRNA	**Double-stranded RNA**
dsRBD	**Double-stranded RNA-binding domain**
DUF	**Domain of unknown function**
EC50	**Half maximal effective concentration**
EGFP	**Enhanced green fluorescent protein**
FAM	**Fluorescein**
endo-siRNA	**Endogenous siRNA**
ER	**Endoplasmic reticulum**
ESC	**Embryonic stem cell**
exo-siRNA	**Exogenous small interfering RNA**
FACS	**Fluorescence-activated cell sorting**
FCS	**Fetal calf serum**
FL	**Firefly luciferase**
Fig.	**Figure**
G	**Guanosine**
GA	**Geographic atrophy**
GTP	**Guanosine triphosphate**
HCV	**Hepatitis C virus**

HDI	**Histone deacetylase inhibitor**
HEK293	**Human embryonic kidney 293 cells**
HEL	**Helicase**
HEPES	**4-(2-hydroxyethyl)-1-piperazineethanesulfonic acid**
hpi	**Hours post infection**
hpt	**Hours post transfection**
HRP	**Horseradish peroxidase**
HTS	**High-throughput screening**
IB-RQ	**IowaBlackRQ**
IC50	**Half maximal inhibitory concentration**
IFN	**Interferon**
IMG	**Institute of Molecular Genetics**
IPTG	**Isopropyl β-D-1-thiogalactopyranoside**
IOCB	**Institute of Organic Chemistry and Biochemistry AS CR**
kDa	**KiloDalton**
LB	**Lysogeny broth**
LOPAC	**Library of pharmacologically active compounds**
LNA	**Lock nucleic acid**
MID	**Middle domain**
mRNA	**Messenger RNA**
miRNA	**MicroRNA**
MVB	**Multivesicular body**
NIH	**National institutes of health**
nt	**Nucleotide**
PB	**P-body**
PBS	**Phosphate Buffered Saline**
PABPC	**Poly(A)-binding protein**
PACT	**Protein activator of the interferon induced protein kinase R**
PAGE	**Polyacrylamide gel electrophoresis**
PASHA	**Partner of Drosha**
PAZ	**Piwi/Argonaute/Zwile**
PCR	**Polymerase chain reaction**
PFU	**Plaque-forming unit**
PGK	**Phosphoglycerate kinase 1**
PIWI	**P-element induced wimpy testis in Drosophila**
piRNA	**Piwi-interacting RNAs**
PKR	**Protein kinase R**
PLL	**Polylysine**

PMSF	**Phenylmethanesulfonylfluoride**
pol II	**RNA polymerase II**
pri-miRNA	**Primary miRNA**
pre-miRNA	**Precursor miRNA**
PTGS	**Post-transcriptional gene silencing**
qPCR	**Quantitative PCR**
RdRP	**RNA-dependent RNA polymerase**
RISC	**RNA-induced silencing complex**
RL	***Renilla* luciferase**
RLU	**Relative luciferase unit**
RLC	**RISC-loading complex**
RNA	**Ribonucleic acid**
RNAi	**RNA interference**
RNase	**Ribonuclease**
RPE	**Retinal pigmented epithelium**
RT-PCR	**Real-time PCR**
SAP	**Shrimp Alkaline Phosphatase**
SDS	**Sodium Dodecil Sulphate**
SEM	**Standard error of the mean**
SG	**Stress granule**
SH3	**Src homology region 3**
shRNA	**Small-hairpin RNA**
siRNA	**Small interfering RNA**
S. pombe	***Schizosaccharomyces pombe***
ss RNA	**Single stranded RNA**
SV40	**Simian virus 40**
Tab.	**Table**
TK	**Thymidine kinase**
TPF	**Trypaflavine**
TRAF	**TNF receptor associated factor**
TRBP2	**Human immunodeficiency virus transactivating response RNA-binding protein 2**
U	**Uridine**
UCT	**University of Chemistry and Technology**
UTR	**Untranslated region**
VSR	**Virus-encoded viral suppressor of RNA silencing**
vsRNA	**Virus-derived small RNA**

1 INTRODUCTION

1.1 RNA silencing

1.1.1 History of RNA silencing

1.1.1.1 Discovery of RNA silencing

RNA silencing is a group of pathways utilizing small, 21-30 nucleotide (nt) long RNAs as sequence-specific guides for inhibition of gene expression. This phenomenon was originally reported more than two decades ago as an unexpected outcome of experiments performed in petunias (Napoli et al., 1990). To deepen purple color of petunia flowers, Napoli *et al.* (1990) (Napoli et al., 1990) over-expressed a chalcone synthase (*CHS*) pigment–producing gene. Instead of the petunias with expected deep purple flowers, they obtained plants with less pigmented, fully or partially white petals indicating that expression of both, the transgene and endogenous *CHS* gene, were considerably reduced. Based on this data, Napoli and coworkers introduced an idea that this effect was mediated by RNA and termed the observed phenomenon post-transcriptional gene silencing (PTGS) (Napoli et al., 1990). A similar trans effect was later observed also in other plant species, in *Neurospora crassa* (termed quelling) (Romano and Macino, 1992) and in animals (Guo and Kemphues, 1995). However, the trigger of RNA silencing was still unknown at that time.

1.1.1.2 RNA interference is triggered by dsRNA

The main question in RNA silencing field was which agent was inducing RNA silencing. Before the discovery of RNA interference (RNAi), one approach to eliminate endogenous gene expression was the introduction of an antisense RNA into cells. It was thought that the exogenous antisense RNA hybridizes with endogenous messenger RNA (mRNA) transcripts forming double stranded RNA (dsRNA) molecules that are subsequently targeted for destruction. The first indication that this view is incomplete came from the control experiments of Guo *et al.* (1995) (Guo and Kemphues, 1995), who found that mRNA could be targeted for degradation even by a sense RNA molecule, which does not hybridize with the endogenous transcript. In 1998, Fire and Mello (Fire et al., 1998) investigated the requirements for the structure of the interfering RNA in *Caenorhabditis elegans* (*C. elegans*). Surprisingly, they found that dsRNA was considerably more effective

in gene silencing than either strand individually (Fire et al., 1998) indicating that the unexpected finding of Guo *et al.* (1995) (Guo and Kemphues, 1995) was probably caused by contamination with dsRNA. The demonstration that only a few molecules of injected dsRNA per cell were sufficient for almost complete degradation of endogenous mRNA indicated existence of some catalytic and/or amplification component in the gene silencing process. Fire and Mello named this dsRNA-mediated gene silencing pathway RNA interference (RNAi); they were awarded the Nobel Prize in Physiology or Medicine for their discovery in 2006.

1.1.1.3 siRNAs - the guiding molecules of RNA interference

Two findings led researchers to the hypothesis that RNAi is mediated by a stable silencing intermediate. First, dsRNA injected into one region of a worm or plant caused systemic silencing (Voinnet and Baulcombe, 1997). Second, gene silencing was passed from a parent to its progeny in *C. elegans* (Grishok et al., 2000). The existence of a stable silencing intermediate was first demonstrated in 1999 by Hamilton and Baulcombe (Hamilton and Baulcombe, 1999), who identified an antisense RNA with estimated length of 25 nt (Hamilton and Baulcombe, 1999). One year later, fractionation of *Drosophila* cells extracts was performed and 21-23 nt small interfering RNAs (siRNAs), which co-purified with RNA interference, were identified (Hammond et al., 2000). In 2001, Elbashir *et al.* (Elbashir et al., 2001b) determined the role of these siRNAs as effector molecules in the RNAi pathway. Upon incubation of *Drosophila* cell extracts with chemically synthesized 21–22 nt dsRNAs targeting a firefly luciferase transcript, the siRNAs served as guides mediating the cleavage of target mRNA near the center of a base paired sequence (Elbashir et al., 2001b). Moreover, it was demonstrated that siRNAs with 2–3 nt overhangs on their 3′ ends reduced the amount of target mRNA more effectively than those with blunt ends (Elbashir et al., 2001b). While siRNAs as the effector molecules of RNAi were discovered, enzymes responsible for their production (from long dsRNA) were still unknown at that time.

1.1.1.4 siRNAs are produced from dsRNA by Dicer

Fractionation of *Drosophila* cell extracts revealed that enzymes responsible for the cleavage of dsRNA into siRNAs differ from those involved in the cleavage of the target mRNA. The enzymatic activity producing siRNAs remained in the supernatant, whereas

the activity cleaving the target mRNA (coined as RNA-induced silencing complex - RISC) was pelleted (Bernstein et al., 2001). Since a prototypical bacterial RNase III was known to cleave dsRNA substrate into shorter fragments, Hannon and colleagues (Bernstein et al., 2001) focused on RNase III family members, in an attempt to determine the enzyme responsible for production of siRNAs from a dsRNA substrate. Selected RNase III homologs were immunoprecipitated from Drosophila S2 cells and analyzed for dsRNA cleavage activity capable of yielding the characteristic 21–23 nt siRNAs with 2-3 nt 3' overhangs. It was found that only the type III enzyme encoded by gene CG4792, later named as Dicer had the required activity (Bernstein et al., 2001). After Dicer identification, researches focused on elucidation of the components of the RISC, particularly on the enzyme necessary for the cleavage of target mRNA.

1.1.1.5 Target mRNAs are sliced by Ago2

In 2002, Martinez *et al.* (Martinez et al., 2002) co-immunoprecipitated siRNA-associated protein complexes from HeLa cells and purified them by a size-exclusion chromatography. Two candidate proteins of ~100 kDa corresponding to Argonaute 1 (AGO1) and Argonaute 2 (AGO2) were identified (Martinez et al., 2002). Although Argonaute proteins had been implicated in RNA silencing across several species (Carmell et al., 2002), the evidence of their slicing activity responsible for the cleavage of target mRNAs was missing until 2004 when Song *et al.* (Song et al., 2004) crystallized the Argonaute protein (PfAgo) from archebacterium *Pyrococcus furiosus*. Crystal structures revealed that the so-called Piwi domain shows a notable similarity to the conserved secondary structure of RNase H enzyme. Moreover, similarly to RNase H, the slicer activity was dependent on divalent cations and left 3′OH, and 5′ phosphate termini (Martinez and Tuschl, 2004). In the same year, Hannon and coworkers (Liu et al., 2004) tagged human AGO1–4 proteins by Myc epitope and immunoprecipitated each complex from human 293T cells. They demonstrated that all Argonaute proteins were able to bound siRNAs, but only AGO2 retained the slicer activity (Liu et al., 2004).

So far, many small RNA species, including siRNAs, microRNAs (miRNAs), PIWI-associated RNAs (piRNAs) and others, have been identified and all of them typically interact with one or more members of Argonaute protein family (Ender and Meister, 2010). As indicated above, some Argonaute proteins carry the catalytically active RNaseH-like domain and can cleave the target RNA in the middle of a base paired sequence. Other

Argonaute proteins usually recruit auxiliary factors helping them to silence the target gene by other mechanisms, including translation repression, formation of repressive chromatin, or DNA deletion (Czech and Hannon, 2011; Ketting, 2011). Small RNAs and RNA silencing pathways can be divided according to several criteria. Here, I use the classification based on the requirement of Dicer protein for small RNAs processing. The history of RNAi is summarized in **Fig.1**.

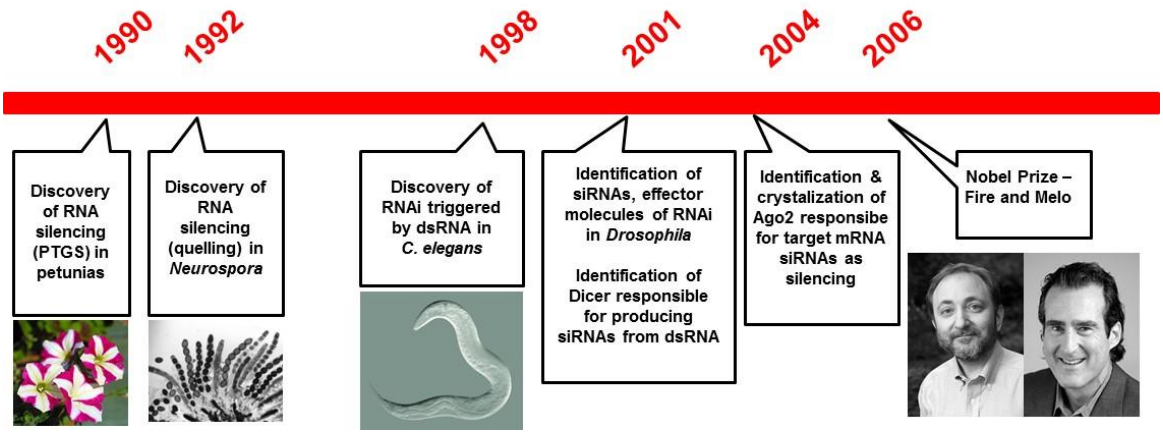

Fig.1: The milestones in the RNAi research

1.1.2 Dicer-dependent pathways

As mentioned above, a number of small RNA species are produced by Dicer (Bernstein et al., 2001). Substrates for Dicer may come from various sources. miRNAs are derived from the genome-encoded hairpins. siRNAs in the RNAi pathway can be processed from a perfectly complementary dsRNA originating from exogenous (exo-siRNAs) or endogenous (endo-siRNAs) sources. Exo-siRNAs can be derived from dsRNA originating, for instance, from viral infection or transfection. In mouse oocytes and *Drosophila melanogaster*, endo-siRNAs can originate from intramolecular long hairpin RNAs or dsRNAs produced by convergent transcription (Czech et al., 2008; Ghildiyal et al., 2008; Okamura et al., 2008; Tam et al., 2008; Watanabe et al., 2008). (**Fig.2A**) In plants, *Schizosaccharomyces pombe (S. pombe)* or *C. elegans*, different types of endo-siRNAs can be produced from dsRNAs synthesized by RNA-dependent RNA polymerases (RdRPs) (Gent et al., 2010; Gent et al., 2009; Grewal, 2010; Pavelec et al., 2009; Voinnet, 2008; Xie

and Qi, 2008) (**Fig.2B**). RNAi and miRNA pathways, the two mammalian Dicer-dependent RNA silencing pathways, are described in more detail in chapters **1.2** and **1.3**.

1.1.3 Dicer-independent pathways

Biogenesis of some small RNA species is Dicer-independent. For example, so-called 22G endo-siRNAs, characterized by the presence of a triphosphate group at 5′ end, are produced directly by the action of RdRP on almost any genomic locus in both germline and soma in *C. elegans* (Aoki et al., 2007; Conine et al., 2010; Gent et al., 2009; Gu et al., 2009b; Pak and Fire, 2007; Sijen et al., 2007) (**Fig.2C**).

The main group of Dicer-independent animal small RNAs are piRNAs. piRNAs interact with PIWI proteins, a subclass of Argonaute protein family (Malone and Hannon, 2009), and are produced in clusters from specific genomic loci. They are 26 – 31 nt long. The 3′ end of piRNAs is 2′-O-methylated by HEN1 enzyme, ensuring an increased stability (Kamminga et al., 2010). Processing of the 5′ end differs according to the mechanism of piRNA biogenesis, and is not yet fully understood.

In *Drosophila* and vertebrates, piRNAs can be generated by two mechanisms (**Fig.2D**): The primary pathway starts with endonucleolytic cleavage of long single stranded RNA (ssRNA) substrate by an unknown nuclease. After the cleavage, piRNAs with uracil at their 5′ end bind one or more PIWI proteins. The primary pathway generates e.g. *Drosophila* piRNAs that can bind PIWI protein (Li et al., 2009; Malone et al., 2009) or mammalian "pachytene" piRNAs located in adult testes. The primary pathway probably precedes the secondary pathway of the piRNA biogenesis, so-called ping-pong pathway that generates predominantly transposon-derived piRNAs. During the ping-pong pathway, piRNAs generated in the primary pathway recognize their complementary targets and cause recruitment of PIWI proteins, mediating the cleavage of transcript in the middle of a base paired region resulting in generating secondary piRNAs (Brennecke et al., 2007; Gunawardane et al., 2007), thus allowing for piRNA amplification.

In *C. elegans*, no ping-pong mechanism equivalent has been found (Batista et al., 2008; Das et al., 2008). 21U RNAs, piRNA-like small RNAs in *C. elegans* (Batista et al., 2008; Das et al., 2008), are distinguished by a consensus motif upstream of their genomic coding sequence (Ruby et al., 2006) (**Fig.2E**). Although the significance of this signal is

not clear, it may represent a transcriptional or RNA processing signal. Like other piRNAs, 21U RNAs are 2´-O-methylated at the 3´ end. The mechanism how 21U RNAs recognize their targets is unclear because, apart from their own locus, no close sequence matches were found in the genome (Batista et al., 2008; Das et al., 2008; Ruby et al., 2006). Nevertheless, the loss of 21U RNAs causes strong defects in spermatogenesis.

piRNAs were suggested to guide RNA silencing through their interaction with PIWI proteins. In mice, PIWI proteins called MIWI, MIWI2 and MILI are essential for spermatogenesis (Thomson and Lin, 2009). Absence of PIWI proteins correlates with an increased expression of transposons. The Piwi-pathway appears involved in both epigenetic and post-transcriptional gene silencing of retrotransposons and other mobile elements in germ cells (Thomson and Lin, 2009).

The next part of the text focuses on two mammalian Dicer-dependent RNA silencing pathways, the canonical RNA interference and the microRNA pathway.

1.2 The canonical RNA interference pathway

Although some authors use the term RNA interference (RNAi) interchangeably with RNA silencing (Ketting, 2011), RNAi was originally defined as a sequence-specific mRNA degradation mediated by small RNAs produced from a long dsRNA. The history of RNAi was described in detail in chapter **1.1.1**. Here, the first section describes the mechanism and the role of RNAi in mammals, while the next section summarizes applications of RNAi in technology.

1.2.1 The mechanism of RNAi in mammals

1.2.1.1 dsRNA recognition and Dicer-mediated cleavage

RNAi is triggered by dsRNA originating from various sources. During the canonical RNAi, a dsRNA molecule is processed into siRNAs by Dicer, a large multidomain protein that belongs to the RNAse III family. Dicer recognizes and efficiently cleaves dsRNA substrates longer than 30 base pairs (bp) with a preference for a 2-nt 3´overhang (Lingel et al., 2003; Ma et al., 2004; Song et al., 2004; Yan et al., 2003), producing small (21 – 23 nt long) RNA duplexes with 2-nt 3´ overhangs, and 5´-monophosphate and 3´-hydroxyl groups at RNA termini. In spite of the preference for dsRNA substrates with 2-nt

overhangs, Dicer is able to cleave also RNA substrates with blunt ends (Provost et al., 2002; Zhang et al., 2002). Although blunt-ended substrates are cleaved predominantly from their termini, an internal RNA duplex cleavage by Dicer also occurs, however with a low frequency (Zhang et al., 2002). Dicer carries two RNAse III domains whose activity depends on magnesium ions (Provost et al., 2002; Zhang et al., 2002). In multicellular eukaryotes, Dicer contains several other domains including the N-terminal DEAD-like (DExD) and helicase superfamily C domains, the Piwi/Argonaute/Zwile (PAZ) domain, the domain of unknown function (DUF283) and the C-terminal dsRNA binding domain (dsRBD) (reviewed in detail in (Jaskiewicz and Filipowicz, 2008; Jinek and Doudna, 2009; Wilson and Doudna, 2013)).

The current view of the Dicer architecture (**Fig.3A**) was established based on the crystal structure of the full-length Dicer from *Giardia intestinalis* complemented by electron microscopy analysis of human Dicer (Lau et al., 2012; MacRae et al., 2007; Macrae et al., 2006). Dicer has an L-shaped structure consisting of a head, a body, and a base (Lau et al., 2012; Sashital and Doudna, 2010). The top of the molecule, the Dicer´s head, is formed by a PAZ domain. The PAZ domain recognizes and binds the end of dsRNA substrate with a high affinity for 3´ protruding overhangs (Lingel et al., 2003; Ma et al., 2004; Song et al., 2004; Yan et al., 2003). The DUF283 domain, tightly associated with the PAZ domain, has a dsRBD-like fold (Dlakic, 2006) and might mediate protein-protein interactions (Qin et al., 2010). The DUF293 domain is also a part of a "platform" domain supporting a "connector" α helix that joins the PAZ domain with the RNAse III catalytic site of Dicer. Thus, Dicer functions as a molecular ruler, measuring the product length as a distance between the PAZ domain and the RNase III domains. Upon the recognition of dsRNA by the PAZ, Dicer cleaves the substrate ~21-23 bps (in mammals) from the open helical end and produces the short interference RNA duplex, with 2-nt overhangs at the 3´ ends (reviewed in (Jinek and Doudna, 2009; Wilson and Doudna, 2013)). Variations in product lengths across species are reflecting the length of non-conserved connector helix. The cleavage of dsRNA is mediated by two RNase III domains, RNase IIIa and RNase IIIb, located in the Dicer´s body. In contrast to prokaryotic RNase III domains, which form a homodimer, the RNase III domains of Dicer form an intramolecular dimer (Zhang et al., 2004).

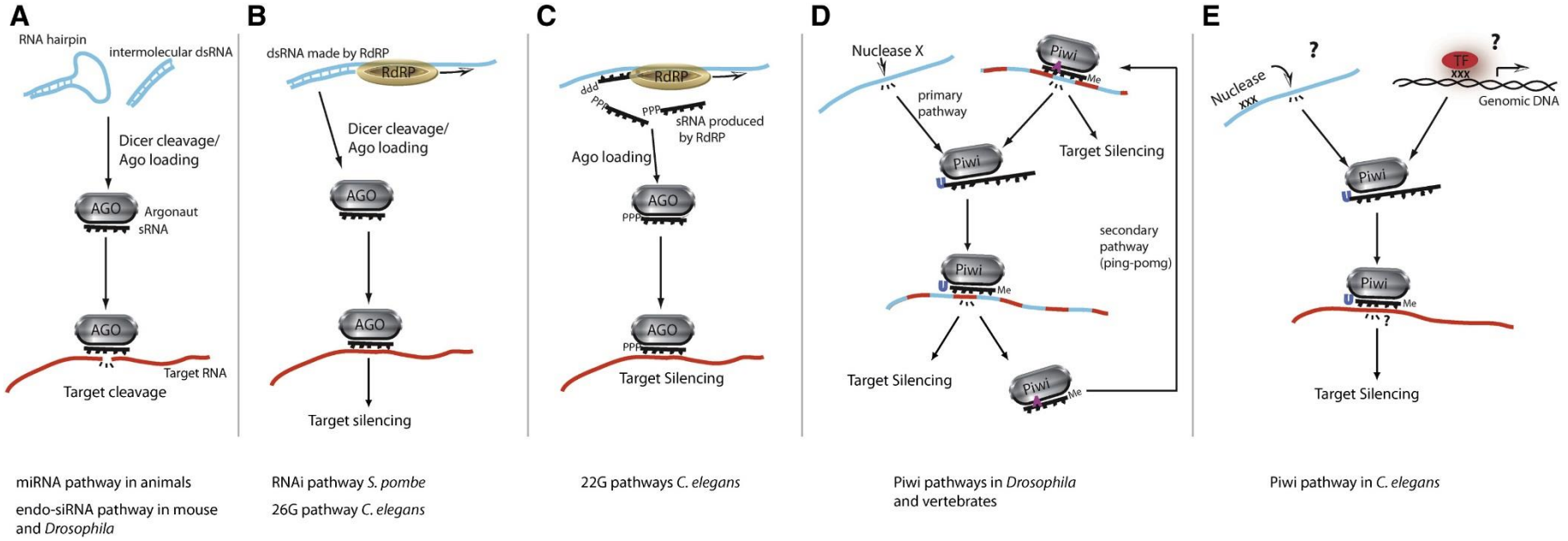

Fig.2*: RNA silencing pathways: A, A ‘‘canonical’’ RNAi pathway (e.g. the endo-siRNA pathways in *Drosophila* and mammals). In both systems, AGO2 is most likely the AGO protein involved. **B,** In *S. pombe* and in *C. elegans*, dsRNA can be generated by RNA-directed RNA polymerase (RdRP). **C,** In *C. elegans*, RdRP enzymes can also directly generate short RNAs that are bound by AGO proteins. The AGO proteins accepting this type of small RNA do not appear to direct target RNA cleavage but do result in a drop in RNA target levels. **D,** A model of piRNA biogenesis and function. ssRNA serves as a source of small RNA and cleavage by either PIWI proteins or an unknown nuclease generates the 5′ ends of the small RNAs. Primary piRNAs carry a 5′-uracil residue, whereas secondary piRNAs either have a 5′-uracil or an adenosine at position 10, due to the cleavage characteristics of AGO proteins. The processing of the 3′ end is poorly understood but is finalized by methylation of the 2′OH group of the last nucleotide. PIWI proteins can cleave their targets, but whether this is required for their silencing activity is not well known. Note that it is difficult to separate target RNA molecules from piRNA substrates, due to the cyclic nature of the process. **E,** Potential models of how piRNAs are generated in *C. elegans* (21U RNAs). A motif (represented as ‘‘xxx’’) is found upstream of 21U RNAs. This motif may function as an RNA processing signal or as a transcriptional signal. Processing of the 3′ end likely resembles the other Piwi pathways. Not much is known about how 21U RNAs silence their targets, but at least in some cases, an RdRP appears to be recruited, triggering the pathway depicted in **C**. Substrate RNAs – depicted in blue, sRNAs - depicted in black, target RNA - depicted in red.***Fig 2** is taken from Ketting , 2011 (Ketting, 2011)

In Dicer, both RNase III domains form a single processing center, in which each domain is responsible for the cleavage of one strand of the substrate (Zhang et al., 2004). The catalytic site of each RNase III domain is formed by four conserved acidic amino-acid residues, which coordinate two metal cations. This suggests that Dicer uses a two-metal-ion mechanism to catalyze the RNA cleavage (Ji, 2008). As mentioned above, although Dicer preferentially cleaves dsRNA substrates from their termini, it is also able to cleave internally, however with a lower efficiency (Zhang et al., 2002). The mechanism of Dicer activity is depicted in **Fig.3B** and recently reviewed for instance in (Ha and Kim, 2014; Wilson and Doudna, 2013).

The fact that most Dicer enzymes carry a DExD helicase domain suggests that it might be involved in the ATP-dependent binding and the remodeling of nucleic acids. It has been shown that *Drosophila* Dicer-2 needs ATP for processive dicing, however, mammalian Dicer does not (Nykanen et al., 2001; Provost et al., 2002; Zhang et al., 2002). Interestingly, the kinetic analysis of mammalian Dicer mutants indicated that the rate of substrate cleavage is attenuated by the Dicer helicase domain (Ma et al., 2008). Deletion of the helicase domain increased the activity of human Dicer up to 65-fold when compared to the intact enzyme (Ma et al., 2008). It was suggested that the helicase domain inhibits the Dicer activity via intramolecular interaction. The inhibitory effect is attenuated by the physical interaction of the helicase domain with other proteins, such as TRBP2 (human immunodeficiency virus transactivating response RNA-binding protein 2). (Ma et al., 2008). TRBP2 binding stimulates the cleavage of various dsRNA substrates by ~5-fold (under multiple-turnover conditions), presumably through the stabilization of Dicer-substrate complexes (Chakravarthy et al., 2010). Recently, electron microscopy analysis of human Dicer provided additional information on the structure of the helicase domain. According to Lau *et al.* (2012), N-terminal helicase domain is situated at the base of Dicer and is composed of three predicted globular subdomains (Lau et al., 2012) (**Fig.3C**). The helicase subdomains form a clamp-shaped structure, which might facilitate recognition or selection Dicer substrates by dsRBD located near the catalytic site (Lau et al., 2012). Architecture and mechanism of Dicer cleavage is demonstrated in **Fig.3**.

Various organisms employ Dicer paralogs with distinct functions and different product lengths. For instance, *Drosophila* Dcr-1 produces miRNAs, while Dcr-2 produces siRNAs (Lee et al., 2004c). Interestingly, four Dicer paralogs were described in

Arabidopsis thaliana (reviewed in (Meins et al., 2005)). In contrast, only a single Dicer is used for the production of both siRNAs and miRNAs in mammals, *C. elegans*, and *Trypanosoma*.

Several protein factors interact with Dicer and facilitate dsRNA recognition and cleavage. In mammals, TRBP is one of two main Dicer-interacting partners. TRBP carries three dsRBDs and was shown to be involved in the miRNA processing and RISC loading (Haase et al., 2005; Chendrimada et al., 2005). It was demonstrated that the complex of TRBP and Dicer associates with AGO2 and recruits it to the siRNA. The TRBP knock-down resulted in destabilization of Dicer and subsequent inhibition of miRNA biogenesis (Chendrimada et al., 2005). However, it is not clear whether TRBP plays a role in the recognition and processing of long dsRNA in canonical RNAi *in vivo* in mammals. Another Dicer interacting partner is a TRBP paralog called PACT (a protein activator of the interferon induced protein kinase R). PACT is able to interact with both Dicer and TRBP and may facilitate the siRNA production (Kok et al., 2007).

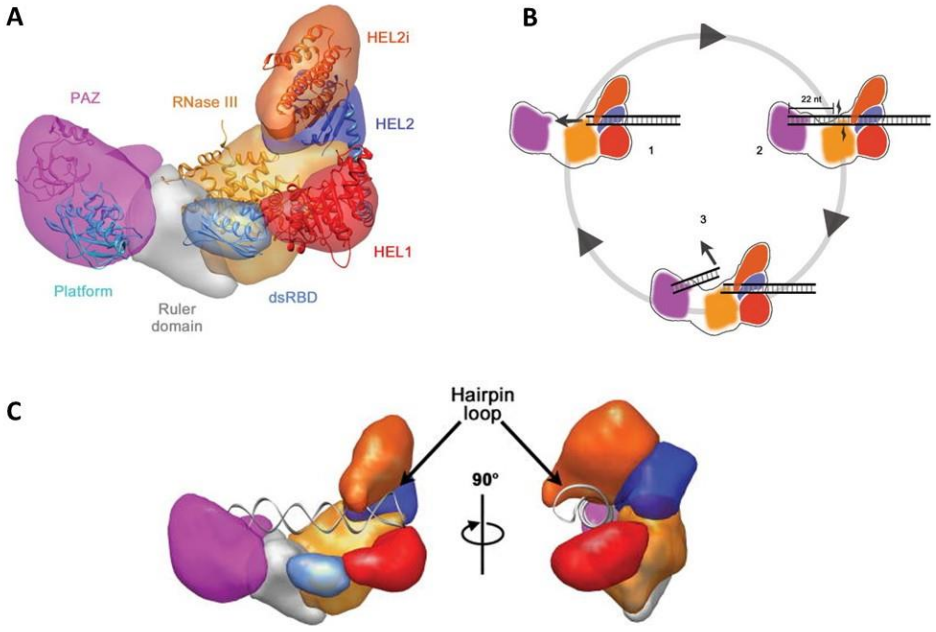

Fig.3*: Architecture and mechanism of Dicer: A Segmented map of human Dicer with crystal structures of homologous domains docked. **B,** Scheme of processive dicing: (1) The helicase translocates dsRNA into the nuclease core. (2) The PAZ domain (purple) recognizes the dsRNA end, positioning RNase III (orange) for cleavage. (3) The siRNA product is released while the dsRNA substrate remains bound to the helicase. **C,** Model for pre-miRNA recognition. A pre-miRNA hairpin is modeled into the proposed binding channel of Dicer with the stem loop fit in the RNA-binding cleft of the helicase. * Fig.3 is taken from Lau *et al.* (2012) (Lau et al., 2012)

1.2.1.2 Argonaute proteins and RISC loading

After dicing, the small RNA duplex is loaded onto effector "RNA-induced silencing complex" (RISC) containing AGO protein. This active process is called the RISC assembly and requires ATP (reviewed in (Ha and Kim, 2014)). Notably, all four human AGO proteins (AGO1-AGO4) can incorporate both, siRNA and miRNA. In miRNA pathway, the effector complex is called miRISC (miRNA-induced silencing complex). AGO protein in the (mi)RISC binds a small RNA strand and uses it as a sequence-specific guide for the recognition of the target mRNA. Some AGO proteins serve as so-called slicers – enzymes catalyzing the endonucleolytic cleavage of target mRNAs, typically in the canonical RNAi pathway (Liu et al., 2004; Meister et al., 2004; Song et al., 2004). After the formation of a perfect siRNA-mRNA duplex, slicing-competent AGO protein cleaves the cognate mRNA in the middle of the base paired sequence. Although only mammalian AGO2 is capable of the cleavage (Liu et al., 2004; Meister et al., 2004; Song et al., 2004), all four mammalian AGO proteins are able to interact with the translation machinery and/or mRNA the decay factors and induce translational repression and subsequent decay of the target mRNA.

The resolution of the crystal structure of eukaryotic (human and yeast) AGO protein (~100 kDa) in complex with a guide strand of small RNA revealed a bilobal architecture composed of an N-terminal lobe comprising of N-terminal domain and the PAZ domain and C-terminal lobe with the middle (MID) domain and the PIWI domain (reviewed in (Ha and Kim, 2014)). As in Dicer, the PAZ domain of AGO protein recognizes and binds 3′-protruding ends of small RNAs in a sequence-independent manner (Lingel et al., 2003; Ma et al., 2004). While the 3′ end of a guide RNA is anchored in the PAZ domain, the 5′ monophosphate is tightly bound in a pocket between MID and PIWI domains (reviewed in (Ha and Kim, 2014; Jinek and Doudna, 2009)). A target mRNA is positioned within AGO protein as follows: the 5′ end of the mRNA enters between the N-terminal and the PAZ domain and its 3′ end exits the AGO protein between the PAZ and the MID domains. The PIWI domain has an RNase H-like fold, which is responsible for slicing of target mRNA between nucleotide positions 10 and 11 opposite of the guide, relative to the 5′end of the guide RNA (Ma et al., 2005; Song et al., 2004; Yuan et al., 2005), and reviewed in (Kunne et al., 2014). The architecture and mechanism of AGO protein is shown in **Fig.4**.

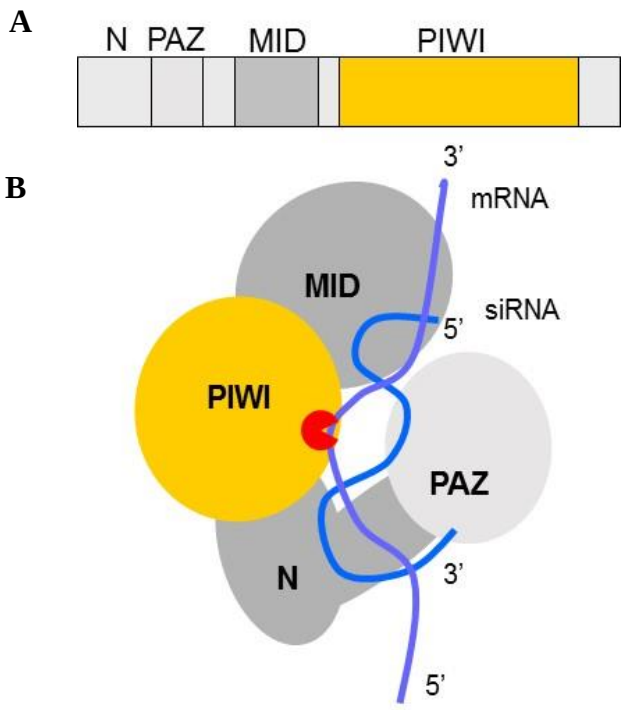

Fig.4: Structure and mode of action of Argonaute protein. A Domains in open reading frames. **B**, The scheme of structural organization depicting roles of both proteins in RNAi. Red "pacman" indicates position of the endonucleolytic activity.

Early studies indicated that Dicer, AGO and TRBP proteins compose the so-called RISC loading complex (RLC) and participate on the RISC loading and strand selection (Gregory et al., 2005; Haase et al., 2005; Chendrimada et al., 2005; MacRae et al., 2008; Martinez et al., 2002). In RLC, TRBP is flexibly bound to the Dicer´s DExH/D domain and assists the release of the RNA duplex by Dicer and its loading on AGO protein (Daniels et al., 2009; Wang et al., 2009a). Moreover, results of several *in vitro* experiments support the hypothesis that in humans, the RISC loading may be coupled to the Dicer-dependent pre-miRNA processing. First, recombinant Dicer-TRBP complex was shown to be able to bind siRNA duplexes *in vitro* (Gredell et al., 2010; Noland et al., 2011). Second, RLC has both target cleavage and pre-miRNA processing activity *in vitro* (Liu et al., 2012). Despite these findings, the detailed composition of the mammalian RLC is still being investigated. Moreover, it has been suggested that Dicer is not required for asymmetric RISC assembly *in vitro* and in cells (Betancur and Tomari, 2012; Kawamata et al., 2009), supporting the idea that in mammals, the RLC is dispensable for small RNA loading onto AGO proteins (reviewed in (Ha and Kim, 2014)).

Each siRNA duplex is comprised from so-called passenger strand, which is degraded and the guide strand, which is incorporated into the RISC. After the small RNA duplex loading, AGO proteins associated with RNA duplexes remove the passenger strand and

generate a mature RISC, independently of ATP. The removal of the passenger strand from the duplex occurs by two different mechanisms. In the case when the RNA duplex is formed at the center and the human RISC contains AGO2, the passenger strand can be sliced by AGO2 (Kim et al., 2007; Matranga et al., 2005; Miyoshi et al., 2005) and subsequently removed using endonuclease C3PO (reviewed in (Ha and Kim, 2014)). When the RNA duplex has central mismatches or RISC carries human AGO1, AGO3 or AGO4, mismatches in the guide strand promote the unwinding of the miRNA duplexes without a previous cleavage. This is typical for miRNA pathway (reviewed in (Ha and Kim, 2014)). Which strand of the miRNA or siRNA duplex is selected as a guide strand, depends on its thermodynamic stability. There are two determinants for the strand selection. First, the strand with a less stable base pairing at the 5' end typically becomes a guide strand, whereas the remaining passenger or star (*) strand is quickly degraded (Khvorova et al., 2003; Schwarz et al., 2003). Second, the strand with U at the first position is preferentially selected by AGO proteins as a guide strand (reviewed in (Ha and Kim, 2014)). Both TRBP (Wang et al., 2009a) and the helicase domain of human Dicer (Noland et al., 2011) were suggested to act as a sensor(s) of the thermodynamic stability of 5´ small RNA in the strand selection during the RISC assembly.

1.2.1.3 Target recognition and cleavage

RISC recognizes the target mRNA based on its complementarity with the guide small RNA. Although siRNAs typically perfectly base pair with their targets, there is a distinct 5´ bias towards the target recognition. It was demonstrated that the 5´ half of small RNA provides the majority of the binding energy between the RISC complex and the target mRNA (Doench et al., 2003; Haley and Zamore, 2004), thus creating a thermodynamic threshold for a stable association (Ameres et al., 2007). Biochemical analysis of target recognition revealed that in mammals, the (mi)RISC neither scans transcripts systematically nor is able to unfold a structured RNA. Instead, it seems that the RISC randomly and transiently contacts ssRNA and promotes siRNA-mRNA base pairing (Ameres et al., 2007; Rana, 2007), and reviewed in (Stroynowska-Czerwinska et al., 2014).

Two models for the target recognition and AGO2-mediated cleavage have been proposed: (i) According to the fixed-end model, both ends of the guide RNA remain bound to the AGO protein during slicing (Wang et al., 2009b). (ii) According to the two-state model (Tomari and Zamore, 2005), the 3´ end of the siRNA is bound by the PAZ domain

and the 5′ end of the siRNA is wedged in the pocket between the MID and the PIWI domains. First, the 5′ end of siRNA interacts with the cognate mRNA, and subsequently the 3′ end is released from the PAZ domain to enable full base pairing. The base pairing in the middle of the siRNA results in the correct orientation of mRNA to the active site and its cleavage (Tomari and Zamore, 2005; Wang et al., 2009b), and reviewed in (Kunne et al., 2014). The siRNA can affect the gene expression not only by AGO2-mediated mRNA cleavage. In case of imperfect complementarity between siRNA and cognate mRNA, siRNA can promote the translational repression and the mRNA decay typical for miRNAs (Doench et al., 2003) (see chapter **1.3**). Schematic overview of the mammalian RNAi and miRNA pathways is demonstrated in **Fig.5**.

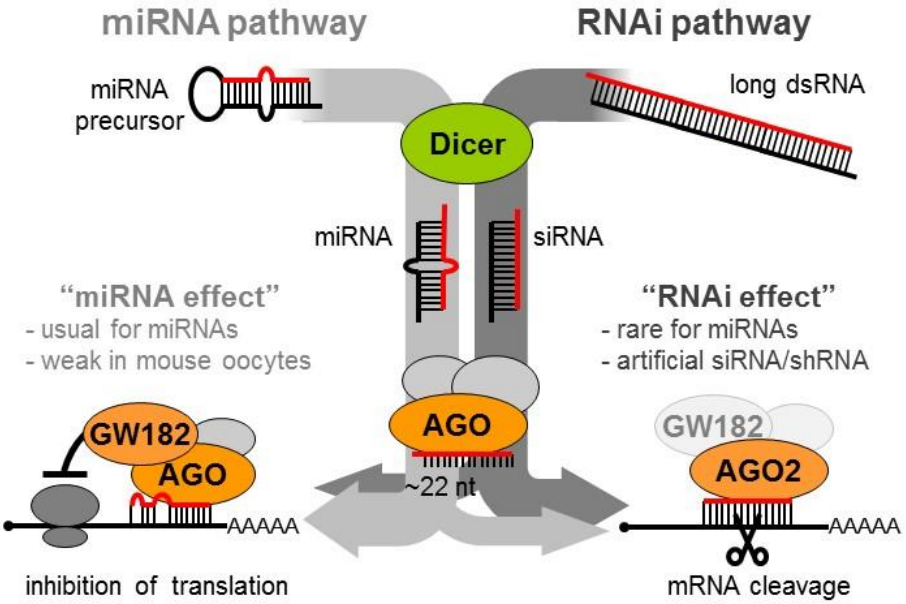

Fig.5*: Overview of mammalian RNAi and miRNA pathways*: In somatic cell, miRNAs are the most abundant and functionally dominant small RNA class. During the miRNA biogenesis, RNase III Dicer cleaves small hairpin precursors (pre-miRNAs) and produces 21–23 nt long miRNAs loaded on the RNA-induced silencing complex (RISC). The RNAi pathway shares protein components with the miRNA pathway. RNAi employs 22 nt long small interfering RNAs (siRNA) produced by Dicer from long dsRNA. The key component of RISC is the AGO protein from the Argonaute protein family. Mammals have four AGO proteins (AGO1–4). All AGO proteins bind miRNAs and siRNAs. AGO1, AGO3, and AGO4 induce a translational repression. Only AGO2 is capable of endonucleolytic cleavage of cognate RNAs, which is the hallmark of RNAi. miRNAs loaded on AGO2 can induce the endonucleolytic cleavage upon the perfect base pairing with targets. However, a typical miRNA binding is imperfect and results in translational repression. miRNAs function as gene-specific inhibitors and miRNA networks provide a combinatorial system of post-transcriptional control of gene expression. The experimental gene knock-down in mammalian cells relies on short RNAs – typically synthetic siRNAs or expressed miRNA-like molecules. *Fig.5 is modified according to Svoboda, 2014 (Svoboda, 2014).

1.2.1.4 Endogenous RNAi in mammals

In mammalian somatic cells, RNAi is poorly induced by long dsRNA, and, according to the next generation sequencing data, the putative endo-siRNA are not abundant. One reason is that RNAi effects in mammalian somatic cells are masked by interferon (IFN) pathway responding to dsRNA in a sequence-independent manner (reviewed in (Sidahmed et al., 2014)). Interestingly, ubiquitous expression of long dsRNA in a transgenic mouse does not induce neither the IFN response, nor robust RNAi effect, and the data from next generation sequencing of small RNAs from tissues expressing dsRNA indicate poor processing of dsRNA into siRNAs (Nejepinska et al., 2012). Although the RNAi in the somatic cells seems to be inefficient, according to several reports RNAi may become rarely functional even in somatic cells (reviewed in (Svoboda, 2014)).

In contrast to somatic cells, in mouse oocytes, in which the IFN pathway is not functional, RNAi can be induced with the microinjected as well as the expressed long dsRNA (Svoboda et al., 2000; Wianny and Zernicka-Goetz, 2000). The loss of Dicer or AGO2 in oocytes results in the meiotic spindle defect indicating the necessity of endo-siRNAs for normal meiotic maturation (Kaneda et al., 2009; Ma et al., 2010; Tang et al., 2007). Recently, high levels of a unique N-terminally truncated Dicer isoform (denoted Dicer^{O}), whose expression is driven by an intronic MT-C retrotransposon promoter, has been reported to be expressed in mouse and rat oocytes (Flemr et al., 2013). **(Fig.6)**. Consistent with a previously reported autoinhibitory function of the N-terminal helicase domain of human Dicer (Ma et al., 2008), Dicer^{O} isoform lacking the DExD helicase domain shows a higher cleavage activity *in vitro* than the full-length Dicer in somatic cells. Moreover, level of endo-siRNAs is increased by the ectopic expression of Dicer^{O} in somatic cells (Flemr et al., 2013). Deletion of an intronic MT-C retrotransposon promoter causes the loss of Dicer^{O} and female sterility. Interestingly, oocytes lacking the MT-C element show meiotic spindle defects, thus phenocopying the maternal Dicer-null phenotype (Flemr et al., 2013).

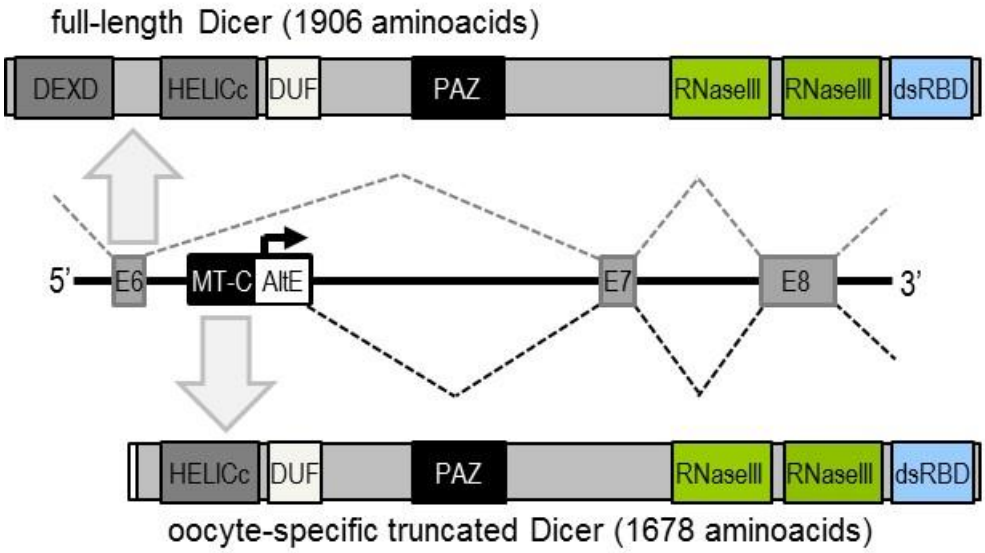

Fig.6*: Schemes of somatic and oocyte-specific Dicer isoforms: Endogenous siRNAs derived from repetitive sequences and processed pseudogenes occur in mouse oocytes because of a unique Dicer isoform adapted for effective processing of long dsRNAs. *Fig.6 is completely adopted from Svoboda, 2014 (Svoboda, 2014).

1.2.1.5 Antiviral RNAi in mammals

Various antiviral systems protect all living organisms from viral infections. In plants (Hamilton and Baulcombe, 1999) and invertebrates (Felix et al., 2011; Lu et al., 2005) and reviewed in (Sidahmed et al., 2014; Svoboda, 2014), RNAi functions as a form of an innate immunity responding to dsRNA that is frequently produced during viral infection. Several concurrent observations demonstrate the antiviral role of RNAi in invertebrates. First, inhibition of RNAi results in the increased viral replication. Next, both virus-encoded viral suppressors of RNA silencing (VSRs) and siRNA derived from viral sequences were found in infected individuals.

In mammals the existence of a natural antiviral RNAi response is discussed for several reasons (reviewed in (Cullen, 2006; Sidahmed et al., 2014; Svoboda, 2014)). First, viral dsRNA triggers the efficient and nonspecific IFN response in the majority of mammalian somatic cells (Goubau et al., 2013). Second, virus-derived small RNAs (vsRNAs) accumulate in various virus-infected mammalian cell types, nevertheless they have unspecified functions and in most cases they are not similar to plant and invertebrate viral siRNAs in terms of biochemical features, size, and distribution patterns (Aliyari et al., 2008). Finally, several mammalian viral proteins display viral suppressor of RNAi (VSR)-like activities. (Haasnoot et al., 2007). Taken together, although there is some evidence for

antiviral RNAi in mammals, the observations described in invertebrates do not occur concurrently under physiological conditions or they are often interpreted alternatively. In spite of the aforementioned facts, there are several studies indicating a possible role of RNAi in controlling viral infections in mammalian cells, and virus-derived endo-siRNAs were reported in mammals (Li et al., 2013; Maillard et al., 2013). Moreover, it was demonstrated that mutations in the RNAi machinery components improve the replication of several viruses in mammalian cells (reviewed in (Li et al., 2013; Maillard et al., 2013; Sidahmed et al., 2014; Svoboda, 2014)).

1.2.2 RNAi technology in mammals

RNAi technology became a powerful experimental tool for addressing fundamental questions in experimental biology and biotechnology, as well as a potential therapeutic strategy. It capitalizes on the fact that transfection of mammalian cells with *in vitro* synthesized siRNAs, which are too short for the activation of the IFN response, induces a robust and specific RNAi in somatic cells (Elbashir et al., 2001a). RNAi is a specific, potent, and highly successful approach for loss-of-function studies in almost all eukaryotic organisms. The RNAi effect is typically achieved by synthetic siRNAs designed to target the gene of interest. However, synthetic siRNAs have limits as their effect is transient, depends on their efficient delivery, and their synthesis is relatively costly. Some of these issues are addressed by vectors expressing shRNAs, which can be delivered transiently or stably integrated in cell lines or animals (Fewell and Schmitt, 2006 126). There are two main classes of vectors for RNAi. The class I hairpins use a covalent connection of siRNA strands with a small loop (Brummelkamp et al., 2002b; McManus et al., 2002; Paddison et al., 2002; van de Wetering et al., 2003). They are typically expressed by RNA polymerase III, which limits their potential use for tissue-specific RNAi. The class II hairpins mimic endogenous miRNA precursors. The siRNA sequence is placed into a pri-miRNA-like transcript that is processed like an endogenous miRNA (Zeng et al., 2002). The class II hairpins are typically expressed by RNA polymerase II (pol II), which makes them more suitable for tissue-specific transgenic RNAi in mammals.

The gene knock-down by RNAi is used similarly to the conventional knock-out to study the function of genes in cell culture and *in vivo*. Generation of transgenic mice with the RNAi-mediated knock-down has some advantages as well as limitations when

compared to producing a knock-out mice. On one hand, it is faster, simpler and, less expensive. On the other hand, the RNAi-mediated knock-down of the target gene is usually not complete and its efficiency differs in various cell types (Dickins et al., 2007; Hasuwa et al., 2002; Peng et al., 2006).

Transgenic RNAi knock-down mice can be produced using different strategies. The most common strategy is an injection of linear DNA fragment into the 1-cell pronucleus, which results in a random integration of concatemers of transgenes. This leads to a high variability in expression levels and a certain risk of site-specific insertion effects (Hasuwa et al., 2002). Another strategy is an introduction of shRNA-expressing vector into mouse embryonic stem cells (ESCs) by electroporation (Carmell et al., 2003; Kunath et al., 2003) or lentiviral infection (Rubinson et al., 2003) and a subsequent injection of selected ESC clones into blastocysts, producing chimeric transgenic animals. The problem with mosaicism overcomes the so-called tetraploid aggregation, an alternative way of producing animals from ESCs (Kunath et al., 2003; Lickert et al., 2004; Nagy et al., 1993). A number of viral systems including retroviral (Brummelkamp et al., 2002a; Hemann et al., 2003), adeno-associated (Boden et al., 2004) and lentiviral vectors have been used for transgenic RNAi (Rubinson et al., 2003; Stewart et al., 2003; Tiscornia et al., 2003). These systems differ in (terms of) transgene integration sites and copy numbers (reviewed in (Podolska and Svoboda, 2011)). Analysis of the gene function *in vivo* can be facilitated by the spatiotemporal control of RNAi, which can be achieved using: (i) a tissue-specific promoter to express a class II hairpin, (ii) a drug-inducible promoter (Dickins et al., 2007; Gupta et al., 2004; Wang et al., 2003) or (iii) the Cre-loxP system, which can be utilized for both conditional activation (Cre-ON) and inactivation (Cre-OFF) of RNAi in an irreversible manner (Coumoul et al., 2004; Dickins et al., 2007; Kasim et al., 2004; Tiscornia et al., 2003; Ventura et al., 2004).

RNAi *in vivo* has already been achieved in different invertebrate model organisms (Ambros et al., 2003; Amdam et al., 2006; Bucher et al., 2002; Fire et al., 1998; Lohmann et al., 1999; Newmark et al., 2003; Orii et al., 2003; Timmons and Fire, 1998), and so far, many siRNA delivery systems have been already tested also in living mammals. Unlike the majority of invertebrate model organisms, mammals do not have the systemic RNAi, so the RNAi approach must rely on the efficient delivery of either synthetic siRNAs or shRNA-expressing plasmids into targeted cells or tissues. First, high levels of plasmid

expression in visceral organs, mostly liver, were achieved by high-pressure tail vein injection (hydrodynamic transfection) (Liu et al., 1999; Zhang et al., 1999b), which was used to deliver siRNAs or shRNA-expressing vectors into adult mice (Giladi et al., 2003; Lewis et al., 2002; McCaffrey et al., 2002; McCaffrey et al., 2003; Song et al., 2003). This invasive method is highly effective only in liver, and induced RNAi effect is transient (Lewis et al., 2002). Next, different non-viral (Gao and Huang, 2009) and adenovirus-based methods were developed to deliver siRNAs or shRNA-expressing vectors into the particular tissues (Ge et al., 2004). Several groups reported efficient knock-down of endogenous genes in some mammalian organs using a local injection, a nasal instillation, oral delivery (Aouadi et al., 2009; Kong et al., 2004; Massaro et al., 2004; Salahpour et al., 2007) or an electroporation (Akaneya et al., 2005; Golzio et al., 2005; Kishida et al., 2004; Kong et al., 2004; Konishi et al., 2004; Matsuda and Cepko, 2004; Paganin-Gioanni et al., 2008). Overview of the current status of the RNAi-induced gene silencing in living mammals is depicted in **Fig.7**.

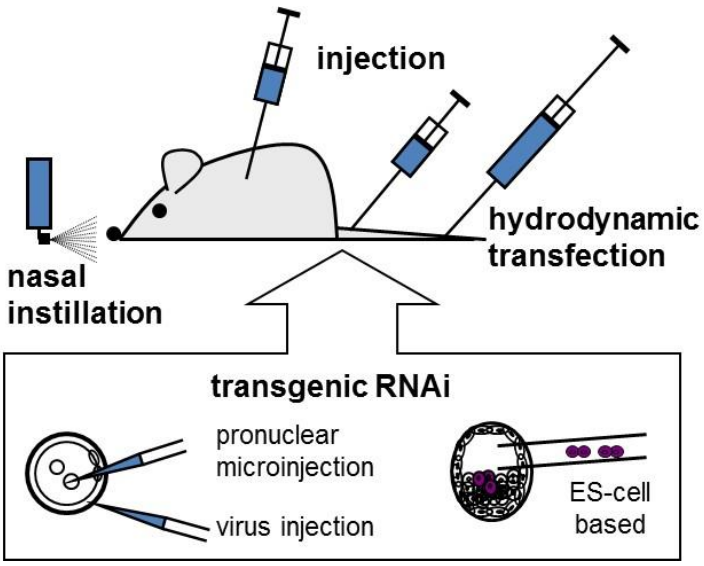

Fig.7*: Schematic depiction of strategies for the RNAi-induced gene silencing in living mammals. RNAi in animals can be induced from a transgene. Transgenic animals are usually produced by one of the three depicted strategies. Different strategies for delivering an RNAi agent (e.g. siRNA- or shRNA-expressing vector) are available to induce RNAi in adult animals. Delivery methods include hydrodynamic transfection, injection into a specific location/tissue, or nasal instillation. *Fig.7 was completely adopted from Podolska *et al.* (2011) (Podolska and Svoboda, 2011)

1.3 Mammalian microRNA pathway

The dominant mammalian RNA silencing pathway is the microRNA pathway. miRNAs participate in almost every cellular process including apoptosis, proliferation and differentiation, and their expression is altered in many diseases, including cancer (Ambros, 2004; Bartel, 2004; Filipowicz et al., 2008).

1.3.1 History of microRNA pathway research

The first miRNA called *lin-4* was discovered by Victor Ambros and Gary Ruvkun groups two decades ago (Bartel, 2004; Lee et al., 1993). *Lin-4* is one of heterochronic genes that control temporal developmental pattern in all larval stages of *C. elegans* (Horvitz and Sulston, 1980; Chalfie et al., 1981). In 1987, Ferguson *et al.* demonstrated that the suppressor mutation of *lin-14* reverts a *lin-4* loss-of-function phenotype (Ferguson et al., 1987). Moreover, the *lin-14* null mutation caused the opposite phenotype of the *lin-4* null mutation (Chalfie et al., 1981; Lee et al., 2004a) indicating that *lin-4* negatively regulates *lin-14* (Lee et al., 2004a). Two years later, Ambros group succeeded in cloning the genomic fragment containing the *lin-4* gene. As neither the start nor the stop codons were found in this region, and mutations introduced into the putative ORF did not affect the *lin-4* function, it became apparent that *lin-4* did not encode a protein (Lee et al., 2004a; Lee et al., 1993). Instead, two small RNAs (66 nt and 22 nt long) were found to be generated from the *lin-4* locus. At the same time, Ruvkun group found that *lin-14* is downregulated post-transcriptionally (Wightman et al., 1993). In 1992, both groups came independently to the same conclusion that *lin-4* transcripts are partially complementary to the 3′UTR of *lin-14* gene and that the small noncoding *lin-4* transcripts negatively regulate *lin-14* through its 3′UTR region (Lee et al., 2004a; Lee et al., 1993; Wightman et al., 1993).

Because *lin-4* is expressed only in *C. elegans*, the widespread prevalence and functional importance of miRNA-dependent gene regulation was first emphasized in *let-7*, which is conserved from worms to human. Similarly to *lin-4*, *let-7* controls temporal transitions during development (Pasquinelli et al., 2000; Reinhart et al., 2000). The discovery of *let-7* in *C. elegans* started a revolution in research of miRNAs. In humans, let-7 was detected at different expression levels in the majority of tissues (Pasquinelli et al., 2000). The latest release (June 2014) of the miRNA database (miRBase) has catalogued

2588 mature miRNAs in humans (http://www.mirbase.org/). These miRNAs potentially regulate over 60% of human protein-coding genes (Friedman et al., 2009).

1.3.2 The mechanism of canonical microRNA pathway in mammals

1.3.2.1 miRNA biogenesis

miRNAs are genome-encoded and have defined sequences. miRNA genes are typically located in the non-coding genomic regions or in the intronic regions of protein-coding genes (reviewed in (Ha and Kim, 2014)). miRNAs are typically transcribed by RNA polymerase II (pol II) as primary miRNAs (pri-miRNAs) carrying local hairpin structures containing the mature miRNA sequence(Cai et al., 2004; Lee et al., 2004b). Like other pol II transcripts, pri-miRNAs carry the 5′ cap and the 3′ poly-A-tail (Cai et al., 2004). Pri-miRNA transcription is regulated by pol II transcription factors and by epigenetic changes, such as DNA methylation or histone modifications (Ha and Kim, 2014). miRNA genes may reside in the genome as single transcription units, but often miRNAs clustered, so that one pri-miRNA transcript carries several local hairpin structures and can be processed into several functional miRNAs (Rodriguez et al., 2004). Although a vast majority of miRNAs is transcribed by pol II, some viral miRNAs are transcribed by RNA polymerase III (Pfeffer et al., 2005).

Pri-miRNAs are further processed by the nuclear Microprocessor complex containing RNase III Drosha and a dsRNA-binding protein DGCR8 (Di George Syndrome critical region gene 8), also known as PASHA (partner of Drosha) in invertebrates (Denli et al., 2004; Gregory et al., 2004; Landthaler et al., 2004; Lee et al., 2003) and reviewed in (Ha and Kim, 2014). Drosha processes pri-miRNA transcripts into relatively short (70–100 bp long) hairpin precursor miRNAs (pre-miRNAs) with phosphorylated 5′ ends and 3′ dinucleotide overhangs (Lee et al., 2003). Drosha is a multidomain nuclear protein that belongs to the family of RNase III-type endonucleases. The N-terminal part of Drosha is rich in prolin, arginine and serine and is necessary for nuclear localization in cells. The C-terminal part of Drosha is formed by tandem RNase III domains and the dsRNA-binding domain (dsRBD). The middle region of Drosha mediates the interaction with DGCR8 (reviewed in (Ha and Kim, 2014)). Although the purified Drosha is capable of a non-specific dsRNA cleavage *in vitro, in vivo* cleavage specificity of hairpins is determined by DGCR8, which presumably binds to the base of the pri-miRNA stem loop and guides

Drosha to the substrate (Han et al., 2006). Drosha cleaves the double-stranded stem of pri-miRNA 11 bp from the basal junction between ssRNA and dsRNA (Gregory et al., 2004; Han et al., 2004; Han et al., 2006) and ~ 22 bp away from the apical junction linked to the terminal loop. Moreover, additional sequence motifs have been demonstrated to be involved in pri-miRNA processing (reviewed in (Ha and Kim, 2014)). The Drosha-mediated cleavage produces a 2-nt long overhang on the 3′end. The mammalian Microprocessor contains several additional accessory protein factors, including DDX5 (p68) and DDX17 (p72), DEAD-box RNA helicases increasing processing by Drosha (Fukuda et al., 2007; Gregory et al., 2004) and reviewed in (Ha and Kim, 2014). The expression level, specificity, and activity of Drosha are regulated by several mechanisms that include: (i) autoregulation between Drosha and DGCR8 maintaining homeostatic activity of the Microprocessor complex, (ii) post-translational modifications regulating protein stability, nuclear localization and processing of the Microprocessor complex and (iii) RNA-binding proteins selectively interacting with Drosha (reviewed in (Ha and Kim, 2014)).

Pre-miRNAs are exported from the nucleus to the cytoplasm by Exportin 5 in a Ran-GTP-dependent manner (Bohnsack et al., 2004; Lund et al., 2004; Yi et al., 2003). Cytosolic pre-miRNAs are cleaved by Dicer near the terminal loop, yielding the mature miRNA duplexes of 22 nt in length with 2 nt 3’ overhangs on both ends (Bartel, 2009; Grishok et al., 2001). As stated above, Dicer binds pre-miRNA with the preference for 2 nt overhang on the 3′end, which is generated by the Drosha-mediated cleavage. In mammals and flies, two counting rules for determination of cleavage sites exist. First, the Dicer cleavage site is located at a fixed distance from the 3′end of the terminus of dsRNA (the 3′counting rule). Second, the Dicer cleavage site is located 22 nt away from the 5′phosphorylated end of the pre-miRNA (the 5′counting rule). The second case occurs when the 5′end of pre-miRNA is thermodynamically unstable (Park et al., 2011). Mammals have only one Dicer, which produces both siRNAs and miRNAs. Although mammalian Dicer cleaves both imperfectly base paired pre-miRNAs hairpins and perfect RNA duplexes, processing of pre-miRNA duplexes is more than hundred times more efficient than processing of perfect long dsRNA under multiple-turnover conditions (Chakravarthy et al., 2010). As already mentioned, several cofactors and products, including TRBP or

PACT, are involved in the control of Dicer activity (reviewed in (Ha and Kim, 2014)). An overview of mammalian miRNA pathway is depicted in **Fig.5**.

1.3.2.2 miRISC loading and mechanism of miRNA target interaction

The loading of small RNA duplex on AGO protein to form an effector complex called miRISC in miRNA pathway and subsequent RNA duplex unwinding and strand selection were described above (see **1.2.1.2.)** and reviewed elsewhere (Czech and Hannon, 2011; Ha and Kim, 2014; Kawamata and Tomari, 2010).

Similarly to siRNAs, miRNAs interact with their mRNA targets via base pairing. Importantly, metazoan miRNAs usually form imperfect hybrids (Bartel, 2009). The most stringent requirement for the target recognition is so-called seed region comprising of 2-7 nt from the 5′ end of a miRNA. The seed region is important for target recognition and nucleating the interaction with an mRNA target. Apart from the seed region, the guide RNA consists of an anchor (nt 1), a central region (nt 9-12), a 3′supplementary region (nt 13-17), and a tail region (nt 19-21). The sites in the target mRNA matching the seed region are known as canonical sites and are typically located in the 3′UTR. Canonical sites usually pair also with position 8 of a miRNA and/or have adenine opposite position 1 of the miRNA (reviewed in (Hausser and Zavolan, 2014)). In contrast to the 5′ seed region, complementarity within the 3′ half and central region of miRNA is quite relaxed, containing mismatches and bulges (Bartel, 2009). Notably, miRNAs carrying bulges or single nucleotide loops in the miRNA seed region can interact with their targets according to non-canonical binding modes. The anatomy of both canonical and non-canonical miRNA-target interactions are reviewed in detail in (Hausser and Zavolan, 2014). Similarly, although most of the predicted and experimentally verified miRNA target sites are located in the 3′UTR, animal miRNAs might also target the 5′UTR and coding regions of mRNAs (Easow et al., 2007; Gu et al., 2009a; Orom et al., 2008). Interestingly, it was reported that the association of miRNAs with 5′UTR target sites can activate translation (Henke et al., 2008; Orom et al., 2008). Model of small RNA-loaded AGO binding to the target RNA is depicted in **Fig.8**.

Usually, multiple sites, either for the same or different miRNAs, are required for the effective repression of the target mRNA expression (Doench and Sharp, 2004; Grimson et al., 2007). Notably, miRNA genes are frequently organized in polycistronic clusters from

which several miRNAs are coexpressed. Such clustered miRNAs frequently form so-called seed families, groups of miRNAs with identical sequences in the seed region (Bartel, 2009). miRNAs belonging to the same seed family frequently share mRNA targets. Interestingly, ~64% of human miRNA are a part of multimember seed families. There are two hypotheses explaining such redundancy: (i) miRNAs belonging to the same seed family could be expressed and active in different tissues and (ii) variability in the 3´end of miRNAs provides slight differences in their sets of targets or in the dynamics of target regulation (reviewed in (Hausser and Zavolan, 2014)).

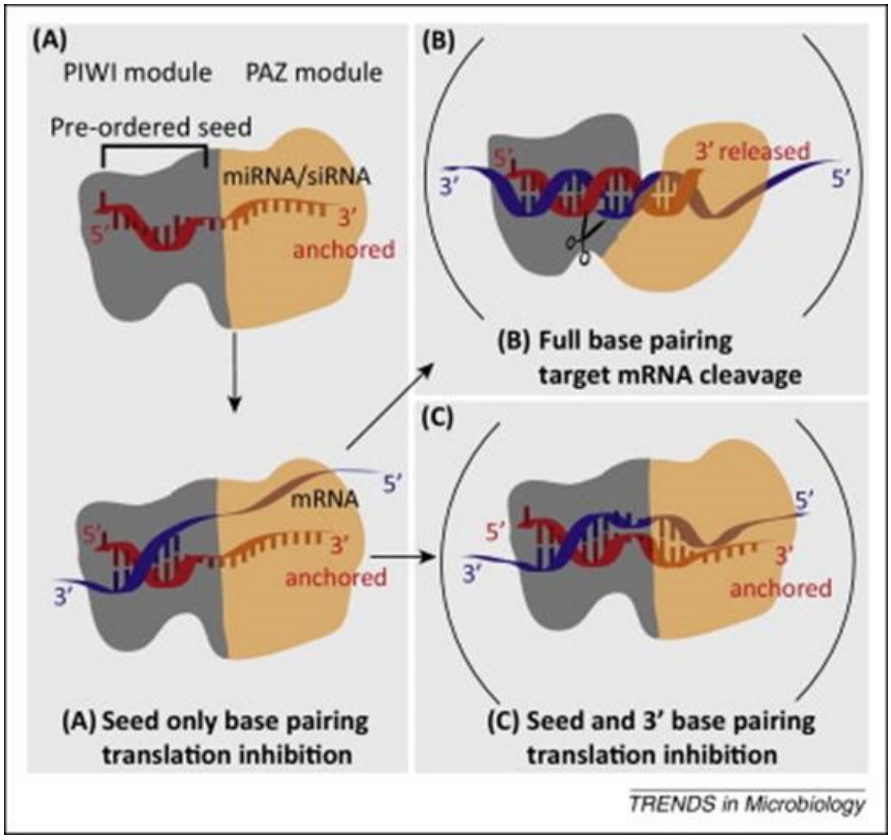

Fig.8: Model of miRNA/siRNA–AGO complex and target binding*. (A) Guide RNA (red) is bound to AGO, stretching (5′–3′) from the PIWI domain (gray) to the PAZ domain (yellow). Nt 2–8 (seed) of the RNA are pre-ordered in a helical conformation; nt 1 is flipped into a binding pocket and is not available for base pairing. The 3′ part of the guide is anchored to the PAZ domain. Recognition of the incoming mRNA (blue) is nucleated through pairing with seed nt 2–8. **(B)** In the case of extensive complementarity between guide and target, base pairing is extended starting from the seed, leading to a conformational change of AGO. Progressive base pairing leads to the release of the 3′ part of the guide from the PAZ domain, allowing guide and target to intertwine, possibly forming a complete helix. Complete binding allows an active AGO to cleave the target mRNA between position 10 and 11 (indicated by scissors). **(C)** In the case of partial 3′ complementarity, the guide and target pair position around nt 13–16, leaving a gap between seed and 3′ pairing. Despite 3′ pairing, the guide remains anchored to AGO. *****Fig.8 was completely adopted from Kunne *et al*. (2014) (Kunne et al., 2014).

1.3.2.3 Mechanism of miRNA-induced repression of gene expression

Although a considerable progress has been made in understanding of the mechanism of miRNA-mediated regulation of gene expression, several controversies still exist. Originally, it was thought that animal miRNAs regulate gene silencing by repression of target mRNA translation. However, it is well documented that animal miRNAs can induce degradation of the target mRNA. The current view is that miRNAs induce translation repression coupled with mRNA destabilization through deadenylases and decapping activities, which are associated with the miRISC (Huntzinger and Izaurralde, 2011).

Huntzinger and Izaurralde (Huntzinger and Izaurralde, 2011) proposed a stepwise model for miRNA-mediated gene silencing in animals. (**Fig.9**). Animal miRNA in a complex with AGO protein recognizes target mRNA via base pairing with partially complementary binding sites predominantly located in the 3′UTR. An AGO protein interact directly with GW182 acting downstream of AGO proteins. Three mammalian GW182 paralogues named TNRC6A (GW182), TNRC6B, and TNRC6C exist (reviewed in (Fabian and Sonenberg, 2012; Huntzinger and Izaurralde, 2011)). The N-terminal domain of GW182 is composed of multiple glycine-tryptophan (GW) repeats and mediates binding to AGO. The middle and C-terminal regions form a bipartite silencing domain (SD) containing two PABPC binding sites: (i) the PAM2 motif mediating the direct binding to the MLLE domain of PABPC and (ii) less defined region interacting with PABPC indirectly probably through additional accessory proteins. The assembly of AGO-GW182 complex triggers target mRNA deadenylation by the major deadenylase complex comprising of CAF1, CCR4, and the NOT complex. Next, depending on the cell type and/or specific target, deadenylated mRNAs are stored in a translationally repressed state, or undergo decapping mediated by the decapping enzyme DCP2 and several decapping activators (DCP1, EDC4, DDX6 etc.) and subsequent rapid degradation by the major 5′-3′exonuclease XRN1 (reviewed in (Huntzinger and Izaurralde, 2011)). Translation inhibition was suggested to occur at both translation initiation level and post-initiation state. However, there is an increasing evidence indicating that animal miRNAs also interfere with the cap-structure and/or with the function of the cap-binding eIF4F complex and therefore, if translation inhibition does occur, it is mostly at initiation level. According to several reports, translation repression precedes mRNA deadenylation and degradation (Bethune et al., 2012; Meijer et al., 2013).

Since mammals have only one Dicer producing both siRNAs and miRNAs, the miRNA pathway and the RNAi mechanistically merge upon dicing. In mammals, all four AGO proteins (AGO1-4) are able to associate with miRNA in the miRISC. Of them, only AGO2 is able to slice (Liu et al., 2004). As described above, the majority of animal miRNAs base pair imperfectly with their target mRNA and regulate gene silencing by repression of translation, deadenylation, and subsequent decay of the mRNA targets. Importantly, the specific silencing effect is not dependent on small RNA's origin but rather on the degree of its complementarity with the target mRNA. A miRNA can guide slicing when it is fully complementary to the target mRNA sequence and is associated with AGO2 (reviewed in (Sontheimer and Carthew, 2005)). One example of such miRNA is miR-196, which can cleave HOXB8 mRNA (Yekta et al., 2004). Likewise, siRNAs that base pair imperfectly with their targets induce the translation repression (Doench et al., 2003; Meister et al., 2004). Taken together, the main mechanistical distinction between mammalian RNAi and miRNA pathway is the type of the Dicer substrate, and not the silencing effect *per se*.

1.3.2.4 Cellular compartmentalization of miRNA repression

There is evidence that miRNA-mediated repression is associated with distinct structures, so-called P-bodies (PBs) (Eulalio et al., 2007a; Parker and Sheth, 2007), discrete cytoplasmic foci that accumulate translationally repressed mRNAs and probably act as sites of final steps of mRNA degradation. PBs are highly dynamic, altering in both size and number during the cell cycle and in response to changes in cellular translation (Eulalio et al., 2007a; Eulalio et al., 2007b; Lian et al., 2006; Parker and Sheth, 2007; Pauley et al., 2006). Proteins involved in mRNA deadenylation (CCR4-NOT1 deadenylase complex, RCK/p54 helicase, HPat1, RAP55, EDC3, Ge-1/Hedls, and the heptameric LSm1-7 complex), mRNA decapping (DCP1-DCP2 decapping complex), mRNA decay (5′-3′exonuclease XRN1), and miRNA repression (AGOs, GW182, miRNAs) are enriched in PBs (reviewed in (Fabian et al., 2010)). At the same time, PBs lack ribosomes and most of the translation initiation factors. Some studies describe an inverse relationship between P-body localization and polysome association of target mRNAs, indicating a correlation between miRNA-mediated translational repression and accumulation of target mRNAs in PBs (Bhattacharyya et al., 2006; Huang et al., 2007; Liu et al., 2005; Pillai et al., 2005).

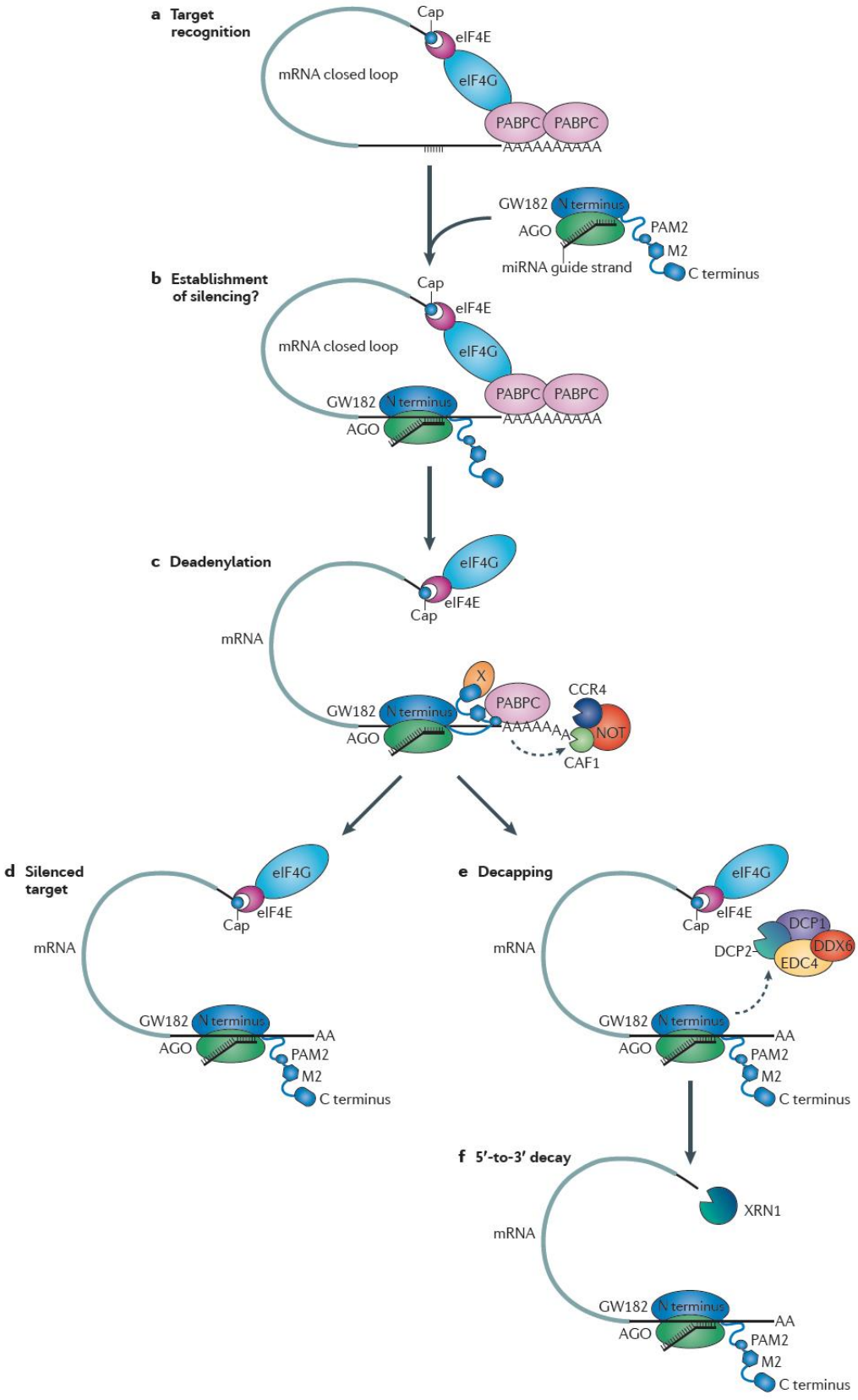
a Target recognition
Cap
eIF4E
eIF4G
mRNA closed loop
PABPC
PABPC
AAAAAAAAAA
GW182
N terminus
AGO
PAM2
M2
C terminus
miRNA guide strand
b Establishment of silencing?
c Deadenylation
mRNA
X
CCR4
NOT
CAF1
d Silenced target
e Decapping
DCP1
DCP2
DDX6
EDC4
f 5′-to-3′ decay
XRN1

Fig.9: Mechanisms of microRNA-mediated gene silencing in animals* (a) The mRNA target is represented in a closed loop conformation, which is achieved through interactions between PABPC bound to the 3′ poly(A) tail and eukaryotic translation-initiation factor 4G (eIF4G) bound to the cap-binding protein eIF4E. **(b,c)** Animal miRNAs bound to AGO recognize their mRNA targets by base pairing to partially complementary binding sites in the mRNA 3′UTR. AGO interacts with GW182 **(b)**, which interacts, in turn, with PABPC bound to the mRNA poly(A) tail **(c)**. GW182 proteins contain two PABPC-binding sites: the PAM2 motif, which confers the direct binding to the PABPC MLLE domain, and the M2 and carboxy-terminal regions, which interact indirectly with PABPC, most likely through additional proteins (indicated as X). The AGO–GW182 complex directs the mRNA to deadenylation **(c)**. **(d)** Depending on the cell type and/or specific target, deadenylated mRNAs can be stored in a translationally repressed state. **(e,f)** In animal cell cultures, deadenylated mRNAs are decapped and rapidly degraded by the major 5′-to-3′ exonuclease XRN1. *****Fig.9 was completely adopted from Huntzinger and Izaurralde (2011) (Huntzinger and Izaurralde, 2011).

Interestingly, although functional miRNA pathway is essential for formation of PBs, microscopically visible PBs seem to be dispensable for miRNA-mediated repression and their occurrence is rather a consequence than a cause of miRNA-induced silencing (Eulalio et al., 2007b; Novotny et al., 2012). In addition, it seems that at least initiation of the miRISC-mediated repression occurs outside of PBs.

Other cellular structures connected to miRNA-mediated repression are stress granules (SGs), which form in response to stress and upon global repression of translation initiation (Kedersha and Anderson, 2007). SGs share some protein components with PBs, and are frequently located adjacent to them, pointing to PB and SG interaction (Kedersha et al., 2005; Wilczynska et al., 2005). It was shown that AGO proteins, artificial miRNAs, and repressed reporter mRNAs accumulate in SGs (Leung et al., 2006). The accumulation of miRISC components in SGs may reflect localized miRNA-mediated repression, but it is also possible that miRISC components aggregate simply due to cellular stress (Leung et al., 2006).

Although RNA silencing was originally thought to be a solely cytosolic process, emerging evidence indicates its connection to several endomembrane systems in plants and animals. First, rough endoplasmic reticulum (ER) was suggested to be the site of the RISC loading and siRNA mediated slicing (reviewed in (Kim et al., 2014)). In fact, mammalian AGO2 was originally identified as GERp95, an ER- and Golgi-associated protein (Cikaluk et al., 1999; Tahbaz et al., 2001). Additional studies reported association of Dicer with ER and Golgi in various cell types (Barbato et al., 2007; Tahbaz et al., 2004). Second, endosomes and multivesicular bodies (MVBs, specialized late endosomal compartments with a characteristic multivesicular morphology that sort endocytosed proteins into

different compartments) were suggested to be possible sites of RISC assembly and turnover (reviewed in (Kim et al., 2014)). In human cells, miRNAs and target mRNAs accumulate in endosomes and MVBs (Gibbings et al., 2009; Lee et al., 2009) and human AGO2 and GW182 co-purified and co-localized both with endosomes and MVBs (Gibbings et al., 2009). Finally, several reports suggested targeting of Dicer and human AGO2 to autophagosomes for degradation, possibly to ensure the homeostatic regulation of miRNA-mediated RNA silencing under various stress conditions (reviewed in (Kim et al., 2014)).

1.3.3 MicroRNAs in pathology

1.3.3.1 miRNAs in human cancer

miRNAs are involved in the majority of cellular processes and their expression changes in various diseases, including cancer. Cancer is a result of a complex, multistep process involving sequential accumulation of mutations that affect the gene function. Aberrant miRNA expression patterns have been implicated in most human malignancies (reviewed in (Farazi et al., 2013)).

Deregulation of miRNAs can be caused by (i) deletion, amplification or mutation in miRNA genes, (ii) deregulation of transcription factors targeting the specific miRNAs, or (iii) epigenetic alterations, such as DNA methylation and histone modifications (reviewed in (Chuang and Jones, 2007; Saito et al., 2006)). There is a mutual relationship between epigenetics and miRNAs - epigenetic mechanisms regulate miRNA expression while miRNAs target the key epigenetic regulators.

The first report suggesting a role of miRNAs in human cancer was a study of tumor suppressors encoded on chromosome 13q14, which is frequently deleted in chronic lymphocytic leukemia (CLL) (Eiring et al., 2010). Surprisingly, it was found that this critical region contains two miRNAs, miR-15a and miR-16-1, expressed in one polycistronic RNA. Since the loss of chromosome 13q14 causes CLL, it was suggested that these miRNAs might be involved in the pathogenesis of human cancer. Moreover, it was discovered that miR-15a and miR-16-1 were absent or downregulated in 69% of CLLs, indicating their tumor suppressive role in this malignancy (Calin et al., 2002; Eiring et al., 2010). So far, the altered miRNA expression has been reported in almost all types of cancer, although it is clear that it is not necessarily a causal factor.

miRNAs can act as oncogenes (oncomirs) or tumor suppressors and function in a variety of pathways frequently deregulated in cancer (reviewed recently in (Chan and Wang, 2015)). For instance: (i) miR-15a and miR-16-1 regulate apoptosis regulation by targeting anti-apoptotic *BCL2* mRNA (Cimmino et al., 2005). (ii) Transcription factor MYC modulates the expression of the miR-17 cluster, which increases the expression of the key cell cycle regulator E2F1, and is upregulated in human lymphomas (O'Donnell et al., 2005). (iii) Overexpression of a single miRNA, miR-21, is sufficient to cause tumor development in B-cells. Results from mice conditionally overexpressing miR-21 showed that pre-B cell lymphoma development and short survival were dependent on miR-21 overexpression, whereas tumor regression and prolonged survival was observed after miR-21 inactivation (Medina et al., 2010). (iv) Increasing number of studies demonstrated involvement of miRNAs in cancer metastasis (reviewed in (Chan and Wang, 2015)). For instance, miR-10b directly stimulates cell migration and invasion via targeting *HOXD10*, which is a transcriptional repressor of RHOC, a key regulator of metastasis (Ma et al., 2007). In contrast, miR-335, miR-126 and miR-206 act as metastasis suppressors in breast cancer. A rescue of miR-126 expression significantly suppressed overall tumor growth while restoration of miR-335 or miR-206 levels altered cell morphology, possibly causing a decrease in cell motility (Tavazoie et al., 2008).

1.3.3.2 MicroRNAs in cardiovascular diseases

miRNAs are also involved in other pathologies, including cardiovascular diseases. For instance, overexpression of miR-1, which is specifically expressed in cardiac and skeletal muscle precursor cells, reduces a pool of proliferating ventricular cardiomyocytes in a developing heart in mice (Zhao et al., 2005). Interestingly, miRNA-1 promotes myogenesis, while miR-133, which clusters together with miR-1 on mouse chromosome 2, stimulates myoblast proliferation (Chen et al., 2006). Microarray analysis identified more than 12 miRNAs deregulated during cardiac hypertrophy and heart failure (van Rooij et al., 2006).

1.3.3.3 MicroRNAs in autoimmune diseases

Many studies showed that miRNAs play a key role in the regulation of immune response and immune system development. Moreover, miRNAs were linked to a variety of autoimmune disorders. The first autoimmune disease in which miRNAs were implicated is

psoriasis, the most prevalent chronic inflammatory skin disease in adults. In this disease, keratinocyte-specific miR-203 is upregulated (Sonkoly et al., 2007). miR-146, other miRNA upregulated in psoriasis, is expressed in immune cells and targets IRAK1 and TRAF6, regulators of the TNF-α signaling pathway (Sonkoly et al., 2007; Taganov et al., 2006). The recent progress in discovery, profiling and characterization of miRNAs in human psoriatic skin was reviewed in (Xia and Zhang, 2014). miRNAs are also deregulated in rheumatoid arthritis, a systemic autoimmune disorder characterized by chronic inflammation of synovial tissues (Smolen et al., 2007), and lupus erythematosus, an autoimmune disorder characterized by excessive production of autoantibodies against various self-antigens (Joseph et al., 2010). The current understanding of the roles of miRNAs in autoimmunity and in various autoimmune diseases is reviewed in (Deng et al., 2014).

1.3.3.4 MicroRNAs in neurodegenerative diseases

A substantial amount of miRNAs is exclusively expressed in the central nervous system and is involved in neuronal development (Fiore et al., 2008). Several reports demonstrated connection between different miRNAs and various neurodegenerative diseases (reviewed in (Maciotta et al., 2013)). For instance, various miRNAs are deregulated in Alzheimer disease (reviewed in (Van den Hove et al., 2014)), Parkinson disease (miR-133b, miR-7, miR-153 etc.) (reviewed in (Heman-Ackah et al., 2013; Ma et al., 2013)), and Huntington disease (miR-486, miR-196a, miR-17-3p, miR-22, miR-485-5p, miR-500 etc.) (reviewed in (Maciotta et al., 2013)).

1.3.3.5 Role of Dicer in age-related macular degeneration

In 2011, Kaneko *et al.* (Kaneko et al., 2011) suggested a role of mammalian Dicer in preventing the inflammatory changes of geographic atrophy. Geographic atrophy (GA) is an untreatable, advanced form of age-related macular degeneration resulting from inflammation-induced retinal pigmented epithelium (RPE) cell degeneration. According to their data, Dicer degrades Alu dsRNA independently of siRNA loading of on the RISC complex in RPE cells in both mice and humans. The reduced Dicer expression in RPE cells allows the accumulation of long dsRNAs derived from Alu elements and thus induces inflammatory changes. Finally, RPE cells are lost, and GA is manifested. GA was recapitulated in the mouse model using RPE cell-specific knock-out of Dicer. This study

demonstrated a miRNA-independent cell survival function of Dicer in suppressing repetitive elements. This opens a new therapeutic possibilities for Dicer stimulators as potential candidates for treatment of age-related macular degeneration, (Kaneko et al., 2011).

1.3.3.6 MicroRNAs in diagnostics and therapy

As mentioned above, specific miRNAs are often associated with a particular disease or disease phase. Therefore, they can be used as biomarkers for diagnosis, prognosis, and therapeutic response prediction, as demonstrated in several types of cancer (Garzon et al., 2009). To provide an alternative to mainly invasive diagnostic techniques, such as biopsy, many studies currently focus on the detection of miRNA biomarkers present in human fluids, including plasma, serum, urine, or saliva by highly sensitive detection methods, such as quantitative real-time polymerase chain reaction (qPCR) (Cortez and Calin, 2009; Wittmann and Jack, 2010).

Deregulated miRNAs also represent potential therapeutic targets. Upregulated miRNAs might be targeted using specifically modified antisense oligonucleotides complementary to miRNAs, known as antagomirs (Rossbach, 2010). Currently, one of the most promising approaches for specific miRNA inhibition *in vivo* is the use of locked nucleic acid (LNA) oligonucleotides, in which the ribose moiety is modified with an extra bridge connecting the 2' oxygen and 4' carbon, thus „locking" the ribose in 3'-*endo* conformation. The LNA modification enhances the base stacking and backbone pre-organization, which significantly increases the hybridization properties of oligonucleotides and augments their sensitivity and specificity. Moreover, LNA modifications provide resistance to nuclease degradation. The most successful application of LNA oligonucleotides is Miravirsen (SPC3649), the first antagomir drug candidate, now in phase IIa clinical trials to treat patients infected with Hepatitis C virus (HCV) (Janssen et al., 2013; Lanford et al., 2010). Miravirsen targets miR-122, a liver-specific miRNA with an important role in the HCV life cycle, and thereby significantly reduces HCV levels in serum of patients chronically infected with HCV with no detectible evidence of resistance. Miravirsed is thought to act mainly by hybridizing to mature miR-122 and blocking its interaction with HCV RNA. However, its target sequence is also present in pri-miR-122 and pre-miR-122, and it was demonstrated that Miravirsen binds to the stem-loop structure of pri- and pre-miR-122 with nanomolar affinity and inhibits both Dicer- and Drosha-

mediated processing of miR-122 precursors, which potentially contributes to the pharmacological activity of the drug (Gebert et al., 2014). Thanks to its unique mechanism of action, Miravirsen represents a new treatment option for HCV patients who do not respond to the current standard therapy.

1.3.4 Analysis of microRNA pathway

1.3.4.1 Analysis of miRNAs expression

The major challenge in the miRNA research is the exact and feasible determination of miRNA expression levels under various physiological and pathological conditions, including development or disease. miRNA expression can be analyzed by several methods including microarrays (Liu et al., 2008), high-throughput sequencing (Creighton et al., 2009), *in situ* hybridization (Shi et al., 2012), or quantitative RT-PCR (Benes and Castoldi, 2010): (i) Microarray technology represents a common approach for miRNA expression profiling (Liu et al., 2008). It is a powerful, high-throughput method that allows genome-wide expression profiling of thousands of small noncoding RNAs within tens of samples processed in parallel in a single experiment. (ii) High-throughput sequencing technology (Creighton et al., 2009) enables simultaneous sequencing of millions of DNA or RNA molecules. It has certain advantages over microarrays. First, it overcomes problems with background and cross-hybridization signals. Second, high-throughput sequencing is not restricted by the array content, allowing for a discovery of novel miRNAs or distinguishing miRNA variants. (iii) Using *in situ* hybridization (Shi et al., 2012; Thompson et al., 2007), miRNAs can be visualized histologically providing valuable data about miRNA expression and function. (iv) Exact quantitative analysis of miRNA expression can be done by quantitative RT-PCR (qPCR) (Benes and Castoldi, 2010); qPCR can be used to validate and calibrate results obtained from a whole-genome profiling using microarrays or deep-sequencing.

1.3.4.2 Target prediction and detection

As miRNAs expression changes under various physiological and pathological conditions, it is of interest to reliably predict miRNA targets. Number of computational algorithms focusing mainly on mRNA canonical sites have been developed for miRNA target prediction: TagetScan, ElMMo, miRecords, PicTar, miRanda, RNAhybrid, DIANA

MicroT analyzer, and others included in MirBase. These algorithms take into account the relevance of seed pairing, the sequence conservation among species, the target site accessibility, and the free energy of miRNA-mRNA binding. Despite the existence of a variety of algorithms, results of miRNA target prediction are often inconsistent, yielding inaccurate results. Thus several methods have been proposed for the experimental miRNA target identification and computational data validation. They include genetic screening, the use of miRNA inhibitors and miRNA mimics in various gene-specific expression assays, usually luciferase reporter assays, quantification of gene expression changes following miRNA transfection, or methods based on AGO crosslinking and immunoprecipitation. All methods with their advantages and disadvantages are reviewed, for example in (Hausser and Zavolan, 2014).

1.3.4.3 Manipulation of miRNA pathway

A common strategy for determining roles of the individual miRNAs in diverse biological processes in mammalian cells is modulation (inhibition or activation) of the miRNA pathway. There are several strategies for modulating RNA silencing. Globally, RNA silencing can be inhibited by knocking-down or knocking-out the key pathway components, such as Dicer or AGO2. However, the onset of inhibition of RNA silencing is dependent on the protein product of the targeted gene and therefore the inhibitory effect cannot be rapidly induced. Delivery of suppressor proteins encoded by plant viruses is another way how to inhibit RNA silencing. For instance, Dunoyer *et al.* (2004) (Dunoyer et al., 2004) reported that tombusviral P19 protein suppressor coimmunoprecipitated with both siRNA and miRNA duplexes suggesting that P19 probably prevents RNA silencing by sequestering both classes of short RNAs (Dunoyer et al., 2004). Although plant protein repressors can function in mammalian cells, their effect depends on achieving their sufficiently high expression. RNA silencing can be also globally enhanced either by eliminating natural inhibitory mechanisms (Timmons, 2004) or by overexpression of important RNA silencing players.

Individual miRNAs can be selectively inhibited using various modified antisense oligonucleotides complementary to mature miRNAs. Successful use of these oligonucleotides, referred to as antagomirs (AMOs), has been reported by many investigators (Esau, 2008). The specific interaction between miRNA and its target mRNA can be prevented by target protectors, such as morpholino-oligonucleotide that interfere

with a single miRNA-mRNA pair by binding specifically to the miRNA target sequence in the 3´UTR (Choi et al., 2007). An enhanced activity of individual miRNAs can be achieved by overexpression or by transfecting cells with so-called miRNA mimics, chemically synthesized dsRNAs, which mimic mature endogenous miRNAs. Although it is possible to modulate RNA silencing by these strategies, they have limits. For example, they are suboptimal for studies of miRNAs during relatively fast transitions between states requiring global transcriptome changes, such as zygotic genome reprogramming or early stages of embryonic stem cell differentiation. Pros & cons of available strategies for miRNA inhibition are summarized in **Tab.1**.

	knock-out	**knock-down**	**suppressor proteins**	**antagomirs**	**target protectors**
onset of inhibition	slow	slow	faster	faster	faster
duration	only stable	stable or transient	stable or transient	transient	transient
work-load	high	medium	low	low	low
cost	high	medium	low	high	high
systemic inhibition	very difficult	tissue-dependent	tissue-dependent	tissue-dependent	?
efficiency	high	high	very low	high	high

Tab.1: Pros & cons of available strategies for miRNA inhibition

1.4 Chemical biology

Chemical biology is an interdisciplinary approach spanning the fields of chemistry and biology. The key idea of chemical biology is to use compounds produced through synthetic chemistry for the study and manipulation of biological systems. High-throughput screening (HTS) is a drug-discovery automation-based method enabling quick and parallel assays of biological or biochemical activities of thousands to millions of small chemical compounds. To minimize the volume of each assay and maximize the number of assays done in a given time, HTS assays are typically performed in "automation-friendly" microtiter plates with 96-, 384-, 1536- or even nanowell formats that permit the assay volumes of several hundred nanolitres. Thus, the time and cost of each assay is reduced to minimum. The key step in HTS is the development and optimization of a robust assay assessing the process of interest. Two types of HTS exist: (i) target-based and (ii) phenotype-based screens.

1.4.1.1 Target-based screens

Target-based screens are used to identify ligands (activators or inhibitors) of for example specific protein of interest. The first step in this type of screen is usually the expression and purification of the protein of interest, however this step is not necessary in all cases. Then, biochemical *in vitro* binding or enzymatic assay is developed and optimized. Typically, small-focused libraries of compounds are tested in a target-based screen. Candidate molecules have to be validated. Only confirmed hits are taken for subsequent analysis of specificity and *in vivo* functionality. Up to now, target-based screens have identified small-molecule or peptide ligands for many proteins, e.g. kinases (Colas et al., 1996), phosphatases (Aramburu et al., 1999), proteases (Apletalina et al., 1998), cell-surface receptors (Tian et al., 1998; Zhang et al., 1999a), E3 ubiquitin ligases (Bottger et al., 1996), steroid receptors (Norris et al., 1999), and many others.

1.4.1.2 Phenotype-based screens

Phenotype-based screens test the ability of each small compound in a library to induce a specific phenotypic outcome in single-cell organisms, such as bacteria (Dolle, 1997) and fungi (Norman et al., 1999) or in cells from multicellular organisms, such as mammals (Mayer et al., 1999; Rosania et al., 2000). Phenotypes can be detected by: (i) various marker genes or proteins in reporter gene assays or antibody-based cellular immunoassays measuring abundance of a specific gene or protein epitope as a marker of a wider cellular phenotype; (ii) functional assays that directly measure cellular activities, such as cell division, metabolism, apoptosis, chemotaxis, or adhesion; (iii) automated microscope-based cell imaging systems that detect changes in cellular morphology or changes in subcellular localization of marker proteins. Up to now, phenotype-based screens have identified reagents that, for example, block mitotic progression (Mayer et al., 1999; Norman et al., 1999), induce or suppress cell cycle arrest (Stockwell et al., 1999), prevent mating pheromone-induced cell cycle arrest (Scott and Smith, 1990), induce apoptosis (Lu et al., 1997), and others. Both types of HTS are schematically shown in **Fig.10**.

So far, data on chemical RNA silencing modulators are rare (reviewed in (Deiters, 2010)). However, several studies have identified potential small compound modulators of the RNA silencing (Deiters, 2010; Chiu et al., 2005; Maiti et al., 2012; Shan et al., 2008; Shum et al., 2012; Tan et al., 2012; Watashi et al., 2010) utilizing both cell-based assays

and biochemical *in vitro* assays. Chiu *et al*. (2005) (Chiu et al., 2005) screened a chemical library of substituted dihydropteridinones and identified a nontoxic, human cell-permeable, and reversible inhibitor of the RNAi pathway, called ATPA-18. They demonstrated that this small compound specifically inhibits an early step in the RNAi pathway, presumably at the level of a passenger strand unwinding or earlier, and that ATPA-18 effects are specific to siRNA duplexes (Chiu et al., 2005). Screening of a library of 2000 small compounds by a cell-based assay identified a small molecule named enoxacin that enhances RNAi and promotes miRNA biogenesis. This result suggests that enoxacin targets the RISC loading step by facilitating the interaction between TRBP and RNAs (Shan et al., 2008). Next, polylysine (PLL) and trypaflavine (TPF) were identified as suppressors of the miRISC activity in a small screen of 530 compounds (Watashi et al., 2010). Interestingly, these two compounds also neutralized tumor growth in a cell-based model (Watashi et al., 2010). A recent biochemical HTS identified three potent small-molecule inhibitors of RISC loading - aurintricarboxylic acid, suramin sodium salt and oxidopamine hydrochloride (Tan et al., 2012).

Importantly, the majority of aforementioned HTSs were performed using relatively small libraries comprising of several hundreds to thousands of compounds. Moreover, identified compounds often showed activity only at non-physiological concentrations, suggesting a nonspecific rather than specific modulation of RNA silencing. Extensive systematic application of chemical biology to explore the area of RNA silencing under highly stringent conditions is needed to identify small molecules allowing for specific and strong stimulation or inhibition of RNA silencing. Taken together, research of RNA silencing modulators represents an interesting and still relatively unexplored area.

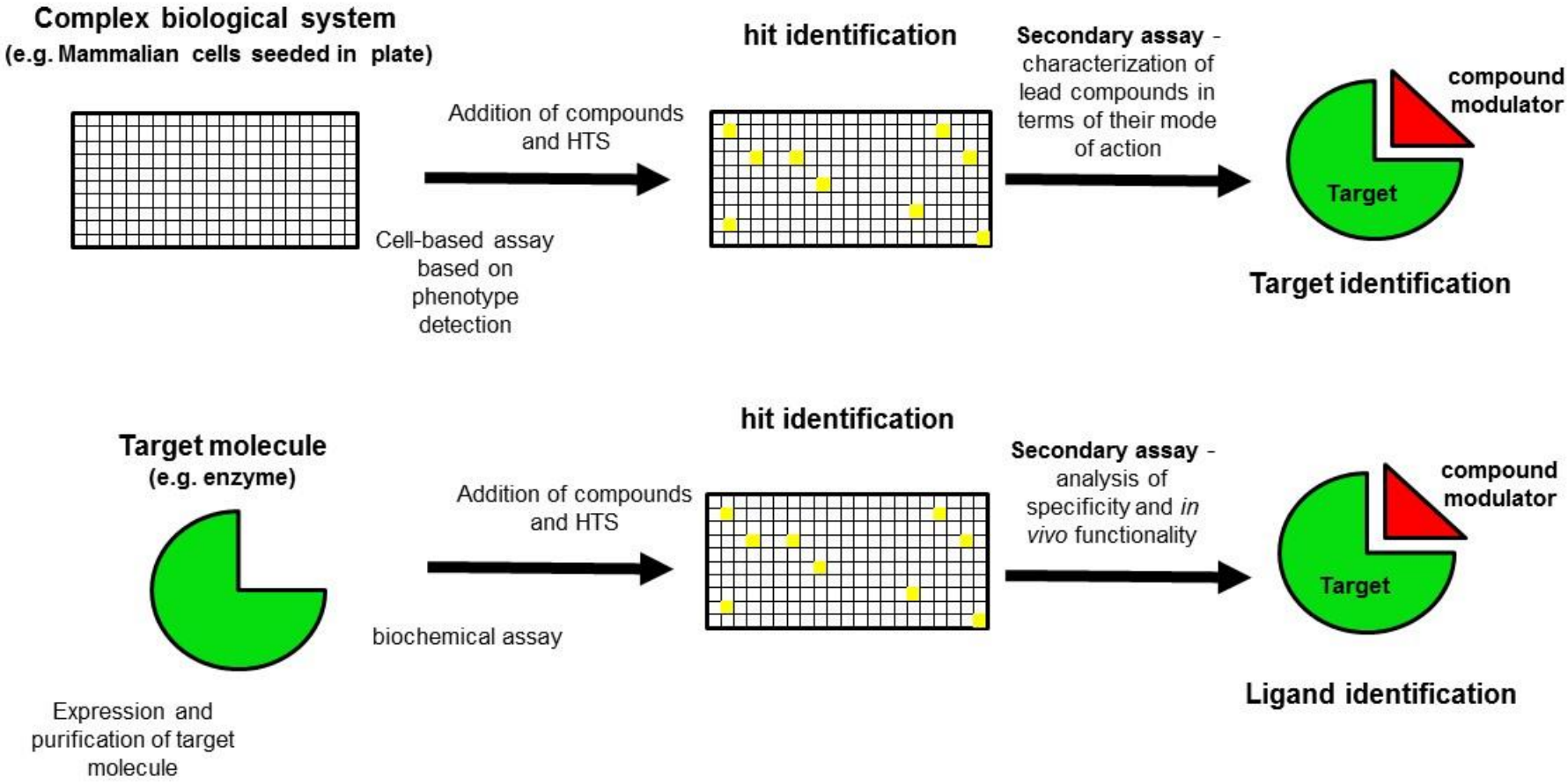

Fig.10: Types of HTS

2 AIMS & SIGNIFICANCE

Potential of chemical biology in the field of RNA silencing has not been fully explored yet. At the same time, small chemical compounds might represent great tools for: (i) a direct modulation of miRNA/RNAi pathways and (ii) a discovering crosstalks between RNA silencing and other cellular pathways.

The direct modulation of RNA silencing offers novel applications in various fields of research. In basic research, small compound modulators would be an excellent tool for studying RNAi and miRNA pathways *in vivo* and *in vitro* and could help to determine essential roles of RNA silencing pathways in different processes in various cell types, tissues, and animal model systems. Moreover, inhibition or activation of RNAi can increase potential of the RNAi technology. In biotechnology, inhibition of RNA silencing could be useful for applications that aim at global reprogramming of gene expression and require a relief of repression of miRNA targets in a differentiated cell type. In therapy, Dicer stimulators are candidates for treatment of age-related macular degeneration, in which Dicer deficiency was implicated (Kaneko et al., 2011). As various miRNAs have been implicated as potential causative agents with opposing roles in tumor suppression and tumor induction (Farazi et al., 2013; Medina and Slack, 2008), modulation of miRNAs can be considered for cancer therapy. As demonstrated by histone-deacetylase-inhibitors (HDIs), global modulation of miRNA pathway might be valuable strategy. While histone deacetylases cause global and complex changes in gene expression, HDIs are used to treat different types of cancer (Bolden et al., 2006; Choudhary et al., 2009; Marks et al., 2004; Richon et al., 2009). Currently, there is a growing number of evidence that small RNA pathways participate in the antiviral response in mammals (Cullen, 2006; Sidahmed et al., 2014; Svoboda, 2014). Therefore, it is tempting to speculate that boosting of RNAi effect by small compound activators could contribute to antiviral therapy.

Many small chemical compounds have been implicated in regulation of specific cellular pathways. Therefore, detailed HTS data analysis is expected to uncover existing mechanisms that regulate the RNA silencing indirectly through signaling, metabolic and other pathways. For the research of such interactions between RNA silencing and other processes, chemical biology provides an excellent choice.

The presented work represents a part of a broader project whose ultimate goal is to obtain a set of small molecules allowing for stimulation or inhibition of RNA silencing. This thesis summarizes the results from the first two phases of the project - (i) development of high-throughput screening assays and (ii) high-throughput screening of available libraries of small compounds.

Specific aims of this thesis were:

- ✓ Development and validation of fluorescence-based biochemical assay for HTS of the Dicer cleavage activity.
- ✓ Development and validation of cell-based reporter assays for monitoring the RNA silencing activity in HTS.
- ✓ HTS of the unique selection of ~30,000 small compounds and initial data analysis.

3 RESEARCH PLAN OVERVIEW

3.1 Research strategy

Our research strategy is to use chemical biology to study and manipulate RNA silencing in mammals. The research goal of the entire project is (i) to provide a set of small compounds allowing for direct stimulation or inhibition of RNA silencing and (ii) to identify crosstalks between RNA silencing and other pathways. The following steps outline the flow of the project (**Fig.11**).

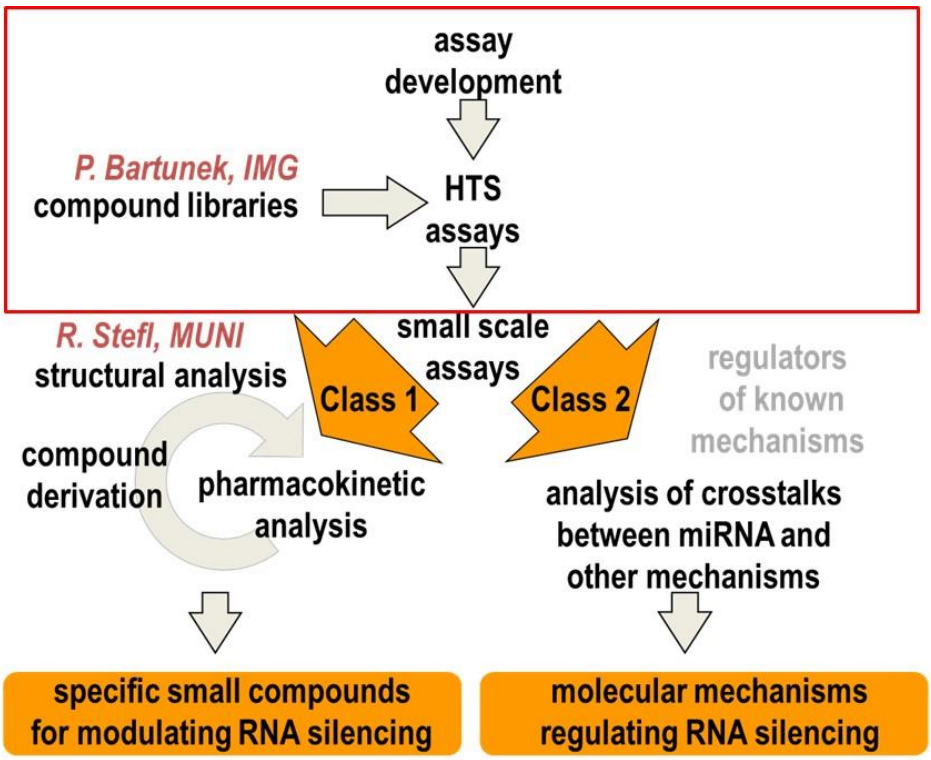

Fig.11: Flowchart of the project. HTS assays will be used (in collaboration with P. Bartunek lab, IMG AS CR, CZ-OPENSCREEN) for screening of ~30,000 compounds. Potential modulators will be further analyzed in small scale assays and divided into two classes. Class 1 compounds (direct regulators) will be studied to define their mode of action and pharmaco-kinetic properties. Lead compounds will be optimized by screening libraries of their derivatives. Compound derivation and synthesis will be performed by M. Hocek and T. Martinu. Structural analysis of interactions with defined domains will be done in collaboration with R. Stefl. Class 2 compounds (annotated regulators of known mechanisms, e.g. signaling, stress response etc.) will be used to define crosstalks between RNA silencing and other cellular pathways. A part of the project covered by this thesis is framed in red.

First, several cell-based reporter assays and one biochemical assay were established and optimized for high-throughput screening (HTS) purposes. Second, the established assays were used for HTS of a unique selection of ~30,000 small compounds in collaboration with P. Bartunek lab at IMG AS CR, CZ-OPENSCREEN. Potential modulators are currently validated. Next, validated candidates will be analyzed in several small scale assays and divided into two classes: (i) Class 1 - putative direct regulators of the RNA silencing and (ii) Class 2 - small compounds affecting the RNA silencing indirectly via targeting other cellular processes, which in turn have impact on RNA silencing. Class 1 compounds will be further studied to define their mode of action and pharmacokinetic properties, and lead compounds will be optimized by screening of their derivates. Structural analysis of potential interactions with defined domains of the key proteins in RNA silencing will be done in collaboration with R. Štefl (MUNI). Class 2 compounds will be used to define crosstalks between RNA silencing and other cellular pathways.

3.2 Assay development

3.2.1 Cell-based assays

The cell-based assays that generated the bulk of HTS data, were developed to monitor endogenous miRNA activity in cells in order to discover both general and miRNA-specific small molecule modifiers of RNA silencing. The principle of the cell-based assay is described in **Fig.12**. The cell-based assays are based on plasmid reporters carrying miRNA binding sites in 3'UTRs **(Fig.12 A, B)**. The principle of the assay is described below. Under normal conditions, endogenous mature miRNAs bind a target sequence on the reporter mRNA and silence it as follows: (i) In case of the reporter containing perfectly complementary binding site(s) ("perfect" reporter), miRNA mediates direct cleavage of the reporter mRNA through AGO2 slicer activity. The minimal requirement for the cleavage is the small RNA bound to AGO2, which form so-called holo-RISC. The perfect reporter thereby reflects the miRNA biogenesis, the efficiency of miRNA loading on AGO2, and the holo-RISC function. (ii) In case of the reporter containing imperfectly complementary binding site(s) (bulged reporter), the central mismatches interfere with short RNA-guided slicer activity of AGO2, and the reporter is repressed by translation repression (Pillai et al., 2005; Schmitter et al., 2006). In addition to AGO and small RNA, this requires additional

accessory proteins in the so-called full-RISC. Thus, the bulged reporter monitors the capability of endogenous miRNAs to induce translational repression by full-RISC and indirect target mRNA degradation on top of miRNA biogenesis. As a result, any interference with miRNA biogenesis or function is detected as an increase in the reporter activity (**Fig.12 A, C**).

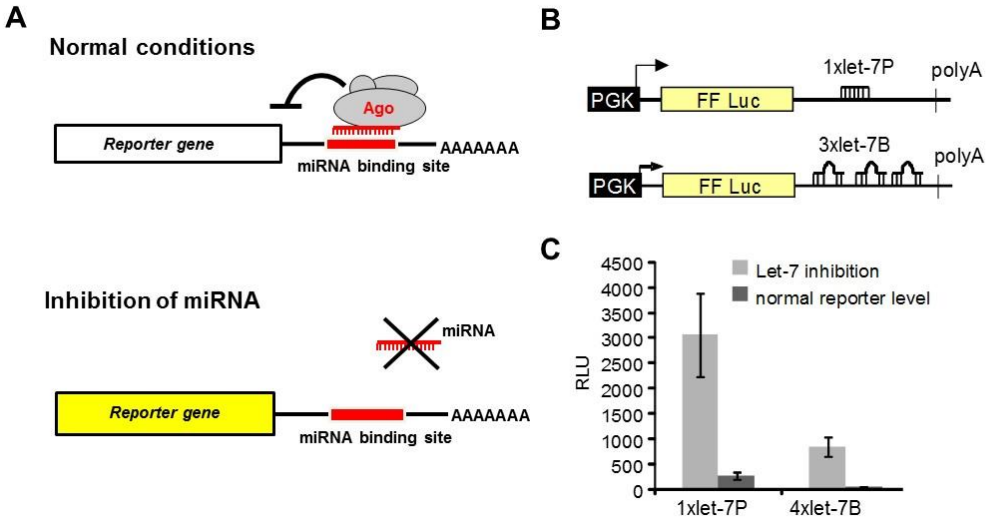

Fig.12: Principle of the cell-based assay. (A) Cell-based assay for quantifying inhibition of the miRNA pathway. The assay is based on the ability of endogenous miRNAs to inhibit the target RNA, the reporter gene carrying binding site(s) for endogenous miRNA in the 3′UTR. Under normal conditions, the reporter is repressed by the effector action of miRNA-loaded RISC, and only basal reporter activity is detectable. Inhibition of miRNA biogenesis or function is detected as an increase in the reporter activity. **(B)** Firefly luciferase reporters carrying perfect (P) and bulged (B) binding sites for let-7 miRNA. **(C)** Relief of reporter repression (luciferase activity) in cells transfected with LNA let-7 family inhibitor.

To obtain optimal reporters, we tested various combinations of (i) promoters (PGK, CMV, SV40, and TK) and poly-A signals, (ii) reporter proteins (EGFP, *Renilla* luciferase (RL) and firefly luciferase (FL)), and (iii) 1-4 bulged or perfect sites for two different miRNAs (let-7, miR-30). These reporters were repressed to different levels and had different sensitivity to inhibition and stimulation of RNA silencing. let-7-targeted reporters were chosen because let-7 is closely associated with pluripotency and differentiation (Bussing et al., 2008; Melton et al., 2010; Viswanathan and Daley, 2010), and finding its specific inhibitors would have a tremendous importance. miR-30 is expressed in both pluripotent and differentiated cells and was selected as its biogenesis has been thoroughly studied (Landgraf et al., 2007; Zeng and Cullen, 2003; Zeng et al., 2002). Reporters were tested in several ways to identify those that would have a robust response to inhibition. During assay optimization, we tested a number of inhibitory approaches (Esau, 2008;

Lakatos et al., 2006; Schmitter et al., 2006) including Dicer and AGO2 knock-downs, plant virus inhibitors p19 and p21 (Dunoyer et al., 2004), locked nucleic acid (LNA) inhibitors from *Exiqon*, or ATPA-18 (Chiu et al., 2005). Finally, stable cell lines expressing the selected reporters were produced and used for HTS.

3.2.2 Florescence-based *in vitro* Dicer cleavage assay

Dicer represents a great target for small compounds. Mammalian RNAi and miRNA pathways are initiated by different RNA molecules but employ a single Dicer producing small RNAs. There are many structural insights into the Dicer function (reviewed in (Jinek and Doudna, 2009)). Dicer is a multidomain protein, and therefore numerous independent modes of modulation are possible. First, autoinhibitory function of the helicase domain (Ma et al., 2008) holds a promise for identifying compounds modulating the Dicer activity via interfering with a substrate binding. Similarly, known structure of Dicer facilitates analysis of interaction of specific compounds with the Dicer PAZ domain. Finally, compounds binding to RNase III domains may interfere with the substrate cleavage.

Activity of Dicer can be monitored *in vitro* by the Dicer cleavage of dsRNA substrate (Zamore et al., 2000). Typically, cleavage assays are based on processing of radiolabeled dsRNA substrates by recombinant Dicer and a detection of cleaved products by electrophoresis (Kolb et al., 2005; Zhang et al., 2002). However, this type of assay is not suitable for HTS. To solve this problem, an assay yielding fluorescence upon cleavage by Dicer (Davies and Arenz, 2006; DiNitto et al., 2010) was developed. Notably, biochemical assays allow for identification of Dicer modulators regardless of their cellular uptake or cytotoxicity, thus enabling a discovery of compounds elusive in cell-based assays.

We developed an assay to monitor the activity of recombinant Dicer by fluorescence as follows (**Fig.13**). As a substrate, we used short (27 bp) perfect RNA duplex containing a 2-nt 3´ overhang at one terminus and a blunt end at the other one. At the blunt end, one RNA strand carries a fluorescent group and the other strand a quencher (**Fig.13**). During the Dicer-mediated cleavage, the 2-nt 3´ overhang is recognized by the PAZ domain, and the cleavage releases a short duplex carrying the fluorophore and the quencher. Subsequent separation of the fluorophore from the quencher can be monitored as fluorescence increasing over time (**Fig.13**). Although it was possible to prepare a substrate resembling a

natural pre-miRNA similarly as previously reported (Davies and Arenz, 2006), we opted for a short (27-nt) RNA duplex, which was easy to synthesize and resembled an artificial extended siRNA structure described earlier (Wu et al., 2003). The sequence of the substrate was derived from a well-characterized human let-7a miRNA, hence allowing for combining our assay with other tools developed for let-7 analysis. To adapt the assay for HTS, we tested several fluorophore/quencher pairs, reaction conditions and volume, concentrations of Dicer and the substrate, and timing of data collection.

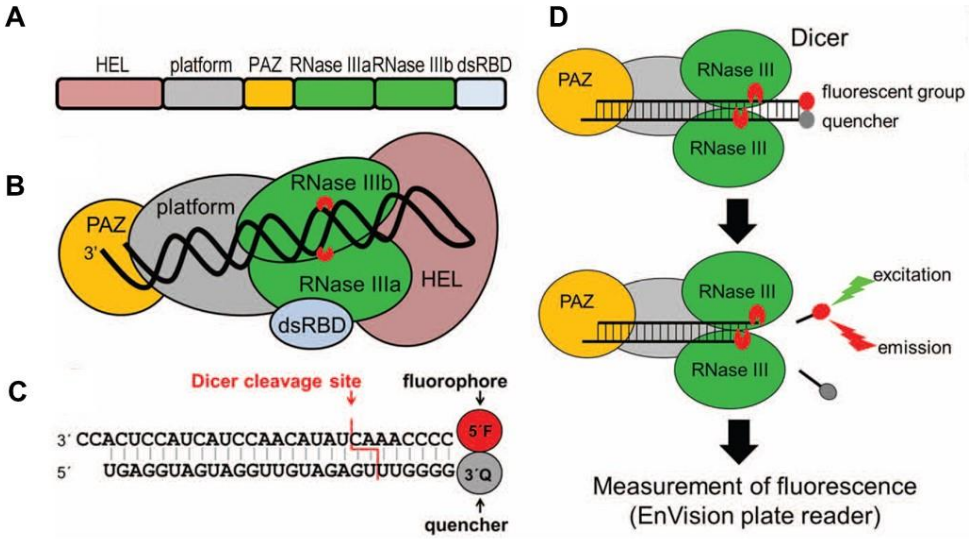

Fig.13: Principle of fluorescence-based *in vitro* Dicer cleavage assay. (**A**) Scheme of domain order in human Dicer protein. HEL, helicase domains; PAZ; dsRBD, double-stranded RNA binding domain. (**B**) A scheme of structural organization of human Dicer and interaction with a pre-microRNA substrate. The scheme is based on available structural data. (Lau et al., 2012) Red "pacmen" indicate active sites of RNase III domains, each of which cleaves one strand of the substrate. (**C**) Dicer substrate for fluorescent cleavage assays. One end contains a 3´ 2-nt overhang, which binds with a high affinity the PAZ domain of the Dicer. The other end of the substrate is blunt and carries a fluorescent group at the 5´ end of one RNA strand and a quencher group at the 3´ end of the other strand. (**D**) The principle of the assay. Fluorescent and quencher group in uncleaved substrate remain in close proximity under assay temperature (37 °C). Dicer binds the 3´ 2-nt overhang with high affinity and cleaves the substrate, producing a short duplex with fluorescent and quencher groups. This short duplex is thermodynamically unstable, resulting in the separation of fluorescent and quencher groups and an increase of fluorescence. Red "pacmen" indicate active sites of RNase III domains.

3.3 Highthroughput screening (HTS)

After assay the establishment and optimization, we performed five HTS of ~30,000 compounds: four (HTS-I – HTS-IV) using cell-based luciferase reporter assays and one (HTS-V) using biochemical fluorescence-based *in vitro* Dicer cleavage assay. All HTS were performed in collaboration with Petr Bartunek group, IMG AS CR, CZ-OPENSCREEN (particularly with David Sedlak), which provided equipment and the

original collection of compounds from 15 libraries including Sigma LOPAC Library, Prestwick Library, NIH Clinical Trial Collection, and several proprietary sublibraries. Our strategy was to generate data allowing for thorough filtering HTS results (see below).

First, we performed a proof-of-concept HTS of ~10,000 compounds to test the feasibility of the screening and to estimate the hit-rate. The screening was performed in HeLa stable cell line carrying the PGK-FL-3xlet-7P reporter containing perfect binding sites for let-7 miRNA (HTS-I). Subsequently, to complement the proof-of- concept HTS and to obtain HTS data from the whole library, we performed HTS of the rest of the library (~20,000 compounds) collection with the same reporter assay (HTS-I). Second, we performed HTS in NIH-3T3 stable cell line carrying the PGK-FL-3xlet-7P reporter containing perfect binding sites for let-7 miRNA (HTS-II) to filter the cell type-specific effects. The data were compared with the data from HTS-I. Third, we performed HTS in HeLa stable cell line carrying the PGK-FL-4xlet-7B reporter containing bulged binding sites for let-7 miRNA (HTS-III) to filter compounds affecting the translation repression (unique in HTS-III) or upstream events (common). Fourth, we performed HTS in HeLa stable cell line carrying the PGK-FL-4xmiR-30B reporter containing bulged binding sites for miR-30 miRNA (HTS-IV) to identify compounds affecting let-7 and miR-30 miRNAs (common regulators) and putative let-7-specific regulators. Finally, we performed kinetic HTS using biochemical fluorescence-based *in vitro* Dicer cleavage assay (HTS-V) to discover potential direct modulators of Dicer activity.

3.4 Compound classification, analysis and further development

3.4.1 Initial HTS data analysis

The goal of the initial round of HTS data mining was to identify compounds ("cherry-picked" compounds) for characterization in secondary assays (**Fig.14**). HTS data were processed using a custom-built searchable database “Chemgen, LIMS”, in house developed in Petr Bartunek group (IMG AS CR, CZ-OPENSCREEN), particularly with help of David Sedlak, who assisted also with normalization and statistical filtering.

First, based on the results from cell-based luciferase reporter assays and compound annotation, compounds were sorted to several groups. The core of the list represented

candidates for general miRNA inhibitors (showing inhibitory activity in all cell-based assays) and let-7 inhibitors (identified in all let-7 assays but not in the miR-30 assay). This core was supplemented by compounds showing activity in HTS-III and HTS-IV (putative general inhibitors of translational repression mediated by miRNAs), any two HTS involving let-7 reporters (weaker candidates for let-7 inhibitors), and HTS-IV and any other HTS (weaker candidates for general miRNA inhibitors). False positives from the cell-based HTS were excluded based on the comparison with the data from the previous cytotoxicity HTS data and HTS of compounds affecting different miRNA-independent firefly reporters. Workflow of compounds analysis and selection is summarized in **Fig.14**.

Next, data from the kinetic HTS using biochemical fluorescence-based *in vitro* Dicer cleavage assay (HTS-V) were analyzed with in-house–developed algorithms and by open source data analytics, reporting and integration platform KNIME (Zurich, Switzerland). To filter false positives and false negatives, several validation assays were performed. Before the data normalization, strongly autofluorescent compounds were filtered out from the analysis as strong autofluorescence prevailing over the fluorescence from the cleavage reaction would impair the data quality. To validate the results of the screen, we will cherry-pick potential candidate compounds and will perform a dose-response validation experiment under the same conditions as those used in the screening. To filter non-specific modulators of the Dicer activity, data from the Dicer screen will be compared with the data from several unrelated enzymatic screens. To filter false positive Dicer inhibitors affecting the Dicer assay by quenching, we will run a standard fluorescent cleavage assay to completion followed by adding putative Dicer inhibitors and monitoring their quenching effects on fluorescence in a completed Dicer assay.

Finally, data from HTS-V will be combined with data from cell-based HTS, and the number of compounds selected for secondary assays will be adjusted according to practical considerations (since downstream assays will be performed in 96- and 384-well plate formats) (**Fig.14**).

3.4.2 Secondary assays

To gain insights into the mechanism of action of individual cherry-picked compounds, several secondary assays (**Fig.14**) will be run to follow two research aims. The first aim is to identify of a small list (<10) of lead compounds, which will form the basis for obtaining efficient miRNA inhibitors and stimulators with low toxicity and good cellular uptake. If needed, lead compounds will be further modified to improve their pharmacokinetic properties and to reduce toxicity (**Fig.14**). Strategies for derivation will be decided either by Michal Hocek (IOCB) or Tomas Martinu (UCT). The second aim will be the investigation of mechanisms regulating the miRNA pathway in mammalian cells. Since many compounds used in HTS have defined effects on the specific signaling or metabolic pathways, data mining should uncover mechanisms regulating the RNA silencing. Although such compounds likely regulate the miRNA pathway indirectly, they will point to specific mechanisms regulating the miRNA pathway, which is of great interest.

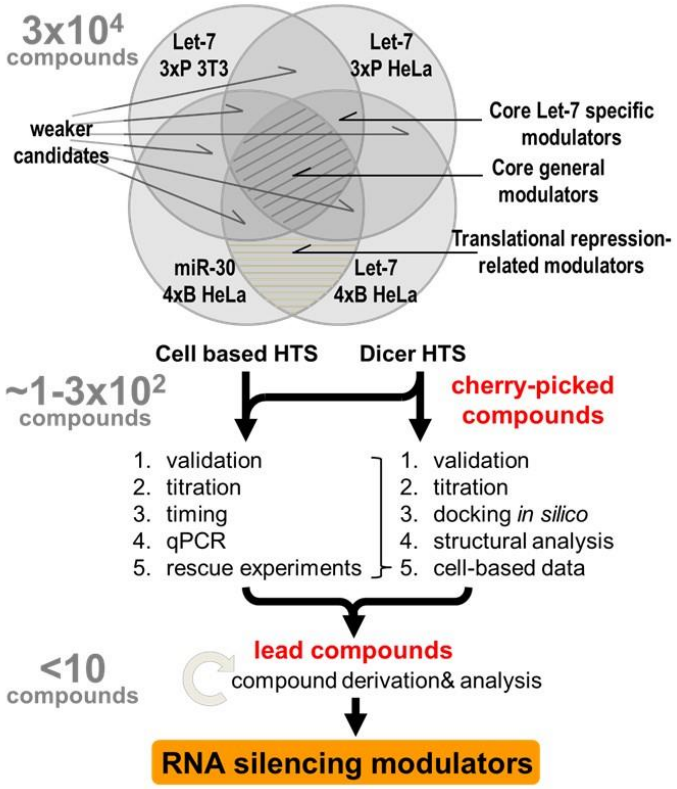

Fig.14: Workflow of Class I compound analysis.

3.4.2.1 Validation assays

The cherry-picked compounds will be assessed using various reporters transiently or stably expressed in cell lines to validate their activity and provide initial kinetic data (concentration and time dependence). The possible application of individual reporters are listed in **Tab.2**. All reporters have already been constructed and are ready to use.

3.4.2.2 Functional assays

To classify the cherry-picked compounds according to their mode of action on RNA silencing, following strategies will be used (**Fig.14**):

(i) ***Fast and slow modulators:*** First, cherry-picked compounds will be sorted according to the time necessary for affecting reporter expression. In case of fast modulators, an early change in the luciferase activity would suggest that regulation occurs directly at the RISC complex as miRNA-loaded effector complexes, already present in cells, are affected. In contrast, delayed change of the luciferase activity would point to the events during miRNA biogenesis and/or to the disruption of some global regulation of the pathway as miRNAs need to be expressed and processed.

(ii) ***Effects on pre-miRNA, pri-miRNA, and mature miRNA levels:*** Next, relative expression of pre-miRNA, pri-miRNA, and mature miRNA will be analyzed by qPCR. Levels of mature miRNA or its precursors will indicate which step of the miRNA biogenesis is affected. Effects of lead compounds will be precisely analyzed by small RNA northern blotting.

(iii) ***Rescue-based classification of inhibitory compounds:*** Cherry-picked compounds with inhibiting properties will be sorted in a cascade of rescue experiments (**Fig.15**). Vectors expressing a minimal pri-miRNA from a ubiquitous promoter are expected to rescue inhibition of the primary transcript production. Expression of a specific ribozyme mimicking pre-miRNA should rescue the inhibition of the microprocessor complex and the upstream events. Transfection of pri-miRNA should rescue the inhibition of the nuclear export and upstream events. Transfection of miRNA mimics should rescue the inhibition of the Dicer cleavage and upstream events, except the RISC loading. Dicer-independent miRNAs would rescue Dicer processing

and perhaps the RISC loading. Effects on bulged reporters would indicate the inhibition of either cleavage or translational repression (**Fig.15**)

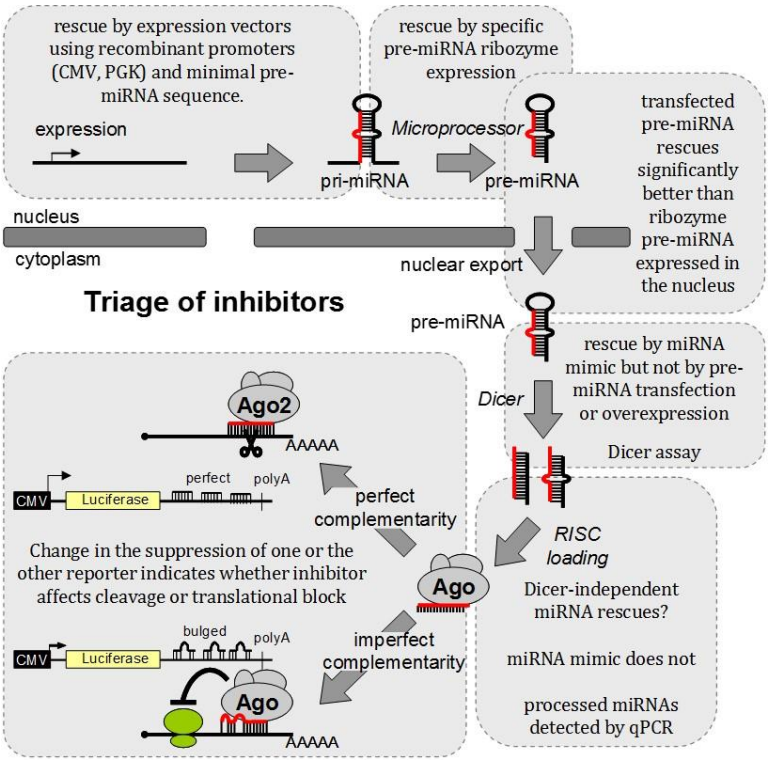

Fig.15: A scheme of rescue experiments. Grey rectangles represent potential places of action of inhibitory compounds and how they can be determined. Vectors expressing a minimal pri-miRNA from a ubiquitous promoter should rescue inhibition of production of the primary transcript. Expression of a specific ribozyme mimicking pre-miRNA should rescue inhibition of the microprocessor complex and upstream. Transfection of pri-miRNA should rescue inhibition of nuclear export and upstream. Transfection of miRNA mimics should rescue inhibition of Dicer cleavage and upstream but not RISC loading. Dicer independent miRNAs will rescue Dicer processing and perhaps RISC loading. Effects on bulged reporters will indicate inhibition of either cleavage or translational repression.

3.4.2.3 Biochemical assays

Two biochemical assays will be used for analysis of the lead compounds: (i) ***Radioactive Dicer assay:*** The best Dicer regulators identified in the fluorescent Dicer cleavage assay will be analyzed in detail using the established Dicer cleavage assay employing recombinant Dicer and radioactively internally labeled dsRNA substrate (Zhang et al., 2004). This will allow for precise quantification of cleavage products and analysis of cleavage fidelity. (ii) ***RISC loading assay:*** The mechanism of action of selected lead compounds will we characterized in detail using the RISC loading assay that closely recapitulates the mammalian RNAi. The RISC loading assay evolved from the published work of Gregory *et al.* (2005), who isolated the human RISC and showed that it is composed of AGO2, Dicer and TRBP (Gregory et al., 2005). Later, the complex was named the RISC-loading complex (RLC) because of its ability to cleave pre-miRNA and to selectively load a guide miRNA into AGO2 (Maniataki and Mourelatos, 2005). MacRae *et al*. (2008) showed that RLC reconstituted from human recombinant proteins *in vitro* has similar activity as the endogenous complex (MacRae et al., 2008). The RLC assay

has two steps: first, equal amounts of RLC and single-stranded 21-nt guide RNA are incubated together, allowing the loading of AGO2 to the guide RNA. Second, a 37-nt long, 5´end ^{32}P-radiolabeled cognate RNA is added to the reaction and cleaved. The cleaved RNA is resolved by electrophoresis and quantified (MacRae et al., 2008).

3.4.2.4 Analysis of crosstalks with other pathways

The library used for HTS combines an original collection of ~30,000 compounds obtained from 15 libraries including Sigma LOPAC Library (a collection of 1,280 characterized compounds), Prestwick Library (a unique collection of 1,119 bioactive compounds), NIH Clinical Trial Collection, and several proprietary libraries. High collection diversity and functional annotation of some compounds will enable us to discover compounds modulating RNA silencing both directly and indirectly via targeting signaling, stress response and other cellular processes, which in turn have impact on RNA silencing. Such indirect modulators of RNA silencing will be used to define crosstalks between RNA silencing and other cellular pathways.

The candidate pathways will be selected based on the results from HTS, secondary assays, and compound annotation. The potential modulators of particular signaling or metabolic pathways will be validated by examining the miRNA activity in cells, where the particular pathway will be stimulated or inhibited. This validation will involve inhibition and stimulation of the pathway by antagonists and agonists and its inhibition by RNAi. Next, the mechanism by which the signaling affects the miRNA pathway or expression of its components will be determined.

The stress response has been linked to inhibition of RNAi and miRNA pathways (Bhattacharyya et al., 2006; Detzer et al., 2011). Therefore, compounds which relieve the let-7-mediated repression of the reporter by inducing the stress will be determined using the microscopic analysis of stress granules and P-bodies in cells treated with putative miRNA inhibitors identified in HTS. For a thorough analysis of stress granules and P-bodies in a 96-well format, ScanR high-throughput microscopy will be applied.

exp. #	reporter	cells	note	usage in secondary assays
1.	pEGFP-SpA-PGK-FL-3xlet-7P-BGHpA	HeLa cell lines	reporter cell lines used in HTS	initial HTS data validation in dose-response and time dependent experiments
	pEGFP-SpA-PGK-FL-4xlet-7B-BGHpA			
	pEGFP-SpA-PGK-FL-4xmiR-30B-BGHpA			
	pEGFP-SpA-PGK-FL-3xlet-7P-BGHpA	NIH-3T3 cell line		
2.	pRep-G418_SV40pA-3xlet-7P-RL←PGK-spA-CMV→FL-BGHpA	HeLa cell lines	bidirectional reporters with miRNA binding sites used HTS, experimental RL reporter	additional HTS data validation using bidirectional reporters enabling precise data normalization, usage of RL as experimental reporter enable us to filter possible modulators of FF activity
	pRep-G418_SV40pA-4xlet-7B-RL←PGK-spA-CMV→FL-BGHpA			
	pRep-G418_SV40pA-4xmiR-30B-RL←PGK-spA-CMV→FL-BGHpA			
3.	pRep-G418_SV40pA-3xlet-7P-invert-RL←PGK-spA-CMV→FL-BGHpA	HeLa transiently	bidirectional reporters with miRNA binding sites in inverted (non-functional) direction	additional HTS data validation - filtering of non-specific compounds
	pRep-G418_SV40pA-4xlet-7B-invert-RL←PGK-spA-CMV→FL-BGHpA			
	pRep-G418_SV40pA-4xmiR-30B-invert-RL←PGK-spA-CMV→FL-BGHpA			
4.	pEGFP-SpA-PGK-FL-4xlet-7M-BGHpA	HeLa transiently	reporters with mutated binding sites for miRNA	additional HTS data validation - filtering of non-specific compounds
	pEGFP-SpA-PGK-FL-4xmiR-30M-BGHpA			
5.	pEGFP-SpA-PGK-FL-3xlet-7P-BGHpA	U20S cell lines	U2OS reporter cells	filtering HTS data using additional cell line (U2OS)
	pEGFP-SpA-PGK-FL-4xlet-7B-BGHpA			
6.	pEGFP-SpA-PGK-FL-1xmiR-24P-BGHpA	HeLa cell lines	reporters with miR-24 binding sites	filtering HTS data using additional miRNA (miR-24)
	pEGFP-SpA-PGK-FL-4xmiR-24B-BGHpA			

Tab.2: Possible usage of available reporter plasmids in validation assays

4 MATERIALS AND METHODS

4.1 Preparation of recombinant Dicer

4.1.1 Generating the recombinant bacmid

4.1.1.1 Preparation of DH10Bac E. coli chemically competent cells

Lysogeny broth (LB) medium supplemented with kanamycin (50 μg/ml) and tetracycline (10 μg/ml) ($LB^{Kan, Tet}$) was inoculated with a single DH10Bac colony, and the culture was shaken vigorously at 37 °C overnight. To bring the cells into the log phase of growth, 4 ml of saturated overnight culture were inoculated into 400 ml of fresh $LB^{Kan, Tet}$ and shaken vigorously at 37 °C until OD_{600} reached 0.4. Cells were centrifuged 10 min at 4,150 g and 4 °C, and the pellet was washed twice with 10 ml of cold 50 mM $CaCl_2$ solution. After the second wash, the bacterial suspension was incubated for 30 min on ice. Finally, pelleted cells were resuspended in 2 ml of cold 50 mM $CaCl_2$ supplemented with 20% glycerol, aliquoted in pre-chilled sterile polypropylene tubes and stored at -80 °C.

4.1.1.2 Transformation of DH10Bac E. coli cells by heat-shock

DH10Bac *E.coli* chemically competent cells were thawed on ice. A 200 μl aliquot was gently mixed with 1 μg of pDest8-Dicer-6His donor vector and incubated for 30 min on ice. Cells were heat-shocked at 42 °C for 45 s and chilled on ice for 2 min. To recover the cells, S.O.C. medium (900 μl) equilibrated to room temperature was added to the transformed cells, and the suspension was shaken at 37 °C for 2 h. Finally, the cell suspension was inoculated onto LB plates containing kanamycin (50 μg/ml), gentamicin (7 μg/ml), tetracycline (10 μg/ml), X-gal (100 μg/ml) and IPTG (Isopropyl β-D-1-thiogalactopyranoside, 40 μg/ml), and plates were incubated at 37 °C for 48 h.

4.1.1.3 Isolation of recombinant bacmid DNA

LB medium (5 ml) supplemented with kanamycin (50 μg/ml), tetracycline (10 μg/ml), and gentamicin (7 μg/ml) ($LB^{Kan,Tet,Gen}$) was inoculated with a single DH10Bac colony, and the culture was shaken vigorously overnight at 37 °C. 5 ml of saturated overnight culture were inoculated into 500 ml of $LB^{Kan,Tet,Gen}$ and shaken vigorously overnight at 37 °C. Recombinant bacmid DNA was isolated using NucleoBondXtraMidi kit (*Machery-Nagel*) according to the manufacturer's recommendations.

4.1.2 Production of the recombinant baculovirus

4.1.2.1 Transfection of insect cells using calcium phosphate method

Sf9 insect cells were cultured in TNM-FH insect medium (*Applichem*) supplemented with 10% fetal calf serum (FCS, *Sigma-Aldrich*), penicillin (100 U/ml, *Life Technologies*), and streptomycin (100 mg/ml, *Life Technologies*) in humidified chamber. Sf9 cells (approximately 20% confluent at the day of transfection) were transfected with recombinant bacmid DNA using a standard calcium phosphate method. The transfection mixture was prepared by mixing 2.5 µg bacmid DNA with 25 µl 2.5 M $CaCl_2$ and 225 µl H_2O. This DNA/$CaCl_2$ pre-mix was added dropwise into 250 µl 2xHEBS buffer (137 mM NaCl, 6 mM glucose, 5 mM KCl, 0.7 mM Na_2HPO_4, 20 mM HEPES) yielding 500 µl of the final transfection mixture. The transfection mixture was incubated for 30 min at room temperature and then added dropwise to cells. TNM-FH culture medium was changed 4 h post-transfection. Then, cells were cultured at 28 °C for 5 days. The protocol was optimized for transfection in a 6-well plate format. The huDicer-HisC expression in Sf9 cells was analyzed by electrophoresis on 6% SDS-PAGE gel followed by Coomassie Brilliant Blue-R250 (CBB-R250) staining and western blotting.

4.1.2.2 Isolation and amplification of P1 baculoviral stock

Before infection, Sf9 insect cells were seeded at concentration 4 x 10^3 cells per 10 cm dish (~20% confluence). After cell attachment (~2 h), the medium was removed and cells were infected with ~10^7 PFU of a baculovirus (~1 ml of P1 viral stock) for 1 h at room temperature with continuous shaking. Next, 10 ml of fresh complete TNM-FH medium were added, and cells were incubated at 28 °C for 48-96 h (P2 viral stock). The viral titer was increasing with prolonged incubation, however, the quality of infected cells was compromised at the same time.

4.1.2.3 Small-scale infection of Sf9 insect cells with baculovirus - monolayer culture

Before infection, Sf9 insect cells were seeded at concentration 4 x 10^3 cells per 10 cm dish (~20% confluence). After attaching cells to a bottom of a culture plate (after ~2 hours), the medium was removed and the cells were infected with ~10^7 PFU of a baculovirus (~1 ml of P1 viral stock) for 1 h at room temperature with continuous shaking. Next, 10 ml of fresh complete TNM-FH insect medium were added, and cells were incubated at 28 °C for 48-96 hours (P2 viral stock). The viral titer was increasing with

prolonged incubation, however, the quality of infected cells was compromised at the same time.

4.1.2.4 Viral Plaque Assay

The baculovirus from the P2 viral stock was cloned using a viral plaque assay. Sf9 insect cells were seeded onto 6 cm dish one day before experiment to reach 30-40% confluence. Cells were infected with 500 µl of the P2 viral stock in dilutions 10^{-2}, 10^{-4}, 10^{-5}, 10^{-6} and 10^{-7} and shaken for 1 h at room temperature to expand the infection. Next, the viral inoculum was removed, and cells were overlaid with 4 ml 1.5% SeaPlaque agarose (*Lonza*) in the complete TNM-FH insect medium warmed to 40 °C. To create plaques, cells were incubated at 28 °C for 7 days. Plaques were counted under a microscope, and the largest plaques collected and used for a new infection of Sf9 cells to amplify the virus clone. The huDicer-HisC expression in Sf9 cells was analyzed by electrophoresis on 6% SDS-PAGE gel followed by CBB-R250 staining and western blotting.

4.1.2.5 Cells lysis

Infected Sf9 cells were collected using a cell scarper, washed with cold PBS containing 2 mM phenylmethanesulfonylfluoride (PMSF, *Sigma-Aldrich*) and lysed in 100 µl of whole cell lysis buffer (PBS, 10% glycerol, 0.5 mM EDTA, 0.2% Triton X-100) supplemented with EDTA-free protease inhibitors mixture (*Roche*) and 2 mM PMSF. Lysates were incubated for 30 min at 4 °C with occasional shaking. Lysates were cleared by centrifugation at 13, 000 g and 4 °C for 10 min, and supernatants were kept at -80 °C until further processing.

4.1.3 Purification of human Dicer-HisC from insect cells

4.1.3.1 Small-scale Dicer-HisC purification – I.

To optimize the purification conditions, three different sets of Dicer purification buffers were prepared. The set "A" was prepared for isolation of huDicer6xHisC under native conditions and contained binding/washing buffer "B/W_a" (20 mM Tris-HCl, pH 7.5, 800 mM NaCl, 1 mM $MgCl_2$, 10% glycerol, 0,5% Triton X-100) and two elution buffers - „E_a-imidazol" (B/W_a + 150 mM imidazol) and E_a-EDTA (B/W_a + 50 mM EDTA). The set "B" was prepared for isolation of huDicer6xHisC under reduction conditions and contained binding/washing buffer "B/W_b" ("B/W_a" + 5 mM β-

mercaptoethanol) and two elution buffers - „E_b-imidazol“ (B/W_b + 150 mM imidazol) and E_b-EDTA (B/W_b + 50 mM EDTA). The set “C” contained binding/washing buffer “B/W_c” (50 mM sodium phosphate, 800 mM NaCl) and two elution buffers - E_c-imidazol (B/W_c + 150 mM imidazol) and E_c-EDTA (B/W_c + 50 mM EDTA).

Sf9 cells (~10^9) infected with recombinant huDicer-HisC baculovirus #2-8 and grown at 28 °C in TNM-FH insect medium supplemented with 10% FCS *(Life Technologies)*, 100 U/ml penicillin *(Life Technologies*), and 100 mg/ml streptomycin *(Life Technologies)* were harvested 72 h after infection. Cells were gently pelleted by centrifugation and divided into three batches, which were consecutively processed as follows: cells were resuspended in 10 ml of ice-cold, EDTA-free protease inhibitor mixture *(Roche)*, and 2 mM PMSF *(Sigma-Aldrich)* supplemented binding/washing buffer B/W_a, B/_b, or B/_c and incubated 30 min on ice. Cells were disrupted by five passages through a 20G needle followed by five passages through a 26G needle. The lysate was cleared by centrifugation at 12,000 g for 1 h at 4 °C, and the protein concentration was determined using Bio-Rad Protein Assay (sample A = 3.5 mg/ml, sample B = 8 mg/ml, sample C = 5 mg/ml). Each sample of cell lysate (30 mg) was applied on 1 ml of Binding/Washing buffer-equilibrated Talon^{TM} affinity resin *(BD Biosciences Clontech, Palo Alto, CA)*, incubated 90 min at 4 °C/shaking and then washed five times, 15 min at 4 °C with 1 ml of binding/washing buffer. The proteins bound to the resin were eluted two times, 15 min at 4 °C with ~ 100 µl of imidazol elution buffer and subsequently 15 min at 4 °C with ~100 µl of EDTA elution buffer. The purity of recovered Dicer was analyzed by electrophoresis on 6% SDS-PAGE gel followed by the CBB-R250 staining and western blotting using (i) primary Dicer 349 rabbit polyclonal antibody (1:5,000) and secondary goat anti-rabbit (IgG H+L), horseradish peroxidase (HRP)-conjugated (1:15,000) antibody and (ii) mouse monoclonal anti-polyHistidine Peroxidase Conjugate antibody (1:2,000; *Sigma-Aldrich*).

4.1.3.2 Small-scale Dicer-HisC purification – II.

The Sf9 insect cells (~10^9) infected with recombinant huDicer-HisC baculovirus #2-8 and harvested 72 h after infection were gently pelleted by centrifugation and resuspended in 30 ml of ice-cold binding buffer (20 mM Tris-HCl, pH 7.5, 100 mM NaCl, 1 mM $MgCl_2$, 10% glycerol, 0,5% Triton X-100) supplemented with EDTA-free protease inhibitor mixture *(Roche)*, and 2 mM PMSF *(Sigma-Aldrich)*. Subsequently, the cells were lysed as

described in 4.1.3.1. The cell lysate (250 mg) was applied on 3 ml of binding buffer-equilibrated Talon™ affinity resin *(BD Biosciences Clontech, Palo Alto, CA)*, incubated for 2 h at 4 °C with continuous shaking and washed five times alternately with 20 ml of binding buffer and washing buffer (binding buffer with 800 mM NaCl). The proteins bound to the resin were eluted with 10 ml of elution buffer (binding buffer with 150 mM imidazole and 50 mM EDTA). Fractions containing Dicer were poooled and dialysed in 10K MWCO Slide-A-Lyzer Dialysis Cassettes *(Thermo Scientific)* against 1 l of dialysis buffer (20 mM Tris-HCl, pH 7.5, 100 mM NaCl, 1 mM $MgCl_2$, 50% glycerol and 0.1% Triton X-100) overnight. All purification steps were carried out at 4 °C. The proteins in dialysis buffer were stored at -80°C. The purity and concentration of recovered Dicer was verified by electrophoresis on 6% SDS-PAGE gel and visualization by CBB-R250 staining and by western blotting using primary Dicer 349 polyclonal rabbit antibody (1:5,000) and secondary goat anti-rabbit (IgG H+L), HRP-conjugated (1:15,000) antibody.

4.1.3.3 Large-scale infection of Sf9 insect cells with baculovirus - suspension culture

50,000,000 of Sf9 cells grown in 40 ml of TNM-FH medium supplemented with 0.1% pluronic (*Sigma-Aldrich*) were infected with ~5 x 10^7 PFU of recombinant baculovirus. Cells were grown in a conical flask, stirring continuously at 28 °C for 72 h.

4.1.3.4 Large-scale human Dicer-HisC purification

Infected cells were gently pelleted by centrifugation and divided into eight batches. Pellets were resuspended in 20 ml of ice-cold binding buffer (20 mM Tris-HCl, pH 7.5, 100 mM NaCl, 1 mM $MgCl_2$, 10% glycerol, 0.5% Triton X-100) supplemented with EDTA-free protease inhibitor mixture, and 2 mM PMSF and disrupted by five subsequent passages through a 20G and 26G needle, respectively. The lysates were cleared by centrifugation at 12,000 g for 1 h at 4 °C. Supernatants were pooled and mixed with 5 ml of binding buffer-equilibrated Talon™ affinity resin (*BD Biosciences Clontech*), washed alternately with binding buffer and washing buffer W800 (supplemented with 800 mM NaCl), then eluted with 10 ml of binding buffer supplemented with 40 mM imidazole. Dicer-containing fractions were pooled and dialysed in 10K MWCO Slide-A-Lyzer Dialysis Cassettes (*Thermo Scientific*) against 1 l of dialysis buffer (20 mM Tris-HCl, pH 7.5, 100 mM NaCl, 1 mM $MgCl_2$, 50% glycerol and 0.1% Triton X-100) overnight. All purification steps were performed at 4 °C. Protein concentration was determined using Bio-

Rad Protein Assay, and dialysed proteins were stored at -80 °C. The purity and concentration of recovered Dicer were analyzed by electrophoresis on 6% SDS-PAGE gel followed by CBB-R250 staining and western blotting.

4.1.3.5 Western blotting

The purified proteins or cell lysate were resolved by 6% SDS-PAGE and semi-dry transferred onto PVDF membrane. The membrane was blocked with blocking buffer (20 mM Tris, pH 7.5, 150 mM NaCl, 0.02% v/v Tween 20, 5% non-fat dry milk) for 30 min rocking at room temperature and incubated with primary antibody* (diluted to blocking buffer) overnight at 4 °C. The excess of the primary antibody was washed three times with blocking buffer (10 min at room temperature) and HRP-conjugated secondary antibody (diluted the blocking buffer was added and rocked for 45 min at room temperature. The excess of the secondary antibody was washed out three times with TTBS buffer (20 mM Tris, pH 7.5, 150 mM NaCl, 0.02% v/v Tween 20), and the signal was developed using SuperSignal West Pico Chemiluminescent Substrate (*Thermo Scientific*). *In case of the mouse monoclonal anti-polyHistidine Peroxidase Conjugate antibody (*Sigma-Aldrich*, 1:2,000), the incubation with secondary HRP-conjugated antibody was omitted.

4.1.3.6 Immuno-dot blot

Protein samples were dropped on a nitrocellulose membrane and processed further as described for western blotting.

4.2 Fluorescence-based *in vitro* Dicer assay

4.2.1 dsRNA substrate preparation

Fluorophore-labeled (2 pmol of each) and quencher–labeled (2 pmol of each) RNA oligonucleotides were mixed with annealing buffer (100 mM NaCl, 50 mM HEPES, pH 7.4) in the final volume of 100 µl. Annealing was performed by heating the mixture at 90 °C for 10 min followed by slow cooling (1 °C/90 s) to 4 °C. The annealed dsRNA was diluted in Dicer assay buffer (30 mM Tris-HCl, pH 8, 50 mM NaCl, 3 mM $MgCl_2$, 0.25% Triton X-100, and 15% glycerol) to the final working concentration.

4.2.2 dsRNA cleavage assay (fluorescence-based in vitro Dicer assay)

The assay was performed in Dicer assay buffer (30 mM Tris-HCl, pH 8, 50 mM NaCl, 3 mM $MgCl_2$, 0.25% Triton X-100, and 15% glycerol) in black, flat-bottom, polystyrene 384-well or 1536-well microplates. The assay was usually performed under single-turnover conditions with Dicer enzyme in molar excess over its substrate. Concentrations of annealed fluorescent dsRNA substrate and concentrations of recombinant Dicer used in particular experiments are indicated in the figure legends in section Results. Samples were incubated at 37 °C under 100% humidity to minimize evaporation. Fluorescence was measured at indicated timepoints using the multilabel reader EnVision (*PerkinElmer*) equipped with a Bodipy TMR optimized filter set for fluorophores Cy5 (excitation filter 647 nm and emission filter 665 nm) and 5(6)-FAM (excitation filter 494 nm and emission filter 519 nm). All experiments were assayed at least in duplicates.

4.2.3 Fractionation of Dicer-cleaved dsRNA substrate

Equal volumes of Dicer-cleaved dsRNA substrate (2 pmol) and 2x RNA Loading Dye (*Thermo Scientific*) were mixed, heated at 96 °C for 3 min and immediately cooled on ice. Samples were resolved by 13.5% polyacrylamide gel containing 7 M urea. The gel was stained with SYBR Gold staining solution (*Life Technologies*) for 1 h at room temperature, protected from light.

4.2.4 Dicer assay-based high-throughput screening (HTS) of chemical libraries

The screened ~ 30,000 compounds were from 15 libraries including Sigma LOPAC Library, Prestwick Library, NIH Clinical Trial Collection, and several proprietary libraries. The libraries were stored in dimethylsulfoxid (DMSO) in 384-well polypropylene plates, and screening was performed on a fully automated robotic platform cell::explorer (*Perkin Elmer*) in a 1536-well format. Recombinant Dicer was diluted to the final concentration of 70 nM in Dicer assay buffer and aliquoted (4 µl per well) into black polystyrene 1536-well plates (*Corning, Inc.*) using Multidrop Combi liquid dispenser (*Thermo Scientific*). The plates were incubated at 4 °C until the screen was initiated. The screening was started by

transferring the compounds from 384-well compound stock plates to 1536-well assay plates using Janus Automated Workstation (*Perkin-Elmer*) integrated to cell::explorer and equipped with 384 Pin tool (*V&P Scientific, Inc.*). Three consecutive transfers of 25 nl of each compound solution were made in order to achieve 15 μM final concentration of the screened compounds. After adding the compounds, each plate was shaken for 30 s using the plate shaker Variomag (*Thermo Scientific*) and incubated for 30 min at 30 °C to allow binding of potential inhibitors to the enzyme. After incubation, 1 μl of 175 nM substrate in Dicer assay buffer was dispensed to each well, the plate was briefly shaken, and fluorescence intensity was recorded with multimode plate reader Envision (*Perkin-Elmer*). The plate was incubated at 30 °C during the screen, and periodic measurements of fluorescent intensity were done every second over the following 25 h.

4.2.5 Dicer assay-based HTS data analysis

Data from the kinetic screen were stored in the internal database and analyzed with the in-house developed algorithms. First, autofluorescent compounds were filtered out, and remaining data were normalized to the background fluorescence of each sample at time=0 h (the first measurement after adding the fluorescent substrate) and to the fluorescence intensity generated by control samples treated with no compounds (these controls were present on each plate in one separate column). Moreover, each row was independently normalized to the control samples to remove artifacts introduced by an uneven performance of individual tubes in Multidrop dispenser. Clustering and diversity analysis of validated hits was performed using JKlustor (JChem 5.11.5, 2013, ChemAxon (http://www.chemaxon.com)).

4.3 Cell culture and transfection

4.3.1 Cell lines

Human HEK293 (ATCC no.: CRL-1573), HeLa (ATCC no.: CCL-2), U2OS (ATCC no. HTB-96), and mouse NIH/3T3 cells (ATCC no.: CRL-1658) were maintained in DMEM (*Sigma-Aldrich*) supplemented with 10% fetal calf serum (FCS, *Sigma-Aldrich*), penicillin (100-U/ml, *Life Technologies*), and streptomycin (100 mg/ml, *Life Technologies*) at 37 °C and 5% CO_2 atmosphere. Insect Sf9 cells (ATCC no.: CRL-1711) were maintained

in TNM-FH insect medium (*Applichem*) supplemented with 10% FCS (*Sigma-Aldrich*), penicillin (100 U/ml, *Life Technologies*), and streptomycin (100 mg/ml, *Life Technologies*) at 28 °C.

4.3.2 Transfections

4.3.2.1 Transfecting cells using TurboFectTM transfection reagent

For delivery of plasmid DNA, cells were plated on 24-well plate, grown to 40% density and transfected using Turbofect Transfection Reagent (*Thermo Scientific*) according to the manufacturer's instructions. The ratio of DNA (µg) to Turbofect transfection reagent (µl) was 1:2 (HeLa cells), 1:1 (HEK-293 and NIH-3T3 cells), and 4:3 (U2OS cells). Cells were analyzed 48 h after transfection.

4.3.2.2 Transfecting cells using Lipofectamine® 2000 Transfection Reagent

For transfections of miRNA antagomirs and miRNA mimics, cells were plated on a 24-well plate, grown to 80% density and transfected using Lipofectamine® 2000 Transfection Reagent (*Life Technologies*) according to the manufacturer's instructions. Cells were analyzed 48 h after transfection.

4.3.2.3 Transfecting cells using Oligofectamine™ Transfection Reagent

For transfections of siRNAs, cells were plated on a 24-well plate, grown to 40% density and transfected using Oligofectamine™ Transfection Reagent (*Life Technologies*) according to the manufacturer's instructions. Cells were analyzed 48 h after transfection.

4.3.3 Establishing stable cell lines

Cells were plated on a 6-well plate, grown to 40% density and transfected using Turbofect transfection reagent. Transfected cells were cultured for 48 h and subsequently selected using puromycin (2 µg/ml) or G418 (800 µg/ml) for additional one or two weeks, respectively. During the selection, resistant cells containing the reporter outgrew non-transfected cells, resulting in the polyclonal population of stably expressing cells (here referred to as pool), which was frozen and kept at -80 °C. Individual clones were selected from each pool. The best performing clone was selected and used in subsequent experiments.

4.4 Flow cytometry

Cells stably expressing pCagEGFP.puro_3xlet-7perfect or pCagEGFP.puro_3xlet-7perfect_invert reporter were plated in 24-well plates and transfected with appropriate DNA. Cells were collected 48 h post-transfection and analyzed using LSRII cytometer (*BD Bioscience*). Data analysis was performed using FlowJo software (*Treestar, Inc.*).

4.5 Bioluminiscence assays

4.5.1 Dual-luciferase reporter assay

Transfected cells grown in 24-well plates were collected 48 h post-transfection, washed with PBS and lysed in 150 µl of Passive Lysis Buffer (*Promega*). Luciferase reporter activity was assessed in 5 µl aliquots using the Dual-Luciferase Reporter Assay (*Promega*) according to the manufacturer's instructions. Luminiscence intensity was measured by Modulus Microplate Multimode Reader (*Turner Biosystems*). Data were normalized to the total protein amount in lysates measured by Bio-rad protein assay (*Bio-Rad*) according to the manufacturer's instructions. Final data were normalized to control transfection.

4.5.2 Validation stable reporter cell lines before pilot HTS

Final analysis of selected reporter cell lines was performed during 5 days. The first day the cells were seeded into 6-well plate at concentration 3.6 x 10^5 HeLa cells/well or 4.5 x 10^5 U2OS cells/well. The second day, the cells were transfected with let-7 family specific antagomirs (*Exiqon*). The third day, the transfected cells were reseeded into 384-well plate at concentration 10,000 cells/well (400 cells/25 µl). The following two days the cells were incubated at 37 °C and 5% CO_2 in humidified atmosphere. Subsequently, the firefly luciferase activity was determined using ONE Glo Luciferase assay system (*Promega*) (for technical details, see chapter **4.5.3.1**), and the *Renilla* luciferase activity was determined using Renilla Glo Luciferase assay system (*Promega*). Luminiscence was measured on EnVision plate reader (*PerkinElmer, Inc.*) using 1 s integration of the luminiscent signal.

4.5.3 Luciferase-based HTS of a chemical library

4.5.3.1 HTS

At the day of the experiment, the selected stable reporter cell lines were harvested into phenol red-free DMEM culture media and diluted to concentration 200 cells/µl. A 25 µl aliquot of the cell suspension was dispensed to white polystyrene 384-well plates (*Corning, Inc.*) by Multidrop Combi liquid dispenser (*Thermo Scientific, Inc.*), and subsequently the compounds were added as described for Dicer HTS assay. The final concentration of the screened compounds was 1 µM. To dissolve the compounds in the medium, each plate was shaken for 30 s using the plate shaker Variomag (*Thermo Scientific*) and then incubated at 37 °C and 5% CO_2 in humidified atmosphere for 48 h. The luciferase activity was determined using One-Glo Luciferase assay system (*Promega*). Briefly, each assay plate removed from the incubator was left at room temperature for 15 min. A 25 µl aliquot of One-Glo reagent, diluted with ddH_2O at ratio 1:3, was dispensed to each well using Multidrop Combi. The assay plate was shaken vigorously for 5 min and then was left on the bench for 10 min before luminiscence was recorded. Luminiscence was measured on EnVision plate reader (*PerkinElmer, Inc.*) using 1 s integration of the luminiscent signal.

4.5.3.2 Data processing and hits identification

Data were stored on the remote server together with information about the position of each sample on the plate to enable linking of corresponding compounds with the database of compounds. Data were normalized using B-score normalization algorithm (Brideau et al., 2003) to remove (i) artifacts arising from the location of the sample on the microtiter plate such as the edge effect or (ii) artifacts arising from the systematical errors introduced by the automated devices used in the HTS process such as a row and a column effect. Samples with values higher than 5x B-score value (for potential inhibitors of RNA silencing) or lower than -5x B-score value (for potential activators of RNA silencing) were identified as hits.

4.6 Polymerase chain reaction (PCR)

4.6.1 OneTaq PCR from bacterial colonies

PCR reaction (10 µl) was prepared as follows: 2 µl of 5x One*Taq* standard reaction buffer, 2 µl of each 4 µM forward and reverse primer, 0.2 µl of 10 mM dNTPs, 5.8 µl of nuclease-free water, and 0.1 U of One*Taq* DNA polymerase (*New England Biolabs*). A single bacterial colony was picked and reinoculated directly into the PCR reaction and simultaneously streaked on a new LB plate with appropriate antibiotic selection. Thermocycling conditions were set to initial denaturation at 94 °C for 30 s followed by 30 cycles of denaturation at 94 °C for 10 s, annealing at 58 °C for 20 s, and elongation at 68 °C for 1 min. The final DNA extension was performed at 68 °C for 5 min.

4.6.2 Standard Taq PCR

Standard DNA amplification of templates shorter than 5 kb was performed using *Taq* DNA polymerase (*Thermo Scientific*). Since this enzyme exhibits deoxynucleotidyl transferase activity, which frequently results in the addition of an extra adenine at the 3'-end of PCR products, the *Taq* DNA polymerase was also used for subsequent TOPO TA cloning (*Life Technologies*) of PCR products according to the manufacturer´s recommendations. The *Taq* PCR reaction (25 µl) was as follows: 2.5 µl 10x *Taq* buffer, 1.5 µl 25 mM $MgCl_2$, 1 µl 50% DMSO, 0.5 µl of each 30 µM forward and reverse primers, 0.5 µl 12.5 mM dNTPs, 1 ng–1 µg of template DNA, 0.5 U of *Taq* DNA polymerase and nuclease-free water to final volume of 25 µl. Thermocycling conditions were set to initial denaturation at 95 °C for 5 min, followed by 25-40 cycles of denaturation at 95 °C for 30 s, annealing at 56-68 °C (based on primers Tm) for 1 min, and elongation at 72 °C for 1 min/kb. The final extension was performed at 72 °C for 3 min.

4.6.3 High Fidelity *Pfu* PCR

Pfu DNA polymerase (*Thermo Scientific*) with a proofreading activity was used whenever high fidelity was necessary for subsequent successful processing of PCR products, e.g. the amplification of DNA insert for molecular cloning into pJet plasmid (*CloneJET PCR Cloning Kit, Thermo Scientific*). The *Pfu* PCR reaction (25 µl) was as

follows: 2.5 µl of *Pfu* polymerase 10x buffer with $MgSO_4$, 0.5 µl of each 30 µM forward and reverse primers, 0.5 µl 12.5 mM dNTPs, 1 ng-1 µg of template DNA, 1.25 U of *Pfu* DNA polymerase, and nuclease-free water to 25 µl. The optimized thermocycling conditions were as follows: initial denaturation at 95 °C for 1 min, followed by 25-30 cycles of denaturation at 95 °C for 30 s, annealing at 56-68 °C (based on primers Tm) for 30 s, and elongation at 68 °C for 90 s. The final extension was performed at 68 °C for 3 min.

4.7 Molecular cloning

4.7.1 Annealing of ssDNA oligonucleotides

To prepare dsDNA insert for cloning, 3 µg of each sense and antisense DNA oligonucleotide were mixed with annealing buffer (100 mM NaCl, 50 mM HEPES, pH 7.4) in the final volume of 50 µl. The annealing was performed by heating the mixture to 90 °C for 10 min followed by a slow (1 °C/90 s) cooling to 4 °C.

4.7.2 Plasmid cloning

Plasmids used for cloning were isolated using GeneJET Plasmid Miniprep Kit (*Thermo Scientific*) according to the manufacturer´s recommendations. Concentration of plasmid DNA was determined using NanoDrop ND-1000 Spectrofotometer (*Thermo Scientific*). One µg of plasmid DNA was digested with 10 U of appropriate restriction enzyme for 1 h at 37 °C. If necessary, plasmid DNA was dephosphorylated by 1 U of Shrimp Alkaline Phosphatase (SAP; *Thermo Scientific*) for 1 h at 37 °C, followed by deactivation of SAP for 15 min at 65 °C. Digested plasmid was resolved by 1% agarose gel in LB buffer (10 mM lithium-borate buffer, pH 8.5) and DNA was extracted from the gel using GeneJET Gel Extraction Kit (*Thermo Scientific*) according to the manufacturer´s recommendations. If gel electrophoresis was not necessary, plasmid DNA was directly purified from the restriction reaction using GeneJET PCR Purification Kit (*Thermo Scientific*) according to the manufacturer´s recommendations. Plasmid DNA (0.5 µg) and DNA insert (plasmid:insert ratio 1:3) were ligated using 2.5 U of T4 ligase (*Fermentas*) for 1 h at room temperature. A 2 µl aliquot of ligation mixture was added to 50 µl of chemically competent *E. coli* cells (TOP 10, *Life Technologies*), and the mixture was incubated for 30 min on ice. Cells were submitted to 45 s lasting heat shock at 42 °C, followed by 2-min

incubation on ice. Transformed cells were transferred to LB medium, vigorously shaken for 1 h at 37 °C, and plated on LB agar plates supplemented with appropriate selection antibiotics (ampicillin or kanamycin). After overnight incubation at 37 °C, individual colonies were picked from the plate and verified for the presence of desired insert by sequencing.

4.8 Construction of reporter plasmids

4.8.1 Construction of EGFP-based reporter plasmids

First, forward (MCS_Insert_Fwd) and reverse (MCS_Insert_Rev) oligonucleotides representing multiple cloning site providing restriction sites necessary for the following cloning steps were annealed and subcloned into BglII and AgeI sites of pEGSH.puro plasmid yielding pPuro plasmid. Next, 1xlet-7P forward (1xlet-7P_Fwd) and 1xlet-7P reverse (1xlet-7P_Rev) oligonucleotides, representing the 1xlet-7P binding site, were annealed and subcloned into BglII site of pCX-EGFP plasmid, yielding pCX-EGFP-1xlet-7P and pCX-EGFP-1xlet-7P_invert plasmids. The proper orientation was checked by sequencing. Finally, expression cassettes were cut out by SalI and HindIII and transferred into pPuro plasmid, yielding final pCagEGFP.puro_1xlet-7P and pCagEGFP.puro_1xlet-7P_invert plasmids. Oligonucleotides used for cloning are listed in **Tab.3/1** and **Tab.3/2**. EGFP-based reporter plasmids carrying 2xlet-7P, 3xlet-7P, and 4xlet-7B binding sites were cloned using the similar strategy **(Tab.4)**.

4.8.2 Construction of bidirectional luciferase-based reporters with G418 resistance

pRep-G418_SV40pA-RL←PGK-spA-CMV→FL-BGHpA reporter plasmid was prepared in six following steps: (i) *pEGFP_FL_BGHpA:* BGHpA sequence was PCR-amplified from pcDNA3.1(-) plasmid using BGH_Fwd_XhoI and BGH_Rev_AgeI_AflII primers and digested using XhoI and AflII. The coding sequence for firefly luciferase was PCR-amplified from pGL4.10 plasmid using pGL_Fwd_seq and FL_Rev_NheI-BamHI-SalI primers and digested using HindIII and SalI. Both amplified sequences were inserted into HindIII and AflII sites of pEGFP-N2 plasmid. (ii) *pEGFP-CMV-FL-BGHpA:* CMV promoter sequence was amplified from pcDNA3.1 (-) plasmid using CMV_Fwd_AseI and

CMV_Rev_HindIII primers and subcloned into HindIII and AseI restriction sites of pEGFP_FL-BGHpA plasmid. (iii) *pEGFP_spA-CMV-FL-BGHpA:* synthetic polyA signal (SpA) sequence was PCR-amplified from pGL4.10 plasmid using spA_Fwd_AseI_XhoI and spA_Rev_NdeI primers and subcloned into AseI restriction site of pEGFP-CMV-FL-BGHpA plasmid. Proper orientation was checked by sequencing. (iv) pEGFP_RL_*SV40pA:* SV40pA sequence was amplified from pcDNA3.1(-) plasmid using SV40pA_Fwd_XhoI and SV40pA_Rev_SalI-AseI primers and digested using XhoI and AseI. The coding sequence for Renilla luciferase was PCR-amplified from phRL-SV40 plasmid using RL_Fwd_NotI and RL_Rev_XbaI-BglII-SalI primers and digested using NotI and SalI. Both amplified sequences were inserted into AseI and NotI sites of pEGFP-N2 plasmid. (v) *pEGFP_PGK-RL-SV40pA:* PGK promoter sequence was amplified from phRL_PGK plasmid using PGK_Fwd_AflII-XhoI and PGK_Rev_NotI primers and subcloned into NotI and AflII sites of pEGFP_RL-SV40pA. pEGFP_TK-RL-SV40pA: TK promoter sequence was amplified from phRL-TK plasmid using TK_Fwd_AflII-XhoI and TK_Rev_NotI primers and digested using NotI and XhoI. Subsequently, the TK promoter sequence was combined with pEGFP-C1 plasmid digested with AseI and XhoI and sub-cloned into NotI and AseI sites of pEGFP_RL-SV40pA plasmid. (vi) *pRep-G418_SV40pA-RL←PGK-spA-CMV→FL-BGHpA:* PGK-RL-SV40pA fragment, obtained from pEGFP_PGK-RL-SV40pA plasmid by AseI and XhoI restriction, was inserted into AseI and XhoI sites of pEGFP_SpA-CMV-FL-BGHpA plasmid. Primers used for cloning are listed in **Tab.3/1** and **Tab.3/2**. Similarly, vectors pRep-G418_SV40pA-RL←CMV-spA-PGK→FL-BGHpA and pRep-G418_SV40pA-RL←TK-spA-PGK→FL-BGHpA were cloned in order to obtain a set of vectors with various combinations of promoters, polyA signals and luciferase reporters (**Tab.5**).

4.8.3 Construction of bidirectional luciferase-based reporters with various miRNA binding site(s)

*pRep-G418_SV40pA-**3xlet-7P**-RL←PGK-spA-CMV→FL-BGHpA:* the 3xlet-7P sites were excised from pCagEGFP.puro_3xlet-7P plasmid with BglII and transferred into BglII site of pRep-G418_SV40pA-RL←PGK-spA-CMV→FL-BGHpA yielding pRep-G418_SV40pA-3xlet-7P-RL←PGK-spA-CMV→FL-BGHpA and pRep-G418_SV40pA-3xlet-7P-invert-RL←PGK-spA-CMV→FL-BGHpA plasmids.

pRep-G418_SV40pA-4xmiR-30B-RL←PGK-spA-CMV→FL-BGHpA: forward (4xmiR-30c_bulge_BglII-Fwd) and reverse (4xmiR-30c_bulge_BglII-Rev) oligonucleotides representing the 4xmiR-30B binding sites were annealed together and subcloned into BglII site of pRep-G418_SV40pA-RL←PGK-spA-CMV→FL-BGHpA, yielding pRep-G418_SV40pA-4xmiR-30B-RL←PGK-spA-CMV→FL-BGHpA and pRep-G418_SV40pA-4xmiR-30B-invert-RL←PGK-spA-CMV→FL-BGHpA. The proper orientation of miRNA binding sites was checked by sequencing. *pRep-G418_SV40pA-RL←PGK-spA-CMV→FL-3xlet-7P-BGHpA*: forward (3xlet-7_Fwd) and reverse (3xlet-7_Rev) oligonucleotides representing the 3xlet-7P binding sites were annealed and inserted into BamHI site of pRep-G418_SV40pA-RL←CMV-spA-PGK→FL-BGHpA. Similarly, additional vectors were cloned in order to obtain a set of vectors with various combinations of promoters, polyA signals, miRNA binding sites, and luciferase reporters (**Tab.6**).

4.8.4 Construction of firefly-based reporters with various miRNA binding site(s)

Forward (1xlet-7P_Fwd) and reverse (1xlet-7P_Rev) oligonucleotides representing the 1xlet-7P binding site were annealed and cloned into BamHI site of pEGFP-SpA-PGK-FL-BGHpA, to obtain pEGFP-SpA-PGK-FL-1xlet-7P-BGHpA. Primers used for cloning are listed in **Tab.3/1** and **Tab.3/2**. Vectors containing different miRNA binding sites were cloned in a similar way (**Tab.7**).

Primer	Sequence
MCS_Insert_Fwd	**GATCTACATGTCGACTCTTAAGCTTCTCA**
MCS_Insert_Rev	**CCGGTGAGAAGCTTAAGAGTCGACATGTA**
1xlet-7P_Fwd	**GATCTACTATACAACCTACTACCTCA**
1xlet-7P_Rev	**GATCTGAGGTAGTAGGTTGTATAGTA**
2xlet-7P_Fwd	**GATCTACTATACAACCTACTACCTCAATTGCGACTATACAACCTACTACCTCA**
2xlet-7P_Rev	**GATCTGAGGTAGTAGGTTGTATAGTCGCAATTGAGGTAGTAGGTTGTATAGTA**
3xlet-7P_Fwd	**GATCTACTATACAACCTACTACCTCATCTAGAACTATACAACCTACTACCTCAATTGCGACTATACAACCTACTACCTCAA**
3xlet-7P_Rev	**GATCTTGAGGTAGTAGGTTGTATAGTCGCAATTGAGGTAGTAGGTTGTATAGTTCTAGATGAGGTAGTAGGTTGTATAGTA**
4xlet-7B_Fwd	**GATCTACTATACAACCGTTCTACCTCATCTAGAACTATACAACCGTTCTACCTCAATTGCGACTATACAACCGTTCTACCTCACGATTGACTATACAACCGTTCTACCTCA**
4xlet-7B_Rev	**GATCTGAGGTAGAACGGTTGTATAGTCAATCGTGAGGTAGAACGGTTGTATAGTCGCAATTGAGGTAGAACGGTTGTATAGTTCTAGATGAGGTAGAACGGTTGTATAGTA**
BGH_Fwd_XhoI	**GTTCTCGAGTGTGCCTTCTAGTTGCCAGC**
BGH_Rev_AgeI_AflII	**GATCTTAAGACCGGTGCCATAGAGCCCACCGCATC**
pGL_Fwd_seq	**GTGCAAGTGCAGGTGCCAGAAC**
FL_Rev_NheI-BamHI-SalI	**GTAGTCGACGGATCCGCTAGCTCATTACACGGCGATCTTGCCGC**
CMV_Fwd_AseI	**CTCATTAATGTTGACATTGATTATTGACTAG**
CMV_Rev_HindIII	**GTGAAGCTTCCTATAGTGAGTCGTATTAAGTACGATAAGCCAGTAAGCAGTGG**
PGK_Fwd_AseI	**CTCATTAATAGGCGCCAACCGGCTCCGTTC**
PGK_Rev_HindIII	**GTGAAGCTTCCTATAGTGAGTCGTATTAAGTACTTGGGCTGCAGGTCGAAAGG**
SV40_Fwd_AseI	**CTCATTAATAGCGCAGCACCATGGCCTG**
SV40_Rev_HindIII	**GTCAAGCTTCCTATAGTGAGTCGTATTAAGTACTTTGCAAAAGCCTAGGCCTC**
TK_Fwd_AseI	**CTCATTAATGAGTCTTCGGACCTCGCG**
TK_Rev_HindIII	**GTGAAGCTTCCTATAGTGAGTCGTATTAAGTACTTAAGCGGGTCGCTGCAGGGTCGC**
spA_Fwd_AseI_XhoI	**GTGATTAATCTCGAGCAATATTATTGAAGCATTTATCAGG**
spA_Rev_NdeI	**CACTGCATATGAGAGAAATGTTCTGGCACCTGC**
SV40pA_Fwd_XhoI	**CACCTCGAGCAACTTGTTTATTGCAGCTTA**
SV40pA_Rev_SalI-AseI	**GAGATTAATGTCGACCGGTATACAGACATGATAAG**
TKpA_Fwd_XhoI	**CACCTCGAGAACACGGAAGGAGACAATACC**
TKpA_Rev_SalI-AseI	**CAGATTAATGTCGACATGAACAAACGACCCAACACC**

Tab.3/1: List of primers

Primer	Sequence
RL_Fwd_NotI	CATGCGGCCGCACCATGGCTTCCAAGGTGTAC
RL_Rev_XbaI-BglII-SalI	GATGTCGACAGATCTAGAACTATTACTGCTCGTTC
CMV_Fwd_AflII-XhoI	CTCCTTAAGCTCGAGGTTGACATTGATTATTGACTAG
CMV_Rev_NotI	GTGGCGGCCGCCCTATAGTGAGTCGTATTAAGTACGATAAGCCAGTAAGCAGTGG
PGK_Fwd_AflII-XhoI	CTCCTTAAGCTCGAGGGCGCCAACCGGCTCCGTTC
PGK_Rev_NotI	GTGGCGGCCGCCCTATAGTGAGTCGTATTAAGTACTTGGGCTGCAGGTCGAAAGG
SV40_Fwd_AflII-XhoI	CTCCTTAAGCTCGAGGCGCAGCACCATGGCCTG
SV40_Rev_NotI	GTCGCGGCCGCCCTATAGTGAGTCGTATTAAGTACTTTGCAAAAGCCTAGGCCTC
TK_Fwd_AflII-XhoI	CAGCTTAAGCTCGAGGAGTCTTCGGACCTCGCG
TK_Rev_NotI	GTGGCGGCCGCCCTATAGTGAGTCGTATTAAGTACTTAAGCGGGTCGCTGCAGGGTCGC
4xmiR-30c_bulge_BglII-Fwd	GATCTGCTGAGAGTGTCAATGTTTACAATTGAGCTGAGAGTGTCAATGTTTACACGATTGCTGAGAGTGTCAATGTTTACATGCATGCTGAGAGTGTCAATGTTTACAA
4xmiR-30c_bulge_BglII-Rev	GATCTTGTAAACATTGACACTCTCAGCATGCATGTAAACATTGACACTCTCAGCAATCGTGTAAACATTGACACTCTCAGCTCAATTGTAAACATTGACACTCTCAGCA
4xlet-7a-mut_Fwd	GATCTACTGAACAACCgttCTACGACATCTAGAACTGAACAACCgttCTACGACAATTGCGACTGAACAACCgttCTACGACACGATTGACTGAACAACCgttCTACGACA
4xlet-7a-mut_Rev	GATCTGTCGTAGAACGGTTGTTCAGTCAATCGTGTCGTAGAACGGTTGTTCAGTCGCAATTGTCGTAGAACGGTTGTTCAGTTCTAGATGTCGTAGAACGGTTGTTCAGTA
1xmiR30P_Fwd	GATCTGCTGAGAGTGTAGGATGTTTACAA
1xmiR30P_Rev	GATCTTGTAAACATCCTACACTCTCAGCA
1xmiR-23P_Fwd	GATCTCTGTTCCTGCTGAACTGAGCCAA
1xmiR-23P_Rev	GATCTTGGCTCAGTTCAGCAGGAACAGA
4xmiR-24B_Fwd	GATCTCTGTTCCTGCTGgctCTGAGCCATCTAGACTGTTCCTGCTGgctCTGAGCCAATTGCGCTGTTCCTGCTGgctCTGAGCCACGATTGCTGTTCCTGCTGgctCTGAGCCAA
4xmiR-24B_Rev	GATCTTGGCTCAGAGCCAGCAGGAACAGCAATCGTGGCTCAGAGCCAGCAGGAACAGCGCAATTGGCTCAGAGCCAGCAGGAACAGTCTAGATGGCTCAGAGCCAGCAGGAACAGA

Tab.3/2: List of primers

final plasmid	host plasmid	insert	source of the insert	oligonucleotides		cloning site(s)	cell line
				fwd	rev		
pPuro	pEGSH.puro	MCS	annealing of oligonucleotides	MCS_Insert_Fwd	MCS_Insert_Rev	BglII/AgeI	NO
pCX-EGFP-1xlet-7_P	pCX-EGFP	1xlet-7P		1xlet-7P_Fwd	1xlet-7P_Rev	Bgl II	NO
pCX-EGFP-1xlet-7_P-invert							NO
pCX-EGFP-2xlet-7_P		2xlet-7P		2xlet-7P_Fwd	2xlet-7P_Rev	Bgl II	NO
pCX-EGFP-2xlet-7_P-invert							NO
pCX-EGFP-3xlet-7_P		3xlet-7P		3xlet-7P_Fwd	3xlet-7P_Rev	Bgl II	NO
pCX-EGFP-3xlet-7_P-invert							NO
pCX-EGFP-4xlet-7_B		4xlet-7P		4xlet-7B_Fwd	4xlet-7B_Rev	Bgl II	NO
pCX-EGFP-4xlet-7_B-invert							NO
pCagEGFP.puro_1xlet-7_P	pPuro	CMV-intron-EGFP-1xlet-7P-PolyA	excision from pCX-EGFP-1xlet-7_P	/	/	SalI/Hind III	NO
pCagEGFP.puro_1xlet-7_P-invert		CMV-intron-EGFP-1xlet-7P_invert-PolyA	excision from pCX-EGFP-1xlet-7_P-invert	/	/	SalI/Hind III	NO
pCagEGFP.puro_2xlet-7_P		CMV-intron-EGFP-2xlet-7P-PolyA	excision from pCX-EGFP-2xlet-7_P	/	/	SalI/Hind III	NO
pCagEGFP.puro_2xlet-7_P-invert		CMV-intron-EGFP-2xlet-7P_invert-PolyA	excision from pCX-EGFP-2xlet-7_P-invert	/	/	SalI/Hind III	NO
pCagEGFP.puro_3xlet-7_P		CMV-intron-EGFP-3xlet-7P-PolyA	excision from pCX-EGFP-3xlet-7_P	/	/	SalI/Hind III	YES
pCagEGFP.puro_3xlet-7_P-invert		CMV-intron-EGFP-3xlet-7P_invert-PolyA	excision from pCX-EGFP-3xlet-7_P-invert	/	/	SalI/Hind III	YES
pCagEGFP.puro_4xlet-7_B		CMV-intron-EGFP-4xlet-7B-PolyA	excision from pCX-EGFP-4xlet-7_B	/	/	SalI/Hind III	NO
pCagEGFP.puro_4xlet-7_B-invert		CMV-intron-EGFP-4xlet-7B_invert-PolyA	excision from pCX-EGFP-4xlet-7_B-invert	/	/	SalI/Hind III	NO

Tab.4: Construction of EGFP-based reporter plasmids carrying 2xlet-7P, 3xlet-7P, and 4xlet-7B binding sites

cloning step	final plasmid	host plasmid	insert(s)	source of the insert	template	primers		cloning sites
						fwd	rev	
1.	pEGFP_FL_BGHpA	pEGFP-N2	BGHpA	PCR	pcDNA3.1(-) plasmid	BGH_Fwd_XhoI	BGH_Rev_AgeI_AflII	HindIII/AflII
			firefly luciferase	PCR	pGL4.10 plasmid	pGL_Fwd_seq	FL_Rev_NheI-BamHI-SalI	
2.	pEGFP-PGK-FL-BGHpA	pEGFP_FL-BGHpA	PGK promoter	PCR	phRL_PGK plasmid	PGK_Fwd_AseI	PGK_Rev_HindIII	HindIII/AseI
	pEGFP_CMV-FL-BGHpA		CMV promoter	PCR	pcDNA3.1 (-) plasmid	CMV_Fwd_AseI	CMV_Rev_HindIII	
	pEGFP-SV40-FL-BGHpA		SV40 promoter	PCR	phRL-SV40 plasmid	SV40_Fwd_AseI	SV40_Rev_HindIII	
	pEGFP-TK-FL-BGHpA		TK promoter	PCR	phRL-TK plasmid	TK_Fwd_AseI	TK_Rev_HindIII	
3.	pEGFP_spA-PGK-FL-BGHpA	pEGFP-PGK-FL-BGHpA	synthetic polyA (SpA)	PCR	pGL4.10 plasmid	spA_Fwd_AseI_XhoI	spA_Rev_NdeI	AseI
	pEGFP_spA_CMV-FL-BGHpA	pEGFP_CMV-FL-BGHpA		PCR				
	pEGFP_spA-SV40-FL-BGHpA	pEGFP-SV40-FL-BGHpA		PCR				
	pEGFP_spA-TK-FL-BGHpA	pEGFP-TK-FL-BGHpA		PCR				
4.	pEGFP_RL_SV40pA	pEGFP-N2 plasmid	SV40pA	PCR	pcDNA3.1(-) plasmid	SV40pA_Fwd_XhoI	SV40pA_Rev_SalI-AseI	AseI/NotI
			Renilla luciferase	PCR	phRL-SV40 plasmid	RL_Fwd_NotI	RL_Rev_XbaI-BglII-SalI	
	pEGFP_RL_TKpA		TKpA	PCR	pEGFP-C1 plasmid	TKpA_Fwd_XhoI	TKpA_Rev_SalI-AseI	
			Renilla luciferase	PCR	phRL-SV40 plasmid	RL_Fwd_NotI	RL_Rev_XbaI-BglII-SalI	
5.	pEGFP_PGK-RL-SV40pA	pEGFP_RL-SV40pA	PGK promoter	PCR	phRL_PGK plasmid	PGK_Fwd_AflII-XhoI	PGK_Rev_NotI	NotI/AflII
	pEGFP_CMV-RL-SV40pA		CMV promoter	PCR	pcDNA3.1 (-) plasmid	CMV_Fwd_AflII-XhoI	CMV_Rev_NotI	
	pEGFP_SV40-RL-SV40pA		SV40 promoter	PCR	phRL-SV40 plasmid	SV40_Fwd_AflII-XhoI	SV40_Rev_NotI	
	pEGFP_PGK-RL-TKpA	pEGFP_RL-TKpA	PGK promoter	PCR	phRL_PGK plasmid	PGK_Fwd_AflII-XhoI	PGK_Rev_NotI	NotI/AflII
	pEGFP_CMV-RL-TKpA		CMV promoter	PCR	pcDNA3.1 (-) plasmid	CMV_Fwd_AflII-XhoI	CMV_Rev_NotI	
	pEGFP_SV40-RL-TKpA		SV40 promoter	PCR	phRL-SV40 plasmid	SV40_Fwd_AflII-XhoI	SV40_Rev_NotI	
	pEGFP_TK-RL-SV40pA	pEGFP_RL-SV40pA	TK promoter	PCR - NotI/XhoI + pEGFP-C1 plasmid - AseI/XhoI	phRL-TK plasmid	TK_Fwd_AflII-XhoI	TK_Rev_NotI	NotI/AseI
					/	/	/	
	pEGFP_TK-RL-TKpA	pEGFP_RL-TKpA	TK promoter	PCR - NotI/XhoI + pEGFP-C1 plasmid - AseI/XhoI	phRL-TK plasmid	TK_Fwd_AflII-XhoI	TK_Rev_NotI	NotI/AseI
					/	/	/	
6.	pRep-G418_SV40pA-RL←PGK-spA-CMV→FL-BGHpA	pEGFP_SpA-CMV-FL-BGHpA	CMV-RL-SV40pA	pEGFP_PGK-RL-SV40pA	/	/	/	AseI/XhoI
	pRep-G418_SV40pA-RL←CMV-spA-PGK→FL-BGHpA	pEGFP_SpA-PGK-FL-BGHpA	PGK-RL-SV40pA	pEGFP_CMV-RL-SV40pA	/	/	/	AseI
	pRep-G418_SV40pA-RL←TK-spA-PGK→FL-BGHpA	pEGFP_SpA-PGK-FL-BGHpA	TK-RL-SV40pA	pEGFP_TK-RL-SV40pA	/	/	/	AseI/XhoI

Tab.5: Construction of dual luciferase reporters

final plasmid	host plasmid	insert	source of the insert	Oligonucleotides		cloning site
				fwd	rev	
pRep-G418_SV40pA-3xlet-7P-RL←CMV-spA-PGK→FL-BGHpA						
pRep-G418_SV40pA-3xlet-7P-invert-RL←CMV-spA-PGK→FL-BGHpA	pRep_SV40pA-RL←CMV-spA-PGK→FL-BGHpA	3xlet-7P	pCagEGFP.puro_3xlet-7P plasmid			
pRep-G418_SV40pA-4xlet-7B-RL←CMV-spA-PGK→FL-BGHpA						
pRep-G418_SV40pA-4xlet-7B-invert-RL←CMV-spA-PGK→FL-BGHpA	pRep_SV40pA-RL←CMV-spA-PGK→FL-BGHpA	4xlet-7B	pCagEGFP.puro_4xlet-7B plasmid			
pRep-G418_SV40pA-3xlet-7P-RL←PGK-spA-CMV→FL-BGHpA						
pRep-G418_SV40pA-3xlet-7P-invert-RL←PGK-spA-CMV→FL-BGHpA	pRep_SV40pA-RL←PGK-spA-CMV→FL-BGHpA	3xlet-7P	pCagEGFP.puro_3xlet-7Pplasmid	/	/	
pRep-G418_SV40pA-4xlet-7B-RL←PGK-spA-CMV→FL-BGHpA						
pRep-G418_SV40pA-4xlet-7B-invert-RL←PGK-spA-CMV→FL-BGHpA	pRep_SV40pA-RL←PGK-spA-CMV→FL-BGHpA	4xlet-7B	pCagEGFP.puro_4xlet-7B plasmid			
pRep-G418_SV40pA-3xlet-7P-RL←TK-spA-PGK→FL-BGHpA						
pRep-G418_SV40pA-3xlet-7P-invert-RL←TK-spA-PGK→FL-BGHpA	pRep_SV40pA-RL←TK-spA-PGK→FL-BGHpA	3xlet-7P	pCagEGFP.puro_3xlet-7Pplasmid			
pRep-G418_SV40pA-4xlet-7B-RL←TK-spA-PGK→FL-BGHpA						
pRep-G418_SV40pA-4xlet-7B-invert-RL←TK-spA-PGK→FL-BGHpA	pRep_SV40pA-RL←TK-spA-PGK→FL-BGHpA	4xlet-7B	pCagEGFP.puro_4xlet-7B plasmid			
pRep-G418_SV40pA-4xmiR-30B-RL←CMV-spA-PGK→FL-BGHpA						
pRep-G418_SV40pA-4xmiR-30B-invert-RL←CMV-spA-PGK→FL-BGHpA	pRep_SV40pA-RL←CMV-spA-PGK→FL-BGHpA					
pRep-G418_SV40pA-4xmiR-30B-RL←PGK-spA-CMV→FL-BGHpA		4xmiR-30B	annealing of oligonucleotides	4xmiR-30c_bulge_BglII-Fwd	4xmiR-30c_bulge_BglII-Rev	BglII
pRep-G418_SV40pA-4xmiR-30B-invert-RL←PGK-spA-CMV→FL-BGHpA	pRep_SV40pA-RL←PGK-spA-CMV→FL-BGHpA					
pRep-G418_SV40pA-4xmiR-30B-RL←TK-spA-PGK→FL-BGHpA						
pRep-G418_SV40pA-4xmiR-30B-invert-RL←TK-spA-PGK→FL-BGHpA	pRep_SV40pA-RL←TK-spA-PGK→FL-BGHpA					
pRep-G418_SV40pA-RL←CMV-spA-PGK→FL-3xlet-7P-BGHpA	pRep-G418_SV40pA-RL←CMV-spA-PGK→FL-BGHpA	3xlet-7P	annealing of oligonucleotides	3xlet-7P_Fwd	3xlet-7P_Rev	BamHI
pRep-G418_SV40pA-RL←PGK-spA-CMV→FL-3xlet-7P-BGHpA	pRep-G418_SV40pA-RL←PGK-spA-CMV→FL-BGHpA					

Tab.6: Construction of a dual luciferase reporter carrying various miRNA binding sites

final plasmid	host plasmid	insert(s)	source of the insert	primers		cloning sites
				fwd	rev	
pEGFP-SpA-PGK-FL-1xlet-7P-BGHpA	pEGFP-SpA-PGK-FL-BGHpA	1xlet-7P	annealing of oligonucleotides	1xlet-7P_Fwd	1xlet-7P_Rev	Bam HI
pEGFP-SpA-PGK-FL-3x-let-7P-BGHpA		3xlet-7P		3xlet-7_Fwd	3xlet-7_Rev	
pEGFP-SpA-CMV-FL-3x-let-7P-BGHpA	pEGFP-SpA-CMV-FL-BGHpA	3xlet-7P		3xlet-7_Fwd	3xlet-7_Rev	
pEGFP-SpA-PGK-FL-4xlet-7B-BGHpA	pEGFP-SpA-PGK-FL-BGHpA	4xlet-7B		4xlet-7B_Fwd	4xlet-7B_Rev	
pEGFP-SpA-PGK-FL-4xmiR-30B-BGHpA		4xmiR-30B		4xmiR-30B_Fwd	4xmiR-30B_Rev	
pEGFP-SpA-PGK-FL-1xmiR-24P-BGHpA		1xmiR-24P		1xmiR-24P_Fwd	1xmiR-24P_Rev	
pEGFP-SpA-PGK-FL-4xmiR-24B-BGHpA		4xmiR-24B		4xmiR-24B_Fwd	4xmiR-24B_Rev	
pEGFP-SpA-PGK-FL-4xlet-7M-BGHpA		4xlet-7M		4xlet-7M_Fwd	4xlet-7M_Rev	
pEGFP-SpA-PGK-FL-4xmiR-30M-BGHpA		4xmiR-30M		4xmiR-30M_Fwd	4xmiR-30M_Rev	

Tab.7: Construction of firefly-based reporters with various miRNA binding site(s)

5 RESULTS

5.1 Fluorescence-based *in vitro* Dicer cleavage assay

5.1.1 Preparation of recombinant human Dicer

5.1.1.1 Expression of recombinant human Dicer-HisC in insect cells

The recombinant human Dicer-HisC was expressed in insect cells using the Bac-to-Bac® Baculovirus Expression System (*Life Technologies*) according to the manufacturer´s instructions. The generation of recombinant baculovirus and the expression of the gene of interest using the Bac-to-Bac® Baculovirus Expression System are depicted in **Fig.16**.

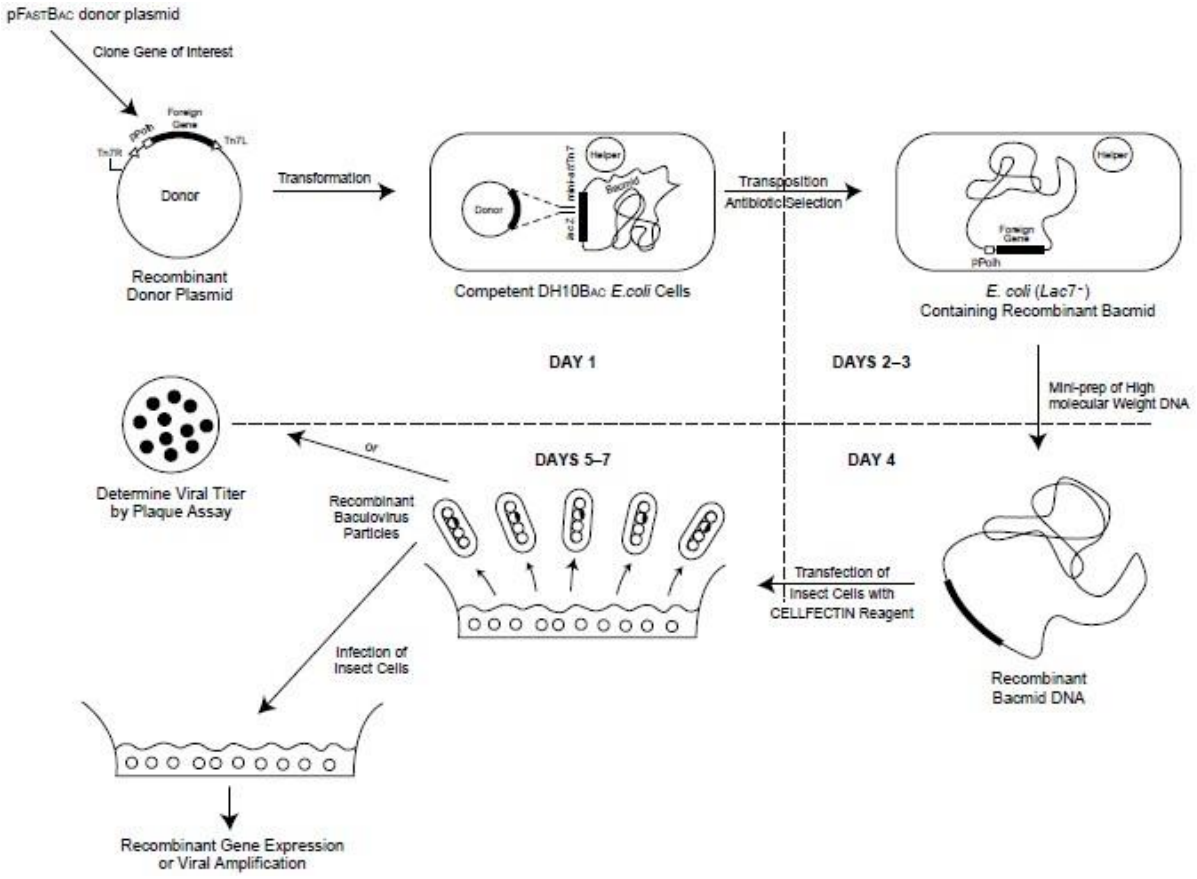

Fig.16: Generation of recombinant baculoviruses and gene expression with the Bac-to-Bac expression system

Purified pDest8-Dicer-6His donor vector carrying the gene for human Dicer equipped with 6xHis-tag on the C-terminus (kindly provided by Dr. Wittold Filipowicz, Friedrich Miescher Institute for Biomedical Research, Basel, Switzerland) was transformed into DH10Bac™ *E. coli*, and subsequently the recombinant bacmid DNA was isolated. Midi-prep isolation of bacmid DNA yielded 27 µg of bacmid #1, 170 µg of bacmid #2, and 160 µg of bacmid #3. The insect Sf9 cells were transfected using calcium phosphate method with three different bacmid DNAs. The transfected cells were lysed 5 days post transfection (dpt) and analyzed for the transgene expression by western blotting using anti-Dicer 349 rabbit polyclonal primary antibody ((Sinkkonen et al., 2010); 1:5,000). The signal was developed using HRP-conjugated goat anti-rabbit secondary antibody (1:15,000). As shown in **Fig.17A**, clear bands corresponding to the molecular weight of human Dicer-6xHisC (~ 220 kDa) were detected in Sf9 cell lysates after transfection with all three bacmids, indicating that all bacmid DNA were recombinant, producing the recombinant human Dicer-HisC baculoviruses.

The P1, a small-scale, low-titer viral stock obtained from the transfection with bacmid #2 was used to infect Sf9 insect cells to generate a high-titer P2 stock. The P2 stock was used for plaque assay to plaque-purify (clone) the virus. After the plaque assay, 10 plaques were collected and, the virus clones were used for new infection of Sf9 cells. The infected cells were harvested and lysed 72 hours post infection (hpi). Cell lysates were analyzed for the transgene expression by western blotting using anti-Dicer 349 polyclonal primary rabbit antibody ((Sinkkonen et al., 2010); 1:5,000) and HRP-conjugated goat anti-rabbit secondary antibody (*Sigma-Aldrich*, 1:15,000). The clear band corresponding to the molecular weight of human Dicer-6xHisC was detected only after infection by virus obtained from plaque #8. Besides, several other bands with lower molecular weight were detected after the infection by virus obtained from plaques #1, #2, #3, #6, #7, #8, #9, and #10. These bands were probably human Dicer-6xHisC degradation products. After the infection by virus obtained from plaques #4 and #5, no signal was detected, so probably these viruses were not recombinant (**Fig.17B**). The virus obtained from plaque #8 was amplified and kept both at -80 °C (in 50% glycerol) and at 4 °C for next experiments.

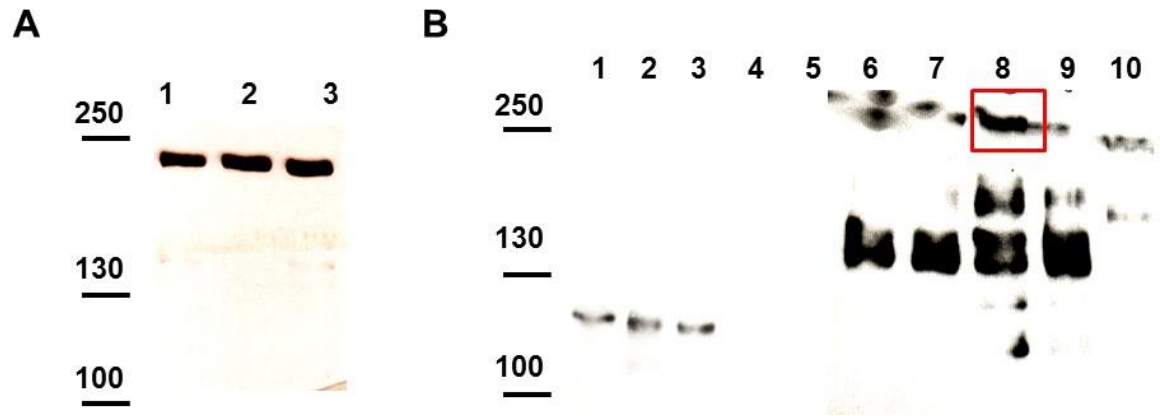

Fig.17: Generating of recombinant baculovirus producing human Dicer-HisC: (A) Western blotting analysis of recombinant human Dicer stained by anti-Dicer 349 rabbit polyclonal primary antibody (1:5,000) and HRP-conjugated goat anti-rabbit secondary antibody (*Sigma-Aldrich*, 1:15,000) after transfection of Sf9 cells using calcium phosphate method. Numbers 1 – 3 mark the individual bacmids. **(B)** Sf9 cells infected by plaque-purified baculovirus, clones 1 – 10. Positions of size marker bands in kDa are indicated on the left.

5.1.1.2 Optimization of human Dicer-HisC purification from insect cells

First, Dicer-HisC was purified from insect cells according to the protocol described in the chapter **4.1.3.1**. Briefly, Dicer-HisC was isolated under three different buffer conditions (A, B, and C). Subsequently, the purity of recovered Dicer was analyzed by electrophoresis on 6% SDS-PAGE gel followed by CBB-R250 staining and by western blotting using: (i) anti-Dicer 349 rabbit polyclonal primary antibody ((Sinkkonen et al., 2010); 1:5,000) and HRP-conjugated goat anti-rabbit secondary antibody (*Sigma-Aldrich*, 1:15,000) and (ii) mouse monoclonal anti-polyHistidine Peroxidase Conjugate antibody (*Sigma-Aldrich*, 1:2,000). The clear band corresponding to the molecular weight of human Dicer-6xHisC after elution with both imidazol- and EDTA-containing elution buffer was detected by SDS-PAGE electrophoresis under all buffer conditions (A, B, and C) tested. Besides, several other bands with lower molecular weight were detected **(Fig.15A)**. According to the western blotting results, these lower bands were presumably Dicer degradation products **(Fig.15B)**.

Second, Dicer-HisC was purified from insect cells according to the protocol described in chapter **4.1.3.2**., and the purity and concentration of recovered Dicer was verified by electrophoresis on 6% SDS-PAGE gel and visualization by the CBB-R250 staining and by western blotting using anti-Dicer 349 rabbit polyclonal primary antibody ((Sinkkonen et al., 2010); 1:5,000) and HRP-conjugated goat anti-rabbit secondary antibody (*Sigma-Aldrich*, 1:15,000). Although the band corresponding to the molecular

weight of human Dicer-6xHisC was slightly visible in elution fractions, the stronger band corresponding to the molecular weight of ~130 kDa was detected both after CBB-R250 staining and western blotting **(Fig.15C, D)**. Although all purification steps were carried out at 4 °C and in the presence of protease inhibitors, the Dicer was massively degraded before and/or during the purification procedure.

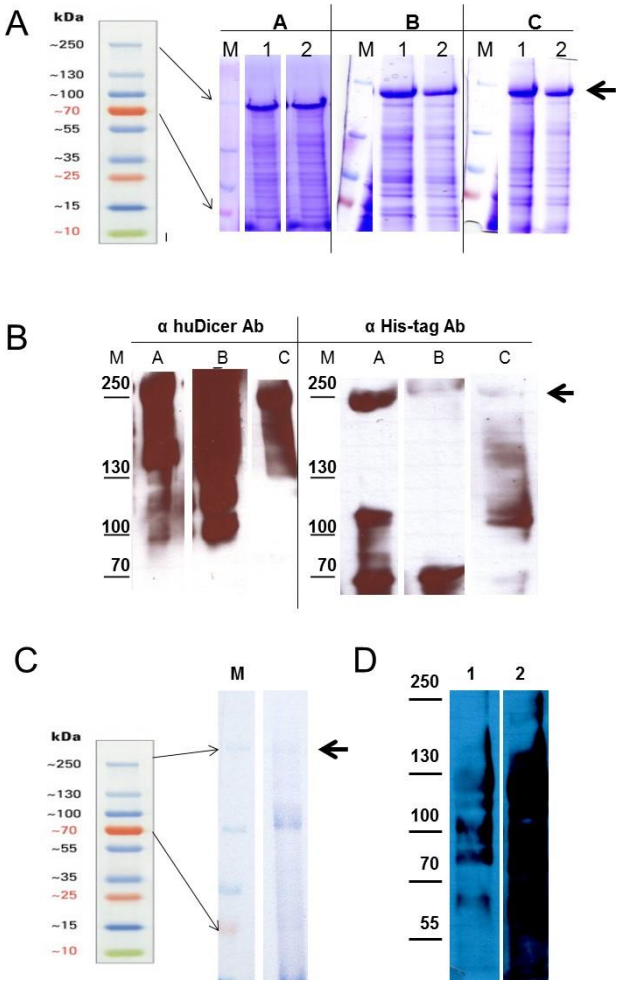

Fig.18: Optimization of human Dicer-HisC purification from insect cells: (A) Dicer purified during the first protocol optimization according to protocol A, B, or C was resolved on 6% polyacrylamide gel and stained by CBB-R250. 1 = Dicer eluted by imidazol, 2 = Dicer eluted by EDTA. **(B)** Western blotting of recombinant human Dicer purified during the first protocol optimization according to protocol A, B, or C and stained by anti-Dicer 349 rabbit polyclonal primary antibody ((Sinkkonen et al., 2010); 1:5,000) and HRP-conjugated goat anti-rabbit secondary antibody (*Sigma-Aldrich*, 1:15,000) or mouse monoclonal anti-polyHistidine Peroxidase Conjugate antibody *(Sigma-Aldrich*, 1:2,000*)*. **(C)** Dicer purified during the second protocol optimization was resolved on 6% polyacrylamide gel and stained by CBB-R250. **(D)** Western blotting of recombinant Dicer purified during the second protocol optimization stained by anti-Dicer 349 rabbit polyclonal primary antibody ((Sinkkonen et al., 2010); 1:5,000) and HRP-conjugated goat anti-rabbit secondary antibody (*Sigma-Aldrich*, 1:15,000) (1) or mouse monoclonal anti-polyHistidine Peroxidase Conjugate antibody *(Sigma-Aldrich*, 1:2000*)* (2). Positions of size marker bands in kDa are indicated on the left. Arrows mark the C-terminally-tagged recombinant human Dicer purified from insect cells.

5.1.2 Assay development

5.1.2.1 Principle of fluorescence-based in vitro Dicer assay

A highly efficient, low-cost, safe, and robust assay is a prerequisite for a successful HTS. Until now, several assays for monitoring Dicer activity *in vitro* have been developed (Davies and Arenz, 2006; DiNitto et al., 2010; Kolb et al., 2005. These assays used different Dicer substrates, such as substrates mimicking the pre-miRNA structure {Davies, 2006 #407) or perfect RNA duplexes of various lengths (30-150 bp) with or without 3´ overhangs

(DiNitto et al., 2010; Kolb et al., 2005; Zhang et al., 2002). Typically, Dicer cleavage assays have been based on the processing of radiolabeled dsRNA substrates by recombinant Dicer and subsequent detection of cleaved products by electrophoresis (Kolb et al., 2005; Zhang et al., 2002). However, this type of assay is not suitable for HTS. A conceivable solution is an assay yielding the fluorescence upon cleavage by Dicer.

Therefore in order to facilitate the rapid screening of potential modulators of Dicer activity in a high-throughput manner without the need for radiolabeling and utilizing native or denaturing PAGE, a fluorescence *in vitro* Dicer assay was developed. This assay is based on the cleavage of a 27-nt long perfect RNA duplex carrying a 2-nt 3′overhang at one terminus and a blunt end at the other terminus, where one strand carries a fluorescent group and the other strand a quencher **(Fig.13C)**. During Dicer cleavage, the 2-nt 3′ overhang is recognized by the PAZ domain, and Dicer cleavage releases a short duplex carrying the fluorophore and the quencher. Subsequent separation of the fluorophore from the quencher yields fluorescence **(Fig.13D)**. Although it was possible to prepare a substrate resembling the structure of natural pre-miRNA similarly as described previously (Davies and Arenz, 2006), we decided for short (27-nt) RNA duplex, which was easy to synthesize and which resembled an artificial siRNA structure described earlier (Kim et al., 2005). The sequence of the substrate was derived from a well characterized human let-7a miRNA, hence allowing for combining our assay with other tools developed for let-7 analysis. Notably, a similar substrate design was also adopted for fluorescence-based Dicer assay by DiNitto *et al.* (2010) (DiNitto et al., 2010).

5.1.2.2 Establishment of the fluorescence-based in vitro Dicer cleavage assay

Unless otherwise stated, all experiments in this section were performed in 20 µl of the starting assay buffer (30 mM Tris-HCl, pH 6.8, 50 mM NaCl, 3 mM $MgCl_2$, 0.1% Triton X-100, and 20% glycerol), adopted from Kolb *et al.* (2005) (Kolb et al., 2005), in black, flat-bottom, polystyrene 384-well microplates (*Corning, Inc., New York, NY*). The reaction was performed at 37 °C and 100% humidity to minimize evaporation. The fluorescence was determined using the multilabel reader EnVision (*PerkinElmer, Waltham, MA*) equipped with a Bodipy TMR optimized filter set (excitation filter 494 nm and emission filter 519 nm) at indicated timepoints.

5.1.2.2.1 Characterization of 5(6)-FAM/3-Dab Dicer substrate

For the assay establishment, a fluorophore-labeled (5(6)-FAM) antisense RNA strand and a quencher-labeled (3-Dab) sense RNA strand were annealed and used as a substrate for recombinant human Dicer-HisC. First, we determined sufficient concentration of the 5(6)-FAM RNA strand, background of the 3-Dab RNA strand, as well as a possible interference of non-annealed quencher-labeled and fluorophore-labeled strands. The 5(6)-FAM RNA and 3-Dab RNA strands were diluted (separately or mixed together) in the starting assay buffer (decimal dilutions, starting at 100 pmol), and the fluorescence was determined as described in the chapter **5.1.2.2**. As shown in **Fig.19**, sufficient concentration of fluorophore-labeled antisense strand is 10^{-1} pmol. At lower concentrations, no fluorescence signal was detected. Although the quencher-labeled sense strand alone had no background signal, the quencher-labeled strand mixed together with the fluorophore-labeled strand partially quenched the fluorescence signal even without their annealing **(Fig.19)**. The fluorescence signal was measured five times with the similar result, indicating a relative stability of the 5(6)-FAM fluorophore in time (data not shown).

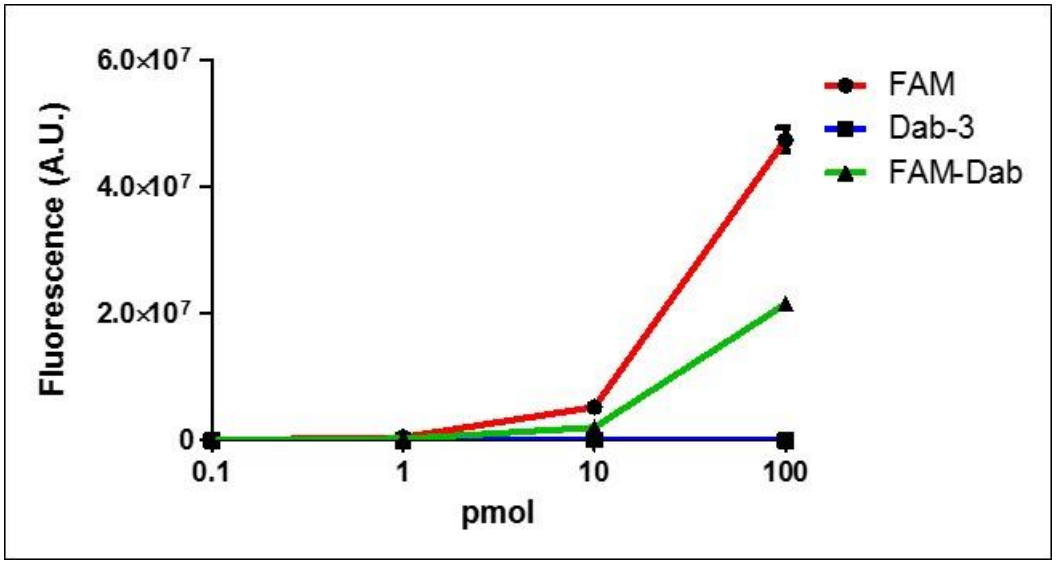

Fig.19: Characterization of 5(6)-FAM antisense and 3-Dab sense RNA strand of Dicer substrate. Fluorophore-labeled (FAM in red) and quencher-labeled (Dab-3 in blue) RNA strands were diluted separately or mixed together (FAM-Dab in green) in starting assay buffer (decimal dilutions, starting at 100 pmol), and the fluorescence was measured by EnVision platform equipped with a Bodipy TMR optimized filter set (excitation filter 494 nm and emission filter 519 nm). The experiment was carried out in black flat-bottom polystyrene 384-well microplate in total volume of 20 µl. Values are reported as mean ± SEM.

5.1.2.2.2 Analysis of purified recombinant human Dicer-HisC activity

To analyze the activity of individual Dicer batches, the fluorescence-based *in vitro* Dicer cleavage assay was performed with 1 µl of non-diluted Dicer. As a Dicer substrate we used 300 nM dsRNA labeled with 5(6)-FAM/3-Dab. Four Dicer batches – Dicer A, B, and C isolated in the first round of Dicer purification (chapter **4.1.3.1**) and Dicer isolated in the second round of Dicer purification (chapter **4.1.3.2**), here referred to as Dicer D, were tested. Fluorescence of the reaction mixture was quantified at time 0 min, 30 min, 90 min, and 150 min of incubation at 37 °C. As shown in **Fig.20**, 2-fold increase of the fluorescence signal after 150 min of incubation at 37 °C was observed for Dicer A and B, indicating a relatively weak enzymatic activity. Although the activity of Dicer D at the end of fluorescence measurement (after 150 min of incubation at 37 °C) was comparable with the activities of Dicer A and B, its reaction progress was slower (**Fig.20)**. The activity of Dicer C was minimal (**Fig.20)**.

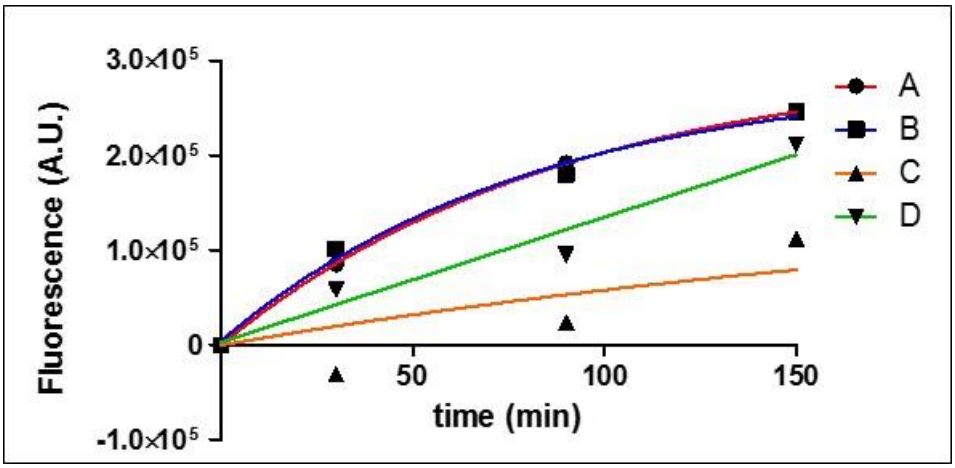

Fig.20: Analysis of the activity of recombinant human Dicer-HisC in fluorescence-based Dicer cleavage assay. Reaction progress curves observed after incubation of four different Dicer batches (1 µl of A, B, C, or D) with the 5(6)-FAM/3-Dab-labeled dsRNA substrate (300 nM). The fluorescence was measured by EnVision platform equipped with a Bodipy TMR optimized filter set (excitation filter 494 nm and emission filter 519 nm). The experiment was carried out in black flat-bottom polystyrene 384-well microplate in total volume of 20 µl.

5.1.2.2.3 Effect of EDTA on Dicer activity

Dicer-catalyzed dsRNA cleavage is Mg^{2+}-dependent (Provost et al., 2002; Zhang et al., 2002). Therefore, chelation of magnesium ions by EDTA should inhibit the Dicer activity. To test this hypothesis, EDTA was added into the reaction to the final concentration of 25 mM. The Dicer cleavage assay was carried out using 200 nM

dsRNA_5(6)FAM/3-Dab Dicer substrate and 1 µl of Dicer A or Dicer D. The fluorescence of the reaction mixture was quantified at time 0 and then after 1, 2, 3, 16, and 24 h of incubation at 37 °C. As expected, chelation of Mg^{2+} ions by 25 mM EDTA completely blocked the Dicer activity, which was manifested as decreasing fluorescence over time **(Fig.21)**.

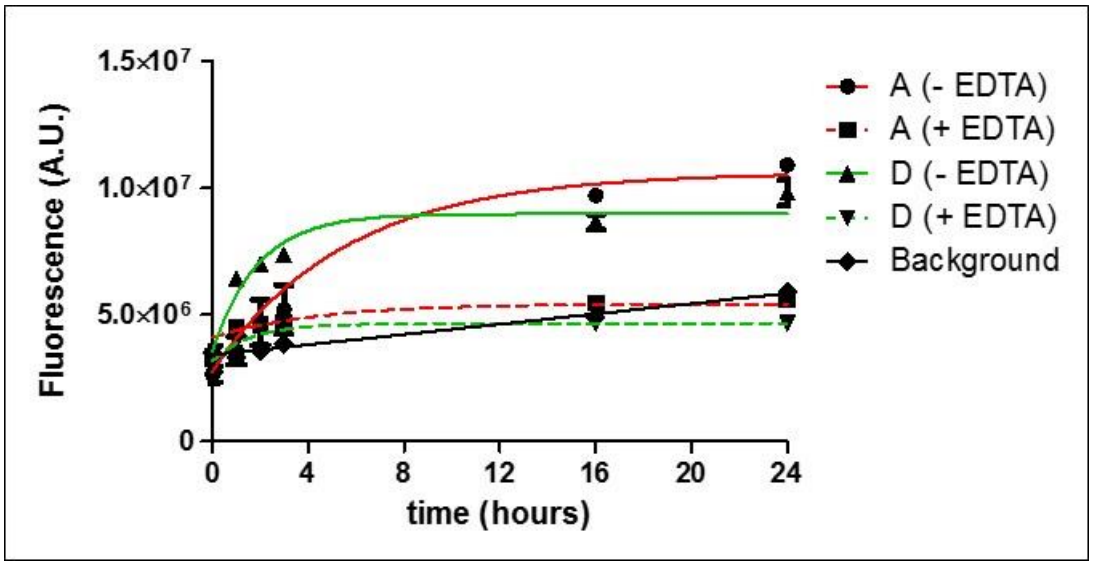

Fig.21: Effect of EDTA on Dicer activity. Reaction progress curves observed after incubation of Dicer A or D with 200 nM 5(6)-FAM/3-Dab labeled dsRNA substrate and with or without 25 mM EDTA. The fluorescence was measured by EnVision platform equipped with a Bodipy TMR optimized filter set (excitation filter 494 nm and emission filter 519 nm). The experiment was carried out in black, flat-bottom, polystyrene 384-well microplate in total volume of 20 µl. Values are reported as mean ± SEM.

5.1.2.2.4 Effect of proteinase K on Dicer activity

Partial degradation of Dicer with proteinase K can stimulate its enzymatic activity (Zhang et al., 2002). To test proteinase K-mediated increase in Dicer activity, roteinase K was added into the reaction to the final concentration of 3 nM or 300 nM. The fluorescence-based *in vitro* Dicer assay was performed using 200 nM dsRNA_5(6)FAM/3-Dab Dicer substrate and 1 µl of Dicer A or Dicer D. Fluorescence of the reaction mixture was quantified at time 0 and then after 1; 2; 3; 16, and 24 h of incubation at 37 °C. Interestingly, proteinase K did not increase the Dicer activity neither at 3 nM, nor at 300 nM concentration. On the contrary, the addition of proteinase K markedly reduced the enzyme activity **(Fig.22)**.

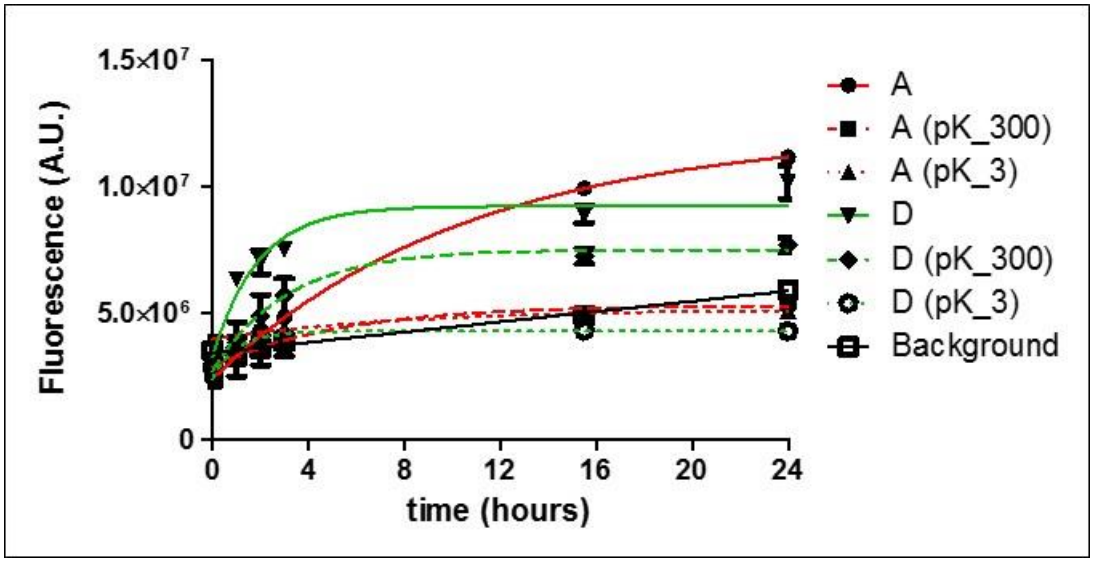

Fig.22: Effect of proteinase K on Dicer activity. Reaction progress curves observed after incubation of Dicer A or D with 200 nM 5(6)-FAM/3-Dab-labeled dsRNA substrate and with or without 3 nM or 300 nM proteinase K. The fluorescence was measured by EnVision platform equipped with a Bodipy TMR optimized filter set (excitation filter 494 nm and emission filter 519 nm). The experiment was carried out in black, flat-bottom, polystyrene 384-well microplate in total volume of 20 µl. Values are reported as mean SEM.

5.1.2.2.5 Effect of RiboLock on Dicer activity

The dsRNA substrate for Dicer can be cleaved by non-specific RNases presented in the environment. To exclude this interference, the RNase inhibitor RiboLock (*Life Technologies)* was added into the reaction. RiboLock specifically inhibits the activity of RNases A, B, and C, however, it should not affect the Dicer activity. The fluorescence-based *in vitro* Dicer assay was carried out using 200 nM dsRNA_5(6)FAM/3-Dab Dicer substrate and 1 µl of Dicer D with or without 0.04 U of RiboLock. Fluorescence of the reaction mixture was quantified at time 0 and then after 1, 2, and 3 h of incubation at 37 °C. As shown in **Fig.23A**, RiboLock did not affect the reaction progress, indicating the specific Dicer-mediated cleavage of dsRNA substrate. However, it should be noted that RiboLock does not inhibit eukaryotic RNases T1, T2, U1, U2, CL3, as well as prokaryotic RNase I and RNase H.

5.1.2.2.6 Fractionation of dsRNA substrate after Dicer-mediated cleavage

To further confirm that the dsRNA substrate is cleaved by Dicer, the Dicer cleavage reaction was performed, and subsequently the products of the cleavage reaction were resolved on denaturing 13.5% PAGE. Briefly, 200 nM dsRNA_5(6)FAM/3-Dab Dicer substrate was mixed with 1 µl of Dicer, and the cleavage reaction was proceeding 3 h at

37 °C. Control samples contained all reagents for the Dicer cleavage assay and either 0,04 U of RiboLock or 25 mM EDTA in addition. As expected, two bands were detected after the cleavage by Dicer regardless of the presence of RiboLock. On the contrary, only one band was observed in the reaction supplemented with EDTA. The presence of only two bands after the Dicer cleavage reaction and the block of dsRNA cleavage in the reaction supplemented with EDTA further confirmed that the dsRNA substrate is specifically cleaved by Dicer. Predicted sizes of the Dicer cleavage products in base pairs are marked by size marker on the left **(Fig.23B)**.

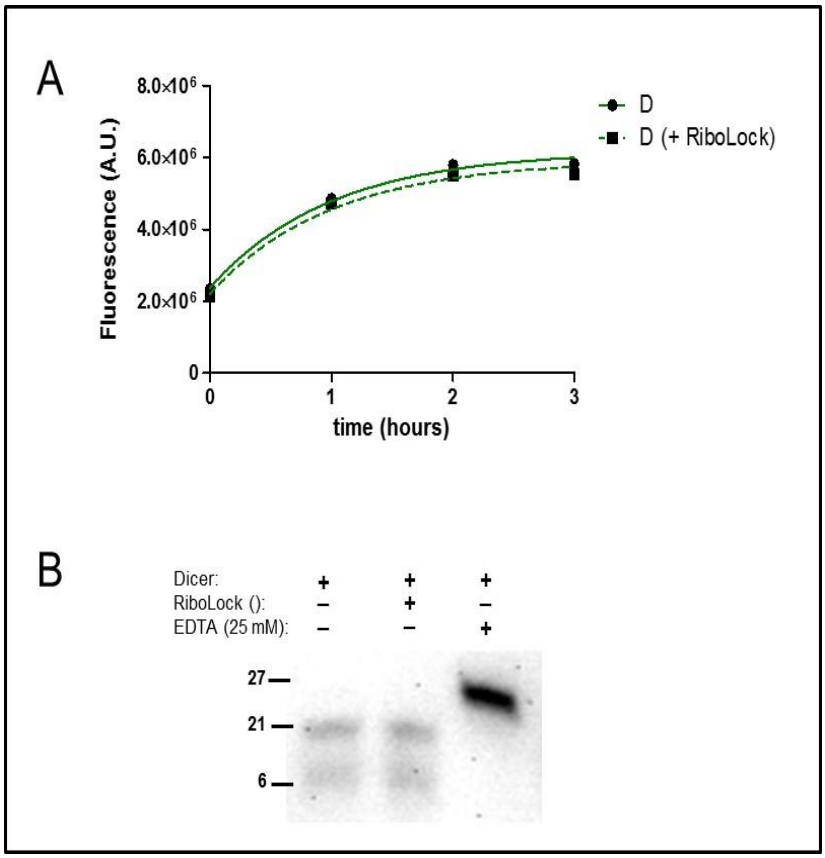

Fig.23: Analysis of potential nonspecific cleavage of dsRNA substrate (A) Reaction progress curves observed after incubation of Dicer D with 200 nM 5(6)-FAM/3-Dab-labeled dsRNA substrate with or without RiboLock. The fluorescence was measured by EnVision platform equipped with a Bodipy TMR optimized filter set (excitation filter 494 nm and emission filter 519 nm) in black flat-bottom polystyrene 384-well microplate in total volume of 20 µl. **(B)** Dicer substrate processed by recombinant Dicer D with or without EDTA or RiboLock was resolved on 13.5% PAGE with 7 M urea and stained by SybrGold. Predicted sizes of the Dicer cleavage products in bp are marked by size marker on left.

5.1.2.3 Optimization of the fluorescence-based Dicer cleavage assay

5.1.2.3.1 Selection of the optimal fluorescent Dicer substrate

To produce an optimal substrate with minimal background activity and maximal fluorescence intensity upon Dicer-mediated cleavage, I tested three Dicer substrates with different combinations of fluorescent and quencher groups. The substrates were selected based on recommendations of providers and the literature (DiNitto et al., 2010) As mentioned above, initially, I tested 5(6)-FAM fluorescent donor- and 3-Dab

quencher-labeled strands (5(6)-FAM/3-Dab; *Exiqon, Vedbaek, Denmark*). Although this combination sufficiently demonstrated feasibility of the assay, two additional combinations of fluorescent and quencher groups were evaluated for HTS. These included: (i) Cy5 fluorescent-labeled and BHQ2 quencher-labeled strands (Cy5/BHQ2; *Sigma-Aldrich*) and (ii) Cy5 fluorescent-labeled and IowaBlackRQ quencher-labeled strands (Cy5/IowaBlackRQ; *Integrated DNA Technologies, Coralville, IA*), the latter combination having been published previously (DiNitto et al., 2010). Dicer cleavage assays were performed under single-turnover conditions, in which Dicer is present in molar excess (233 nM) over the substrate (33 nM). Under these reaction conditions, the rate of product formation is not limited by the product release, since each enzyme molecule reacts at most with one substrate molecule. Notably, the different combinations of fluorophore and quencher yielded different ranges of the assay in terms of detected fluorescence (**Tab.8, Fig.24A**). While the fluorescence released after Dicer-mediated cleavage of the substrate labeled with Cy5/BHQ2 or 5(6)-FAM/3-Dab increased only 2-fold after 3 h, the combination Cy5/IowaBlackRQ achieved an 8-fold increase of fluorescence (**Fig.24A**). Since Cy5/IowaBlackRQ yielded the best result, it was used for further experiments.

	5(6)-FAM/3-Dab	Cy5/BHQ2	Cy5/IowaBlackRQ
Fluorescence at t = 0 h (AU)	2,587,095	39,856.75	31,077.75
Fluorescence at t = 3 h (AU)	4,944,355	104,162.5	252,221.5
Increase in fluorescence (AU)	2,357,260	64,305.75	221,143.75
Fold change (t = 3 h)/(t = 0 h)	1.9	2.6	8.1

Tab.8: Comparison of substrate performance with fluorophore and quencher combinations: Fluorescence was measured on the EnVision (*PerkinElmer*, Waltham, MA) multilabel reader equipped with a Bodipy TMR optimized filter set (excitation filter 647 nm and emission 665 nm for fluorophore Cy5; excitation filter 494 nm and emission 519 nm for fluorophore 5(6)-FAM). AU, arbitrary units.

5.1.2.3.2 Selection of the optimal ratio of Cy5 fluorophore and IB-RQ quencher

To reduce the Dicer substrate background values to minimum and to increase the fluorescence intensity upon Dicer cleavage to maximum, four different quencher-to-fluorophore ratios (0.8:1; 1:1; 1.2:1 and 1.5:1) of IowaBlackRQ (IB-RQ, *Integrated DNA Technologies, Coralville, IA*) quencher to Cy5 fluorophore group were tested. Dicer assay was performed under single-turnover conditions with 233 nM enzyme and 33 nM substrate. As expected, the different ratios of quencher to fluorophore group yielded different ranges of the assay (**Tab.9**). While the fluorescence released after Dicer cleavage of the substrate

annealed in ratio 0.8:1 increased only 2.5-fold after 3 h, the ratios 1:1 and 1.2:1 achieved ~8.5-fold increase of fluorescence and finally the ratio 1.5:1 increased even 12.5-fold (**Fig.24B**). The low fluorescence increase observed for ratio 0.8:1 was naturally caused by insufficient quenching. The annealing in ratios of 1:1 and 1.2:1 yielded similar results. The ratio 1:1 was used for common small-scale experiments, in which the higher background activity of the substrate, as a result of pipetting error, can be simply overcome by preparing a new annealing reaction. Since the insufficient dynamic range of the assay resulting from the high background activity of the substrate would mean useless loss of money, as a safeguard, the ratio 1.2:1 was used for HTS purposes. Although the fluorescence released after the Dicer-mediated cleavage of the substrate annealed in ratio 1.5:1, achieved the highest increase of fluorescence, usage of this ratio was rejected because of the insufficient amount of quencher stock.

IB-RQ : Cy5	**1 : 0.8**	**1 : 1**	**1 : 1.2**	**1 : 1.5**
Fluorescence at t = 0 h (AU)	128,388.5	27,920.0	25,165.0	14,694.0
Fluorescence at t = 3 h (AU)	316,597.5	228,947.0	214,347.0	184,084.0
Increase of fluorescence (AU)	188,209.0	201,027.0	189,182.0	169,390.0
Fold change (t = 3 h)/(t = 0 h)	2.5	8.2	8.5	12.5

Tab.9: Comparison of Cy5/IB-RQ substrate performance in different quencher:fluorophore ratio: Fluorescence was measured on the EnVision (*PerkinElmer, Waltham, MA*) multilabel reader equipped with a Bodipy TMR optimized filter set (excitation filter = 647 nm and emission = 665 nm), AU, arbitrary units.

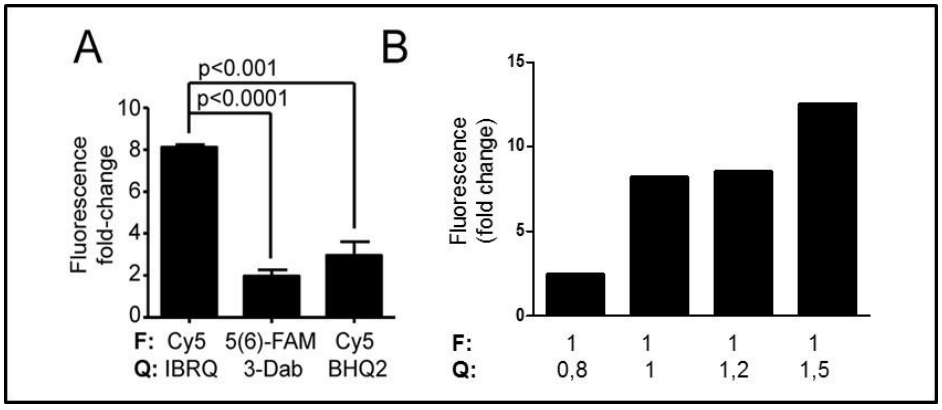

Fig.24: Analysis of the fluorescent Dicer substrates: (A) Fluorescence fold change produced by different substrates. Recombinant Dicer (233 nM) was incubated with a 28-bp perfect duplex RNA substrate (33 nM) labeled with indicated combinations of fluorophore (F) and quencher (Q). Graph depicts fluorescence at t = 3 h/fluorescence at t = 0 h. Values are reported as mean SEM. **(B)** Fluorescence fold change produced by Cy5/IB-RQ (*Integrated DNA Technologies, Coralville, IA*) in different quencher:fluorophore ratios. Recombinant Dicer (233 nM) was incubated with a 28-bp perfect duplex RNA substrate (33 nM) labeled with Cy5/IB-RQ in indicated quencher:fluorophore ratios. Graph depicts fluorescence at t=3 h/fluorescence at t = 0 h. The experiment was performed in singlet. Both experiments were carried out in a black flat-bottom polystyrene 384-well microplate in total volume of 20 µl (n = 4). Fluorescence was measured on the EnVision (*PerkinElmer, Waltham, MA*) multilabel reader equipped with a Bodipy TMR optimized filter set (excitation filter = 647 nm and emission = 665 nm).

5.1.2.3.3 Effect of EDTA – dose response experiment

To test if EDTA is able to inhibit Dicer in a concentration-dependent manner, a dose-response experiment (0.5 mM–5 mM EDTA) was performed. Consistent with requirements of Mg^{2+}, chelation of magnesium ions by EDTA did inhibit the Dicer activity in a dose-dependent manner. Whereas 5 mM EDTA achieved almost 80% inhibition, 500 μM EDTA inhibited the enzyme only by 6% over 3 h. EDTA inhibited the Dicer activity with IC50=271 mM after 3 h of reaction (**Fig.25A**). Surprisingly, neither 5 mM, nor 10 mM EDTA added into the reaction after 1 h of incubation at 37 °C was not able to decrease the fluorescence relieved by Dicer cleavage **(Fig.25B**). One explanation could be that 233 nM Dicer managed to bind the total amount of 33 nM substrate in the single-turnover reaction in the first hour, and that the progressing increase of fluorescence in next hours was caused by progressive release of cleavage product.

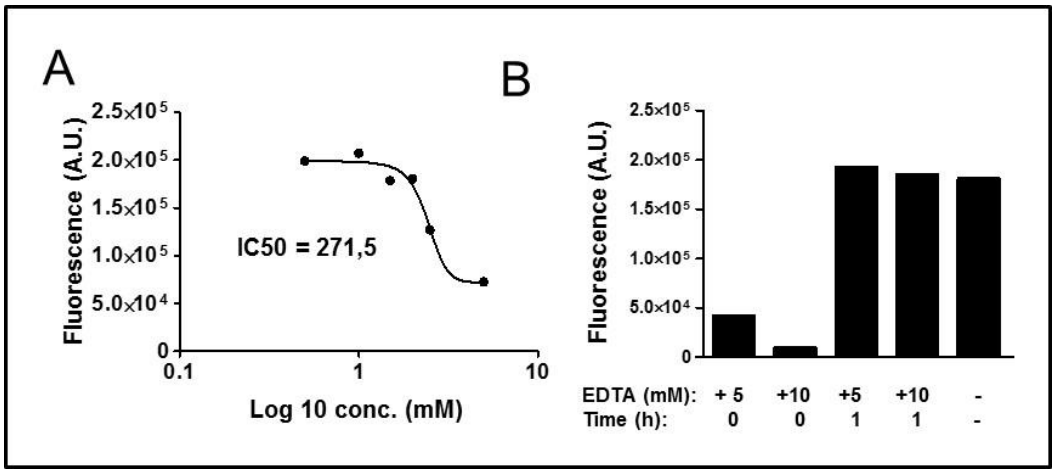

Fig.25: Effect of EDTA on Dicer activity. (A) Inhibition constant (IC) for EDTA as Dicer activity inhibitor. Inhibition constant of EDTA was determined after 3 h of reaction using the fluorescence *in vitro* Dicer assay using 233 nM Dicer and 33 nM substrate. **(B)** Effect of 5 mM or 10 mM EDTA added into cleavage reaction at t = 0 or t = 1 h of incubation at 37 °C.

5.1.2.3.4 Effect of Mg^{2+} ions and NaCl on the Dicer activity

To find optimal conditions of the assay, I determined the influence of Mg^{2+} concentration under the single-turnover conditions. As a starting assay buffer we adopted the Dicer assay buffer (30 mM Tris-HCl, pH 6.8, 50 mM NaCl, 3 mM $MgCl_2$, 0.1% Triton X-100, and 15-20% glycerol) published by Kolb *et al.* (2005) (Kolb et al., 2005). Dicer-mediated dsRNA cleavage is dependent on Mg^{2+} ions. Therefore, I tested how different $MgCl_2$ concentrations (2 mM-10 mM) affect the assay. Surprisingly, there was no

significant difference among all tested conditions. Therefore, we decided to keep the original buffer Mg^{2+} concentration of 3 mM (**Fig.26A**). Next, I tested effects of various concentrations of NaCl (50 – 200 mM). Similarly to Mg^{2+}, addition of NaCl up to 200 mM did not show any significant effect on the assay (**Fig.26B**).

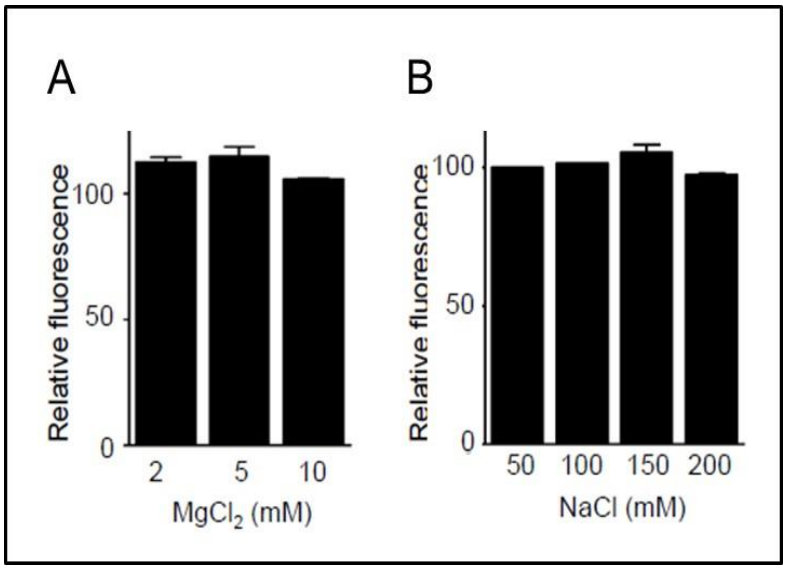

Fig.26: Effect of Mg^{2+} ions (A) and NaCl (B) on the Dicer activity. Fluorescence fold change observed after 3 h incubation of recombinant Dicer (233 nM) with the Cy5/IB-RQ substrate (35 nM). The original buffers conditions (30 mM Tris-HCl, pH 6.8, 50 mM NaCl, 3 mM MgCl2, 0.1% Triton X-100, and 15-20% glycerol) were set as 100. All experiments were carried out in black flat-bottom polystyrene 384-well microplate in total volume of 60 µl. Values are reported as mean ± SEM.

5.1.2.3.5 Effect of buffer additives on the Dicer activity

To test optimal conditions of the assay, I assessed the influence of several buffer additives including PEG4000, glycerol, Triton X-100, and DMSO on the Dicer activity under the single-turnover conditions. PEG4000 is frequently used as enzyme "stabilizer". Therefore I tested, if addition of PEG4000 (5% v/v) would affect the Dicer activity. Surprisingly, the addition of PEG4000 rather decreased than increased the fluorescence released after the Dicer-mediated cleavage. Therefore PEG4000 was excluded from the final buffer (**Fig.27A**). Combinations of glycerol (up to 20% v/v) and Triton X-100 (up to 1% v/v) had only mild effects. In particular, final concentrations of Triton X-100 exceeding 0.75% and glycerol concentrations below 10% reduced the Dicer activity by tens of percent. Based on these data, 0.25% Triton X-100 and 15% glycerol were selected as optimal concentrations for the Dicer assay (**Fig.27B**). Since DMSO is the most frequently used solvent for chemical libraries, I examined how addition of DMSO affects theDicer activity. The effect of DMSO in the reaction buffer was negligible at least up to 5% (v/v). As the final DMSO concentration generally does not exceed 1% (v/v), the HTS should not be affected (**Fig.27C**).

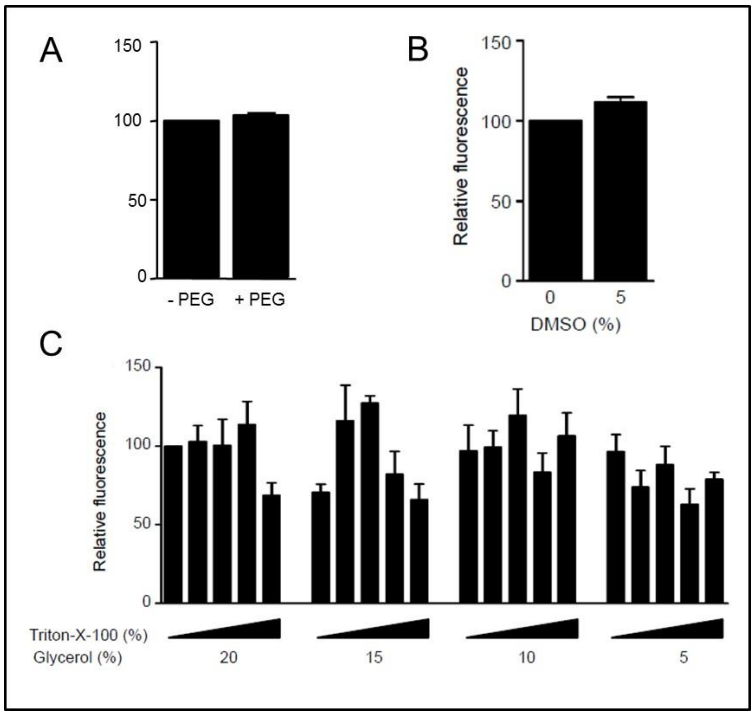

Fig.27: Effect of buffer additives on Dicer activity. Fluorescence fold change observed after 3 h incubation of recombinant Dicer (233 nM) with the Cy5/IB-RQ substrate (35 nM) (fluorescence at t = 3h/fluorescence at 0h). **(A)** Effect of PEG4000 addition. **(B)** Effect of DMSO addition. **(C)** Effect of combination of Triton X-100 and glycerol concentration. Increasing Triton X-100 concentrations were 0.1%, 0.25%, 0.5%, 0.75%, and 1%. The original buffers conditions (30 mM Tris-HCl, pH 6.8, 50 mM NaCl, 3 mM MgCl2, 0.1% Triton X-100, and 15-20% glycerol) were set as 100. All experiments were carried out in black flat-bottom polystyrene 384-well microplate in total volume of 60 µl. Values are reported as mean ± SEM.

5.1.2.3.6 Effect of pH and reaction temperature on Dicer activity

To test optimal conditions of the assay, I analyzed the influence of pH and reaction temperature on the Dicer activity under the single-turnover conditions. The effect was tested for pH values ranging from 6 to 9. The best dynamic range of the assay was observed using the Tris-HCl buffer at pH range 7.0 to 8.0, whereas pH 6.0 and 9.0 showed a 2-fold lower absolute fluorescence activity relative to the original buffer. Since reaction in the buffer at pH 8 was superior in some experiments, we adjusted the pH of original buffer from 6.8 to 8 (**Fig.28A**). Next, I tested the difference between reaction temperatures 30 °C and 37 °C. Notably, although there was only a mild difference between both conditions, the reaction performed at 30 °C was slightly slower, which enabled to measure the Dicer activity at 30 °C during the HTS and so to reduce evaporation (**Fig.28B**).

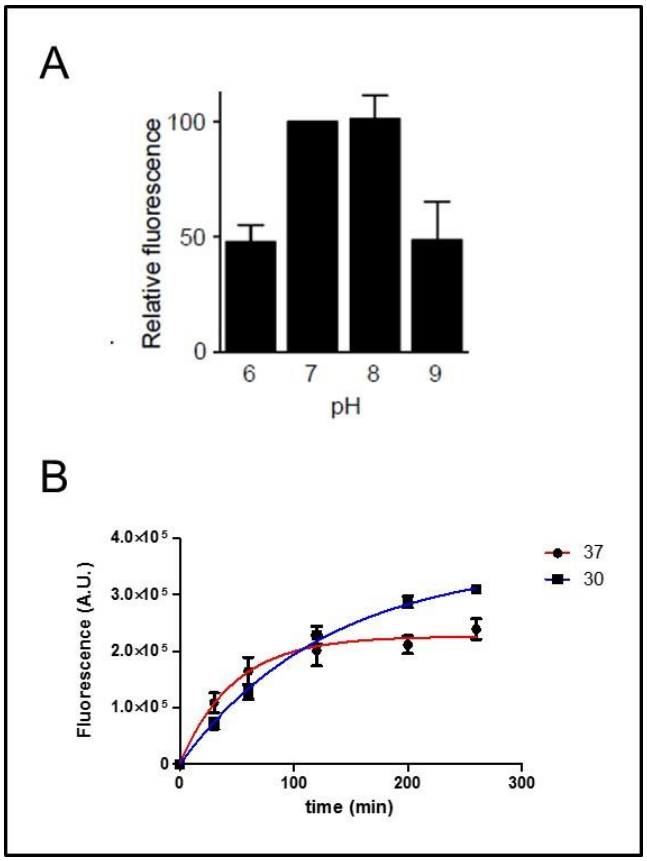

Fig.28: Effect of pH and reaction temperature on Dicer activity. (A) Effect of buffer pH. Fluorescence fold change observed after 3 h incubation of recombinant Dicer (233 nM) with the Cy5/IB-RQ substrate (35 nM) (fluorescence at t = 3h/fluorescence at t = 0 h). **(B)** Effect of reaction temperature: Reaction progress curves observed after incubation of Dicer (233 nM) with 35 nM substrate at 30 °C (blue) or 37 °C (red). Experiments were carried out in black flat-bottom polystyrene 384-well microplate in total volume of 60 µl. Values are reported as mean ± SEM.

5.1.3 Adaptation of the fluorescence-based *in vitro* Dicer assay for HTS

To meet specific requirements for the fully integrated HTS robotic station, we have downscaled the assay to total volume of 5 µl per well suitable for black, flat-bottom, polystyrene 1536-well microtiter plates (*Corning, Inc., New York, NY*). All experiments were performed in optimized Dicer assay buffer (30 mM Tris-HCl, pH 6.8, 50 mM NaCl, 3 mM $MgCl_2$, 0.25% Triton X-100, and 15% glycerol). Unless otherwise stated, the reaction was performed at 37 °C and 100% humidity to minimize evaporation. The fluorescence was determined using the multilabel reader EnVision (*PerkinElmer, Waltham, MA*) equipped with a Bodipy TMR optimized filter set (excitation filter 494 nm and emission filter 519 nm) at indicated timepoints.

5.1.3.1 Large-scale purification of huDicerHisC from insect cells

Based on the results from the small-scale optimization of recombinant human Dicer-HisC purification and based on the literature, I selected the final protocol (for details, see Material and methods) for large-scale purification of the protein. Briefly, Dicer was

isolated from ~2 x 10^9 Sf9 insect cells infected with the recombinant baculovirus. These cells were divided into eight batches, which were processed consecutively. The presence of Dicer protein in individual elution fraction was tested during the elution by Bio-Rad Protein Assay (*Bio-Rad*) (**Fig.29A**) and after the elution by imuno-dot-blot using anti-Dicer 349 rabbit polyclonal primary antibody ((Sinkkonen et al., 2010); 1:5,000) and HRP-conjugated goat anti-rabbit secondary antibody (*Sigma-Aldrich*, 1:15,000) (**Fig.29B**). Based on the results from Bio-Rad Protein Assay and immune-dot-blot, the fractions containing Dicer were pooled, dialysed and the purity of recovered Dicer was analyzed by electrophoresis on 6% SDS-PAGE gel followed by the CBB-R250 staining (**Fig.29C**) and by western blotting using the mouse monoclonal anti-polyHistidine Peroxidase Conjugate antibody (*Sigma-Aldrich*, 1:2,000). (**Fig.29D**).

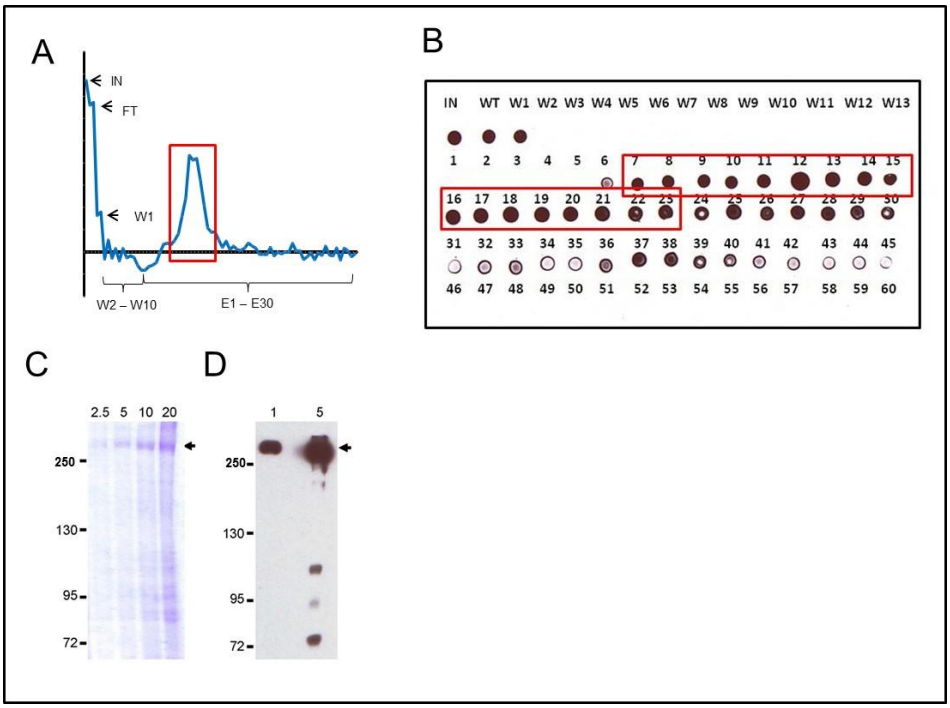

Fig.29: Recombinant Dicer used for HTS - purification: (A) Protein concentration in individual steps of Dicer purification determined using Bio-rad protein assay (*Bio-Rad*). IN = input, FT = flow-through, W1-W10 = washes, E1-E30 = elution fractions. **(B)** Imuno-Dot-Blot of recombinant Dicer in individual steps of its purification stained by anti-Dicer 349 rabbit polyclonal primary antibody ((Sinkkonen et al., 2010); 1:5,000) and HRP-conjugated goat anti-rabbit secondary antibody (*Sigma-Aldrich*, 1:15,000). **(C)** Indicated amounts (in microliters) of purified Dicer were resolved on a 6% polyacrylamide gel and stained by CBB R-250. **(D)** Western blotting of 1 and 5 µl of recombinant Dicer stained by mouse monoclonal anti-polyHistidine Peroxidase Conjugate antibody. Positions of size marker bands in kDa are indicated on the left side. Arrows mark the C-terminally tagged recombinant human Dicer purified from insect cells.

5.1.3.1.1 Analysis of Dicer activity in individual batches

After processing of all Sf9 cells expressing the Dicer protein, the individual Dicer batches were analyzed for Dicer activity in the Dicer cleavage assay under the single-turnover conditions. Notably, all batches contained sufficiently active Dicer (**Fig.30A**) and therefore, all of them were pooled. The activity of pooled Dicer was sufficient as determined by comparison with Dicer batch used in the previous experiments under the same assay conditions (**Fig.30B**). The concentration of pooled Dicer protein was estimated by the Bio-rad Protein Assay (*Bio-Rad*) and was 7 µg/µl. The final yield of the recombinant protein was ~25 mg. The concentration of the purified recombinant Dicer was estimated as total protein content in the recombinant Dicer batch. Therefore, recombinant Dicer concentrations reported here should be considered as the upper limit, while the concentration of the active recombinant Dicer was presumably lower.

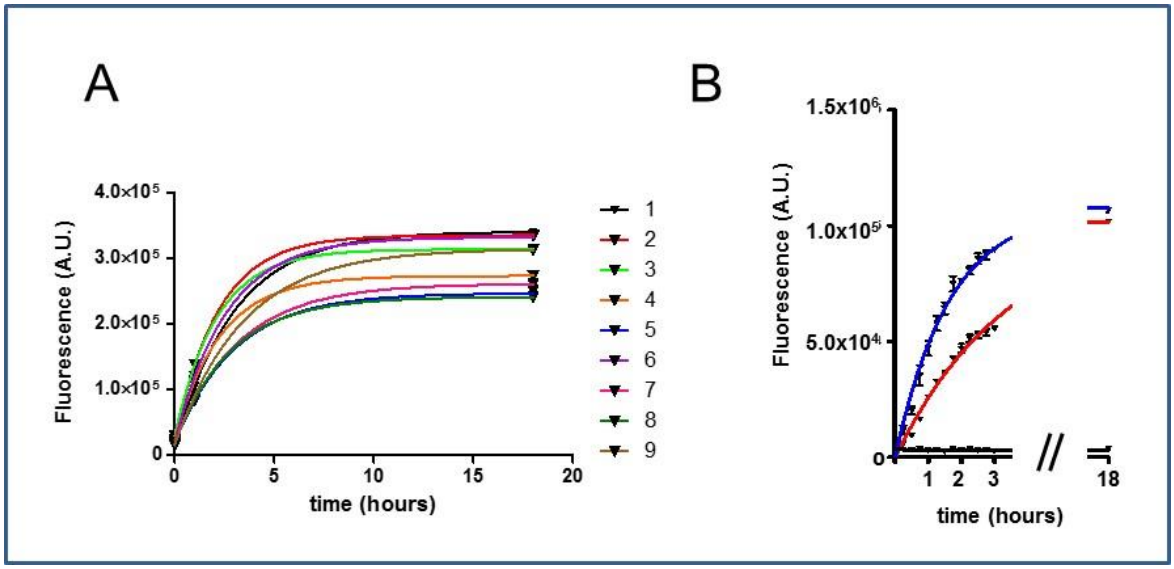

Fig.30: Recombinant Dicer used for HTS – analysis of activity. (A) Reaction progress curves observed after incubation of 1 µl of Dicer from individual Dicer batches with 3 nM substrate. **(B)** Reaction progress curves observed after incubation of Dicer pool (red) or Dicer batch 1 (blue) (233 nM) with 35 nM substrate. Experiments were carried out in black flat-bottom polystyrene 384-well microplate in total volume of 60 µl. Values are reported as mean ± SEM.

5.1.3.2 The enzyme and substrate concentrations

Several parameters influenced the selection of the substrate concentration for HTS, including the dynamic range, sensitivity, costs, available amount of recombinant Dicer, the conversion rate of the substrate, and finally the feasibility of the kinetic measurement in the HTS mode. First, I analyzed the range of substrate concentrations giving an acceptable

signal-to-noise ratio by processing different concentrations of fluorescently labeled dsRNA substrate by excess of Dicer. In particular, 3 to 333 nM of the dsRNA substrate was processed with 230 nM Dicer, and the fluorescent product was recorded for several hours until the reaction rate decreased to a minimum (**Fig.31A**). Since the sensitivity of the assay is dependent on the concentration of the substrate, we were looking for the lowest acceptable concentration of the substrate in the reaction. Starting from the ~15 nM initial substrate concentration, the reaction generated acceptable signal at 50% of substrate conversion (**Fig.31A**). When the reaction was performed to reach higher levels of substrate conversion, substrate concentrations below ~15 nM generated the acceptable signal at later timepoints as well. Although the measurement at relatively high levels of substrate conversion improves the dynamic range of the assay, it sacrifices sensitivity at the same time (Wu et al., 2003). While the lowest acceptable substrate concentration was determined as 15 nM, 35 nM substrate was used in the later assay development to balance the quality and sensitivity of the assay. The optimal Dicer concentration was determined by titrating the fixed concentration of the dsRNA substrate (35 nM) with different Dicer concentrations ranging from 23 nM to 2.3 μM (**Fig.31B**). At the highest concentrations, the Dicer was present in large molar excess over the substrate, and the reaction was performed under the single-turnover conditions, under which the reaction rate was not limited by the product release and enzyme recovery. At these concentrations, the reaction progression was relatively fast ($t_{1/2}$ ~45 min), and the intensity of the fluorescent signal quickly reached the maximum level corresponding to complete substrate conversion (**Fig.31B**). At equimolar concentration of Dicer to substrate, the reaction rate was considerably slower ($t_{1/2}$ ~3–4 h). We also observed that the fluorescent signal did not reach the maximum when the reaction rate declined to zero (**Fig.31B**). To use the full dynamic range of the reaction at a given substrate concentration while keeping the Dicer concentration as low as possible, we selected 70 nM as the optimal concentration for Dicer in the assay.

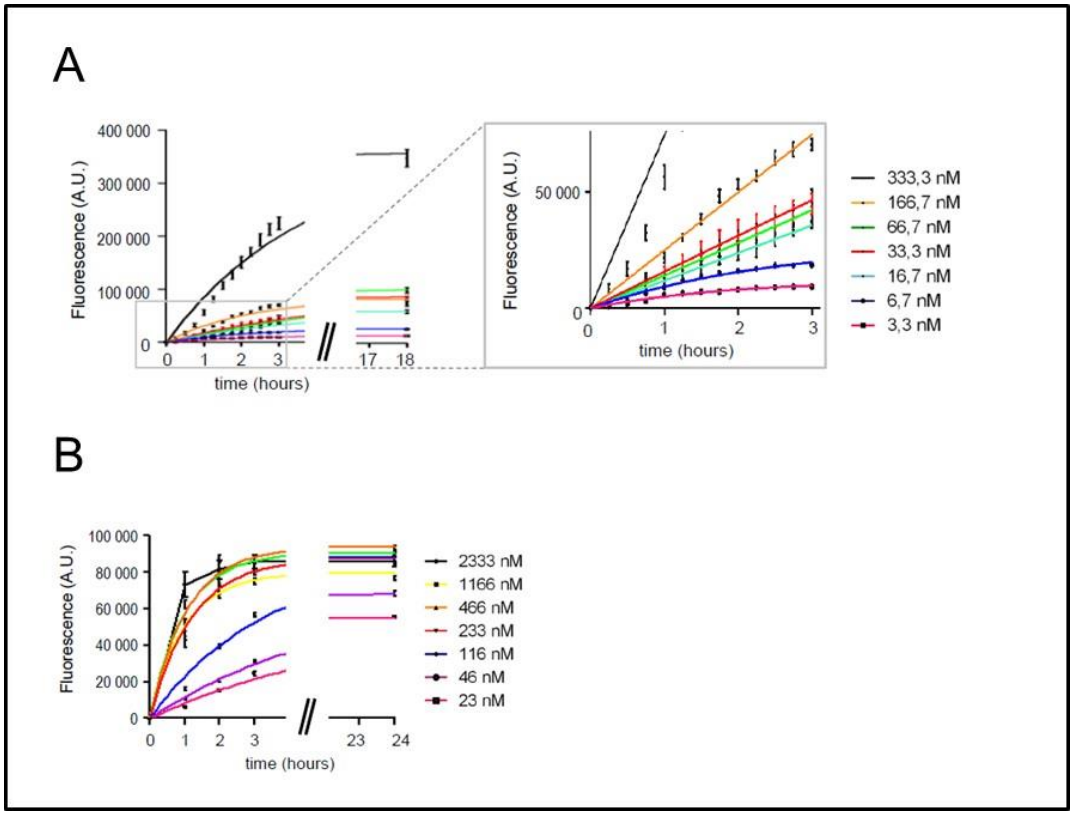

Fig.31: Optimization of substrate and Dicer concentrations. (A) Reaction progress curves under constant Dicer amount (233 nM) and variable Dicer substrate amounts (3.3 nM – 333 nM) conditions. The experiment was carried out in black flat-bottom polystyrene 1536-well microplate in total volume of 5 µl. Error bars = SEM. **(B)** Reaction progress curves under variable Dicer amount (2333 nM – 23 nM) and constant substrate amount (35 nM) conditions. Experiment was performed in black flat-bottom polystyrene 1536-well microplate in total volume of 5 µl. Values are reported as mean ± SEM.

5.1.3.3 Effect of kanamycin on Dicer activity

To further evaluate the assay conditions, I used kanamycin, whose inhibition of Dicer activity has already been shown *in vitro* (Davies and Arenz, 2006). To test the influence of kanamycin A on the Dicer activity, a dose-response experiment was performed under the single-turnover conditions optimized for HTS. We were able to detect inhibitory effects of kanamycin with IC50 = 20.3 µM (**Fig.32A**). Results obtained at the 100 µM concentration were comparable to previous results (Davies and Arenz, 2006).

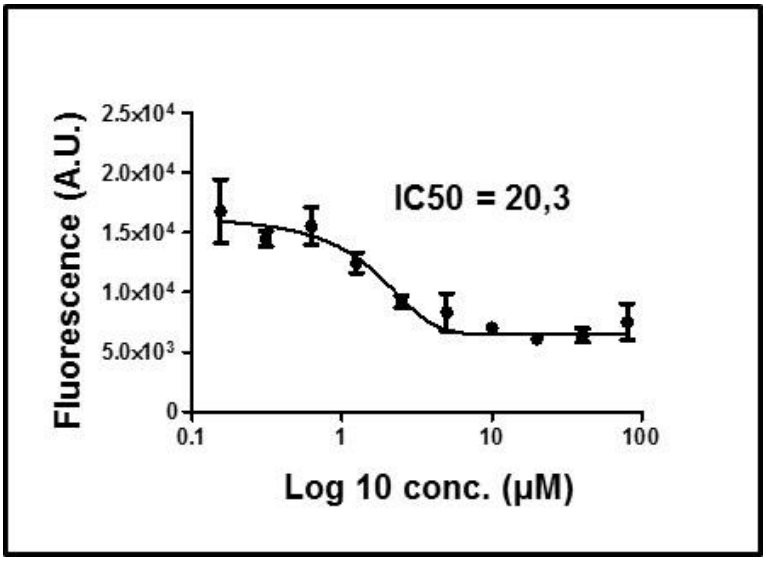

Fig.32: Effect of kanamycin on Dicer activity. Inhibition constant (IC) for kanamycin A determined using the fluorescence *in vitro* Dicer assay using 70 nM Dicer and 35 nM substrate. Experiments were carried out in black flat-bottom polystyrene 384-well microplate in total volume of 60 µl. Values are reported as mean ± SEM.

5.1.3.4 The final optimization of Dicer cleavage assay for HTS

To meet specific requirements for the fully integrated HTS robotic station, we downscaled the assay to a total volume of 5 µl per well suitable for 1536-well microplates. To assess feasibility of the assay under HTS conditions, we ran the kinetic experiment for 18 h with previously determined concentrations of substrate (35 nM) with or without 70 nM Dicer and with or without randomly selected 15 µM compounds (**Fig.32A**). As shown in **Fig.31A**, the pilot kinetic experiment confirmed the feasibility of the assay in the HTS format. Slight increase of the fluorescence in the reaction without Dicer indicated the decreasing stability of the fluorescent Dicer substrate over time, which should not influence the result of the HTS.

To assess the stability and quality of the assay over time, we ran the kinetic experiment for 24 h with previously determined concentrations of substrate (35 nM) with or without 70 nM Dicer and measured the *Z´* factor for different times of the reaction (**Fig.32B**). The *Z´* factor is a measure of statistical effect size quantifying the suitability of a particular assay for use in HTS. The *Z´* factor reached the maximum around 6 h of the reaction time and subsequently declined. This drop in the quality of the assay at later timepoints of the reaction was presumably due to the instability of the annealed fluorescent dsRNA substrate, which resulted in the increasing fluorescent background signal over time in the absence of Dicer even when RNase inhibitors were added. However, the measurement of the reaction progression should be done at lower substrate conversion points, preferentially before 50% of the substrate is converted, corresponding to the

reaction time of ~4 h. At this time, the effect of the increased background fluorescence is minimal and does not strongly affect the quality of the assay.

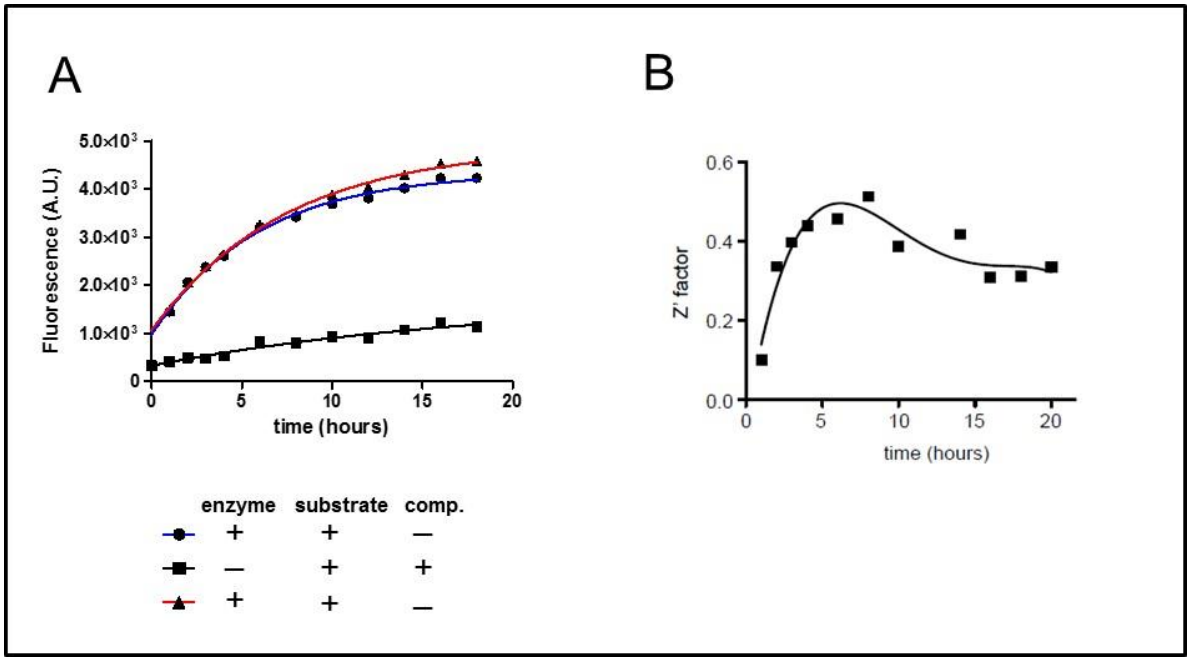

Fig.33: The kinetic pilot screen: (A) Reaction progress curves observed after incubation of the Dicer substrate (35 nM) with or without (black) 70 nM Dicer and with (blue) or without (red) randomly selected 15 μM compounds. **(B)** Changes in Z´ factor during the course of a kinetic experiment. Z´ factor was estimated for different times of reaction. Experiments were carried out in black flat-bottom polystyrene 1536-well microplate in total volume of 5 μl. Values are reported as mean ± SEM.

5.1.4 HTS screen of Dicer stimulators and inhibitors

We performed a kinetic HTS with the collection of ~30,000 compounds from 15 libraries including Sigma LOPAC Library, Prestwick Library, NIH Clinical Trial Collection, and several proprietary libraries. The screen was carried out in 1536-well plates and in the kinetic mode for 25 h. The first data were collected at t = 0 h and then after 1 h, 2 h, 3 h, 4 h, 6 h, 8 h, 10 h, 13 h, 15 h, 17 h, 19 h, 20 h, 21 h, 23 h, and 25 h. Notably, this was the first extensive kinetic screen performed in the Czech Republic. The compounds were tested at the final concentration of 15 μM. The **Fig.34** shows schematic representation of successive steps in the HTS process. The HTS process is described in detail in chapter **4.2.4**. The values were normalized to the background fluorescence at time = 0 h and to the control samples in which no compounds were added. The data normalization is described in detail in chapter **4.2.5**. Here we describe: (i) the partial HTS result of a bioactive

collection of 2816 compounds, which has already been published in Podolska *et al*. (2014) (Podolska et al., 2014), and (ii) the initial data mining from the whole Dicer HTS.

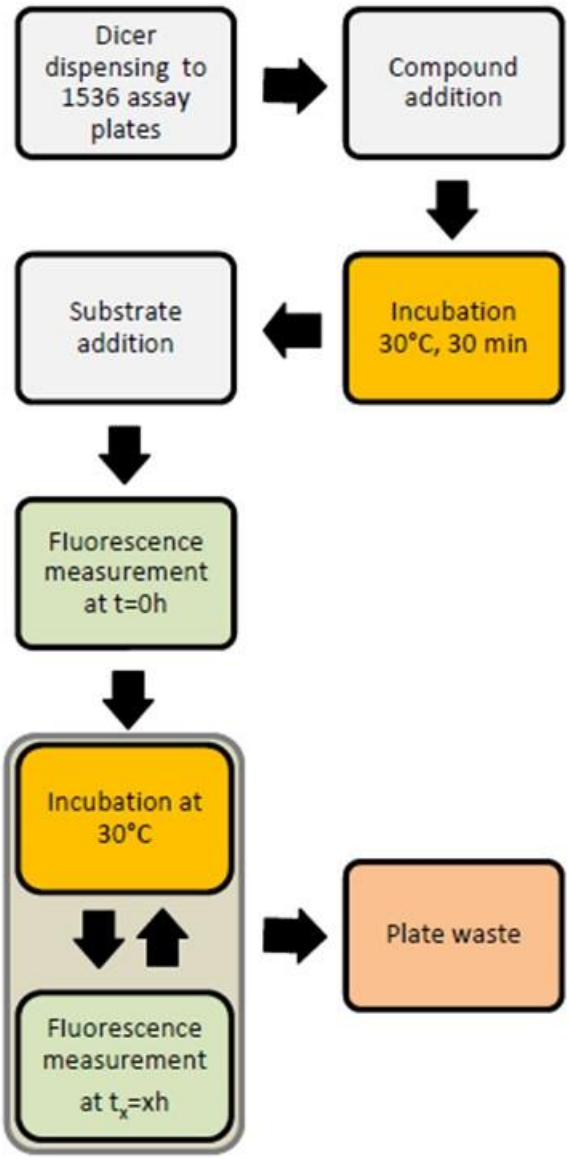

Fig.34: Schematic representation of successive steps in the HTS process. The enzymatic Dicer assay was carried out in 1536 plates in the kinetic mode for 25 h.

To identify Dicer-inhibiting compounds in the bioactive collection of 2816 compounds, we analyzed the normalized values from the measurements corresponding to 4 h of the reaction time and selected only those compounds that inhibited the assay by at least 50% (**Fig.35**). Furthermore, strongly autofluorescent compounds were removed from the analysis as strong autofluorescence prevailing over fluorescence from the cleavage reaction would impair the data quality. Using these criteria, we found 40 potential inhibitors.

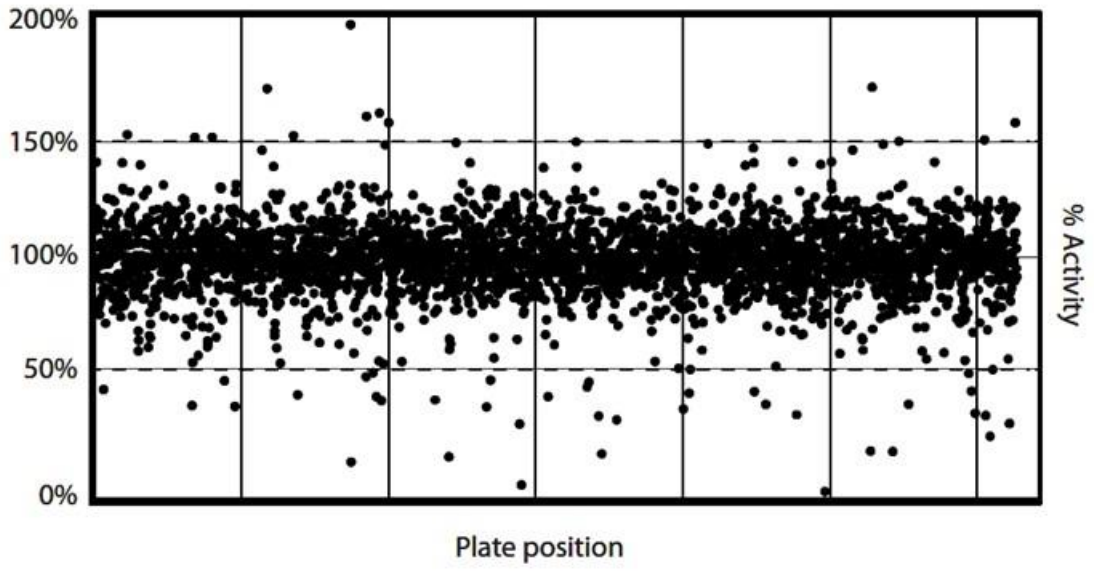

Fig.35: Distribution of activities of 2816 tested compounds. The activities of all tested compounds from the kinetic screen were measured after 4 h from the initiation of the assay, and normalized values were plotted as a function of their respective position in the screened library.

To validate the results of the HTS, we cherry-picked all 40 potential inhibitor compounds and performed a dose-response experiment in the concentration range from 200 nM to 20 μM under the HTS conditions. Of them, 22 compounds revealed reproducible dose-response inhibitory activity in the tested concentration range. The remaining 18 compounds did not show a clear dose response or the inhibition effect did not reach 50% of the inhibition in the tested concentration range. The potency of the validated hits was in the range from 0.5 μM to higher concentrations. Validated compounds were diverse in terms of their structure and annotated pharmacokinetic properties. Since no established Dicer inhibitor was available, the way how to assess the specificity of the identified potential inhibitors of Dicer was limited. First, we performed structure analysis of 22 validated compounds using JKlustor (*ChemAxon*). The analysis revealed 3 scaffolds present in 11 validated hits (**Tab.10**). The other half of compounds did not share any obvious structural similarity. Compounds in clusters I and II are highly related both functionally and structurally. They belong to the same class of biologically active compounds. These scaffolds were enriched in the set of validated hits indicating that the described Dicer assay enables to reproducibly detect specific scaffold-containing small molecules with inhibitory activity. However, the exact mechanism of how these compounds interfere with the assay remains to be elucidated. Second, we compared 22 validated hits from the Dicer screen with a list of validated hits from several unrelated

enzymatic screens. We found 5 compounds that were active in the Dicer assay and at the same time in at least 70% of all unrelated screens, suggesting that these compounds modulate enzymatic activity of Dicer by a nonspecific manner (**Tab.10**). Interestingly, none of these frequent hitters overlapped with the compounds in clusters I and II. On the other hand, compounds from the cluster III were repeatedly found active in other unrelated screens too, which makes them unlikely candidates for specific Dicer inhibitors.

Cluster	Scaffold MW[a]	Compounds[b]	MW Range[c]	IC_{50} Range[d]	Frequent Hitters[e]
I	148	3	220 to 448	1.9 to >20	0
II	256	3	445 to 538	1.9 to 2.9	0
III	138	4	213 to 458	1.0 to 2.0	3
Not clustered	No	12	129 to 804	0.5 to >20	2

Tab.10: Structural analysis of the validated hits. Scaffold identification and scaffold-based compound clustering was carried out with JKlustor (*ChemAxon, Budapest, Hungary*). Three scaffolds were detected and used for compound clustering. **(a)** Molecular weight of the detected scaffold. **(b)** Number of compounds in the cluster. **(c)** Molecular weight range of compounds in the cluster. **(d)** IC50 values for compounds in one cluster were calculated from the validation dose-response curves using GraphPad Prism software (*GraphPad Software, La Jolla, CA*) and nonlinear regression function Y = Bottom + (Top – Bottom)/ (1+10(LogIC50 −X)*Hill slope). **(e)** Number of potentially nonspecific inhibitors detected by the analysis of the hits from unrelated biochemical screens.

To identify potential Dicer modulators in the whole collection of ~30,000 compounds, the data were normalized using B-score method (Brideau et al., 2003) and subsequently subjected to a process aiming to identify active compounds. B-score normalization removed differences between different plates and artifacts, such as the edge effects affecting outer position in the plate and row and column effects introduced by different devices in the workflow of the screen (Brideau et al., 2003). Notably, strongly autofluorescent compounds were removed from the analysis. The normalized values from the measurements were analyzed in reaction times 6 h or 15 h. Potential Dicer inhibitors were identified by applying a cut-off either 9xB-score value (for reaction time 6 h) or 11xB-score value (for reaction time 15 h) of all measured values in the screen excluding the control samples. Potential Dicer activators were identified by applying a cut-off -5.5xB-score value of all measured values in the screen excluding the control samples for both reaction times. Using these criteria, we found 170 potential inhibitors (9xB-score) and 36 potential activators (-5.5xB-score) of Dicer activity at time 6 of the reaction time, 38 (11xB-score) potential inhibitors and 36 potential activators (-5.5xBscore) of Dicer activity at time 15of the reaction time. In total, 279 compounds, of them 72 potential Dicer activators and 207 potential Dicer inhibitors, were cherry-picked and

prepared for next dose-response validation experiments. Development of the assay and results from the analysis of a bioactive collection of 2816 compounds were summarized in a publication "Fluorescence-based high-throughput screening of dicer cleavage activity" (Podolska et al., 2014).

Cell-based assays

5.1.5 Principle of the cell-based assays

I developed several cell-based assays to monitor the endogenous miRNA activity in cells in order to discover both general and miRNA-specific small-molecule modifiers of RNA silencing. The cell-based assays employ plasmid reporters containing the target sequence(s) of mature endogenous miRNAs in the 3´UTR, downstream of a reporter CDS. Under normal conditions, endogenous miRNAs bind to their target sequence on the reporter mRNA and, according to the type of the miRNA binding site, either suppress translation or induce the degradation of mRNAs, thus silencing the reporter. Therefore, any interference with miRNA biogenesis or function can be detected as an increase in the reporter activity (**Fig.12A**).

5.1.6 Assay development

5.1.6.1 EGFP-based reporter

For assaying the let-7 effects, I first examined EGFP-reporter containing three perfect binding sites for let-7 miRNA in the 3´UTR (pCagEGFP.puro_3xlet-7P) as a part of our search for an optimal reporter system for HTS. The EGFP-based reporter was selected for the following reasons. First, EGFP requires no additional substrates or cofactors. Second, the EGFP fluorescence can be easily and cheaply detected by a fluorometer. Importantly, reporters containing perfect binding sites are efficiently repressed mainly by a slicing action of endogenous miRNA loaded on AGO2. We decided to start with the EGFP reporter containing three perfect let-7 binding sites based on assumption that more perfect miRNA binding sites in the target mRNA increase the chance of interaction with miRNA.

First, the functionality of pCagEGFP.puro_3xlet-7P reporter was analyzed as followed. The pCagEGFP.puro_3xlet-7P reporter or control EGFP plasmid, in which

3xlet-7 binding sites were inserted in an antisense (non-functional) direction were transiently transfected into HEK293 cells, and subsequently the fluorescent activity was analyzed using fluorescent microscopy and fluorescence-activated cell sorting (FACS), 48 hours post transfection (hpt). As expected, the EGFP signal of control plasmid was detected using both methods (FACS data – **Fig.36A**). However, the shift in fluorescence intensity between non-transfected cells and cells transfected with pCagEGFP.puro_3xlet-7P reporter was detected only using a more sensitive FACS (**Fig36**).

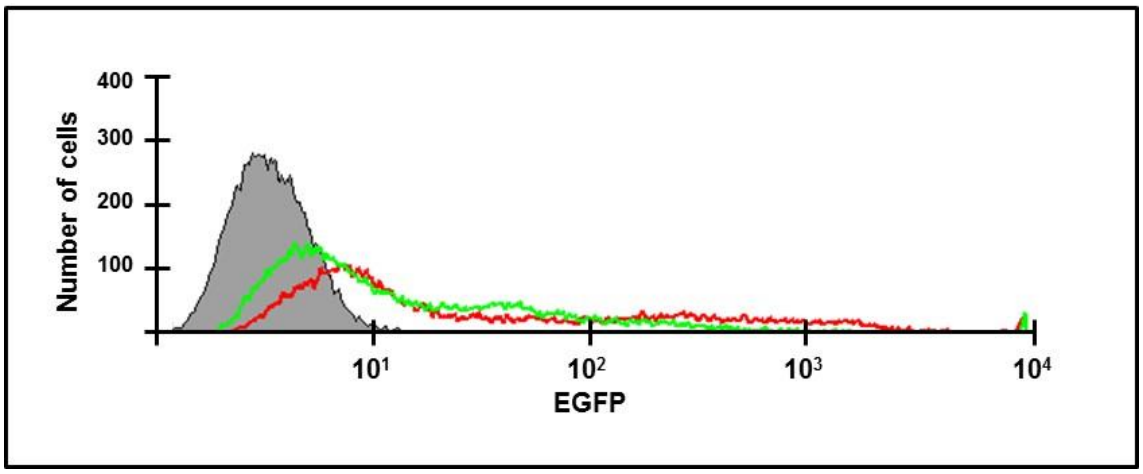

Fig.36: Transient transfection of HEK293 cells with EGFP reporter carrying 3xlet-7 perfect binding sites in 3'UTR: HEK 293 cells were co-transfected with 100 ng/well of pCagEGFP.puro_3xlet-7perfect or with 100 ng/well of pCagEGFP.puro_3xlet-7perfect_invert plasmid and 500 ng/well of pTer plasmid. Transfection was performed using TurboFect transfection reagent. EGFP expression was analyzed 48 hpt by FACS. x axis = EGFP fluorescence intensity. y axis = cell count. Colored curves show distribution of EGFP signal as follows: grey curve = un-transfected cells, green curve = pCagEGFP.puro_3xlet-7perfect + pTer co-transfection and red curve = pCagEGFP.puro_3xlet-7perfect_invert + pTer co-transfection.

For HTS purposes, stable reporter cell lines needed to be established to reduce the number of manipulations and to increase the reproducibility and robustness of the assay. To establish the stable reporter cell line, the pCagEGFP.puro_3xlet-7P vector encoding a puromycin resistance marker was transfected into either HeLa or HEK293 cells. HeLa and HEK293 cells were selected for stable cell lines establishment for their high efficiency of transfection, high levels of endogenous let-7 miRNA, and a large amount of data available for data comparison. Stable clones were selected using an optimal puromycin

concentration. The sensitivity of established reporter cell lines to miRNA pathway inhibition was tested as follows.

First, the biogenesis of endogenous let-7 miRNA was inhibited by knocking-down Dcr1 or *AGO2*. Individual HeLa and HEK293 clones carrying a stably integrated pCagEGFP.puro_3xlet-7P reporter were transfected with a plasmid expressing shRNA targeting Dcr1 or *AGO2*, and changes in EGFP fluorescence were analyzed by FACS, 72 hpt (**Fig.37A, B**). Although knock-down of either Dcr1 (data not shown) or *AGO2* (**Fig.37A, B**) increased EGFP fluorescence intensity in comparison to un-transfected reporter cells, both fluorescence signals were overlapping, thus making distinguishing of the inhibitory effect difficult.

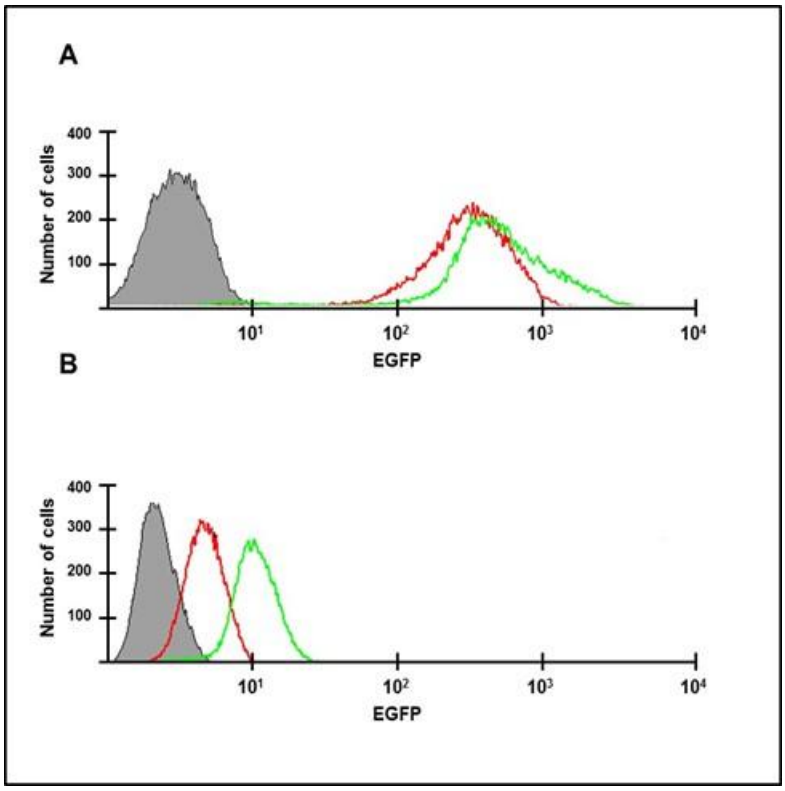

Fig.37: Analysis of HeLa and HEK293 stable cell lines carrying EGFP reporter with 3xlet-7 perfect binding sites in 3'UTR: (A) HEK293 cells carrying stably integrated pCagEGFP.puro_3xlet-7perfect, clone #B4 or **(B)** HeLa cells carrying stably integrated pCagEGFP.puro_3xlet-7perfect, clone #C4, were transfected with 2 µg/well of pTer-Ago2_shRNA plasmid. Transfection was performed using TurboFect transfection reagent. EGFP expression was analyzed 72 hpt by FACS. x axis = EGFP fluorescence intensity. y axis = cell count. Colored curves show distribution of EGFP signal as follows: grey curve = un-transfected cells, red curve = un-tranfected reporter cells, green curve = pTer-Ago2_shRNA transfection.

Second, miRNA pathway was inhibited globally using plant virus suppressor proteins. HeLa_pCagEGFP.puro_3xlet-7P reporter cells (clone #C4) were transfected with (i) P19 plant virus suppressor protein (pcDNA_P19 plasmid) (**Fig.38A**) or (ii) P21 plant virus suppressor protein (pcDNA_P21 plasmid) (**Fig.38B**) and analyzed by FACS 48 hpt. As expected, P19- and P21-mediated inhibition of RNAi increased EGFP fluorescence in comparison to un-transfected reporter cells, however, the shift in fluorescence signal was only mild, similarly to Dcr-1 and *AGO2* knock-downs.

Third, let-7 miRNAs were specifically inhibited using let-7-specific antagomir (AMOs, miRCURY LNA mm-let-7a). HeLa_pCagEGFP.puro_3xlet-7P reporter cells (clone #C4) were transfected with AMOs and analyzed by FACS 48 hpt (**Fig.38C**). Transfection of 40 pmol miRCURY LNA mm-let-7a in combination with 1 μg of pcDNA3.1 plasmid as a stuffer DNA resulted in the increase in fluorescence in comparison to un-transfected reporter cells, or reporter cells transfected with 1 μg of pcDNA3.1 plasmid alone. As a stuffer DNA is referred a "neutral" DNA, for example a simple cloning plasmid without functional mammalian sequences, which is added to the transfection mixture to maintain the constant amount of transfected DNA per sample. Although transfection with 4 pmol of miRCURY LNA mm-let-7a also resulted in a mild increase in EGFP fluorescence in comparison to un-transfected reporter cells, the shift was comparable with a control transfection with pcDNA3.1 stuffer plasmid alone, indicating that transfection with a stuffer plasmid alone can influence the EGFP signal (**Fig.38C**).

Taken together, the functionality of EGFP reporter cell-based assay was confirmed by different strategies of miRNA pathway inhibition. However, due to a low fluorescence signal change upon the miRNA pathway inhibition and relatively high background fluorescence, the assay was unsatisfactory. The increase in fluorescence was detectable only by flow cytometry, making the assay suboptimal for the HTS format. Thus, for further development of the HTS assay we opted for luciferase reporters.

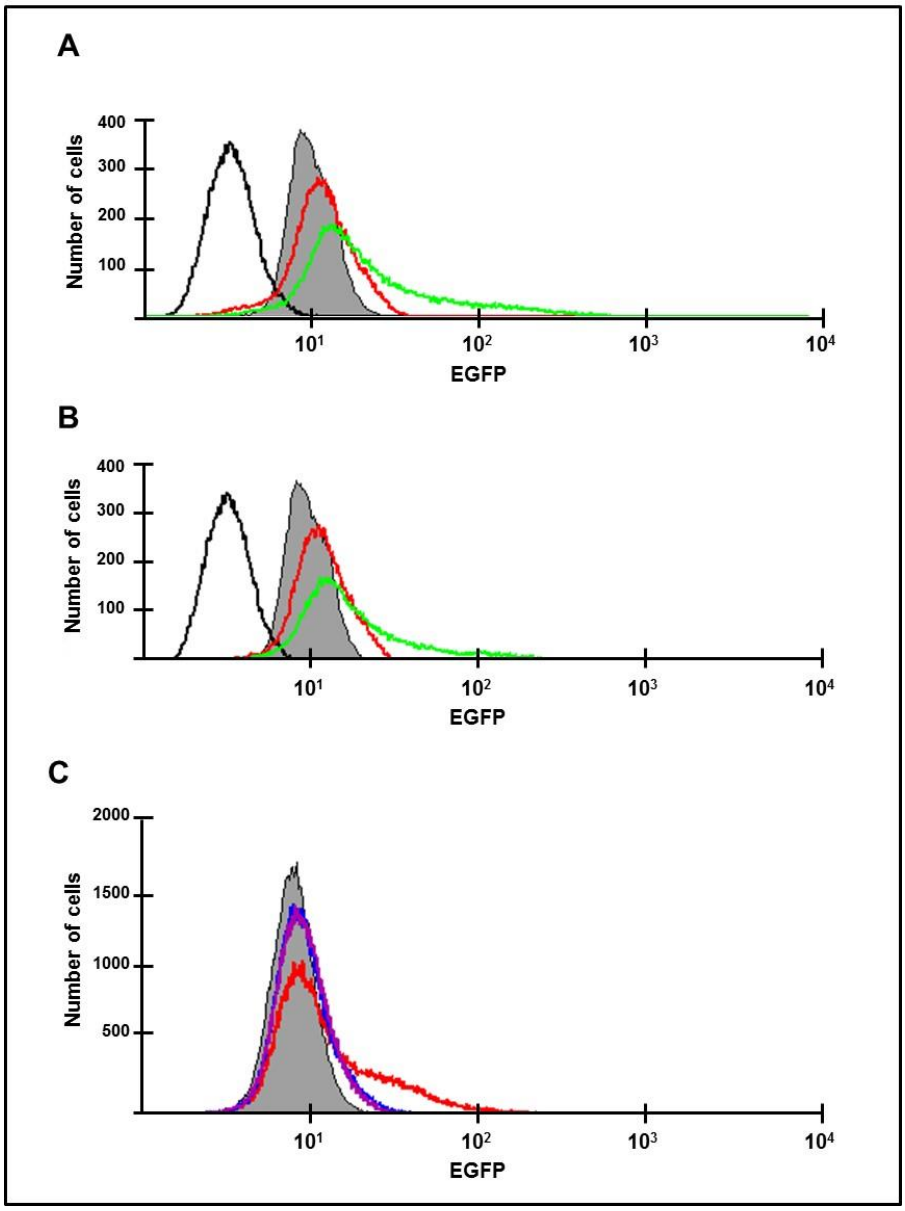

Fig.38: Analysis of HeLa cells carrying stably integrated 3xlet-7 perfect reporter clone #C4: (A) Transfection with 1 µg of pcDN3.1(-)_P19 plasmid, or co-transfection with 100 ng of pcDNA 3.1(-)_P19 plasmid and 900 ng of pcDNA 3.1(-) plasmid. **(B)** Transection with 1 µg of pcDN3.1(-)_P21 plasmid, or co-transfection with 100 ng of pcDNA 3.1(-)_P21 plasmid and 900 ng of pcDNA 3.1(-) plasmid. Transfection was performed using TurboFect transfection reagent (*Life Technologies*). EGFP expression was analyzed 48 hpt by FACS. x axis = EGFP fluorescence intensity. y axis = cell count. Colored curves show distribution of EGFP signal as follows: black = un-transfected cells, grey = un-transfected reporter cells, red = transfection with 1 µg of pcDNA 3.1(-)_P19 plasmid or 1 µg of pcDNA 3.1(-)_P21 plasmid, green = co-transfection with 100 ng of pcDNA 3.1(-)_P19 plasmid or 100 ng of pcDNA 3.1(-)_P21 plasmid + 900 ng of pcDNA 3.1(-) plasmid. **(C)** Co-transfection with 4 pmol or 40 pmol of miRCURY LNA mm-let-7a AMOs and 1 µg of pcDNA 3.1(-) plasmid as a stuffer. As a negative control, cells were transfected only with 1 µg of pcDNA 3.1(-) plasmid. Transfection was performed using Lipofectamine 2000 transfection reagent (*Life Technologies*). EGFP expression was analyzed 48 hpt by FACS. x axis = EGFP fluorescence intensity. y axis = cell count. Colored curves show distribution of EGFP signal as follows: grey = un-transfected reporter cells, violet = transfection with 1 µg of pcDNA 3.1(-), blue = co-transfection with 1 µg of pcDNA 3.1(-) + 4 pmol of miRCURY LNA mmLet-7a AMOs, red curve = co-transfection with 1 µg of pcDNA 3.1(-) + 40 pmol of miRCURY LNA mmLet-7a AMOs.

5.1.6.2 Dual luciferase-based reporter

Dual luciferase-based reporters were developed and analyzed as the second step of searching for an optimal reporter system for HTS. Although a luciferase-based reporter assay is much more sensitive when compared to EGFP-based reporters, it has several disadvantages, such as the costs or necessity of adding substrates and having a luminometer for measuring luminiscence.

First, we decided to test a bidirectional luciferase-based reporter containing both a *Renilla* luciferase and an independently transcribed firefly luciferase reporter gene. In this reporter, binding sites for endogenous miRNA were inserted downstream of *Renilla* CDS, and the firefly reporter was used for normalization purposes to account for variation in transfection efficiency and cell viability (**Fig.39**). The principle of the method is the same as for EGFP-reporters. Briefly, mature endogenous miRNAs will suppress the *Renilla* luciferase. After inhibition of miRNA, the *Renilla* luciferase expression will recover and yield an increased *Renilla* luciferase signal. Since this reporter system is based on an increase instead of a decrease in the luciferase expression in the presence of an active inhibitor, false positives caused by compound toxicity are minimized.

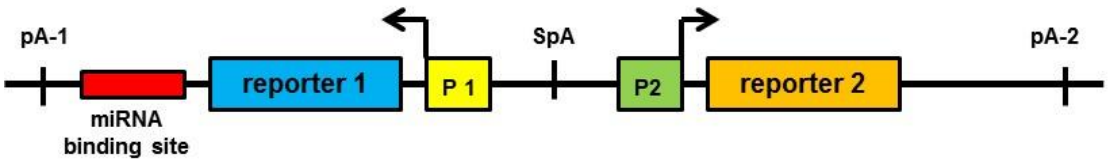

Fig.39: Scheme of the dual luciferase-based reporter. pA = polyadenylation signal, SpA = synthetic polyadenylation signal, P = promoter.

To obtain optimal reporters, I constructed and tested combinations of promoters (PGK, CMV, SV40, and TK), polyA sites (SV40pA, TKpA, BGHpA), and miRNA biding sites (1-4 bulged or perfect sites) for different miRNAs (let-7, miR-30). As described below, such reporters were repressed to different levels and had different sensitivity to repression and stimulation of RNA silencing.

The first set of analyses examined the impact of different combination of promoters on the activity of reporters containing 3xlet-7P binding sites downstream *Renilla* luciferase. The ability of the reporters to detect endogenous let-7 miRNA was analyzed by transient transfection with one of the following reporters into HeLa cells:

(i) pRep-G418_SV40pA-3xlet-7P-RL←**CMV**-spA-**PGK**→FL-BGHpA

(ii) pRep-G418_SV40pA-3xlet-7P-RL←**PGK**-spA-**CMV**→FL-BGHpA

(iii) pRep-G418_SV40pA-3xlet-7P-RL←**TK**-spA-**PGK**→FL-BGHpA

The assay was validated by co-transfection with let-7 family-specific LNA AMOs (*Exiqon*) as a positive control. Luciferase reporter activity was assessed using the Dual-Luciferase Reporter Assay (*Promega*) 48 hpt. Transfection details are described in particular figure legends. Notably, the analysis revealed that combination of different promoters in bidirectional luciferase-based reporters has only a slight impact on their activity. A 65-fold increase in luciferase activity was observed in HeLa cells after a transient co-transfection with let-7-specific AMOs in comparison to the activity obtained after a transfection with pRep-G418_SV40pA-3xlet-7P-RL←**PGK**-spA-**CMV**→FL-BGHpA plasmid alone (**Fig.40A**). The activities of pRep-G418_SV40pA-3xlet-7P-RL←**PGK**-spA-**CMV**→FL-BGHpA was almost twice as high as the activity of pRep-G418_SV40pA-3xlet-7P-RL←**TK**-spA-**PGK**→FL-BGHpA (**Fig.40A**). No significant differences were found between the activity of pRep-G418_SV40pA-3xlet-7P-RL←**PGK**-spA-**CMV**→FL-BGHpA and pRep-G418_SV40pA-3xlet-7P-RL←**CMV**-spA-**PGK**→FL-BGHpA (data not shown).

The second set of analyses examined the impact of different miRNA binding sites on the bidirectional luciferase reporter activity. HeLa cells were transiently transfected with one of the following reporters:

(i) pRep-G418_SV40pA-3xlet-7P-RL←**PGK**-spA-**CMV**→FL-BGHpA,

(ii) pRep-G418_SV40pA-4xlet-7B-RL←**PGK**-spA-**CMV**→FL-BGHpA

(iii) pRep-G418_SV40pA-4xmiR-30B-RL←**PGK**-spA-**CMV**→FL-BGHpA.

To knock-down let-7 or miR-30 activity, the co-transfection with miRNA specific LNA AMOs was performed. The activity of the reporters was assessed using the Dual-Luciferase Reporter Assay (*Promega*), 48 hpt. Transfection details are described in the legend of **Fig.40**. It is apparent that different miRNA binding sites affect the reporter activity (**Fig.40B**). Notably, the activity increase of the perfect reporter was up to 15-fold higher than the increase of both bulged reporters, whose activity was similar. The reporter containing three perfect binding sites for let-7 miRNA (pRep-G418_SV40pA-3xlet-7P-

RL←PGK-spA-CMV→FL-BGHpA) showed a 65-fold increase of luminiscence after let-7 inhibition and was selected for a stable cell line establishment.

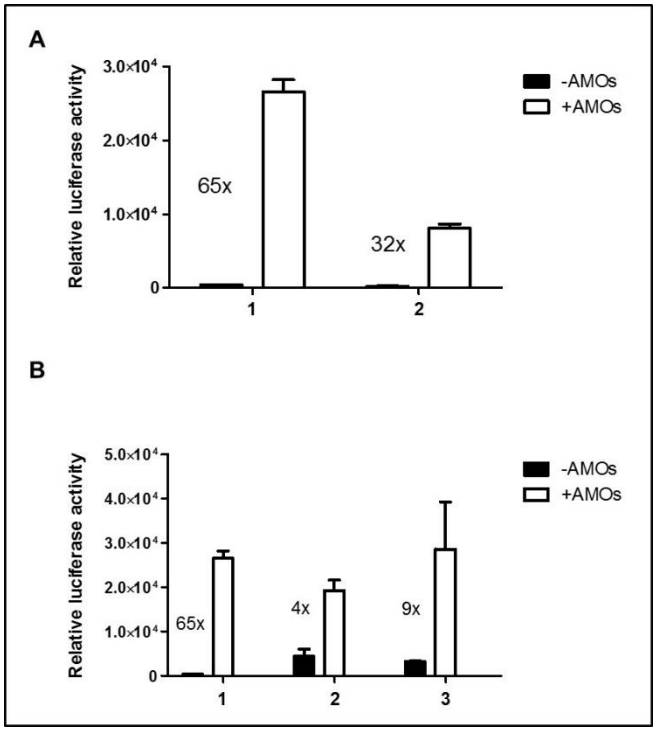

Fig.40: Effect of (A) different combination of promoters on luciferase reporters or (B) different miRNA binding sites on luciferase activity. HeLa cells co-transfected with 5 pmol/well of let-7- or miR-30-specific LNA AMOs (white bars), 500 ng/well of pBS and 2.5 ng /well of luciferase reporter. For control reactions (black bars), AMOs were omitted. (A) x axis: 1 = pRep-G418_SV40pA-3xlet-7P-RL←PGK-spA-CMV→FL-BGHpA, 2 = pRep-G418_SV40pA-3xlet-7P-RL←TK-spA-PGK→FL-BGHpA. (B) x axis: 1 = pRep-G418_SV40pA-3xlet-7P-RL←PGK-spA-CMV→FL-BGHpA, 2 = pRep-G418_SV40pA-4xlet-7B-RL←PGK-spA-CMV→FL-BGHpA, 3 = plasmid pRep-G418_SV40pA-4xmiR-30B-RL←PGK-spA-CMV→FL-BGHpA. y axis: *Renilla* normalized to firefly. Fold increase is indicated next to the bars. Values are reported as mean ± SEM.

To establish a stable reporter cell line, the pRep-G418_SV40pA-3xlet-7P-RL←PGK-spA-CMV→FL-BGHpA vector encoding a neomycin resistance marker was transfected into HeLa cells. Stable clones were selected using optimal G418 concentration. Resistant clones were transfected with let-7-specific LNA AMOs and assayed for the presence of the luciferase reporter using a Dual Luciferase Assay (*Promega*). The best clones were selected based on the level of luciferase expression, and the response to let-7 AMOs transfection. Surprisingly, more than a half of analyzed resistant clones expressed only the firefly luciferase. Of clones expressing both, *Renilla* and firefly luciferase, the clone #B5 with 55-fold increase of luminiscence after let-7 inhibition showed the best dynamic range of the assay and was selected for next experiments. This clone provided ~6-fold higher dynamic range of the assay comparing with the second best clone #A2 (**Fig.41A**). Similarly as for HeLa cells, U2OS stable cell line carrying the pRep-G418_SV40pA-3xlet-7P-RL←PGK-spA-CMV→FL-BGHpA reporter was established and analyzed. The U2OS human bone osteosarcoma epithelial cells were chosen for their easy maintenance in the cell culture, good so-far experience in HTS, and existing data from counter screen searching for cytotoxic compounds. The 22-fold increase of luminiscence

was observed after inhibition of let-7 by specific AMOs in the heterogeneous population of reporter cells (**Fig.41B**). Finally, four different clones with the highest release of luminiscence after let-7 inhibition by AMOs were selected for next experiments: clone #6 (22-fold change), clone #2 (36-fold change), clone #15 (28-fold change), and clone #22 (24-fold change) (data not shown).

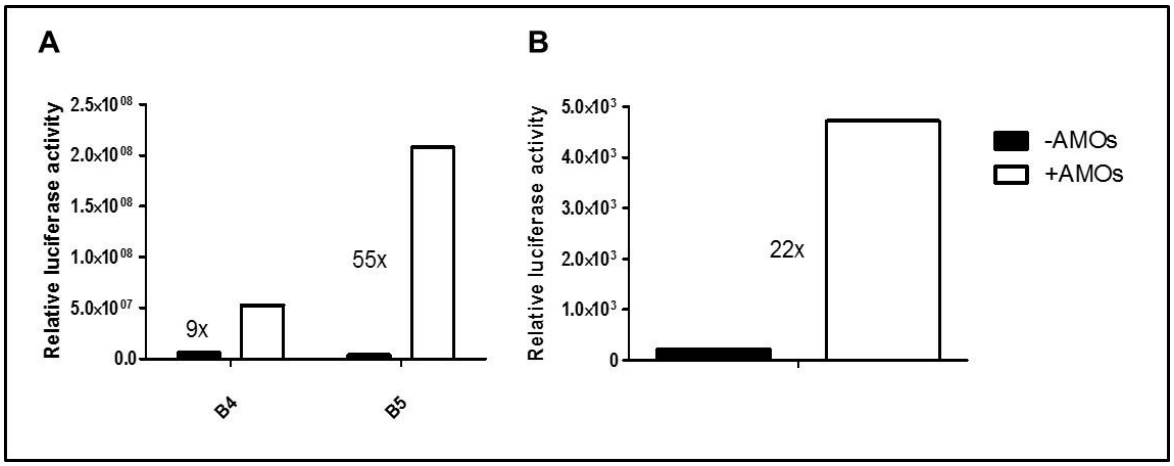

Fig.41: Analysis of stable cell lines carrying bidirectional luciferase-based reporter with 3xlet-7 perfect binding sites: Individual clones of HeLa cells (individual clones designated B4 and B5) **(A)** or heterogeneous population of U2OS cells **(B)** carrying pRep-G418_SV40pA-3xlet-7P-RL←PGK-spA-CMV→FL-BGHpA reporter were transfected with 5 pmol/well of let-7 family-specific LNA AMOs (white bars). For control reactions (black bars) AMOs were omitted. y axis: *Renilla* normalized to firefly. Fold increase is indicated next to the bars.

Taken together, dual luciferase-based reporters carrying miRNA binding sites in 3´UTR of *Renilla* CDS were developed and optimized in terms of type of used promoters, polyA sites, or number and type of miRNA binding sites. Subsequently, HeLa-based and U2OS-based stable reporter cell lines were established and analyzed. Bidirectional luciferase assays employing the selected HeLa and U2OS clones showed satisfactory dynamic range. However, regardless of our so-far good experience with small-scale bidirectional luciferase assays employing *Renilla* as the experimental target, the use of this system for HTS turned out to be problematic for two reasons. First, the EnVision plate reader used for measurement of luminescence signal during HTS experiments does not allow the measurement of *Renilla* and firefly luciferase signals sequentially. Second, the usage of Renilla-glo (*Promega*) steady substrate for *Renilla* luciferase was not established and optimized well at that time. Importantly, the pilot HTS with Renilla-glo substrate showed poor reproducibility (data not shown) for reasons that were not further studied. Therefore, we decided for developing a firefly luciferase-based reporter system.

5.1.6.3 Firefly-based reporter

Tens of cell-based HTSs employing the firefly luciferase reporters have already been successfully performed in the collaborating group of Petr Bartunek, IMG AS CR, CZ-OPENSCREEN, providing a large volume of existing data for data comparison. Therefore, we finally decided to adopt a firefly-based reporter assay as the reporter system for HTS. First, I constructed reporters carrying 3xlet-7P binding sites in the 3´UTR behind the firefly luciferase (pEGFP-SpA-PGK-FL-3xlet-7P-BGHpA). Next, HeLa stable cell lines carrying the pEGFP-SpA-PGK-FL-3xlet-7P-BGHpA encoding a neomycin resistance marker were established. Resistant clones were transfected with let-7-specific LNA AMOs and assayed for the presence of the luciferase reporter using a Dual Luciferase Assay (*Promega*), 48 hpt. The clones were then selected based on the level of luciferase expression and the response to let-7 inhibition. Finally, three different clones with the highest release of luminiscence after let-7 inhibition by AMOs were selected for next experiments and storage: clone #10 (14-fold change), clone #13 (40-fold change), and clone #16 (8-fold change) (**Fig.42A**). Similarly to HeLa stable cell lines, U2OS stable cell lines carrying the pEGFP-SpA-PGK-FL-3xlet-7P-BGHpA reporter were established and tested. Finally, three different clones with the highest increase of luminiscence after let-7 inhibition by AMOs were selected for next experiments and storage: clone #2 (10-fold change), clone #9 (3.5-fold change), and clone #10 (6.5-fold change) (**Fig.42B**).

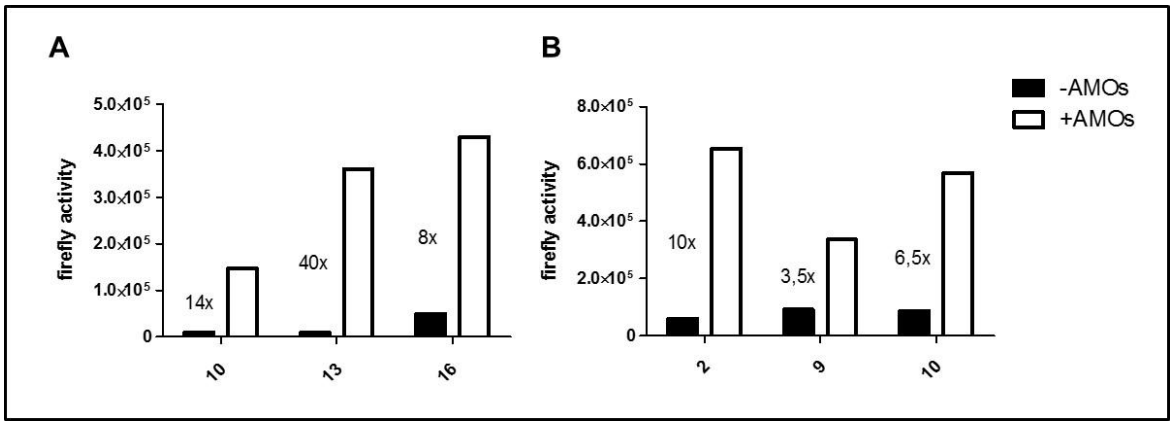

Fig.42: Analysis of stable cell lines carrying firefly-based reporter with 3xlet-7 perfect binding sites: Individual clones of HeLa cells **(A)** or U2OS cells **(B)** carrying pEGFP-SpA-PGK-FL-3xlet-7P-BGHpA reporter were transfected with 5 pmol/well of let-7 family-specific LNA AMOs (white bars). For control reactions (black bars), AMOs were omitted. x axis: Numbers of individual clones. y axis: Firefly luciferese normalized to the total protein amount in lysates. Fold increase is indicated next to the bars.

5.1.6.4 Final selection of the stable reporter cell line for pilot HTS

Four cell lines carrying a stably integrated luciferase reporter were selected for the final analysis before HTS: (i) HeLa_ pEGFP-SpA-PGK-FL-3xlet-7P-BGHpA#13, (ii) HeLa_pRep-G418_SV40pA-3xlet-7P-RL←PGK-spA-CMV→FL-BGHpA#B5, (iii) U2OS_pEGFP-SpA-PGK-FL-3xlet-7P-BGHpA#2, and (iv) U2OS_pRep-G418_SV40pA-3xlet-7P-RL←PGK-spA-CMV→FL-BGHpA#2. Briefly, the cells were transfected with let-7 family specific AMOs (*Exiqon*). The presence of the firefly luciferase reporter was assayed using a One-Glo luciferase assay system (*Promega*), 48 hpt. The presence of *Renilla* luciferase reporter was assayed using Renilla-Glo luciferase assay system (*Promega*), 48 hpt. The results obtained from the preliminary analysis of the reporter cell lines are compared in **Fig.43**. Of the bidirectional reporters in which *Renilla* was the targeted luciferase, the U2OS_pRep-G418_SV40pA-3xlet-7P-RL←PGK-spA-CMV→FL-BGHpA#2 reporter provided ~7-fold higher dynamic range of the assay compared to the HeLa_pRep-G418_SV40pA-3xlet-7P-RL←PGK-spA-CMV→FL-BGHpA#B5 (**Fig.43, A and B**). From firefly reporters, the HeLa_pEGFP-SpA-PGK-FL-3xlet-7P-BGHpA#13 reporter provided ~ 6.5-fold higher dynamic range of the assay compared to U2OS_ pEGFP-SpA-PGK-FL-3x-let-7P-BGHpA#2 (**Fig.43, C and D**). Finally, HeLa_pEGFP-SpA-PGK-FL-3x-let-7P-BGHpA#13 reporter cell line was selected as the best for the pilot HTS for following reasons: (i) it provided reasonable dynamic range of the assay (~11x), (ii) it provided higher basal reporter activity potentially enabling to discover both inhibitors and activators of miRNA pathway, (iii) HTS-based on measurement of firefly luciferase was well established in collaborating group of Petr Bartunek, IMG AS CR, CZ-OPENSCREEN, providing a large amount of data for results comparison.

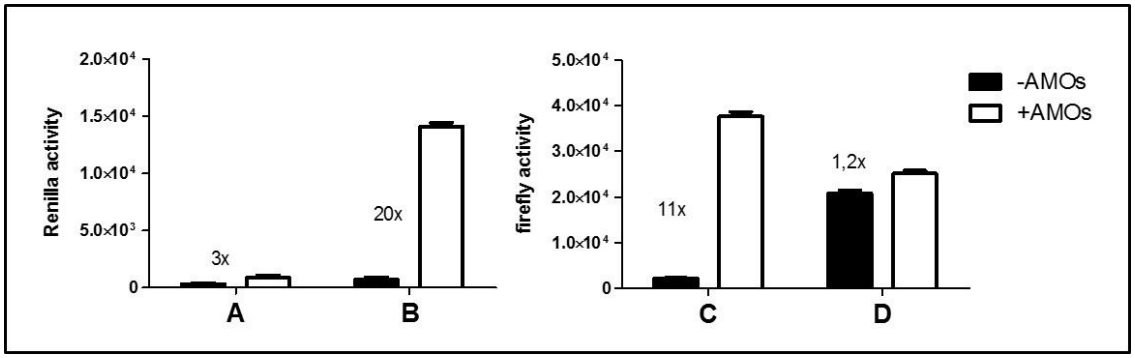

Fig.43: Selection of the stable luciferase cell line for HTS. Reporter cells were transfected with 25 pmol/well of let-7 family-specific LNA AMOs (white bars). For control reactions (black bars), AMOs were omitted. Fold increase is indicated next to the bars. Experiment was carried out in white flat-bottom polystyrene 384-well microplate in total volume of 25 µl. Luminescence was measured by EnVision. Values are reported as mean ± SEM.

y axis: Luciferase activity.

x axis: A = HeLa_pRep-G418_SV40pA-3xlet-7P-RL←PGK-spA-CMV→FL-BGHpA #B5 stable cell line,
B = U2OS_pRep-G418_SV40pA-3xlet-7P-RL←PGK-spA-CMV→FL-BGHpA #2 stable cell line,
C = HeLa_pEGFP-SpA-PGK-FL-3xlet-7P-BGHpA #13 stable cell line,
D = U2OS_pEGFP-SpA-PGK-FL-3xlet-7P-BGHpA #2 stable cell line.

5.1.6.5 Additional firefly-based reporters for HTSs

To obtain data allowing for filtering of HTS results according to different parameters, we decided to develop additional cell-based luciferase assays. First, to filter cell type-specific effects, NIH-3T3 stable cell line carrying the PGK-FL-3xlet-7 perfect reporter encoding a neomycin resistance marker was established. The mixed population of resistant cells (pool) was transfected with let-7-specific LNA AMOs, and the presence of the luciferase reporter was tested using a Dual Luciferase Assay (*Promega*), 48 hpt. The pool showed 7.5-fold increase of luminescence after let-7 inhibition (data not shown). The resistant clones were selected and tested by the same way as the mixed population of resistant cells. The best clones were selected based on the level of luciferase expression and the response to let-7 inhibition. Finally, four different clones were selected for next experiments and storage. The clones #A21, #A33, #A45, and #A10 showed 20-fold, 46-fold, 68-fold, and 72-fold increase in luminescence after let-7 inhibition using specific AMOs, respectively (**Fig.44A**).

Second, to filter the compounds affecting a translation repression or upstream steps, HeLa stable cell line carrying the PGK-FL-4xlet-7 bulged reporter encoding a neomycin resistance marker was established. The mixed population of resistant cells (pool) was transfected with let-7-specific LNA AMOs, and the presence of the luciferase reporter was tested using a Dual Luciferase Assay (*Promega*), 48 hpt. The results obtained from the

analysis of the mixed population of resistant cells are presented in **Fig.44B**. The pool showed 8-fold increase of luminescence after let-7 inhibition providing a satisfactory dynamic range of the assays for HTS.

Third, to identify compounds affecting let-7 and miR-30 miRNAs (putative common regulators) and putative let-7-specific regulators, HeLa stable cell line carrying the PGK-FL-4xmiR-30 bulged reporter encoding a neomycin resistance marker was established. The mixed population of resistant cells (pool) was transfected with miR-30-specific LNA AMOs, and the presence of the luciferase reporter was analyzed using a Dual Luciferase Assay (*Promega*), 48 hpt. As can be seen from the graph in **Fig.44B**, the pool showed 29-fold increase of luminescence after the miR-30 inhibition providing satisfactory dynamic range of the assays for HTS.

Notably, HeLa cell lines stably expressing a firefly luciferase reporters carrying four bulged binding sites for either let-7 (pEGFP-SpA-PGK-FL-4xlet-7B-BGHpA) or miR-30 (pEGFP-SpA-PGK-FL-4xmiR-30B-BGHpA) in its 3′UTR were used in study of Novotny *et al*. (2012) (Novotny et al., 2012) to test whether the increased number of P-bodies caused by LSm8 knock-down had any consequences for miRNA-mediated repression of translation (Novotny et al., 2012).

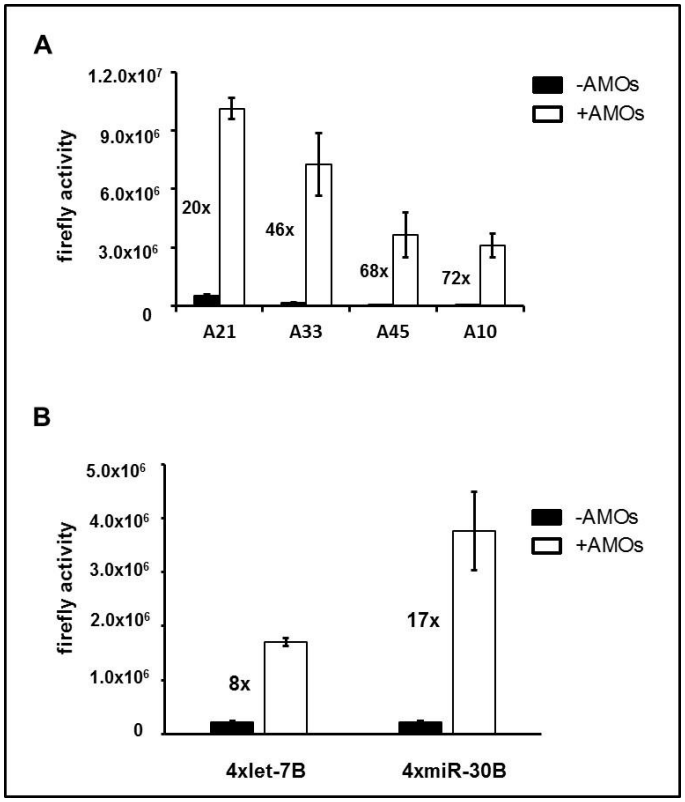

Fig.44: Analysis of stable cell lines carrying firefly-based reporter with 3xlet-7P, 4xlet-7B, or 4xmiR-30B binding sites: (A) Individual clones of NIH-3T3 cells carrying pEGFP-SpA-PGK-FL-3x-let-7P-BGHpA were transfected with 5 pmol/well of let-7 family-specific LNA AMOs (white bars). **(B)** Mixed population of HeLa cells carrying pEGFP-SpA-PGK-FL-4xlet-7B-BGHpA, or pEGFP-SpA-PGK-FL-4xmiR-30B-BGHpA were transfected with 5 pmol/well of let-7 family-specific LNA AMOs, or miR-30 family-specific LAM AMOs, respectively (white bars). For control reactions (black bars), AMOs were omitted. x axis: Numbers of individual clones. y axis: Firefly 123uciferase normalized to the total protein amount in lysates. Fold increase is indicated next to the bars. Values are reported as mean ± SEM.

5.1.6.6 Pilot HTS

After the assay establishment and optimization, we first performed a proof-of-concept HTS of part of the collection (~10 000 compounds) to test: (i) selectivity and robustness of the assay in HTS format and (ii) feasibility of the screening to estimate the hit-rate. The screening was performed in HeLa stable cell line carrying the PGK-FL-3xlet-7 perfect reporter (HeLa_pEGFP-SpA-PGK-FL-3xlet-7P-BGHpA#13), and it is termed HTS-I hereafter. The pilot HTS was performed in collaboration with group of Petr Bartunek, IMG, AS CR, CZ-OPENSCREEN, who provided equipment, original collection of compounds from 15 libraries, including Sigma LOPAC Library, Prestwick Library, NIH Clinical Trial Collection, and several proprietary libraries and data analysis. The pilot screen was carried out in a 384-well format at concentration 1 μM. Collected data from the pilot screen were normalized using a robust B-score method (Brideau et al., 2003). B-score normalization removed differences between different plates and artifacts, such as the edge effects affecting the outer position in the plate and row and column effects introduced by different devices in the workflow of the screen (Brideau et al., 2003). Normalized data were further analyzed in order to identify the active compounds. For hit selection, different cut-off values were examined for potential inhibitors and activators. Hits were identified by applying a cut-off either 5x B-score value of all measured values in the screen excluding control samples for the identification of potential miRNA pathway inhibitors or a cut-off – 1.8x B-score value of all measured values in the screen excluding control samples for the identification of potential miRNA pathway activators (Brideau et al., 2003). Under these conditions, the pilot HTS identified 180 potential inhibitors and 27 of potential activators of the miRNA pathway. Of those, 22 hits were removed due to cytotoxic effects on HL-60 and/or HEK293 cells. Previously, cytotoxicity tests have been performed in the collaborating group of Petr Bartunek, IMG AS CR, CZ-OPENSCREEN. **Fig.45** shows a graphical representation of the pilot screen, which resulted in hit selection visualized in **Fig.46**. Taken together, the pilot screen validated the ability to discover small-molecule inhibitors and activators of miRNA function. Moreover, the pilot screen identified several tens of hits that are necessary to be validated using the secondary assays.

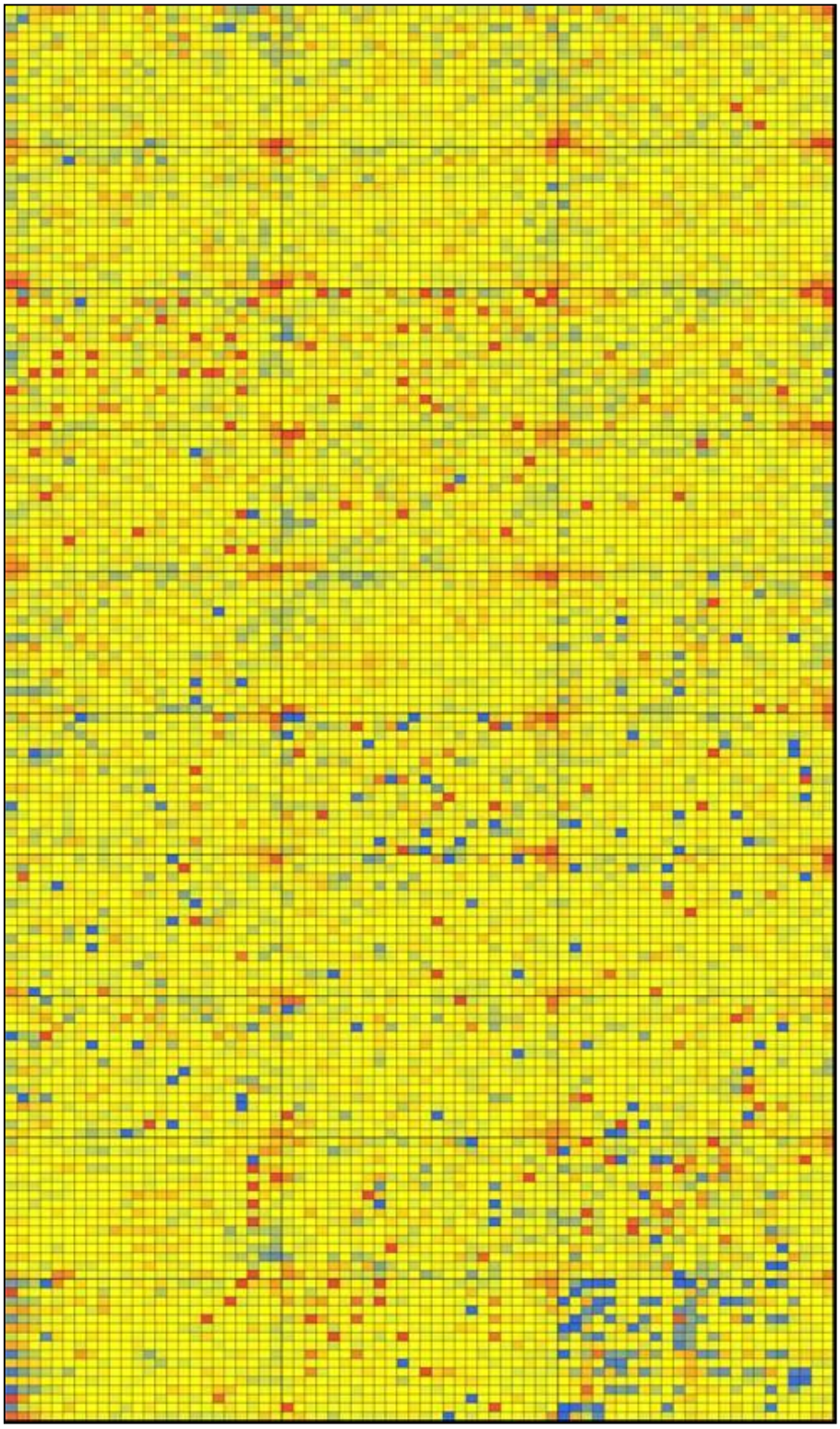

Fig.45: Graphical representation of the pilot HTS: ~10,000 compounds were screened in the pilot screen using HeLa_pEGFP-SpA-PGK-FL-3xlet-7P-BGHpA#13 reporter cell line. Activities of the compounds in the assay are represented in the color scale ranging from the blue (low activity = potential activators) to the red color (high activity = potential inhibitors). The screen was performed in thirty 384-well plates representing 11 520 measured values.

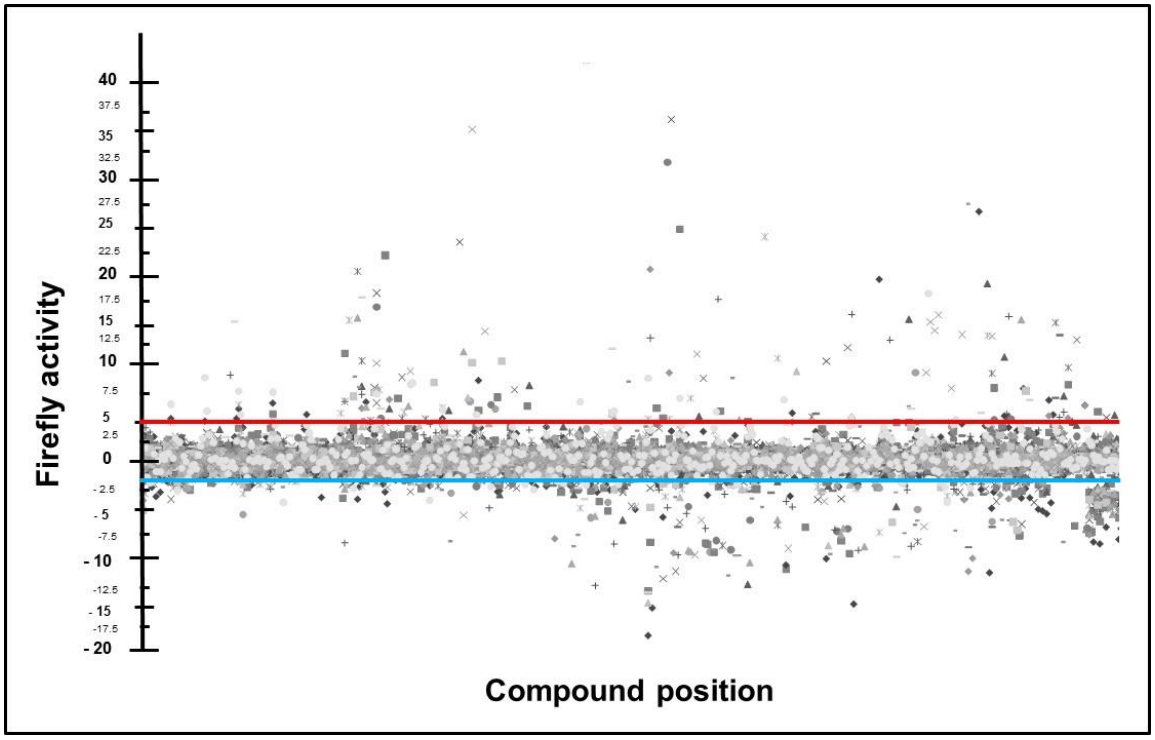

Fig.46: Hit identification: ~10.000 compounds were screened using HeLa_pEGFP-SpA-PGK-FL-3xlet-7P-BGHpA#13 reporter cell line. B-score-normalized data were used for hit selection. Hits were identified by applying a cut-off either 5x B-score value of all measured values in the screen for the identification of potential miRNA pathway inhibitors (here represented by the red line) or a cut-off – 1.8x B-score value of all measured values in the screen for the identification of potential miRNA pathway activators (here represented by the blue line).

5.1.6.7 HTS

After validation of selectivity and robustness of the firefly reporter cell-based assay in the pilot HTS, we decided to continue and perform several additional cell-based screens of ~30,000 compounds allowing us to generate data necessary for filtering of HTS results according to different parameters (**Fig.14**). As for the pilot HTS, all additional HTSs were performed in collaboration with Petr Bartunek group, IMG AS CR, CZ-OPENSCREEN, providing the equipment, the compounds library and data analysis and were carried out in a 384-well format and at concentration 1 μM. Collected data from the screens were normalized using the aforementioned B-score method (Brideau et al., 2003) and subsequently subjected to a process aiming to identify active compounds. Hits were identified by applying a cut-off either 5x B-score value of all measured values in the screen excluding control samples for the identification of potential miRNA pathway inhibitors, or a cut-off –5x B-score value of all measured values in the screen excluding control samples for the identification of potential miRNA pathway activators (Brideau et al., 2003).

First, to complete the results from the pilot HTS and thus obtain HTS data from the whole library, we performed HTS of the rest of the library collection (~20,000 compounds) using the same reporter assay (HTS-I – HeLa_PGK-FL-3xlet-7 perfect). Taken together, the HTS-I identified 624 potential inhibitors (5xB-score) and 791 potential activators (-5xB-score) of the miRNA pathway. Second, we performed HTS in NIH-3T3 stable cell line carrying the PGK-FL-3xlet-7 perfect reporter (HTS-II) to filter cell type-specific effects. The HTS-II identified 903 potential inhibitors (5xB-score) and 489 of potential activators (-5xB-score) of the miRNA pathway. The data from HTS-II were compared with the data from HTS-I. Third, we performed HTS in HeLa stable cell line carrying the PGK-FL-4xlet-7 bulged reporter (HTS-III) to filter compounds affecting translation repression (unique in HTS-III) or upstream steps (common). The HTS-III identified 367 potential inhibitors (5xB-score) and 56 of potential activators (-5xB-score) of the miRNA pathway. The data from HTS-III were compared with the data from HTS-I and HTS-2. Fourth, we performed HTS in HeLa stable cell line carrying the PGK-FL-4xmiR-30 bulged reporter (HTS-IV) to identify compounds affecting let-7 and miR-30 miRNAs (common regulators) and putative let-7-specific regulators. The HTS-IV has identified 587 potential inhibitors (5xB-score) and 229 of potential activators (-5xB-score) of the miRNA pathway.

Venn diagrams in **Fig.47** represent an overview of the most interesting hits generated after data comparison from all HTS performed. As indicated in the center intersection of all HTS results, 227 (-5xB-score) potential general miRNA inhibitors and 15 (5xB-score) potential general miRNA activators were identified. The comparison of the results from the let-7–based screens with the results from the miR-30-based screen revealed 21 (-5xB-score) potential let-7-specific inhibitors and 1 (5xB-score) potential let-7-specific activator. HTS-III and HTS-IV identified 27 (-5xB-score) putative inhibitors and 10 (5xB-score) putative activators of translation repression mediated by miRNAs. Total hit numbers generated by individual screens are summarized in **Tab.11**.

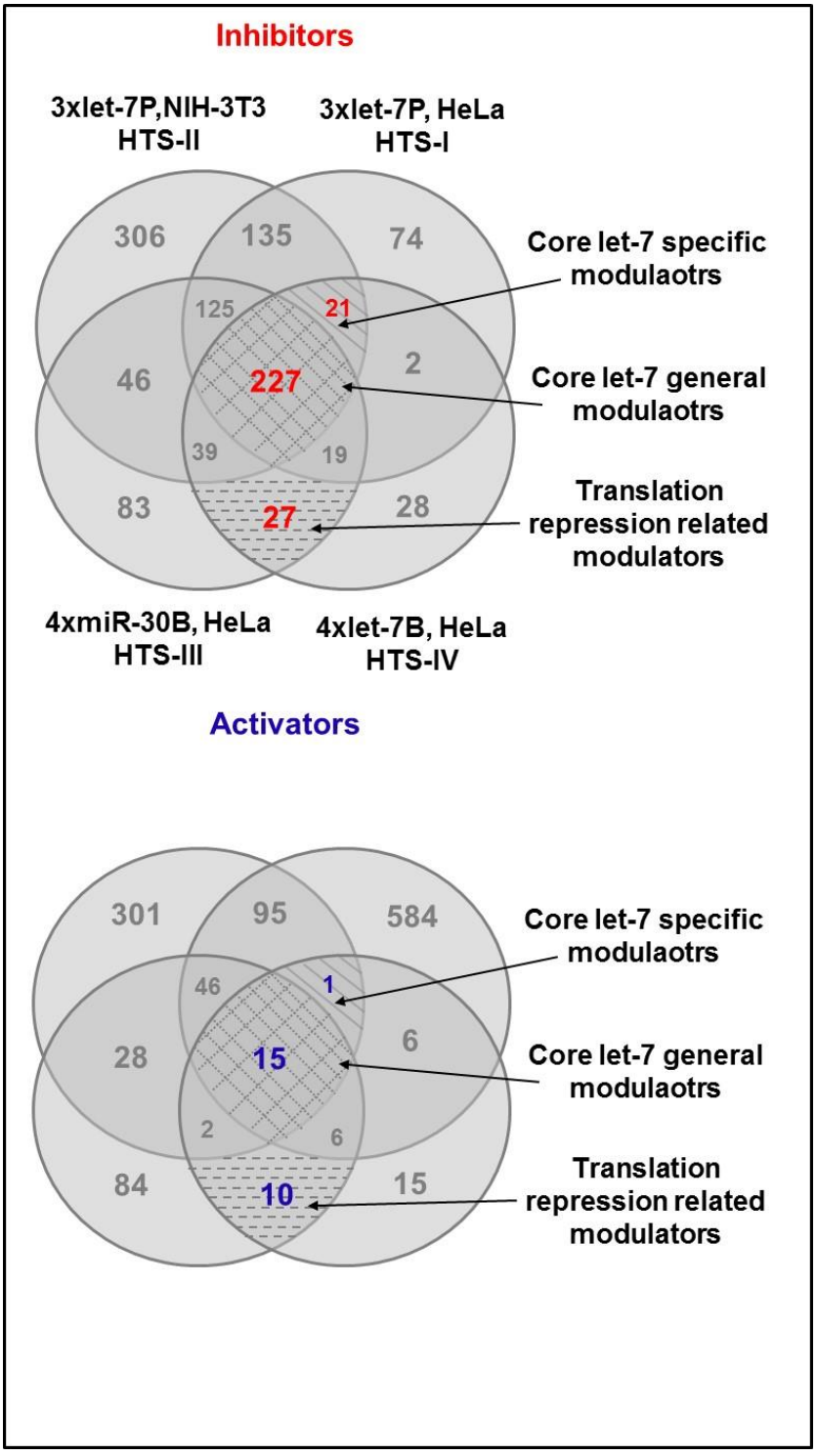

Fig.47: Graphical representation of HTS results: Venn diagrams represent the most interesting hits generated after data comparison from all cell-based HTS (I-IV) performed. As indicated in the center intersection of all HTS results, 227 (-5xB-score) potential general miRNA inhibitors and 15 (5xB-score) potential general miRNA activators were identified. The comparison of the results from the let-7–based screens with the results from the miR-30-based screen revealed 21 (-5xB-score) potential let-7-specific inhibitors and 1 (5xB-score) potential let-7-specific activator. HTS-III and HTS-IV identified 27 (-5xB-score) putative inhibitors and 10 (5xB-score) putative activators of translation repression mediated by miRNAs.

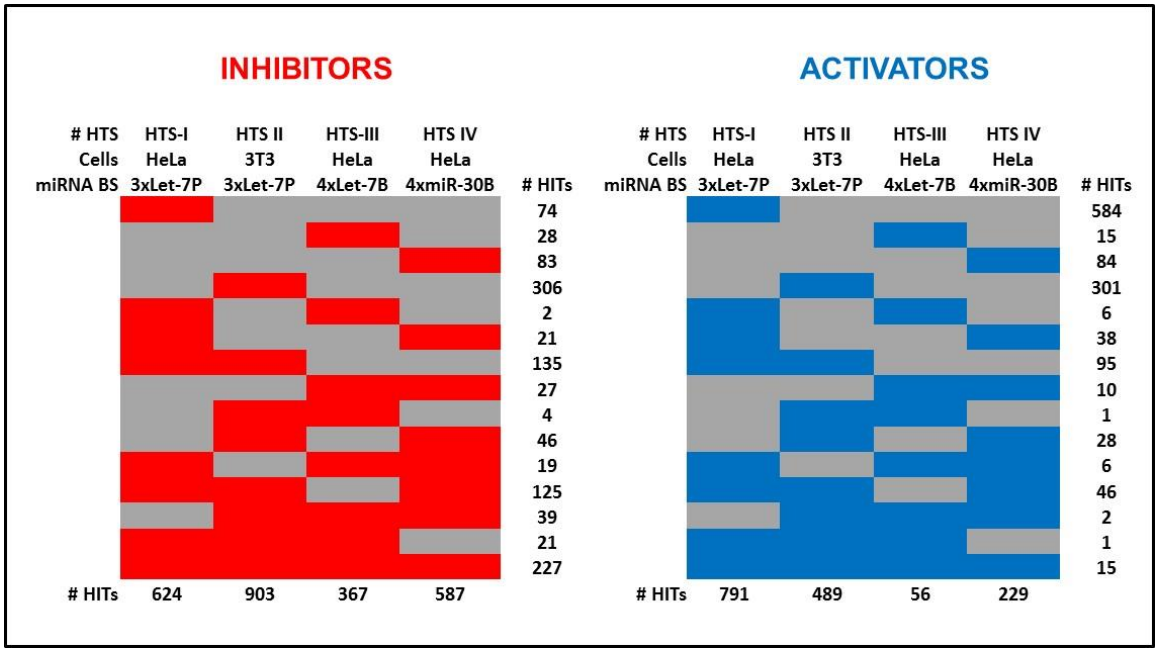

Tab.11: Summary of total his generated by individual cell-based HTS: Columns represent individual screens (HTS-I, HTS-II, HTS III, and HTS-IV) using different reporters in HeLa or NIH-3T3 cell lines (HeLa_PGK-FL-3xlet7-P, 3T3_PGK-FL-3xlet7-P, HeLa_PGK-FL-4xlet7-BP, and HeLa_PGK-FL-4xmiR-30-BP, respectively). Numbers of compounds unique to a particular screen (for example 74 hits unique for HTS-I in case of inhibitors and 584 in case of activators) or scoring in several screens (for example 19 for HTS-I, II, and IV in case of inhibitors and 6 in case of activators) are listed on the right and are graphically represented by red (inhibitors) or blue (activators) fields on the grey background. Numbers of total hits in individual screens are stated in the bottom row.

6 DISCUSSION

The presented work is a part of a large scientific project that aims to obtain a set of small molecules allowing for stimulation or inhibition of RNA silencing. This thesis summarizes the first two phases of the project: (i) development of high-throughput screening assays and (ii) high-throughput screening (HTS) of a library of ~30,000 small compounds. Highly efficient, low-cost, safe, and robust assays represent a prerequisite for a successful HTS. During the first part of the thesis project, one biochemical and several cell-based assays were developed to monitor the miRNA pathway activity. Both types of assays, as well as the results of HTSs, are discussed below.

6.1 Aspects of fluorescence-based *in vitro* Dicer cleavage assay

To identify compounds modulating the Dicer activity, we developed a fluorescence-based *in vitro* Dicer cleavage assay. Conventionally, the Dicer cleavage activity is characterized using a "classical" *in vitro* Dicer cleavage assay employing a 5´-end radioactively labeled (γ-^{32}P-ATP) dsRNA Dicer substrate and electrophoretic analysis of the samples after the Dicer cleavage reaction (Chakravarthy et al., 2010; Kolb et al., 2005; Zhang et al., 2002). Although this type of assay enables the precise analysis of the Dicer cleavage reaction kinetics, it is suboptimal for high-throughput experiments. Therefore, we developed a high-throughput assay for Dicer activity and used it to screen a compound library.

The assay is adapted for HTS in several aspects. Although it would be possible to prepare a substrate resembling a structure of a natural pre-miRNA similar to that done previously, (Davies and Arenz, 2006), we opted for a short (27-nt) RNA duplex that was easy to synthesize and resembled an artificial siRNA structure described earlier (Kim et al., 2005). Two reasons lead us to this decision: first, under the single-turnover conditions *in vitro*, Dicer cleaves small hairpin miRNA precursors relatively fast ($t_{1/2}$<5 min) (Chakravarthy et al., 2010), which would be unfavorable for HTS. Therefore, a long perfect RNA duplex, whose processing is considerably slower ($t_{1/2}$~80 min in a single-turnover assay with >25-fold molar excess of Dicer for a 35-bp duplex with 2-nt overhangs at both

ends) (Chakravarthy et al., 2010), was found to be a more suitable type of RNA substrate for HTS. Second, a perfect RNA duplex can be easily modified into a substrate that produces fluorescence upon cleavage. Notably, the sequence of the substrate was derived from a well-characterized human let-7a miRNA, hence allowing for combining our assay with other tools developed for let-7 analysis.

An important feature of the RNA substrate for Dicer is the optimal combination of the fluorophore and the quencher. I tested three combinations: (i) 5(6)-FAM fluorescent donor and 3-Dab quencher (*Exiqon, Vedbaek, Denmark*), (ii) Cy5 fluorescent donor and IowaBlackRQ (IB-RQ) quencher (*Integrated DNA Technologies, Coralville, IA*), and (iii) Cy5 fluorescent donor and BHQ2 quencher (*Sigma-Aldrich*). Of them, the Cy5/IB-RQ combination was clearly superior to others. Numerous factors could contribute to the worse performance of Cy5/BHQ2 and 5(6)-FAM/3-Dab substrates. For instance, it could be a consequence of suboptimal compatibility of fluorescent and quencher group interactions. The 5(6)-FAM/3-Dab substrate had the highest background fluorescence, which could contribute to the low fluorescence increase during the experiment. It is not clear, what was the cause of the different results obtained with Cy5/BHQ and Cy5/IB-RQ substrates carrying the same fluorophore. Although the background fluorescence of both substrates was similar, the relative fluorescence released by Dicer was ~4-fold higher with the Cy5/IB-RQ substrate. It is not clear whether BHQ2 would affect Dicer binding or whether labeling efficiency and BHQ2 quenching activity could contribute to the lower increase in fluorescence. Notably, a similar substrate for fluorescence-based Dicer cleavage assay was independently designed and used by DiNitto *et al.* (2010) (DiNitto et al., 2010). Their fluorescent substrate is one nucleotide longer, carries a different sequence, uses UU dinucleotide as a 3′ overhang, but carries the same fluorophore and quencher combination and yields comparable results (DiNitto et al., 2010).

The reaction buffer for our *in vitro* Dicer assay was adopted from Kolb *et al*. (2005) (Kolb et al., 2005) with only minor modifications. Conventionally, the "classical" Dicer cleavage assays are performed under conditions enabling to determine the precise Dicer kinetics (e.g. dsRNA substrate in molar excess over the Dicer enzyme). In contrast, we performed fluorescent Dicer cleavage assay under the single-turnover conditions under which Dicer is present in the molar excess over the substrate. Under these reaction conditions, the rate of the product formation is not limited by the product release, since

each enzyme molecule reacts with one substrate molecule at most. There were several reasons for the selection of this option: (i) insufficient amount of available dsRNA substrate stock, (ii) a high background activity of the dsRNA substrate at concentrations over ~100 nM and (iii) insufficient activity of Dicer at concentrations bellow ~50 nM (an estimate based on the results from several experiments, data not shown). Therefore, the HTS reaction was downscaled to 5 μl, and 35 nM substrate and 70 nM Dicer was used. This combination yielded an acceptable signal-to-noise ratio and a relatively slow substrate processing rate ($t_{1/2}$~4 h), which provided enough flexibility for the robust monitoring of a large number of reactions at multiple timepoints in a continuous assay. Notably, due to usage of lower substrate concentrations, the assay described here is primarily aimed to screen for Dicer inhibitors and may be suboptimal for analyzing Dicer stimulators.

The screen of a library of ~30,000 compounds was performed in a kinetic manner. During the HTS, the readings were taken at times 0, 1, 2, 3, 4, 6, 8, 10, 13, 15, 17, 19, 21, 23, and 25 h. Importantly, the number of selected hits is influenced by both time at which the reading was taken, and the selected cut-off conditions (the precise cut-off conditions that were set up for the hit selection are presented in the chapter **5.1.4.**). Under the conditions when the readings were taken at time 6 and 15 h, 207 compounds significantly inhibiting the assay and 72 compounds potentially activating the assay were identified A dose-response assay performed on 2,816 selected potential Dicer inhibitors originating from the library containing annotated bioactive compounds validated 22 compounds (reaction time 4 h from the initiation of the assay) (Podolska et al., 2014).

Interestingly, three common scaffolds were found among the validated compounds, which suggests that some common themes exist in the manner by which compounds interfere with the assay. Inhibitory compounds could interfere with the Dicer cleavage in many ways. At this point it is difficult to distinguish between the compounds inhibiting Dicer specifically and the compounds which affect the assay but are not Dicer-specific inhibitors. Such non-specific assay modulators could be, for example: (i) compounds that nonspecifically denature or aggregate proteins, (ii) compounds that affect the substrate structure (intercalating compounds), or (iii) compounds that interfere with the fluorescence. The compounds generally affecting the enzymes can be filtered using the comparison with the results from other enzymatic assays. We identified 5 such compounds among 22 validated hits. Remarkably, some of these compounds overlapped with one of the three

identified scaffolds, while none overlapped with the other two. That quenching caused by compounds can yield false positives, as is exemplified by ruthenium red. Ruthenium red showed IC50 = 6.2 μM and reached 100% of Dicer inhibition at 20 μM concentration. Ruthenium red is a hextapositive complex cation stabilizing DNA and RNA helices against thermal denaturation (Karpel et al., 1981). Therefore it was an interesting candidate for a Dicer inhibitor. Since ruthenium red has its absorption maximum (534 nm; *Sigma-Aldrich*) sufficiently below that of the Cy5 label (excitation maximum 646 nm/emission maximum 664 nm) used in the HTS, the fluorescent quenching was unlikely. However, when ruthenium red (2.5–10 μM) was added to a completed fluorescent cleavage assay (at the 22 h timepoint), we observed up to 56% lower fluorescence. This indicates that ruthenium red was reducing the fluorescence produced by the Dicer cleavage and not the Dicer activity per se. Therefore, we recommend to include the analysis of quenching activity of putative Dicer inhibitors by running a standard fluorescent cleavage assay to completion followed by adding the putative Dicer inhibitors and monitoring their quenching effects on the fluorescence in a completed Dicer cleavage assay (Podolska et al., 2014).

Regarding the Dicer-specific compounds, future experiments will validate them and describe their mode of action. Since Dicer is a multidomain protein, numerous independent modes of inhibition are possible. For example, compounds binding the PAZ or helicase domains may interfere with the substrate binding, and compounds binding to RNase III domains may interfere with substrate cleavage. Therefore, to further classify the compounds identified by the Dicer cleavage assay described here, additional assays need to be developed. For example, it is possible to replace the PAZ domain with RNA-binding spliceosomal protein U1A, which binds a loop of specific sequence that can replace the 2-nt overhang of the current substrate (MacRae et al., 2007). Such Dicer would cleave such hairpin substrate at a fixed distance from the loop and would be resistant to inhibitors binding the PAZ domain. The fact that our results did not show any overlap with previous analyses is not surprising. While we used a biochemical assay directly aimed at compounds modulating Dicer, the previous screens were mainly cell-based and monitored performance of an entire RNA silencing pathway (Deiters, 2010). In addition, our assay would poorly detect inhibitors with IC50>15 μM, such as kanamycin.

Taken together, the fluorescence-based Dicer cleavage assay was adapted for HTS and successfully used for identifying candidate modulators of the key step in miRNA and RNAi pathways.

6.2 Aspects of cell-based assays

To identify potential global small-molecule modulators of RNA silencing pathways, especially the miRNA pathway, several cell-based assays were developed. These assays are based on reporters carrying miRNA binding sites in 3´UTR. In the assay, the endogenous miRNA suppresses reporter activity, thus reflecting the activity of selected miRNA levels. In the presence of a small molecule inhibitor, the reporter repression is relieved, resulting in the increased reporter signal. Since this reporter system monitors an increase of reporter signal in the presence of an active inhibitor, the majority of false positives due to the compound cytotoxicity should be excluded. Importantly, although data processing after HTS included analysis of both miRNA pathway inhibitors and activators, the presented cell-based assays are primarily aimed to screen for miRNA pathway inhibitors and are suboptimal for identification of miRNA pathway stimulators.

To perform a HTS, stable reporter cell lines were established to reduce the number of manipulations and to increase the reproducibility and robustness of the assay. Interestingly, the assay development went through several turns and twists and sometimes lad us to dead ends. To select a suitable reporter, an EGFP-based reporter was examined first because EGFP fluorescence requires no additional substrates or cofactors and the EGFP fluorescence can be easily and cheaply detected by a fluorometer. Although functionality of the EGFP reporter cell-based assay was confirmed, due to a low fluorescence signal induction upon the miRNA pathway inhibition and a relatively high background fluorescence, the assay was found not suitable for HTS.

As the second option during our search for an optimal reporter system for HTS we examined luciferase reporters. At that time, a bidirectional luciferase-based reporter system containing both an experimental *Renilla* luciferase and an independently transcribed firefly luciferase reporter gene was established in our laboratory. Therefore, the first choice was the establishment of a bidirectional luciferase-based reporter in which the binding sites for an endogenous miRNA were inserted downstream of *Renilla* CDS, and the firefly reporter

was used for normalization purposes to account for variation in transfection efficiency and cell viability. However, despite our so far good experience with small-scale bidirectional luciferase assays employing *Renilla* luciferase as the experimental target, the use of this system for HTS turned out to be problematic for the following reasons: (i) the EnVision plate reader, which was used for measurement of luminescence signal during HTS experiments, did not allow to measure *Renilla* and firefly luciferase signals sequentially and (ii) the usage of Renilla-glo (*Promega*) steady substrate for *Renilla* luciferase was not established and optimized well at that time. Furthermore, the pilot HTS with Renilla-glo substrate showed a poor reproducibility. The reasons of inconsistent results were not further studied. Instead, we decided for firefly luciferase-based reporter system, because tens of cell-based HTSs employing firefly luciferase reporters were already successfully performed in the collaborating group of Petr Bartunek, IMG AS CR, CZ-OPENSCREEN, providing a large volume of existing data for data comparison. Therefore, the HTS results presented here are the outcome of a long way of assay development starting from the EGFP-based reporters and leading through the bidirectional *Renilla* luciferase-based reporters to the single firefly luciferase-based reporters.

During the assay development, tens of reporters varying in type of promoters, polyA sites and miRNA biding sites were tested. Such reporters were repressed to different levels and had a different sensitivity to repression and stimulation of RNA silencing. Endogenous miRNAs target reporters with perfect complementary sites by RNAi-like cleavage while reporters with imperfect complementary (bulged) sites are inhibited by translation repression (Pillai et al., 2005; Schmitter et al., 2006). Moreover, it was reported that the number of miRNA binding sites in the reporter affects the extent of miRNA-mediated reporter repression (Doench et al., 2003). Increasing number of perfectly complementary binding sites increases the probability of the single necessary cleavage event and thus also the level of gene silencing by RNAi (Doench et al., 2003). Similarly, increasing number of bulged binding sites in the reporter increases the level of translation repression. Notably, the effects of binding multiple miRNA complexes to the 3′UTR are likely cooperative (Doench et al., 2003). Therefore, to obtain optimal reporters, various combinations of both types of miRNA binding sites were constructed and analyzed. This should allow to: (i) distinguish compounds affecting translation repression and acting upstream of it and (ii) select a reporter yielding the best dynamic range of the assay. Finally, reporters containing

binding sites for two endogenous miRNAs, let-7 and miR-30, were tested. Notably, let-7-targeted reporters were selected because let-7 is closely associated with pluripotency and differentiation (reviewed in (Svoboda and Flemr, 2010)) and finding its specific inhibitors would have great importance. miR-30 was chosen because its biogenesis was thoroughly studied (Zeng and Cullen, 2003, 2004) and is expressed in both pluripotent and differentiated cells (Landgraf et al., 2007).

To test a selectivity and a robustness of the assay in the HTS format and to verify a feasibility of the HTS to estimate the hit rate, we first performed a proof-of concept HTS of a part of the collection (~10,000 compounds). For the pilot HTS, the assay based on HeLa stable cell line carrying the firefly luciferase reporter with three perfect let-7 binding sites was used for its good dynamic range and a higher basal activity compared with other stable cell lines tested, potentially enabling to discover both inhibitors and activators of the miRNA pathway. Surprisingly, the pilot HTS produced a satisfactory hit rate. The hit rate is dependent on the cut-off value chosen for data analysis. Due to a relatively high amount of compounds stimulating the firefly activity, we decided to set 5xB-score cut-off value for potential miRNA pathway inhibitors. On this cut-off value, 180 potential miRNA inhibitors were identified. In contrast, due to a relatively poor amount of compounds inhibiting the firefly activity, we decided to set -1,8xB-score cut-off value for potential miRNA pathway activators. On this cut-off value, 27 potential miRNA activators were identified, however 22 of them were removed due to their cytotoxicity. Notably, tens of identified hits were already annotated bioactive compounds. Subsequent data analysis revealed the diversity in terms of the compound association with various cellular processes. There were for example compounds causing DNA damage, blocking translation, blocking cell cycle, corticosteroids or compounds interfering with different signaling pathways. Importantly, identification of compounds interfering with miRNA pathway indirectly would enable to discover crosstalks between RNA silencing and other cellular pathways.

The proof-of-concept HTS validated the selectivity and robustness of the firefly reporter cell-based assay. To continue, four HTSs of ~30,000 compounds were performed allowing us to filter the HTS data according to the following parameters: (i) cell type-specific vs. cell type-non-specific modulators of miRNA pathway, (ii) let-7 miRNA-specific vs. global modulators of miRNA pathway, and (iii) miRNA pathway-specific compounds affecting translation repression vs. compounds affecting the upstream steps of

RNA silencing pathways. The cut-off values for hit rate determination were set to 5xB-score value for potential miRNA pathway inhibitors and -5xB-score value for potential miRNA pathway stimulators. We identified: (i) 227 potential general miRNA inhibitors and 15 potential general miRNA pathways activators, (ii) 21 potential let-7 specific inhibitors and 1 potential let-7-specific activator, or (iii) 27 putative general inhibitors and 10 putative activators of translation repression.

HTSs generated several groups of interesting hits. First, global small compound modulators would be a great tool for studying RNA silencing pathways *in vivo* and *in vitro* and they would have also a therapeutic potential. miRNAs are associated with cancer and can act as oncogenes or tumorsuppresors (Medina and Slack, 2008). Finding that miRNAs inhibit senescence in cancer cells (Badiola et al., 2015) indicates that cancer cells could be more sensitive to the global inhibition of miRNA pathway then the normal cells, which opens a possible strategy for cancer therapy. Moreover, as exemplified by histone-deacetylase inhibitors, the global modulation of the highly complex miRNA pathway is valuable. While histone deacetylases cause global and complex changes in gene expression, histone-deacetylase inhibitors are used to treat different types of cancer (Bolden et al., 2006; Choudhary et al., 2009; Marks et al., 2004; Richon et al., 2009). Interestingly, Dicer activators are candidates for the therapy of age-related macular degeneration, in which Dicer deficiency has been implicated (Kaneko et al., 2011). Next, some biotechnological applications may benefit from the inhibition of RNA silencing pathways. let-7 inhibits the induction of pluripotent stem cells and vice versa the inhibition of let-7 miRNA in differentiated cells contributes to a higher efficiency of iPS formation (Worringer et al., 2014). Therefore let-7-specific inhibitors would have a great potential in the research of pluripotency and stem cells. Finally, potential modulators of miRNA-mediated translation repression may contribute to the functional analysis of the full-RISC complex.

The data on small compound modulators of RNA silencing are scarce. However, several studies have identified small compound modulators of RNA silencing (Deiters, 2010; Chiu et al., 2005; Maiti et al., 2012; Shan et al., 2008; Shum et al., 2012; Tan et al., 2012; Watashi et al., 2010), utilizing both cell-based assays and biochemical *in vitro* assays. Several compounds identified in previous HTSs were in our collection as well, enabling the data comparison. First, enoxacin has been shown to promote the miRNA biogenesis and to enhance the miRNA function in a dose-dependent manner, with a median effective

concentration (EC50) ~30 μM (Shan et al., 2008). Importantly, enoxacin did not show any remarkable activity in our hands. It is not surprising as we used fifty times lower compound screening concentration than was the concentration used in the study of Shan *et al.* (2008) (Shan et al., 2008). Moreover, Shum *et al.* (Shum et al., 2012) showed that enoxacin is inactive at lower screening concentration (10 μM) (Shum et al., 2012). A recent biochemical HTS has identified three potent small-molecule inhibitors of the RISC loading: (i) aurintricarboxylic acid, (ii) suramin sodium salt, and (iii) oxidopamine hydrochloride (Tan et al., 2012). Of them, the first two were present in our library as well. Although suramin sodium salt did not show any activity in our HTSs at screening concentration hundred times lower than the screening concentration used in study of Tan *et al.* (2012) (Tan et al., 2012), aurintricarboxylic acid (Tan et al., 2012) was identified as a potential Dicer inhibitor in our Dicer HTS. Finally, five of six compounds identified as inhibitors of the miRNA-21 biogenesis in the recent study utilizing an image-based biosensor assay (Shum et al., 2012) were also present in our collection. Four of them (N,N-dipropyldopamine hydrobromide, 8-hydroxy-DPAT hydrobromide, deoxycorticosterone and flutamide) were inactive in our HTS, in which the screening concentration was ten times lower than that used in the study of Shum *et al.* (2012) (Shum et al., 2012). Interestingly, one of them, neurotoxin "6-Hydroxy-DL-DOPA" (Shum et al., 2012), was identified as a potential Dicer inhibitor in our Dicer HTS as well.

The analysis of the data from the pilot HTS revealed known inhibitors of particular signaling pathways, potential inducers of the stress response, or modulators of specific metabolic pathways. It is unlikely that these compounds regulate the miRNA pathway directly. Instead, they point to other mechanisms that can regulate the miRNA pathway. For instance, it was reported that after the stress induction the miRNA pathway is blocked and the AGO2 with the miRNA is relocalized from P bodies or cytoplasm into the stress granules indicating that there is a link between the stress induction and inhibition of miRNA pathway (Bhattacharyya et al., 2006; Detzer et al., 2011). Therefore, primary candidates on the secondary modulation of miRNA pathway would be those inducing cellular stress. Surprisingly, analysis of ~200 compounds that were cherry-picked based on the results from the proof-of-concept screen revealed that only 4% of compounds induced the formation of the stress granules (data not shown), and therefore the majority of identified compounds inhibits the miRNA pathways by other mechanisms than stress induction. The

fact that one of the compounds capable of the stress granules induction was emetine, which has been linked to stress induction in the past (Kedersha et al., 2000), confirmed the cell-based assay robustness and credibility of HTS data. How cells regulate the miRNA pathway activity is of great interest. Chemical biology offers an attractive approach to identify such regulating mechanisms in mammalian cells since many compounds used in the HTS have the defined effects on specific signaling or metabolic pathways.

As mentioned before, several reports have already used chemical biology to study the RNA silencing. However, there are some technical differences between HTSs performed so far and our HTSs. First, in contrast to earlier studies, which were performed on relatively small libraries comprising several hundreds to ~7,000 compounds (Deiters, 2010; Chiu et al., 2005; Maiti et al., 2012; Shan et al., 2008; Shum et al., 2012; Tan et al., 2012; Watashi et al., 2010), we screened an extensive collection of ~30,000 compounds that varied in terms of their structure. Second difference between our HTSs and HTSs, which were done in the past, is the compound concentration. Whereas we used 1 μM compound concentration enabling us to identify only very specific modulators of RNA silencing, the majority of previously identified RNA silencing modulators showed considerable activity only at much higher concentrations (Deiters, 2010; Chiu et al., 2005; Maiti et al., 2012; Shan et al., 2008; Shum et al., 2012; Tan et al., 2012; Watashi et al., 2010). Therefore, it is not surprising that the majority of compounds, which were identified in previous HTSs and which were in our collection as well, did not show any remarkable activity in our HTSs. Taken together, in contrast to previous studies, our HTS strategy was to set up the screening conditions enabling the identification of highly specific and potent modulators of RNA silencing.

Although the first two key phases of the project - the assay development and the HTS - were already completed within the thesis, the way leading to very specific and potent inhibitor or activator of RNA silencing is still almost at the beginning. Further work is required to validate the HTS-generated data in dose- and time-dependent experiments and to provide an insight into the mode of action of individual cherry-picked compounds using various secondary assays. The design of experiments leading to the compound classification and further development is described in the chapter **Research plan overview** (pages # 59-62).

7 CONCLUSION

In summary, one biochemical fluorescence-based *in vitro* Dicer cleavage assay focused on searching for Dicer modulators and four cell based assays focused on searching for modulators of RNA silencing pathways were developed and used for HTS of ~30,000 small chemical compounds. These HTSs were unique in terms of extensiveness of the compound library and the low compound screening concentration, thus promising the identification of very specific and potent small compound modulators of RNA silencing. Moreover, no assay similar to the fluorescence-based *in vitro* Dicer cleavage assay has been used in such an extensive kinetic HTS so far. Although our HTSs generated a lot of interesting data, first it is necessary to verify them in dose- and time-dependent experiments, and subsequently the best candidates need to be characterized in various secondary assays to find out their mode of action. Taken together, the aims of the dissertation were completely achieved, and the project can enter into the next stage – validation and characterization of the cherry-picked compound.

8 REFERENCES

Akaneya, Y., Jiang, B., Tsumoto, T., 2005. RNAi-induced gene silencing by local electroporation in targeting brain region. J Neurophysiol 93, 594-602.

Aliyari, R., Wu, Q., Li, H.W., Wang, X.H., Li, F., Green, L.D., Han, C.S., Li, W.X., Ding, S.W., 2008. Mechanism of induction and suppression of antiviral immunity directed by virus-derived small RNAs in Drosophila. Cell Host Microbe 4, 387-397.

Ambros, V., 2004. The functions of animal microRNAs. Nature 431, 350-355.

Ambros, V., Lee, R.C., Lavanway, A., Williams, P.T., Jewell, D., 2003. MicroRNAs and other tiny endogenous RNAs in C. elegans. Curr Biol 13, 807-818.

Amdam, G.V., Norberg, K., Page, R.E., Jr., Erber, J., Scheiner, R., 2006. Downregulation of vitellogenin gene activity increases the gustatory responsiveness of honey bee workers (Apis mellifera). Behav Brain Res 169, 201-205.

Ameres, S.L., Martinez, J., Schroeder, R., 2007. Molecular basis for target RNA recognition and cleavage by human RISC. Cell 130, 101-112.

Aoki, K., Moriguchi, H., Yoshioka, T., Okawa, K., Tabara, H., 2007. In vitro analyses of the production and activity of secondary small interfering RNAs in C. elegans. EMBO J 26, 5007-5019.

Aouadi, M., Tesz, G.J., Nicoloro, S.M., Wang, M., Chouinard, M., Soto, E., Ostroff, G.R., Czech, M.P., 2009. Orally delivered siRNA targeting macrophage Map4k4 suppresses systemic inflammation. Nature 458, 1180-1184.

Apletalina, E., Appel, J., Lamango, N.S., Houghten, R.A., Lindberg, I., 1998. Identification of inhibitors of prohormone convertases 1 and 2 using a peptide combinatorial library. J Biol Chem 273, 26589-26595.

Aramburu, J., Yaffe, M.B., Lopez-Rodriguez, C., Cantley, L.C., Hogan, P.G., Rao, A., 1999. Affinity-driven peptide selection of an NFAT inhibitor more selective than cyclosporin A. Science 285, 2129-2133.

Badiola, I., Santaolalla, F., Garcia-Gallastegui, P., Del Rey, A.S., Unda, F., Ibarretxe, G., 2015. Biomolecular bases of the senescence process and cancer. A new approach to oncological treatment linked to ageing. Ageing Res Rev.

Barbato, C., Ciotti, M.T., Serafino, A., Calissano, P., Cogoni, C., 2007. Dicer expression and localization in post-mitotic neurons. Brain research 1175, 17-27.

Bartel, D.P., 2004. MicroRNAs: genomics, biogenesis, mechanism, and function. Cell 116, 281-297.

Bartel, D.P., 2009. MicroRNAs: target recognition and regulatory functions. Cell 136, 215-233.

Batista, P.J., Ruby, J.G., Claycomb, J.M., Chiang, R., Fahlgren, N., Kasschau, K.D., Chaves, D.A., Gu, W., Vasale, J.J., Duan, S., Conte, D., Jr., Luo, S., Schroth, G.P., Carrington, J.C., Bartel, D.P., Mello, C.C., 2008. PRG-1 and 21U-RNAs interact to form the piRNA complex required for fertility in C. elegans. Mol Cell 31, 67-78.

Benes, V., Castoldi, M., 2010. Expression profiling of microRNA using real-time quantitative PCR, how to use it and what is available. Methods 50, 244-249.

Bernstein, E., Caudy, A.A., Hammond, S.M., Hannon, G.J., 2001. Role for a bidentate ribonuclease in the initiation step of RNA interference. Nature 409, 363-366.

Betancur, J.G., Tomari, Y., 2012. Dicer is dispensable for asymmetric RISC loading in mammals. RNA 18, 24-30.

Bethune, J., Artus-Revel, C.G., Filipowicz, W., 2012. Kinetic analysis reveals successive steps leading to miRNA-mediated silencing in mammalian cells. EMBO Rep 13, 716-723.

Bhattacharyya, S.N., Habermacher, R., Martine, U., Closs, E.I., Filipowicz, W., 2006. Relief of microRNA-mediated translational repression in human cells subjected to stress. Cell 125, 1111-1124.

Boden, D., Pusch, O., Lee, F., Tucker, L., Ramratnam, B., 2004. Efficient gene transfer of HIV-1-specific short hairpin RNA into human lymphocytic cells using recombinant adeno-associated virus vectors. Mol Ther 9, 396-402.

Bohnsack, M.T., Czaplinski, K., Gorlich, D., 2004. Exportin 5 is a RanGTP-dependent dsRNA-binding protein that mediates nuclear export of pre-miRNAs. RNA 10, 185-191.

Bolden, J.E., Peart, M.J., Johnstone, R.W., 2006. Anticancer activities of histone deacetylase inhibitors. Nature reviews. Drug discovery 5, 769-784.

Bottger, V., Bottger, A., Howard, S.F., Picksley, S.M., Chene, P., Garcia-Echeverria, C., Hochkeppel, H.K., Lane, D.P., 1996. Identification of novel mdm2 binding peptides by phage display. Oncogene 13, 2141-2147.

Brennecke, J., Aravin, A.A., Stark, A., Dus, M., Kellis, M., Sachidanandam, R., Hannon, G.J., 2007. Discrete small RNA-generating loci as master regulators of transposon activity in Drosophila. Cell 128, 1089-1103.

Brideau, C., Gunter, B., Pikounis, B., Liaw, A., 2003. Improved statistical methods for hit selection in high-throughput screening. Journal of biomolecular screening 8, 634-647.

Brummelkamp, T.R., Bernards, R., Agami, R., 2002a. Stable suppression of tumorigenicity by virus-mediated RNA interference. Cancer Cell 2, 243-247.

Brummelkamp, T.R., Bernards, R., Agami, R., 2002b. A system for stable expression of short interfering RNAs in mammalian cells. Science 296, 550-553.

Bucher, G., Scholten, J., Klingler, M., 2002. Parental RNAi in Tribolium (Coleoptera). Curr Biol 12, R85-86.

Bussing, I., Slack, F.J., Grosshans, H., 2008. let-7 microRNAs in development, stem cells and cancer. Trends in molecular medicine 14, 400-409.

Cai, X., Hagedorn, C.H., Cullen, B.R., 2004. Human microRNAs are processed from capped, polyadenylated transcripts that can also function as mRNAs. RNA 10, 1957-1966.

Calin, G.A., Dumitru, C.D., Shimizu, M., Bichi, R., Zupo, S., Noch, E., Aldler, H., Rattan, S., Keating, M., Rai, K., Rassenti, L., Kipps, T., Negrini, M., Bullrich, F., Croce, C.M., 2002. Frequent deletions and down-regulation of micro- RNA genes miR15 and miR16 at 13q14 in chronic lymphocytic leukemia. Proc Natl Acad Sci U S A 99, 15524-15529.

Carmell, M.A., Xuan, Z., Zhang, M.Q., Hannon, G.J., 2002. The Argonaute family: tentacles that reach into RNAi, developmental control, stem cell maintenance, and tumorigenesis. Genes Dev 16, 2733-2742.

Carmell, M.A., Zhang, L., Conklin, D.S., Hannon, G.J., Rosenquist, T.A., 2003. Germline transmission of RNAi in mice. Nat Struct Biol 10, 91-92.

Cikaluk, D.E., Tahbaz, N., Hendricks, L.C., DiMattia, G.E., Hansen, D., Pilgrim, D., Hobman, T.C., 1999. GERp95, a membrane-associated protein that belongs to a family of proteins involved in stem cell differentiation. Mol Biol Cell 10, 3357-3372.

Cimmino, A., Calin, G.A., Fabbri, M., Iorio, M.V., Ferracin, M., Shimizu, M., Wojcik, S.E., Aqeilan, R.I., Zupo, S., Dono, M., Rassenti, L., Alder, H., Volinia, S., Liu, C.G., Kipps, T.J., Negrini, M., Croce, C.M., 2005. miR-15 and miR-16 induce apoptosis by targeting BCL2. Proc Natl Acad Sci U S A 102, 13944-13949.

Colas, P., Cohen, B., Jessen, T., Grishina, I., McCoy, J., Brent, R., 1996. Genetic selection of peptide aptamers that recognize and inhibit cyclin-dependent kinase 2. Nature 380, 548-550.

Conine, C.C., Batista, P.J., Gu, W., Claycomb, J.M., Chaves, D.A., Shirayama, M., Mello, C.C., 2010. Argonautes ALG-3 and ALG-4 are required for spermatogenesis-specific 26G-RNAs and thermotolerant sperm in Caenorhabditis elegans. Proc Natl Acad Sci U S A 107, 3588-3593.

Cortez, M.A., Calin, G.A., 2009. MicroRNA identification in plasma and serum: a new tool to diagnose and monitor diseases. Expert opinion on biological therapy 9, 703-711.

Coumoul, X., Li, W., Wang, R.H., Deng, C., 2004. Inducible suppression of Fgfr2 and Survivin in ES cells using a combination of the RNA interference (RNAi) and the Cre-LoxP system. Nucleic Acids Res 32, e85.

Creighton, C.J., Reid, J.G., Gunaratne, P.H., 2009. Expression profiling of microRNAs by deep sequencing. Briefings in bioinformatics 10, 490-497.

Cullen, B.R., 2006. Is RNA interference involved in intrinsic antiviral immunity in mammals? Nat Immunol 7, 563-567.

Czech, B., Hannon, G.J., 2011. Small RNA sorting: matchmaking for Argonautes. Nat Rev Genet 12, 19-31.

Czech, B., Malone, C.D., Zhou, R., Stark, A., Schlingeheyde, C., Dus, M., Perrimon, N., Kellis, M., Wohlschlegel, J.A., Sachidanandam, R., Hannon, G.J., Brennecke, J., 2008. An endogenous small interfering RNA pathway in Drosophila. Nature 453, 798-802.

Daniels, S.M., Melendez-Pena, C.E., Scarborough, R.J., Daher, A., Christensen, H.S., El Far, M., Purcell, D.F., Laine, S., Gatignol, A., 2009. Characterization of the TRBP domain required for dicer interaction and function in RNA interference. BMC Mol Biol 10, 38.

Das, P.P., Bagijn, M.P., Goldstein, L.D., Woolford, J.R., Lehrbach, N.J., Sapetschnig, A., Buhecha, H.R., Gilchrist, M.J., Howe, K.L., Stark, R., Matthews, N., Berezikov, E., Ketting, R.F., Tavare, S., Miska, E.A., 2008. Piwi and piRNAs act upstream of an endogenous siRNA pathway to suppress Tc3 transposon mobility in the Caenorhabditis elegans germline. Mol Cell 31, 79-90.

Davies, B.P., Arenz, C., 2006. A homogenous assay for micro RNA maturation. Angewandte Chemie 45, 5550-5552.

Deiters, A., 2010. Small molecule modifiers of the microRNA and RNA interference pathway. The AAPS journal 12, 51-60.

Deng, X., Su, Y., Wu, H., Wu, R., Zhang, P., Dai, Y., Chan, T.M., Zhao, M., Lu, Q., 2014. The role of microRNAs in autoimmune diseases with skin involvement. Scandinavian journal of immunology.

Denli, A.M., Tops, B.B., Plasterk, R.H., Ketting, R.F., Hannon, G.J., 2004. Processing of primary microRNAs by the Microprocessor complex. Nature 432, 231-235.

Detzer, A., Engel, C., Wunsche, W., Sczakiel, G., 2011. Cell stress is related to re-localization of Argonaute 2 and to decreased RNA interference in human cells. Nucleic Acids Res 39, 2727-2741.

Dickins, R.A., McJunkin, K., Hernando, E., Premsrirut, P.K., Krizhanovsky, V., Burgess, D.J., Kim, S.Y., Cordon-Cardo, C., Zender, L., Hannon, G.J., Lowe, S.W., 2007. Tissue-specific and reversible RNA interference in transgenic mice. Nat Genet 39, 914-921.

DiNitto, J.P., Wang, L., Wu, J.C., 2010. Continuous fluorescence-based method for assessing dicer cleavage efficiency reveals 3' overhang nucleotide preference. BioTechniques 48, 303-311.

Dlakic, M., 2006. DUF283 domain of Dicer proteins has a double-stranded RNA-binding fold. Bioinformatics 22, 2711-2714.

Doench, J.G., Petersen, C.P., Sharp, P.A., 2003. siRNAs can function as miRNAs. Genes Dev 17, 438-442.

Doench, J.G., Sharp, P.A., 2004. Specificity of microRNA target selection in translational repression. Genes Dev 18, 504-511.

Dolle, R.E., 1997. Comprehensive survey of chemical libraries yielding enzyme inhibitors, receptor agonists and antagonists, and other biologically active agents: 1992 through 1997. Molecular diversity 3, 199-233.

Dunoyer, P., Lecellier, C.H., Parizotto, E.A., Himber, C., Voinnet, O., 2004. Probing the microRNA and small interfering RNA pathways with virus-encoded suppressors of RNA silencing. The Plant cell 16, 1235-1250.

Easow, G., Teleman, A.A., Cohen, S.M., 2007. Isolation of microRNA targets by miRNP immunopurification. RNA 13, 1198-1204.

Eiring, A.M., Harb, J.G., Neviani, P., Garton, C., Oaks, J.J., Spizzo, R., Liu, S., Schwind, S., Santhanam, R., Hickey, C.J., Becker, H., Chandler, J.C., Andino, R., Cortes, J., Hokland, P., Huettner, C.S., Bhatia, R., Roy, D.C., Liebhaber, S.A., Caligiuri, M.A., Marcucci, G., Garzon, R., Croce, C.M., Calin, G.A., Perrotti, D., 2010. miR-328 functions as an RNA decoy to modulate hnRNP E2 regulation of mRNA translation in leukemic blasts. Cell 140, 652-665.

Elbashir, S.M., Harborth, J., Lendeckel, W., Yalcin, A., Weber, K., Tuschl, T., 2001a. Duplexes of 21-nucleotide RNAs mediate RNA interference in cultured mammalian cells. Nature 411, 494-498.

Elbashir, S.M., Lendeckel, W., Tuschl, T., 2001b. RNA interference is mediated by 21- and 22-nucleotide RNAs. Genes Dev 15, 188-200.

Ender, C., Meister, G., 2010. Argonaute proteins at a glance. J Cell Sci 123, 1819-1823.

Esau, C.C., 2008. Inhibition of microRNA with antisense oligonucleotides. Methods 44, 55-60.

Eulalio, A., Behm-Ansmant, I., Izaurralde, E., 2007a. P bodies: at the crossroads of post-transcriptional pathways. Nat Rev Mol Cell Biol 8, 9-22.

Eulalio, A., Behm-Ansmant, I., Schweizer, D., Izaurralde, E., 2007b. P-body formation is a consequence, not the cause, of RNA-mediated gene silencing. Mol Cell Biol 27, 3970-3981.

Fabian, M.R., Sonenberg, N., 2012. The mechanics of miRNA-mediated gene silencing: a look under the hood of miRISC. Nature Structural & Molecular Biology 19, 586-593.

Fabian, M.R., Sonenberg, N., Filipowicz, W., 2010. Regulation of mRNA translation and stability by microRNAs. Annu Rev Biochem 79, 351-379.

Farazi, T.A., Hoell, J.I., Morozov, P., Tuschl, T., 2013. MicroRNAs in human cancer. Advances in experimental medicine and biology 774, 1-20.

Felix, M.A., Ashe, A., Piffaretti, J., Wu, G., Nuez, I., Belicard, T., Jiang, Y., Zhao, G., Franz, C.J., Goldstein, L.D., Sanroman, M., Miska, E.A., Wang, D., 2011. Natural and experimental infection of Caenorhabditis nematodes by novel viruses related to nodaviruses. PLoS Biol 9, e1000586.

Ferguson, E.L., Sternberg, P.W., Horvitz, H.R., 1987. A genetic pathway for the specification of the vulval cell lineages of Caenorhabditis elegans. Nature 326, 259-267.

Fewell, G.D., Schmitt, K., 2006. Vector-based RNAi approaches for stable, inducible and genome-wide screens. Drug Discov Today 11, 975-982.

Filipowicz, W., Bhattacharyya, S.N., Sonenberg, N., 2008. Mechanisms of post-transcriptional regulation by microRNAs: are the answers in sight? Nat Rev Genet 9, 102-114.

Fiore, R., Siegel, G., Schratt, G., 2008. MicroRNA function in neuronal development, plasticity and disease. Biochim Biophys Acta 1779, 471-478.

Fire, A., Xu, S., Montgomery, M.K., Kostas, S.A., Driver, S.E., Mello, C.C., 1998. Potent and specific genetic interference by double-stranded RNA in Caenorhabditis elegans. Nature 391, 806-811.

Flemr, M., Malik, R., Franke, V., Nejepinska, J., Sedlacek, R., Vlahovicek, K., Svoboda, P., 2013. A Retrotransposon-Driven Dicer Isoform Directs Endogenous Small Interfering RNA Production in Mouse Oocytes. Cell 155, 807-816.

Friedman, R.C., Farh, K.K., Burge, C.B., Bartel, D.P., 2009. Most mammalian mRNAs are conserved targets of microRNAs. Genome Res 19, 92-105.

Fukuda, T., Yamagata, K., Fujiyama, S., Matsumoto, T., Koshida, I., Yoshimura, K., Mihara, M., Naitou, M., Endoh, H., Nakamura, T., Akimoto, C., Yamamoto, Y., Katagiri, T., Foulds, C., Takezawa, S., Kitagawa, H., Takeyama, K., O'Malley, B.W., Kato, S., 2007. DEAD-box RNA helicase subunits of the Drosha complex are required for processing of rRNA and a subset of microRNAs. Nat Cell Biol 9, 604-611.

Gao, K., Huang, L., 2009. Nonviral methods for siRNA delivery. Mol Pharm 6, 651-658.

Garzon, R., Calin, G.A., Croce, C.M., 2009. MicroRNAs in Cancer. Annual review of medicine 60, 167-179.

Ge, Q., Filip, L., Bai, A., Nguyen, T., Eisen, H.N., Chen, J., 2004. Inhibition of influenza virus production in virus-infected mice by RNA interference. Proc Natl Acad Sci U S A 101, 8676-8681.

Gebert, L.F., Rebhan, M.A., Crivelli, S.E., Denzler, R., Stoffel, M., Hall, J., 2014. Miravirsen (SPC3649) can inhibit the biogenesis of miR-122. Nucleic Acids Res 42, 609-621.

Gent, J.I., Lamm, A.T., Pavelec, D.M., Maniar, J.M., Parameswaran, P., Tao, L., Kennedy, S., Fire, A.Z., 2010. Distinct phases of siRNA synthesis in an endogenous RNAi pathway in C. elegans soma. Mol Cell 37, 679-689.

Gent, J.I., Schvarzstein, M., Villeneuve, A.M., Gu, S.G., Jantsch, V., Fire, A.Z., Baudrimont, A., 2009. A Caenorhabditis elegans RNA-directed RNA polymerase in sperm development and endogenous RNA interference. Genetics 183, 1297-1314.

Ghildiyal, M., Seitz, H., Horwich, M.D., Li, C., Du, T., Lee, S., Xu, J., Kittler, E.L., Zapp, M.L., Weng, Z., Zamore, P.D., 2008. Endogenous siRNAs derived from transposons and mRNAs in Drosophila somatic cells. Science 320, 1077-1081.

Gibbings, D.J., Ciaudo, C., Erhardt, M., Voinnet, O., 2009. Multivesicular bodies associate with components of miRNA effector complexes and modulate miRNA activity. Nat Cell Biol 11, 1143-1149.

Giladi, H., Ketzinel-Gilad, M., Rivkin, L., Felig, Y., Nussbaum, O., Galun, E., 2003. Small interfering RNA inhibits hepatitis B virus replication in mice. Mol Ther 8, 769-776.

Golzio, M., Mazzolini, L., Moller, P., Rols, M.P., Teissie, J., 2005. Inhibition of gene expression in mice muscle by in vivo electrically mediated siRNA delivery. Gene Ther 12, 246-251.

Goubau, D., Deddouche, S., Reis e Sousa, C., 2013. Cytosolic sensing of viruses. Immunity 38, 855-869.

Gredell, J.A., Dittmer, M.J., Wu, M., Chan, C., Walton, S.P., 2010. Recognition of siRNA asymmetry by TAR RNA binding protein. Biochemistry 49, 3148-3155.

Gregory, R.I., Chendrimada, T.P., Cooch, N., Shiekhattar, R., 2005. Human RISC couples microRNA biogenesis and posttranscriptional gene silencing. Cell 123, 631-640.

Gregory, R.I., Yan, K.P., Amuthan, G., Chendrimada, T., Doratotaj, B., Cooch, N., Shiekhattar, R., 2004. The Microprocessor complex mediates the genesis of microRNAs. Nature 432, 235-240.

Grewal, S.I., 2010. RNAi-dependent formation of heterochromatin and its diverse functions. Curr Opin Genet Dev 20, 134-141.

Grimson, A., Farh, K.K., Johnston, W.K., Garrett-Engele, P., Lim, L.P., Bartel, D.P., 2007. MicroRNA targeting specificity in mammals: determinants beyond seed pairing. Mol Cell 27, 91-105.

Grishok, A., Pasquinelli, A.E., Conte, D., Li, N., Parrish, S., Ha, I., Baillie, D.L., Fire, A., Ruvkun, G., Mello, C.C., 2001. Genes and mechanisms related to RNA interference regulate expression of the small temporal RNAs that control C. elegans developmental timing. Cell 106, 23-34.

Grishok, A., Tabara, H., Mello, C.C., 2000. Genetic requirements for inheritance of RNAi in C. elegans. Science 287, 2494-2497.

Gu, S., Jin, L., Zhang, F., Sarnow, P., Kay, M.A., 2009a. Biological basis for restriction of microRNA targets to the 3' untranslated region in mammalian mRNAs. Nat Struct Mol Biol 16, 144-150.

Gu, W., Shirayama, M., Conte, D., Jr., Vasale, J., Batista, P.J., Claycomb, J.M., Moresco, J.J., Youngman, E.M., Keys, J., Stoltz, M.J., Chen, C.C., Chaves, D.A., Duan, S., Kasschau, K.D., Fahlgren, N., Yates, J.R., 3rd, Mitani, S., Carrington, J.C., Mello, C.C., 2009b. Distinct argonaute-mediated 22G-RNA pathways direct genome surveillance in the C. elegans germline. Mol Cell 36, 231-244.

Gunawardane, L.S., Saito, K., Nishida, K.M., Miyoshi, K., Kawamura, Y., Nagami, T., Siomi, H., Siomi, M.C., 2007. A slicer-mediated mechanism for repeat-associated siRNA 5' end formation in Drosophila. Science 315, 1587-1590.

Guo, S., Kemphues, K.J., 1995. par-1, a gene required for establishing polarity in C. elegans embryos, encodes a putative Ser/Thr kinase that is asymmetrically distributed. Cell 81, 611-620.

Gupta, S., Schoer, R.A., Egan, J.E., Hannon, G.J., Mittal, V., 2004. Inducible, reversible, and stable RNA interference in mammalian cells. Proc Natl Acad Sci U S A 101, 1927-1932.

Ha, M., Kim, V.N., 2014. Regulation of microRNA biogenesis. Nat Rev Mol Cell Biol 15, 509-524.

Haase, A.D., Jaskiewicz, L., Zhang, H., Laine, S., Sack, R., Gatignol, A., Filipowicz, W., 2005. TRBP, a regulator of cellular PKR and HIV-1 virus expression, interacts with Dicer and functions in RNA silencing. EMBO Rep 6, 961-967.

Haasnoot, J., de Vries, W., Geutjes, E.J., Prins, M., de Haan, P., Berkhout, B., 2007. The Ebola virus VP35 protein is a suppressor of RNA silencing. PLoS Pathog 3, e86.

Haley, B., Zamore, P.D., 2004. Kinetic analysis of the RNAi enzyme complex. Nat Struct Mol Biol 11, 599-606.

Hamilton, A.J., Baulcombe, D.C., 1999. A species of small antisense RNA in posttranscriptional gene silencing in plants. Science 286, 950-952.

Hammond, S.M., Bernstein, E., Beach, D., Hannon, G.J., 2000. An RNA-directed nuclease mediates post-transcriptional gene silencing in Drosophila cells. Nature 404, 293-296.

Han, J., Lee, Y., Yeom, K.H., Kim, Y.K., Jin, H., Kim, V.N., 2004. The Drosha-DGCR8 complex in primary microRNA processing. Genes Dev 18, 3016-3027.

Han, J., Lee, Y., Yeom, K.H., Nam, J.W., Heo, I., Rhee, J.K., Sohn, S.Y., Cho, Y., Zhang, B.T., Kim, V.N., 2006. Molecular basis for the recognition of primary microRNAs by the Drosha-DGCR8 complex. Cell 125, 887-901.

Hasuwa, H., Kaseda, K., Einarsdottir, T., Okabe, M., 2002. Small interfering RNA and gene silencing in transgenic mice and rats. FEBS Lett 532, 227-230.

Hausser, J., Zavolan, M., 2014. Identification and consequences of miRNA-target interactions--beyond repression of gene expression. Nat Rev Genet 15, 599-612.

Heman-Ackah, S.M., Hallegger, M., Rao, M.S., Wood, M.J., 2013. RISC in PD: the impact of microRNAs in Parkinson's disease cellular and molecular pathogenesis. Frontiers in molecular neuroscience 6, 40.

Hemann, M.T., Fridman, J.S., Zilfou, J.T., Hernando, E., Paddison, P.J., Cordon-Cardo, C., Hannon, G.J., Lowe, S.W., 2003. An epi-allelic series of p53 hypomorphs created by stable RNAi produces distinct tumor phenotypes in vivo. Nat Genet 33, 396-400.

Henke, J.I., Goergen, D., Zheng, J., Song, Y., Schuttler, C.G., Fehr, C., Junemann, C., Niepmann, M., 2008. microRNA-122 stimulates translation of hepatitis C virus RNA. EMBO J 27, 3300-3310.

Horvitz, H.R., Sulston, J.E., 1980. Isolation and genetic characterization of cell-lineage mutants of the nematode Caenorhabditis elegans. Genetics 96, 435-454.

Huang, J., Liang, Z., Yang, B., Tian, H., Ma, J., Zhang, H., 2007. Derepression of microRNA-mediated protein translation inhibition by apolipoprotein B mRNA-editing enzyme catalytic polypeptide-like 3G (APOBEC3G) and its family members. J Biol Chem 282, 33632-33640.

Huntzinger, E., Izaurralde, E., 2011. Gene silencing by microRNAs: contributions of translational repression and mRNA decay. Nat Rev Genet 12, 99-110.

Chakravarthy, S., Sternberg, S.H., Kellenberger, C.A., Doudna, J.A., 2010. Substrate-specific kinetics of Dicer-catalyzed RNA processing. J Mol Biol 404, 392-402.

Chalfie, M., Horvitz, H.R., Sulston, J.E., 1981. Mutations that lead to reiterations in the cell lineages of C. elegans. Cell 24, 59-69.

Chan, S.H., Wang, L.H., 2015. Regulation of cancer metastasis by microRNAs. Journal of biomedical science 22, 9.

Chen, J.F., Mandel, E.M., Thomson, J.M., Wu, Q., Callis, T.E., Hammond, S.M., Conlon, F.L., Wang, D.Z., 2006. The role of microRNA-1 and microRNA-133 in skeletal muscle proliferation and differentiation. Nat Genet 38, 228-233.

Chendrimada, T.P., Gregory, R.I., Kumaraswamy, E., Norman, J., Cooch, N., Nishikura, K., Shiekhattar, R., 2005. TRBP recruits the Dicer complex to Ago2 for microRNA processing and gene silencing. Nature 436, 740-744.

Chiu, Y.L., Dinesh, C.U., Chu, C.Y., Ali, A., Brown, K.M., Cao, H., Rana, T.M., 2005. Dissecting RNA-interference pathway with small molecules. Chemistry & biology 12, 643-648.

Choi, W.Y., Giraldez, A.J., Schier, A.F., 2007. Target protectors reveal dampening and balancing of Nodal agonist and antagonist by miR-430. Science 318, 271-274.

Choudhary, C., Kumar, C., Gnad, F., Nielsen, M.L., Rehman, M., Walther, T.C., Olsen, J.V., Mann, M., 2009. Lysine acetylation targets protein complexes and co-regulates major cellular functions. Science 325, 834-840.

Chuang, J.C., Jones, P.A., 2007. Epigenetics and microRNAs. Pediatric research 61, 24R-29R.

Janssen, H.L.A., Reesink, H.W., Lawitz, E.J., Zeuzem, S., Rodriguez-Torres, M., Patel, K., van der Meer, A.J., Patick, A.K., Chen, A., Zhou, Y., Persson, R., King, B.D., Kauppinen, S., Levin, A.A., Hodges, M.R., 2013. Treatment of HCV Infection by Targeting MicroRNA. New Engl J Med 368, 1685-1694.

Jaskiewicz, L., Filipowicz, W., 2008. Role of Dicer in posttranscriptional RNA silencing. Curr Top Microbiol Immunol 320, 77-97.

Ji, X., 2008. The mechanism of RNase III action: how dicer dices. Curr Top Microbiol Immunol 320, 99-116.

Jinek, M., Doudna, J.A., 2009. A three-dimensional view of the molecular machinery of RNA interference. Nature 457, 405-412.

Joseph, A., Brasington, R., Kahl, L., Ranganathan, P., Cheng, T.P., Atkinson, J., 2010. Immunologic rheumatic disorders. The Journal of allergy and clinical immunology 125, S204-215.

Kamminga, L.M., Luteijn, M.J., den Broeder, M.J., Redl, S., Kaaij, L.J., Roovers, E.F., Ladurner, P., Berezikov, E., Ketting, R.F., 2010. Hen1 is required for oocyte development and piRNA stability in zebrafish. EMBO J 29, 3688-3700.

Kaneda, M., Tang, F., O'Carroll, D., Lao, K., Surani, M.A., 2009. Essential role for Argonaute2 protein in mouse oogenesis. Epigenetics Chromatin 2, 9.

Kaneko, H., Dridi, S., Tarallo, V., Gelfand, B.D., Fowler, B.J., Cho, W.G., Kleinman, M.E., Ponicsan, S.L., Hauswirth, W.W., Chiodo, V.A., Kariko, K., Yoo, J.W., Lee, D.K., Hadziahmetovic, M., Song, Y., Misra, S., Chaudhuri, G., Buaas, F.W., Braun, R.E., Hinton, D.R., Zhang, Q., Grossniklaus, H.E., Provis, J.M., Madigan, M.C., Milam, A.H., Justice, N.L., Albuquerque, R.J., Blandford, A.D., Bogdanovich, S., Hirano, Y., Witta, J., Fuchs, E., Littman, D.R., Ambati, B.K., Rudin, C.M., Chong, M.M., Provost, P., Kugel, J.F., Goodrich, J.A., Dunaief, J.L., Baffi, J.Z., Ambati, J., 2011. DICER1 deficit induces Alu RNA toxicity in age-related macular degeneration. Nature 471, 325-330.

Karpel, R.L., Shirley, M.S., Holt, S.R., 1981. Interaction of the ruthenium red cation with nucleic acid double helices. Biophysical chemistry 13, 151-165.

Kasim, V., Miyagishi, M., Taira, K., 2004. Control of siRNA expression using the Cre-loxP recombination system. Nucleic Acids Res 32, e66.

Kawamata, T., Seitz, H., Tomari, Y., 2009. Structural determinants of miRNAs for RISC loading and slicer-independent unwinding. Nat Struct Mol Biol 16, 953-960.

Kawamata, T., Tomari, Y., 2010. Making RISC. Trends Biochem Sci 35, 368-376.

Kedersha, N., Anderson, P., 2007. Mammalian stress granules and processing bodies. Methods Enzymol 431, 61-81.

Kedersha, N., Cho, M.R., Li, W., Yacono, P.W., Chen, S., Gilks, N., Golan, D.E., Anderson, P., 2000. Dynamic shuttling of TIA-1 accompanies the recruitment of mRNA to mammalian stress granules. J Cell Biol 151, 1257-1268.

Kedersha, N., Stoecklin, G., Ayodele, M., Yacono, P., Lykke-Andersen, J., Fritzler, M.J., Scheuner, D., Kaufman, R.J., Golan, D.E., Anderson, P., 2005. Stress granules and processing bodies are dynamically linked sites of mRNP remodeling. J Cell Biol 169, 871-884.

Ketting, R.F., 2011. The many faces of RNAi. Dev Cell 20, 148-161.

Khvorova, A., Reynolds, A., Jayasena, S.D., 2003. Functional siRNAs and miRNAs exhibit strand bias. Cell 115, 209-216.

Kim, D.H., Behlke, M.A., Rose, S.D., Chang, M.S., Choi, S., Rossi, J.J., 2005. Synthetic dsRNA Dicer substrates enhance RNAi potency and efficacy. Nat Biotechnol 23, 222-226.

Kim, K., Lee, Y.S., Carthew, R.W., 2007. Conversion of pre-RISC to holo-RISC by Ago2 during assembly of RNAi complexes. RNA 13, 22-29.

Kim, Y.J., Maizel, A., Chen, X., 2014. Traffic into silence: endomembranes and post-transcriptional RNA silencing. EMBO J 33, 968-980.

Kishida, T., Asada, H., Gojo, S., Ohashi, S., Shin-Ya, M., Yasutomi, K., Terauchi, R., Takahashi, K.A., Kubo, T., Imanishi, J., Mazda, O., 2004. Sequence-specific gene silencing in murine muscle induced by electroporation-mediated transfer of short interfering RNA. J Gene Med 6, 105-110.

Kok, K.H., Ng, M.H., Ching, Y.P., Jin, D.Y., 2007. Human TRBP and PACT directly interact with each other and associate with dicer to facilitate the production of small interfering RNA. J Biol Chem 282, 17649-17657.

Kolb, F.A., Zhang, H., Jaronczyk, K., Tahbaz, N., Hobman, T.C., Filipowicz, W., 2005. Human dicer: purification, properties, and interaction with PAZ PIWI domain proteins. Methods Enzymol 392, 316-336.

Kong, X.C., Barzaghi, P., Ruegg, M.A., 2004. Inhibition of synapse assembly in mammalian muscle in vivo by RNA interference. EMBO Rep 5, 183-188.

Konishi, Y., Stegmuller, J., Matsuda, T., Bonni, S., Bonni, A., 2004. Cdh1-APC controls axonal growth and patterning in the mammalian brain. Science 303, 1026-1030.

Kunath, T., Gish, G., Lickert, H., Jones, N., Pawson, T., Rossant, J., 2003. Transgenic RNA interference in ES cell-derived embryos recapitulates a genetic null phenotype. Nat Biotechnol 21, 559-561.

Kunne, T., Swarts, D.C., Brouns, S.J.J., 2014. Planting the seed: target recognition of short guide RNAs. Trends Microbiol 22, 74-83.

Lakatos, L., Csorba, T., Pantaleo, V., Chapman, E.J., Carrington, J.C., Liu, Y.P., Dolja, V.V., Calvino, L.F., Lopez-Moya, J.J., Burgyan, J., 2006. Small RNA binding is a common strategy to suppress RNA silencing by several viral suppressors. EMBO J 25, 2768-2780.

Landgraf, P., Rusu, M., Sheridan, R., Sewer, A., Iovino, N., Aravin, A., Pfeffer, S., Rice, A., Kamphorst, A.O., Landthaler, M., Lin, C., Socci, N.D., Hermida, L., Fulci, V., Chiaretti, S., Foa, R., Schliwka, J., Fuchs, U., Novosel, A., Muller, R.U., Schermer, B., Bissels, U., Inman, J., Phan, Q., Chien, M., Weir, D.B., Choksi, R., De Vita, G., Frezzetti, D., Trompeter, H.I., Hornung, V., Teng, G., Hartmann, G., Palkovits, M., Di Lauro, R., Wernet, P., Macino, G., Rogler, C.E., Nagle, J.W., Ju, J., Papavasiliou, F.N., Benzing, T., Lichter, P., Tam, W., Brownstein, M.J., Bosio, A., Borkhardt, A., Russo, J.J., Sander, C., Zavolan, M., Tuschl, T., 2007. A mammalian microRNA expression atlas based on small RNA library sequencing. Cell 129, 1401-1414.

Landthaler, M., Yalcin, A., Tuschl, T., 2004. The human DiGeorge syndrome critical region gene 8 and Its D. melanogaster homolog are required for miRNA biogenesis. Curr Biol 14, 2162-2167.

Lanford, R.E., Hildebrandt-Eriksen, E.S., Petri, A., Persson, R., Lindow, M., Munk, M.E., Kauppinen, S., Orum, H., 2010. Therapeutic Silencing of MicroRNA-122 in Primates with Chronic Hepatitis C Virus Infection. Science 327, 198-201.

Lau, P.W., Guiley, K.Z., De, N., Potter, C.S., Carragher, B., MacRae, I.J., 2012. The molecular architecture of human Dicer. Nat Struct Mol Biol 19, 436-440.

Lee, R., Feinbaum, R., Ambros, V., 2004a. A short history of a short RNA. Cell 116, S89-92, 81 p following S96.

Lee, R.C., Feinbaum, R.L., Ambros, V., 1993. The C. elegans heterochronic gene lin-4 encodes small RNAs with antisense complementarity to lin-14. Cell 75, 843-854.

Lee, Y., Ahn, C., Han, J., Choi, H., Kim, J., Yim, J., Lee, J., Provost, P., Radmark, O., Kim, S., Kim, V.N., 2003. The nuclear RNase III Drosha initiates microRNA processing. Nature 425, 415-419.

Lee, Y., Kim, M., Han, J., Yeom, K.H., Lee, S., Baek, S.H., Kim, V.N., 2004b. MicroRNA genes are transcribed by RNA polymerase II. EMBO J 23, 4051-4060.

Lee, Y.S., Nakahara, K., Pham, J.W., Kim, K., He, Z., Sontheimer, E.J., Carthew, R.W., 2004c. Distinct roles for Drosophila Dicer-1 and Dicer-2 in the siRNA/miRNA silencing pathways. Cell 117, 69-81.

Lee, Y.S., Pressman, S., Andress, A.P., Kim, K., White, J.L., Cassidy, J.J., Li, X., Lubell, K., Lim do, H., Cho, I.S., Nakahara, K., Preall, J.B., Bellare, P., Sontheimer, E.J., Carthew, R.W., 2009. Silencing by small RNAs is linked to endosomal trafficking. Nat Cell Biol 11, 1150-1156.

Leung, A.K., Calabrese, J.M., Sharp, P.A., 2006. Quantitative analysis of Argonaute protein reveals microRNA-dependent localization to stress granules. Proc Natl Acad Sci U S A 103, 18125-18130.

Lewis, D.L., Hagstrom, J.E., Loomis, A.G., Wolff, J.A., Herweijer, H., 2002. Efficient delivery of siRNA for inhibition of gene expression in postnatal mice. Nat Genet 32, 107-108.

Li, C., Vagin, V.V., Lee, S., Xu, J., Ma, S., Xi, H., Seitz, H., Horwich, M.D., Syrzycka, M., Honda, B.M., Kittler, E.L., Zapp, M.L., Klattenhoff, C., Schulz, N., Theurkauf, W.E., Weng, Z., Zamore, P.D., 2009. Collapse of germline piRNAs in the absence of Argonaute3 reveals somatic piRNAs in flies. Cell 137, 509-521.

Li, Y., Lu, J., Han, Y., Fan, X., Ding, S.W., 2013. RNA interference functions as an antiviral immunity mechanism in mammals. Science 342, 231-234.

Lian, S., Jakymiw, A., Eystathioy, T., Hamel, J.C., Fritzler, M.J., Chan, E.K., 2006. GW bodies, microRNAs and the cell cycle. Cell Cycle 5, 242-245.

Lickert, H., Takeuchi, J.K., Von Both, I., Walls, J.R., McAuliffe, F., Adamson, S.L., Henkelman, R.M., Wrana, J.L., Rossant, J., Bruneau, B.G., 2004. Baf60c is essential for function of BAF chromatin remodelling complexes in heart development. Nature 432, 107-112.

Lingel, A., Simon, B., Izaurralde, E., Sattler, M., 2003. Structure and nucleic-acid binding of the Drosophila Argonaute 2 PAZ domain. Nature 426, 465-469.

Liu, C.G., Calin, G.A., Volinia, S., Croce, C.M., 2008. MicroRNA expression profiling using microarrays. Nature protocols 3, 563-578.

Liu, F., Song, Y., Liu, D., 1999. Hydrodynamics-based transfection in animals by systemic administration of plasmid DNA. Gene Ther 6, 1258-1266.

Liu, J., Carmell, M.A., Rivas, F.V., Marsden, C.G., Thomson, J.M., Song, J.J., Hammond, S.M., Joshua-Tor, L., Hannon, G.J., 2004. Argonaute2 is the catalytic engine of mammalian RNAi. Science 305, 1437-1441.

Liu, J., Valencia-Sanchez, M.A., Hannon, G.J., Parker, R., 2005. MicroRNA-dependent localization of targeted mRNAs to mammalian P-bodies. Nat Cell Biol 7, 719-723.

Liu, X., Jin, D.Y., McManus, M.T., Mourelatos, Z., 2012. Precursor microRNA-programmed silencing complex assembly pathways in mammals. Mol Cell 46, 507-517.

Lohmann, J.U., Endl, I., Bosch, T.C., 1999. Silencing of developmental genes in Hydra. Dev Biol 214, 211-214.

Lu, R., Maduro, M., Li, F., Li, H.W., Broitman-Maduro, G., Li, W.X., Ding, S.W., 2005. Animal virus replication and RNAi-mediated antiviral silencing in Caenorhabditis elegans. Nature 436, 1040-1043.

Lu, X.P., Fanjul, A., Picard, N., Pfahl, M., Rungta, D., Nared-Hood, K., Carter, B., Piedrafita, J., Tang, S., Fabbrizio, E., Pfahl, M., 1997. Novel retinoid-related molecules as apoptosis inducers and effective inhibitors of human lung cancer cells in vivo. Nat Med 3, 686-690.

Lund, E., Guttinger, S., Calado, A., Dahlberg, J.E., Kutay, U., 2004. Nuclear export of microRNA precursors. Science 303, 95-98.

Ma, E., MacRae, I.J., Kirsch, J.F., Doudna, J.A., 2008. Autoinhibition of human dicer by its internal helicase domain. J Mol Biol 380, 237-243.

Ma, J., Flemr, M., Stein, P., Berninger, P., Malik, R., Zavolan, M., Svoboda, P., Schultz, R.M., 2010. MicroRNA Activity Is Suppressed in Mouse Oocytes. Current Biology 20, 265-270.

Ma, J.B., Ye, K., Patel, D.J., 2004. Structural basis for overhang-specific small interfering RNA recognition by the PAZ domain. Nature 429, 318-322.

Ma, J.B., Yuan, Y.R., Meister, G., Pei, Y., Tuschl, T., Patel, D.J., 2005. Structural basis for 5'-end-specific recognition of guide RNA by the A. fulgidus Piwi protein. Nature 434, 666-670.

Ma, L., Teruya-Feldstein, J., Weinberg, R.A., 2007. Tumour invasion and metastasis initiated by microRNA-10b in breast cancer. Nature 449, 682-688.

Ma, L., Wei, L., Wu, F., Hu, Z., Liu, Z., Yuan, W., 2013. Advances with microRNAs in Parkinson's disease research. Drug design, development and therapy 7, 1103-1113.

Maciotta, S., Meregalli, M., Torrente, Y., 2013. The involvement of microRNAs in neurodegenerative diseases. Frontiers in cellular neuroscience 7, 265.

MacRae, I.J., Ma, E., Zhou, M., Robinson, C.V., Doudna, J.A., 2008. In vitro reconstitution of the human RISC-loading complex. Proc Natl Acad Sci U S A 105, 512-517.

MacRae, I.J., Zhou, K., Doudna, J.A., 2007. Structural determinants of RNA recognition and cleavage by Dicer. Nat Struct Mol Biol 14, 934-940.

Macrae, I.J., Zhou, K., Li, F., Repic, A., Brooks, A.N., Cande, W.Z., Adams, P.D., Doudna, J.A., 2006. Structural basis for double-stranded RNA processing by Dicer. Science 311, 195-198.

Maillard, P.V., Ciaudo, C., Marchais, A., Li, Y., Jay, F., Ding, S.W., Voinnet, O., 2013. Antiviral RNA interference in mammalian cells. Science 342, 235-238.

Maiti, M., Nauwelaerts, K., Herdewijn, P., 2012. Pre-microRNA binding aminoglycosides and antitumor drugs as inhibitors of Dicer catalyzed microRNA processing. Bioorganic & medicinal chemistry letters 22, 1709-1711.

Malone, C.D., Brennecke, J., Dus, M., Stark, A., McCombie, W.R., Sachidanandam, R., Hannon, G.J., 2009. Specialized piRNA pathways act in germline and somatic tissues of the Drosophila ovary. Cell 137, 522-535.

Malone, C.D., Hannon, G.J., 2009. Small RNAs as guardians of the genome. Cell 136, 656-668.

Maniataki, E., Mourelatos, Z., 2005. A human, ATP-independent, RISC assembly machine fueled by pre-miRNA. Genes Dev 19, 2979-2990.

Marks, P.A., Richon, V.M., Miller, T., Kelly, W.K., 2004. Histone deacetylase inhibitors. Advances in cancer research 91, 137-168.

Martinez, J., Patkaniowska, A., Urlaub, H., Luhrmann, R., Tuschl, T., 2002. Single-stranded antisense siRNAs guide target RNA cleavage in RNAi. Cell 110, 563-574.

Martinez, J., Tuschl, T., 2004. RISC is a 5' phosphomonoester-producing RNA endonuclease. Genes Dev 18, 975-980.

Massaro, D., Massaro, G.D., Clerch, L.B., 2004. Noninvasive delivery of small inhibitory RNA and other reagents to pulmonary alveoli in mice. Am J Physiol Lung Cell Mol Physiol 287, L1066-1070.

Matranga, C., Tomari, Y., Shin, C., Bartel, D.P., Zamore, P.D., 2005. Passenger-strand cleavage facilitates assembly of siRNA into Ago2-containing RNAi enzyme complexes. Cell 123, 607-620.

Matsuda, T., Cepko, C.L., 2004. Electroporation and RNA interference in the rodent retina in vivo and in vitro. Proc Natl Acad Sci U S A 101, 16-22.

Mayer, T.U., Kapoor, T.M., Haggarty, S.J., King, R.W., Schreiber, S.L., Mitchison, T.J., 1999. Small molecule inhibitor of mitotic spindle bipolarity identified in a phenotype-based screen. Science 286, 971-974.

McCaffrey, A.P., Meuse, L., Pham, T.T., Conklin, D.S., Hannon, G.J., Kay, M.A., 2002. RNA interference in adult mice. Nature 418, 38-39.

McCaffrey, A.P., Nakai, H., Pandey, K., Huang, Z., Salazar, F.H., Xu, H., Wieland, S.F., Marion, P.L., Kay, M.A., 2003. Inhibition of hepatitis B virus in mice by RNA interference. Nat Biotechnol 21, 639-644.

McManus, M.T., Petersen, C.P., Haines, B.B., Chen, J., Sharp, P.A., 2002. Gene silencing using micro-RNA designed hairpins. RNA 8, 842-850.

Medina, P.P., Nolde, M., Slack, F.J., 2010. OncomiR addiction in an in vivo model of microRNA-21-induced pre-B-cell lymphoma. Nature 467, 86-90.

Medina, P.P., Slack, F.J., 2008. microRNAs and cancer: an overview. Cell Cycle 7, 2485-2492.

Meijer, H.A., Kong, Y.W., Lu, W.T., Wilczynska, A., Spriggs, R.V., Robinson, S.W., Godfrey, J.D., Willis, A.E., Bushell, M., 2013. Translational repression and eIF4A2 activity are critical for microRNA-mediated gene regulation. Science 340, 82-85.

Meins, F., Jr., Si-Ammour, A., Blevins, T., 2005. RNA silencing systems and their relevance to plant development. Annu Rev Cell Dev Biol 21, 297-318.

Meister, G., Landthaler, M., Patkaniowska, A., Dorsett, Y., Teng, G., Tuschl, T., 2004. Human Argonaute2 mediates RNA cleavage targeted by miRNAs and siRNAs. Mol Cell 15, 185-197.

Melton, C., Judson, R.L., Blelloch, R., 2010. Opposing microRNA families regulate self-renewal in mouse embryonic stem cells. Nature 463, 621-626.

Miyoshi, K., Tsukumo, H., Nagami, T., Siomi, H., Siomi, M.C., 2005. Slicer function of Drosophila Argonautes and its involvement in RISC formation. Genes Dev 19, 2837-2848.

Nagy, A., Rossant, J., Nagy, R., Abramow-Newerly, W., Roder, J.C., 1993. Derivation of completely cell culture-derived mice from early-passage embryonic stem cells. Proc Natl Acad Sci U S A 90, 8424-8428.

Napoli, C., Lemieux, C., Jorgensen, R., 1990. Introduction of a Chimeric Chalcone Synthase Gene into Petunia Results in Reversible Co-Suppression of Homologous Genes in trans. The Plant cell 2, 279-289.

Nejepinska, J., Malik, R., Filkowski, J., Flemr, M., Filipowicz, W., Svoboda, P., 2012. dsRNA expression in the mouse elicits RNAi in oocytes and low adenosine deamination in somatic cells. Nucleic Acids Res 40, 399-413.

Newmark, P.A., Reddien, P.W., Cebria, F., Sanchez Alvarado, A., 2003. Ingestion of bacterially expressed double-stranded RNA inhibits gene expression in planarians. Proc Natl Acad Sci U S A 100 Suppl 1, 11861-11865.

Noland, C.L., Ma, E., Doudna, J.A., 2011. siRNA repositioning for guide strand selection by human Dicer complexes. Mol Cell 43, 110-121.

Norman, T.C., Smith, D.L., Sorger, P.K., Drees, B.L., O'Rourke, S.M., Hughes, T.R., Roberts, C.J., Friend, S.H., Fields, S., Murray, A.W., 1999. Genetic selection of peptide inhibitors of biological pathways. Science 285, 591-595.

Norris, J.D., Paige, L.A., Christensen, D.J., Chang, C.Y., Huacani, M.R., Fan, D., Hamilton, P.T., Fowlkes, D.M., McDonnell, D.P., 1999. Peptide antagonists of the human estrogen receptor. Science 285, 744-746.

Novotny, I., Podolska, K., Blazikova, M., Valasek, L.S., Svoboda, P., Stanek, D., 2012. Nuclear LSm8 affects number of cytoplasmic processing bodies via controlling cellular distribution of Like-Sm proteins. Mol Biol Cell 23, 3776-3785.

Nykanen, A., Haley, B., Zamore, P.D., 2001. ATP requirements and small interfering RNA structure in the RNA interference pathway. Cell 107, 309-321.

O'Donnell, K.A., Wentzel, E.A., Zeller, K.I., Dang, C.V., Mendell, J.T., 2005. c-Myc-regulated microRNAs modulate E2F1 expression. Nature 435, 839-843.

Okamura, K., Chung, W.J., Ruby, J.G., Guo, H., Bartel, D.P., Lai, E.C., 2008. The Drosophila hairpin RNA pathway generates endogenous short interfering RNAs. Nature 453, 803-806.

Orii, H., Mochii, M., Watanabe, K., 2003. A simple "soaking method" for RNA interference in the planarian Dugesia japonica. Dev Genes Evol 213, 138-141.

Orom, U.A., Nielsen, F.C., Lund, A.H., 2008. MicroRNA-10a binds the 5'UTR of ribosomal protein mRNAs and enhances their translation. Mol Cell 30, 460-471.

Paddison, P.J., Caudy, A.A., Bernstein, E., Hannon, G.J., Conklin, D.S., 2002. Short hairpin RNAs (shRNAs) induce sequence-specific silencing in mammalian cells. Genes Dev 16, 948-958.

Paganin-Gioanni, A., Bellard, E., Couderc, B., Teissie, J., Golzio, M., 2008. Tracking in vitro and in vivo siRNA electrotransfer in tumor cells. J RNAi Gene Silencing 4, 281-288.

Pak, J., Fire, A., 2007. Distinct populations of primary and secondary effectors during RNAi in C. elegans. Science 315, 241-244.

Park, J.E., Heo, I., Tian, Y., Simanshu, D.K., Chang, H., Jee, D., Patel, D.J., Kim, V.N., 2011. Dicer recognizes the 5' end of RNA for efficient and accurate processing. Nature 475, 201-205.

Parker, R., Sheth, U., 2007. P bodies and the control of mRNA translation and degradation. Mol Cell 25, 635-646.

Pasquinelli, A.E., Reinhart, B.J., Slack, F., Martindale, M.Q., Kuroda, M.I., Maller, B., Hayward, D.C., Ball, E.E., Degnan, B., Muller, P., Spring, J., Srinivasan, A., Fishman, M., Finnerty, J., Corbo, J., Levine, M., Leahy, P., Davidson, E., Ruvkun, G., 2000. Conservation of the sequence and temporal expression of let-7 heterochronic regulatory RNA. Nature 408, 86-89.

Pauley, K.M., Eystathioy, T., Jakymiw, A., Hamel, J.C., Fritzler, M.J., Chan, E.K., 2006. Formation of GW bodies is a consequence of microRNA genesis. EMBO Rep 7, 904-910.

Pavelec, D.M., Lachowiec, J., Duchaine, T.F., Smith, H.E., Kennedy, S., 2009. Requirement for the ERI/DICER complex in endogenous RNA interference and sperm development in Caenorhabditis elegans. Genetics 183, 1283-1295.

Peng, S., York, J.P., Zhang, P., 2006. A transgenic approach for RNA interference-based genetic screening in mice. Proc Natl Acad Sci U S A 103, 2252-2256.

Pfeffer, S., Sewer, A., Lagos-Quintana, M., Sheridan, R., Sander, C., Grasser, F.A., van Dyk, L.F., Ho, C.K., Shuman, S., Chien, M., Russo, J.J., Ju, J., Randall, G., Lindenbach, B.D., Rice, C.M., Simon, V., Ho, D.D., Zavolan, M., Tuschl, T., 2005. Identification of microRNAs of the herpesvirus family. Nat Methods 2, 269-276.

Pillai, R.S., Bhattacharyya, S.N., Artus, C.G., Zoller, T., Cougot, N., Basyuk, E., Bertrand, E., Filipowicz, W., 2005. Inhibition of translational initiation by Let-7 MicroRNA in human cells. Science 309, 1573-1576.

Podolska, K., Sedlak, D., Bartunek, P., Svoboda, P., 2014. Fluorescence-based high-throughput screening of dicer cleavage activity. Journal of biomolecular screening 19, 417-426.

Podolska, K., Svoboda, P., 2011. Targeting genes in living mammals by RNA interference. Briefings in functional genomics 10, 238-247.

Provost, P., Dishart, D., Doucet, J., Frendewey, D., Samuelsson, B., Radmark, O., 2002. Ribonuclease activity and RNA binding of recombinant human Dicer. EMBO J 21, 5864-5874.

Qin, H., Chen, F., Huan, X., Machida, S., Song, J., Yuan, Y.A., 2010. Structure of the Arabidopsis thaliana DCL4 DUF283 domain reveals a noncanonical double-stranded RNA-binding fold for protein-protein interaction. RNA 16, 474-481.

Rana, T.M., 2007. Illuminating the silence: understanding the structure and function of small RNAs. Nat Rev Mol Cell Biol 8, 23-36.

Reinhart, B.J., Slack, F.J., Basson, M., Pasquinelli, A.E., Bettinger, J.C., Rougvie, A.E., Horvitz, H.R., Ruvkun, G., 2000. The 21-nucleotide let-7 RNA regulates developmental timing in Caenorhabditis elegans. Nature 403, 901-906.

Richon, V.M., Garcia-Vargas, J., Hardwick, J.S., 2009. Development of vorinostat: current applications and future perspectives for cancer therapy. Cancer letters 280, 201-210.

Rodriguez, A., Griffiths-Jones, S., Ashurst, J.L., Bradley, A., 2004. Identification of mammalian microRNA host genes and transcription units. Genome Res 14, 1902-1910.

Romano, N., Macino, G., 1992. Quelling: transient inactivation of gene expression in Neurospora crassa by transformation with homologous sequences. Molecular microbiology 6, 3343-3353.

Rosania, G.R., Chang, Y.T., Perez, O., Sutherlin, D., Dong, H., Lockhart, D.J., Schultz, P.G., 2000. Myoseverin, a microtubule-binding molecule with novel cellular effects. Nat Biotechnol 18, 304-308.

Rossbach, M., 2010. Small non-coding RNAs as novel therapeutics. Current molecular medicine 10, 361-368.

Rubinson, D.A., Dillon, C.P., Kwiatkowski, A.V., Sievers, C., Yang, L., Kopinja, J., Rooney, D.L., Zhang, M., Ihrig, M.M., McManus, M.T., Gertler, F.B., Scott, M.L., Van Parijs, L., 2003. A lentivirus-based system to functionally silence genes in primary mammalian cells, stem cells and transgenic mice by RNA interference. Nat Genet 33, 401-406.

Ruby, J.G., Jan, C., Player, C., Axtell, M.J., Lee, W., Nusbaum, C., Ge, H., Bartel, D.P., 2006. Large-scale sequencing reveals 21U-RNAs and additional microRNAs and endogenous siRNAs in C. elegans. Cell 127, 1193-1207.

Saito, Y., Liang, G., Egger, G., Friedman, J.M., Chuang, J.C., Coetzee, G.A., Jones, P.A., 2006. Specific activation of microRNA-127 with downregulation of the proto-oncogene BCL6 by chromatin-modifying drugs in human cancer cells. Cancer Cell 9, 435-443.

Salahpour, A., Medvedev, I.O., Beaulieu, J.M., Gainetdinov, R.R., Caron, M.G., 2007. Local knockdown of genes in the brain using small interfering RNA: a phenotypic comparison with knockout animals. Biol Psychiatry 61, 65-69.

Sashital, D.G., Doudna, J.A., 2010. Structural insights into RNA interference. Curr Opin Struct Biol 20, 90-97.

Scott, J.K., Smith, G.P., 1990. Searching for peptide ligands with an epitope library. Science 249, 386-390.

Shan, G., Li, Y., Zhang, J., Li, W., Szulwach, K.E., Duan, R., Faghihi, M.A., Khalil, A.M., Lu, L., Paroo, Z., Chan, A.W., Shi, Z., Liu, Q., Wahlestedt, C., He, C., Jin, P., 2008. A small molecule enhances RNA interference and promotes microRNA processing. Nat Biotechnol 26, 933-940.

Shi, Z., Johnson, J.J., Stack, M.S., 2012. Fluorescence In Situ Hybridization for MicroRNA Detection in Archived Oral Cancer Tissues. Journal of oncology 2012, 903581.

Shum, D., Bhinder, B., Radu, C., Farazi, T., Landthaler, M., Tuschl, T., Calder, P., Ramirez, C.N., Djaballah, H., 2012. An image-based biosensor assay strategy to screen for modulators of the microRNA 21 biogenesis pathway. Combinatorial chemistry & high throughput screening 15, 529-541.

Schmitter, D., Filkowski, J., Sewer, A., Pillai, R.S., Oakeley, E.J., Zavolan, M., Svoboda, P., Filipowicz, W., 2006. Effects of Dicer and Argonaute down-regulation on mRNA levels in human HEK293 cells. Nucleic Acids Res 34, 4801-4815.

Schwarz, D.S., Hutvagner, G., Du, T., Xu, Z., Aronin, N., Zamore, P.D., 2003. Asymmetry in the assembly of the RNAi enzyme complex. Cell 115, 199-208.

Sidahmed, A., Abdalla, S., Mahmud, S., Wilkie, B., 2014. Antiviral innate immune response of RNA interference. J Infect Dev Ctries 8, 804-810.

Sijen, T., Steiner, F.A., Thijssen, K.L., Plasterk, R.H., 2007. Secondary siRNAs result from unprimed RNA synthesis and form a distinct class. Science 315, 244-247.

Sinkkonen, L., Hugenschmidt, T., Filipowicz, W., Svoboda, P., 2010. Dicer is associated with ribosomal DNA chromatin in mammalian cells. PLoS One 5, e12175.

Smolen, J.S., Aletaha, D., Koeller, M., Weisman, M.H., Emery, P., 2007. New therapies for treatment of rheumatoid arthritis. Lancet 370, 1861-1874.

Song, E., Lee, S.K., Wang, J., Ince, N., Ouyang, N., Min, J., Chen, J., Shankar, P., Lieberman, J., 2003. RNA interference targeting Fas protects mice from fulminant hepatitis. Nat Med 9, 347-351.

Song, J.J., Smith, S.K., Hannon, G.J., Joshua-Tor, L., 2004. Crystal structure of Argonaute and its implications for RISC slicer activity. Science 305, 1434-1437.

Sonkoly, E., Wei, T., Janson, P.C., Saaf, A., Lundeberg, L., Tengvall-Linder, M., Norstedt, G., Alenius, H., Homey, B., Scheynius, A., Stahle, M., Pivarcsi, A., 2007. MicroRNAs: novel regulators involved in the pathogenesis of psoriasis? PLoS One 2, e610.

Sontheimer, E.J., Carthew, R.W., 2005. Silence from within: endogenous siRNAs and miRNAs. Cell 122, 9-12.

Stewart, S.A., Dykxhoorn, D.M., Palliser, D., Mizuno, H., Yu, E.Y., An, D.S., Sabatini, D.M., Chen, I.S., Hahn, W.C., Sharp, P.A., Weinberg, R.A., Novina, C.D., 2003. Lentivirus-delivered stable gene silencing by RNAi in primary cells. RNA 9, 493-501.

Stockwell, B.R., Haggarty, S.J., Schreiber, S.L., 1999. High-throughput screening of small molecules in miniaturized mammalian cell-based assays involving post-translational modifications. Chemistry & biology 6, 71-83.

Stroynowska-Czerwinska, A., Fiszer, A., Krzyzosiak, W.J., 2014. The panorama of miRNA-mediated mechanisms in mammalian cells. Cellular and molecular life sciences : CMLS 71, 2253-2270.

Svoboda, P., 2014. Renaissance of mammalian endogenous RNAi. Febs Letters 588, 2550-2556.

Svoboda, P., Flemr, M., 2010. The role of miRNAs and endogenous siRNAs in maternal-to-zygotic reprogramming and the establishment of pluripotency. EMBO Rep 11, 590-597.

Svoboda, P., Stein, P., Hayashi, H., Schultz, R.M., 2000. Selective reduction of dormant maternal mRNAs in mouse oocytes by RNA interference. Development 127, 4147-4156.

Taganov, K.D., Boldin, M.P., Chang, K.J., Baltimore, D., 2006. NF-kappaB-dependent induction of microRNA miR-146, an inhibitor targeted to signaling proteins of innate immune responses. Proc Natl Acad Sci U S A 103, 12481-12486.

Tahbaz, N., Carmichael, J.B., Hobman, T.C., 2001. GERp95 belongs to a family of signal-transducing proteins and requires Hsp90 activity for stability and Golgi localization. J Biol Chem 276, 43294-43299.

Tahbaz, N., Kolb, F.A., Zhang, H., Jaronczyk, K., Filipowicz, W., Hobman, T.C., 2004. Characterization of the interactions between mammalian PAZ PIWI domain proteins and Dicer. EMBO Rep 5, 189-194.

Tam, O.H., Aravin, A.A., Stein, P., Girard, A., Murchison, E.P., Cheloufi, S., Hodges, E., Anger, M., Sachidanandam, R., Schultz, R.M., Hannon, G.J., 2008. Pseudogene-derived small interfering RNAs regulate gene expression in mouse oocytes. Nature 453, 534-538.

Tan, G.S., Chiu, C.H., Garchow, B.G., Metzler, D., Diamond, S.L., Kiriakidou, M., 2012. Small molecule inhibition of RISC loading. ACS chemical biology 7, 403-410.

Tang, F., Kaneda, M., O'Carroll, D., Hajkova, P., Barton, S.C., Sun, Y.A., Lee, C., Tarakhovsky, A., Lao, K., Surani, M.A., 2007. Maternal microRNAs are essential for mouse zygotic development. Genes Dev 21, 644-648.

Tavazoie, S.F., Alarcon, C., Oskarsson, T., Padua, D., Wang, Q., Bos, P.D., Gerald, W.L., Massague, J., 2008. Endogenous human microRNAs that suppress breast cancer metastasis. Nature 451, 147-152.

Thompson, R.C., Deo, M., Turner, D.L., 2007. Analysis of microRNA expression by in situ hybridization with RNA oligonucleotide probes. Methods 43, 153-161.

Thomson, T., Lin, H., 2009. The biogenesis and function of PIWI proteins and piRNAs: progress and prospect. Annu Rev Cell Dev Biol 25, 355-376.

Tian, S.S., Lamb, P., King, A.G., Miller, S.G., Kessler, L., Luengo, J.I., Averill, L., Johnson, R.K., Gleason, J.G., Pelus, L.M., Dillon, S.B., Rosen, J., 1998. A small, nonpeptidyl mimic of granulocyte-colony-stimulating factor [see commetns]. Science 281, 257-259.

Timmons, L., 2004. Endogenous inhibitors of RNA interference in Caenorhabditis elegans. BioEssays : news and reviews in molecular, cellular and developmental biology 26, 715-718.

Timmons, L., Fire, A., 1998. Specific interference by ingested dsRNA. Nature 395, 854.

Tiscornia, G., Singer, O., Ikawa, M., Verma, I.M., 2003. A general method for gene knockdown in mice by using lentiviral vectors expressing small interfering RNA. Proc Natl Acad Sci U S A 100, 1844-1848.

Tomari, Y., Zamore, P.D., 2005. Perspective: machines for RNAi. Genes Dev 19, 517-529.

van de Wetering, M., Oving, I., Muncan, V., Pon Fong, M.T., Brantjes, H., van Leenen, D., Holstege, F.C., Brummelkamp, T.R., Agami, R., Clevers, H., 2003. Specific inhibition of gene expression using a stably integrated, inducible small-interfering-RNA vector. EMBO Rep 4, 609-615.

Van den Hove, D.L., Kompotis, K., Lardenoije, R., Kenis, G., Mill, J., Steinbusch, H.W., Lesch, K.P., Fitzsimons, C.P., De Strooper, B., Rutten, B.P., 2014. Epigenetically regulated microRNAs in Alzheimer's disease. Neurobiology of aging 35, 731-745.

van Rooij, E., Sutherland, L.B., Liu, N., Williams, A.H., McAnally, J., Gerard, R.D., Richardson, J.A., Olson, E.N., 2006. A signature pattern of stress-responsive microRNAs that can evoke cardiac hypertrophy and heart failure. Proc Natl Acad Sci U S A 103, 18255-18260.

Ventura, A., Meissner, A., Dillon, C.P., McManus, M., Sharp, P.A., Van Parijs, L., Jaenisch, R., Jacks, T., 2004. Cre-lox-regulated conditional RNA interference from transgenes. Proc Natl Acad Sci U S A 101, 10380-10385.

Viswanathan, S.R., Daley, G.Q., 2010. Lin28: A microRNA regulator with a macro role. Cell 140, 445-449.

Voinnet, O., 2008. Use, tolerance and avoidance of amplified RNA silencing by plants. Trends Plant Sci 13, 317-328.

Voinnet, O., Baulcombe, D.C., 1997. Systemic signalling in gene silencing. Nature 389, 553.

Wang, H.W., Noland, C., Siridechadilok, B., Taylor, D.W., Ma, E., Felderer, K., Doudna, J.A., Nogales, E., 2009a. Structural insights into RNA processing by the human RISC-loading complex. Nat Struct Mol Biol 16, 1148-1153.

Wang, J., Tekle, E., Oubrahim, H., Mieyal, J.J., Stadtman, E.R., Chock, P.B., 2003. Stable and controllable RNA interference: Investigating the physiological function of glutathionylated actin. Proc Natl Acad Sci U S A 100, 5103-5106.

Wang, Y., Juranek, S., Li, H., Sheng, G., Wardle, G.S., Tuschl, T., Patel, D.J., 2009b. Nucleation, propagation and cleavage of target RNAs in Ago silencing complexes. Nature 461, 754-761.

Watanabe, T., Totoki, Y., Toyoda, A., Kaneda, M., Kuramochi-Miyagawa, S., Obata, Y., Chiba, H., Kohara, Y., Kono, T., Nakano, T., Surani, M.A., Sakaki, Y., Sasaki, H., 2008. Endogenous siRNAs from naturally formed dsRNAs regulate transcripts in mouse oocytes. Nature 453, 539-543.

Watashi, K., Yeung, M.L., Starost, M.F., Hosmane, R.S., Jeang, K.T., 2010. Identification of small molecules that suppress microRNA function and reverse tumorigenesis. J Biol Chem 285, 24707-24716.

Wianny, F., Zernicka-Goetz, M., 2000. Specific interference with gene function by double-stranded RNA in early mouse development. Nat Cell Biol 2, 70-75.

Wightman, B., Ha, I., Ruvkun, G., 1993. Posttranscriptional regulation of the heterochronic gene lin-14 by lin-4 mediates temporal pattern formation in C. elegans. Cell 75, 855-862.

Wilczynska, A., Aigueperse, C., Kress, M., Dautry, F., Weil, D., 2005. The translational regulator CPEB1 provides a link between dcp1 bodies and stress granules. J Cell Sci 118, 981-992.

Wilson, R.C., Doudna, J.A., 2013. Molecular mechanisms of RNA interference. Annual review of biophysics 42, 217-239.

Wittmann, J., Jack, H.M., 2010. Serum microRNAs as powerful cancer biomarkers. Biochim Biophys Acta 1806, 200-207.

Worringer, K.A., Rand, T.A., Hayashi, Y., Sami, S., Takahashi, K., Tanabe, K., Narita, M., Srivastava, D., Yamanaka, S., 2014. The let-7/LIN-41 pathway regulates reprogramming to human induced pluripotent stem cells by controlling expression of prodifferentiation genes. Cell Stem Cell 14, 40-52.

Wu, G., Yuan, Y., Hodge, C.N., 2003. Determining appropriate substrate conversion for enzymatic assays in high-throughput screening. Journal of biomolecular screening 8, 694-700.

Xia, J., Zhang, W., 2014. MicroRNAs in normal and psoriatic skin. Physiological genomics 46, 113-122.

Xie, Z., Qi, X., 2008. Diverse small RNA-directed silencing pathways in plants. Biochim Biophys Acta 1779, 720-724.

Yan, K.S., Yan, S., Farooq, A., Han, A., Zeng, L., Zhou, M.M., 2003. Structure and conserved RNA binding of the PAZ domain. Nature 426, 468-474.

Yekta, S., Shih, I.H., Bartel, D.P., 2004. MicroRNA-directed cleavage of HOXB8 mRNA. Science 304, 594-596.

Yi, R., Qin, Y., Macara, I.G., Cullen, B.R., 2003. Exportin-5 mediates the nuclear export of pre-microRNAs and short hairpin RNAs. Genes Dev 17, 3011-3016.

Yuan, Y.R., Pei, Y., Ma, J.B., Kuryavyi, V., Zhadina, M., Meister, G., Chen, H.Y., Dauter, Z., Tuschl, T., Patel, D.J., 2005. Crystal structure of A. aeolicus argonaute, a site-specific DNA-guided endoribonuclease, provides insights into RISC-mediated mRNA cleavage. Mol Cell 19, 405-419.

Zamore, P.D., Tuschl, T., Sharp, P.A., Bartel, D.P., 2000. RNAi: double-stranded RNA directs the ATP-dependent cleavage of mRNA at 21 to 23 nucleotide intervals. Cell 101, 25-33.

Zeng, Y., Cullen, B.R., 2003. Sequence requirements for micro RNA processing and function in human cells. RNA 9, 112-123.

Zeng, Y., Cullen, B.R., 2004. Structural requirements for pre-microRNA binding and nuclear export by Exportin 5. Nucleic Acids Res 32, 4776-4785.

Zeng, Y., Wagner, E.J., Cullen, B.R., 2002. Both natural and designed micro RNAs can inhibit the expression of cognate mRNAs when expressed in human cells. Mol Cell 9, 1327-1333.

Zhang, B., Salituro, G., Szalkowski, D., Li, Z., Zhang, Y., Royo, I., Vilella, D., Diez, M.T., Pelaez, F., Ruby, C., Kendall, R.L., Mao, X., Griffin, P., Calaycay, J., Zierath, J.R., Heck, J.V., Smith, R.G., Moller, D.E., 1999a. Discovery of a small molecule insulin mimetic with antidiabetic activity in mice. Science 284, 974-977.

Zhang, G., Budker, V., Wolff, J.A., 1999b. High levels of foreign gene expression in hepatocytes after tail vein injections of naked plasmid DNA. Hum Gene Ther 10, 1735-1737.

Zhang, H., Kolb, F.A., Brondani, V., Billy, E., Filipowicz, W., 2002. Human Dicer preferentially cleaves dsRNAs at their termini without a requirement for ATP. EMBO J 21, 5875-5885.

Zhang, H., Kolb, F.A., Jaskiewicz, L., Westhof, E., Filipowicz, W., 2004. Single processing center models for human Dicer and bacterial RNase III. Cell 118, 57-68.

Zhao, Y., Samal, E., Srivastava, D., 2005. Serum response factor regulates a muscle-specific microRNA that targets Hand2 during cardiogenesis. Nature 436, 214-220.

9 PUBLICATIONS and SUPPLEMENTS

During my Ph.D., I co-authored three impacted publications:

(i) A review summarizing the use of RNAi *in vivo*:

Podolska, K., Svoboda, P., 2011. Targeting genes in living mammals by RNA interference. Briefings in functional genomics 10, 238-247. (Supplement I.)

(ii) Reporters, which I developed for HTS were used in the following study, in which I monitored miRNA activity upon inhibition of Lsm8.

Novotny, I., Podolska, K., Blazikova, M., Valasek, L.S., Svoboda, P., Stanek, D., 2012. Nuclear LSm8 affects number of cytoplasmic processing bodies via controlling cellular distribution of Like-Sm proteins. Mol Biol Cell 23, 3776-3785. (Supplement II.)

(iii) An article summarizing development of Dicer HTS:

Podolska, K., Sedlak, D., Bartunek, P., Svoboda, P., 2014. Fluorescence-based high-throughput screening of dicer cleavage activity. Journal of biomolecular screening 19, 417-426. (Supplement III.)

In addition, a manustript summarizing cell-based assay results is currently in preparation.